Physico-chemical methods to determine the trace rare elements in Goan ore rejects and beneficiate the ore to get pure iron oxide useful for high-tech ferrite manufacture

A   THESIS

SUBMITTED TO THE

GOA   UNIVERSITY

FOR THE DEGREE OF

DOCTOR OF PHILOSOPHY

IN

INORGANIC   CHEMISTRY

BY

PANDURANG Y. SAWANT

DEPARTMENT OF CHEMISTRY
GOA   UNIVERSITY
TALEIGAO PLATEAU
GOA – 403206
INDIA

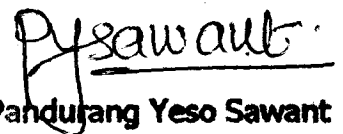DECEMBER 1998

Dedicated to

MY GURUS

STATEMENT

I hereby state that this thesis for the Ph.D. degree on "Physico-chemical methods to determine the trace rare elements in Goan ore rejects and beneficiate the ore to get pure iron oxide useful for high-tech ferrite manufacture" is my original work and that it has not previously formed the basis for the award of any degree, diploma, associateship and or any other similar title to the best of my knowledge and information.

Dr.K.S.Rane

(Research Guide)

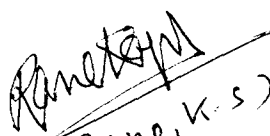Pandurang Yeso Sawant

(candidate)

Dr. Jayant C. Pradhan

Goa 403 206

CERTIFICATE

As required under University ordinance, I certify that the thesis entitled "Physico-chemical methods to determine the trace rare elements in Goan ore rejects and beneficiate the ore to get pure iron oxide useful for high-tech ferrite manufacture" submitted by Mr. Pandurang Yeso Sawant for the award of Doctor of Philosophy in Chemistry is a record of research done by the candidate during the period of study under my guidance and that it has not previously formed the basis for the award to the candidate of any degree, diploma, associateship, fellowship or other similar titles.

Date: 18 December 1998

Dr. K. S. Rane,
Research Guide,
Department of Chemistry,
Goa University.

Dr K. S. Rane
(Rane, K. S) (Internal examiner)
29/7/99

Prof. K. A. Nararajan
(external examiner)

ACKNOWLEDGEMENT

breakdown of the instruments used for the purpose along with his associates Mr.Gend and Jayprakash Kamat.

I am immensely indepted to Dr. V. M. S. Verenkar for his all kinds of assistance and cooperation in various phases of my work.

I am thankful to Dr. B. D. Dessai, Dr. A. V. Salkar, Dr. J. B. Fernandes, Dr. B. Dasgupta, Dr. R. N. Shirsat, Dr. J. Kirtany, Dr. S. P. Kamat, Dr. V. S. Nadkarni and Dr. S. G. Tilve for their encouragement and suggestions.

I express my thanks to Dr. Ganpat Naik, Dr. Sajo Naik, Dr. Shridhar Gurav, Dr. Kamalesh Pai Fondekar, Mr. Samant, Mr. Sachin Kakodkar and Mr. Sadanand Hinde for their valuable suggestions.

I greatfully thank Mrs. Sunita Verenkar for the computerisation of this work without which this presentation would not have been in time and success.

Finally but not the least I extend my thanks to my research colleagues Mr. Rajesh, Tushar, Teotone, Ratnakar, Adlete, Neel, Mrs. Deepa, Purnakala, Harsha, Vidya and Asha for their various suggestions and cooperation.

My thanks also goes to Mr. Ravi Chavan and Mr. M. R. Potdar for tracing figures.

However, this work could not have been carried out without the help and cooperation of office and laboratory staff of our chemistry department.

ABSTRACT

Iron oxides, α-Fe_2O_3 (hematite), Fe_3O_4 (magnetite) and γ-Fe_2O_3 (maghemite) have wide industrial applications as pigments, catalysts and magnetic materials. The iron oxides in combination with divalent metals, M^{2+}, form a class of magnetic materials called ferrites of general formula, MFe_2O_4. The ferrites possess interesting magnetic and electric properties and find use in electronic industries as device materials as cores in radio transistors, televisions and VCR's, microwave equipments, high frequency transformers (power ferrites), magnetic tape recorders etc.

The demand for iron oxides and ferrites in ever expanding electronic industries has increased tremendously in 1990's. The estimated world ferrites production, by the turn of this century, is ~ 974,000 metric tons per year (MTPY). During 1970's and 1980's India's contribution in the world ferrites material was mere 2(%) and the present scenario is also not that encouraging.

In ferrite industries the major raw material, Fe_2O_3, for the production is about 70% and the important source for this ferrite grade iron oxide is upgraded hematite and spray roasted acid pickle solution of steel industries. Considering the rich iron oxide sources in India, there is enough scope for our country to be a leader in the ferrites market, if we exploit the iron oxide ores effectively. But then, we are envisaging to exploit the iron ore rejects to synthesize chemically the ferrite grade iron oxides used in ferrites manufacture.

The thesis deals with the chemical beneficiation of iron ore rejects to prepare iron oxides of low impurity contents to use in the synthesis of $MgFe_2O_4$ and $(Mn_{1/2}Zn_{1/2})Fe_2O_4$.

Two iron ore samples consisting of 57.49 (%) Fe_2O_3, 23.33 (%) Al_2O_3, 9.15 (%) SiO_2, 0.83 (%) MnO (study sample I) and 76.36 (%) Fe_2O_3, 6.41 (%) Al_2O_3, 5.24 (%) SiO_2, 2.36(%) MnO (study sample II) are chosen for the chemical beneficiation to get high purity Fe_2O_3.

The acid extract of the ores are precipitated as metal (iron) hydroxides using precipitants like NaOH, NH_3, $NaOH+NH_3$ and Na_2CO_3. The hydroxides on decomposition yield α-Fe_2O_3 of purity 92-98.38 (%) depending on the precipitants.

The metal (iron) hydroxides were further converted into metal (iron) formates and the decomposed products are mainly γ-Fe_2O_3 of purity 96.5 - 98.67 (%).

The acid extract on extracting with methyl isobutyl ketone (MIBK) and precipitating as hydroxide yielded 99.73 (%) pure iron oxide on decomposition.

The metal (iron) hydroxides / formates on equilibration with hydrazine in a desiccator containing 99.99 (%) hydrazine hydrate when exposed to air decomposed instantaneously to magnetic γ-Fe_2O_3.

The iron oxides, both α- and γ-Fe_2O_3, thus obtained by chemical beneficiation of iron ore are used to prepare $MgFe_2O_4$ and $(Mn_{1/2}Zn_{1/2})Fe_2O_4$ by ceramic technique.

A single phase $MgFe_2O_4$ that obtained are characterized for their important magnetic and electric properties and compared their results with the ferrite prepared from commercial hematite, commercial red oxide and standard γ-Fe_2O_3. A mixture of $MgFe_2O_4$ + α-Fe_2O_4 is observed in the ferrite synthesized from commercial hematite

indicating incomplete formation of the ferrite, while all the other ferrites samples are characterized as single phase $MgFe_2O_4$. Hence, the properties of the ferrite obtained from commercial hematite showed low saturation magnetization, high porosity, high Curie temperature; all other $MgFe_2O_4$ that prepared from chemically beneficiated iron oxide gave uniform properties.

The $(Mn_{1/2}Zn_{1/2})Fe_2O_4$ system is a complicated one as the preparation of the ferrite needs stringent process control due to the fact that manganese has tendency to vary its oxidation state. In our investigations we have restricted ourselves to the synthesis aspects of the ferrite. And, a fairly good quality $(Mn_{1/2}Zn_{1/2})Fe_2O_4$ was achieved using chemically beneficiated iron ore (study sample II).

An important iron oxide of γ-Fe_2O_3 form has been studied to investigate the presence of protons in its spinel structure on the octahedral sites. And, the lithiation of the oxide has enabled us to establish the presence of the protons in the oxide.

CONTENTS

CHAPTER I

I

CHAPTER II

CHEMICAL BENEFICIATION OF IRON ORE REJECTS

CHAPTER III

PREPARATION AND CHARACTERIZATION OF IRON OXIDE FROM IRON
HYDROXIDES, IRON FORMATES AND THEIR HYDRAZINATED COMPLEXES

CHAPTER IV

STUDIES ON THE MAGNESIUM AND MANGANESE ZINC FERRITES

PART – I

MICROSTRUCTURE AND PROPERTY CORRELATION OF $MgFe_2O_4$(ore rejec s[46])

PART – II

SYNTHESIS AND CHARACTERIZATION OF $MgFe_2O_4$ (Study Sample – I)

PART III

SYNTHESIS AND CHARACTERIZATION OF $Mn_{1/2}Zn_{1/2}Fe_2O_4$ (Study Sample – II)

CHAPTER V

STRUCTURAL ASPECTS OF γ-Fe_2O_3: HYDROGEN IRON OXIDE OR HYDROGEN

CHAPTER VI

CONCLUSIONS

LIST OF TABLES

CHAPTER – I

CHAPTER – II

CHAPTER – III

CHAPTER – IV

PART - I

LIST OF FIGURES

XI

from their oxides

CHAPTER – V

General Introduction

Magnetite, Fe_3O_4, probably the first ever known magnetic material which was put into practical use by ingenious navigators in early days in the form of magnetic needle in compass as to get guided the direction of their voyages. Its saturation magnetization was measured in 1890 by Du Bois [1] and considered it as ferrous ferrite, $FeO.Fe_2O_3$. Manganese zinc ferrite is a naturally occuring mineral called franklinite discovered by Berthier in 1819. It has been found in only two places around Franklin, New Jersey. The mineral is slightly magnetic because of contamination and oxidation and it was Snoek [2] who synthesized it first and recognised its potential as a high frequency magnetic core material. Manganese zinc ferrite is an isomorph of magnetite and as such has the cubic spinel structure. A variety of synthetic ferrites were then prepared by Hilpert [3] who

1

suggested the basic formula for the ferrites as $MO.Fe_2O_3$, where M is the divalen metal ion.

Ever since the realisation of the application of these natural magnetic ma erials, several magnetic materials of interesting compositions have been synthesized, characterized and put them in use for the benefit of humanity. Three basic types or classes of magnetic crystal structures have found wide applications in electronic industries and other industrial persuits. Each of these types contains families of completely different compositions all of which possess unique properties and characteristic applications. These three classes of ferrimagnetic oxides are ferrites (spinels), garnets and hexagonal materials.

The ferrites are further classified as soft and hard, depending on their magnetic characteristics. During the early days (some 60 years ago) ferrites, especially soft ferrites, found use primarily in the communication areas. When television arrived, they were used as flyback transformers or as deflection yokes. In telephones, they were used as channel filters and in tone generators circuits ferrites find applications in touch-tone phones. Of ten million telephones that manufactured by Western Electric in early 1970's [4] about 3 million were touch-tone dials. At that time MnZn ferrite was the only material that met all the requirements that are important viz. High Q, good stability with time and temperature, small size, low cost.

In 1930's a transistor switched power supplies created a need for ferrite material operating at much higher flux levels and frequencies than those encountered in telecommunications. MnZn ferrites were the materials that found use, that time, but then with the increase in switch-mode power supply market, requirement of magnetic characteristics also changed. Power ferrites are thus arrived. The power ferrites needed to be operated at higher frequencies. Frequency of operation kept increasing as the solid

state industry developed enabling to prepare newer ferrites. The need for small compact power supplies for computers, microprocessors and VCR's have further triggered a great demand for power ferrites. The new power ferrites have to have two new attributes [5] that not previously needed in other applications: 1) they have to possess high saturation, Bs and 2) they should have low core loss at higher flux densities (near the position of μ_{max}) and at fairly high frequencies.

MnZn ferrites are materials of low resistivity which impedes their use in high frequency applications due to several losses like eddy current etc. A higher resistivity materials, MgZn ferrites are now replacing MnZn ferrites in certain applications. A comparison of important properties between MgZn and MnZn ferrites reveals that, although permeability and saturation reduced from 900 – 1000 and 3000 – 4000 Gauss in MnZn ferrites to 350 – 500 and 2400 – 2700 Gauss in MgZn ferrites, the loss factor remained almost constant at $\sim 10^{-6}$. But, there is tremendous increase in resistivity observed in MgZn ferrites of $\sim 10^{7} - 10^{8}$ Ω cm, while MnZn ferrites show low resistivity, $\sim 10^{2}$ Ω cm.

Infact, Mg ferrites and allied compounds have found widespread applications in microwave devices. They are considered as the most versatile ferrites in electronic industry [6] because of their comparatively low magnetic and dielectric losses obtainable. In particular, these possess high resistivities which can be obtained by the selection of suitable minor additives and using appropriate firing procedures. Among the various magnesium ferrites, MgZn ferrites have been most thoroughly examined. MgAl ferrites are the other examples which have been widely studied when useful frequency ranges of microwave devices have to be extended for low microwave bands and ultra high frequency devices. These materials of $MgFe_2O_4$ group are of much interest because they

exhibit low saturation magnetization, high resistivity and uniform and reproducible characteristics needed for microwave device applications.

Spinels, thus, of general formula MFe_2O_4 find applications when additives are present in divalent form. MnZn ferrite is achieved on substituting Zn^{2+} from $ZnFe_2O_4$ by Mn^{2+} or Mn^{2+} from $MnFe_2O_4$ by Zn^{2+}. A 50 % substitution of Zn^{2+} from $ZnFe_2O_4$ leads to $Mn_{1/2}Zn_{1/2}Fe_2O_4$. A solid solution of $MnFe_2O_4$ and $ZnFe_2O_4$ is thus achieved: $Mn_{1-x}Zn_xFe_2O_4$, where x = 0.5. Similarly a solid solution of $MgFe_2O_4$ and $ZnFe_2O_4$ may be written as $Mg_{1-x}Zn_xFe_2O_4$, where x = 0.5. However, a complete range of solid solutions can be obtained by varying x from 0.00 to 1.00 in many spinels. Such a wide range of solid solutions show interesting properties, as literature survey reveals, many different spinels of different additives. Last seven to eight decades ferrites researchers realised many interesting properties of these from both academic and application point of view by using more than one additives in the spinel structure. If ferrites are considered as materials containing mostly iron which are derived from magnetite Fe_3O_4, ($Fe^{2+}O.Fe^{3+}_2O_3$) by substituting Fe^{2+} by divalent metals, M^{2+}, a wide range of ferrites can be produced. The more common divalent metal ions that are being used are Mn, Fe, Co, Ni, Cu, Zn, Mg, Cd, and Ge. Trivalent metal Fe^{3+} from Fe_3O_4 is also substituted by trivalent metals such as, Al, Cr, Ga, Mn. Monovalent Li and tetravalent Ti and Sn are even incorporated into the lattice of the spinel by the respective decrease or increase in the Fe^{2+}/Fe^{3+} ratio. When such additives are introduced, it becomes quite involved research as far as their synthesis is concerned, as single phase ferrite is needed to be formed to achieve desired properties. And, hence, the synthesis of the ferrites becomes main objective of any researcher who enters this field.

Synthesis of Ferrites

Ferrites synthesis needs a thorough understanding of chemistry aspects. Since

ferrites are oxide solid ceramic materials, high temperatures are needed to prepare them. As solid state reactions are sluggish, reactivity of starting materials requires to be increased. Fine grained starting materials are therefore used. A homogeneous mixing ensures close proximity of individual reactants with each other. Instead of heating directly the ground mixtures to high temperatures, preheating is done to initiate the reactions. This preheating is normally done in pelletised powders to ensure better reactions. The preheated samples are then cooled, ground and repelletised then further heat treatment is done at much high temperatures. Many a times, one more grinding and pelletising is carried to go for final sintering at the desired temperatures to get well dense, fully grown microstructures. Ferrites preparation is laborious, as one has to make a compromise between their intrinsic and extrinsic properties to realise a material of optimum characteristics.

Intrinsic and Extrinsic properties

The intrinsic properties of ferrites are saturation magnetization, magnetostriction, anisotropy, permeability and Curie temperatures whereas the extrinsic properties are hysteresis, resistivity, dielectric constants etc. The parameters such as porosity grain size, impurities, etc. affect the extrinsic properties. The extrinsic properties are also referred to as structure sensitive properties. Single phase ferrites of the desired compositions are must to achieve the required magnetization and Curie temperature values.

Importance of extrinsic properties

Ferrites of optimum properties are difficult to achieve and hence the preparation of polycrystalline magnetic materials is considered to be difficult and complex. It is now well understood that the control of extrinsic properties is most desired to achieve the

5

required properties for device applications. Hence, the knowledge of the parameters of microstructure such as density, grain size and porosity and their intra and interg anular distribution are important in controlling the extrinsic properties. The knowle lge of chemistry and crystal structure along with the microstructural aspects becoi ie the important criteria in the study of ferrites.

Chemistry, crystal structure and microstructure of ferrites

Ferrites of general formula MFe_2O_4, where M is a divalent metal, are struc turally similar to the mineral spinel $MgAl_2O_4$. Conventionally they are writt en as $(M^{2+})_{tet}[Fe^{3+}_2]_{oct} O_4$, where tet = tetrahedral site and oct = octahedral site. Spine has a close packed cubic structure of oxygen atoms with 8 formula units per unit cell ε nd the unit cell structural formula is written as, $(M^{2+}_8)^A_{tet}[Fe^{3+}_{12}]^B_{oct} O_{32}$, where ( ) = A s te and [ ] = B site. The unit cell consists of in all 64 tetrahedral sites and 32 octahedral sites of which $^1/_8$ tetrahedral sites and ½ octahedral sites are occupied.

Normal spinel

All divalent metal ions, M^{2+}, when occupy the tetrahedral sites a normal s inel is arrived. $ZnFe_2O_4$ is an example of such a spinel with formula, $Zn^{2+}[Fe^{3+}_2]O_4$. T ie ( ) bracket can be omitted.

Inverse spinel

Divalent metals here enter the octahedral sites replacing the trivalent metals which then go to tetrahedral sites as in Fe_3O_4, $Fe^{3+}[Fe^{2+}Fe^{3+}]O_4$. Nickel ferrite is nother example, $NiFe_2O_4$, $Fe^{3+}[Ni^{2+}Fe^{3+}]O_4$.

Random spinel

An intermediate between normal and inverse spinels are observed when diva lent

6

metals occupy both A and B sites. Examples are many, depending on number of such distributions. In $MgFe_2O_4$ the divalent cation distribution is $Fe^{3+}_{0.9}Mg^{2+}_{0.1}[Mg^{2+}_{0.9}Fe^{3+}_{1.1}]O_4$. The other member of this class is $MnFe_2O_4$, $Mn^{2+}_{0.8}Fe^{3+}_{0.2}[Mn^{2+}_{0.2}Fe^{3+}_{1.8}]O_4$.

Vacancy spinel

Although all 8 tetrahedral and 16 octahedral sites are occupied by metal ions as in normal and inverse spinels, there are instances wherein few vacancies are observed in spinel structure. The vacancies are due to non occupation of few of 8 tetrahedra or 16 octahedral sites of the spinel structure. A good example is the oxidation product of magnetite itself. Fe_3O_4, $Fe^{3+}[Fe^{2+}Fe^{3+}]O_4$ on oxidation, all Fe^{2+} on octahedral sites convert into Fe^{3+} and results into gamma ferric oxide, γ-Fe_2O_3, $Fe^{3+}[Fe^{3+}_{5/3}\square_{1/3}]O_4$, where $\square$ represents vacancy. The spinel lattice can tolerate a high concentration of cation vacancies.

This tendency to form cation vacancies increases in spinels [7] of practical application, $(M_A+M_B)_{1-x}Fe_{2+x}O_4$, when there are two or more metals besides iron and when x varies between –0.3 to 0.3. The ferrite is considered to be stoichiometric from formula stand point when x = 0 (or Fe_2O_3 = 50 mole %). In contrast to this formula stoichiometry, there can exist an atomic stoichiometry where there are exactly 3 metal atoms for every 4 oxygen atoms.

The tendency to form cation vacancies increases as x increases from 0 to a more positive value by the combination of excess α-Fe_2O_3 with rhombohedral structure dissolving into a ferrite spinel structure,

$$4Fe^{3+}_2O_3(rh) \longrightarrow 3Fe^{3+}_{8/3}\square_{1/3}O_4(sp) \quad \text{------------ ( )}$$
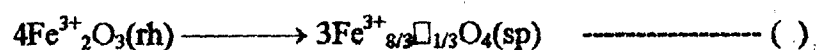
and the equilibration of the dissolved species with temperature and atmosphere,

7

$$3Fe^{3+}_{8/3} \square_{1/3} O_4 \Longleftrightarrow 8/3 Fe^{2+}Fe^{3+}_2 O_4 + O_2 \uparrow \quad \Delta H = 23 kcal/mole \quad \text{------- (2)}$$
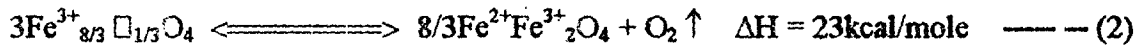
Increased temperature and decreased atmospheric oxygen tend to reduce the cation vacancy content. From this analysis, atomic stoichiometry can exist without having formula stoichiometry. Cation vacancies play an extremely important role in the ferrite's sintering kinetics and magnetic properties.

Chemistry

Ferrites of spinel structure exhibit magnetism, ferro-, ferri- and antiferro- due to i) unpaired 3d electrons ii) super exchange between adjacent metal ions and iii) non equivalence in number of A and B sites. Magnetic moment of free state magnetic atom is the sum of the electron spin and orbital moments, while the atoms in spinel exhibit only spin magnetic moments as quenching of orbitals takes place due to the electronic fields caused by the surrounding oxygen about the metal ion. Therefore, atomic magnetic moment (m) is simply its electronic spin moment and is equivalent to $m = \mu_B n$ where μ_B is a Bohr magnetone unit and n is the number of unpaired electrons.

In spinel both A and B sites are capable of accommodating variety of metal ions, magnetic and non magnetic. Since these two sites have two different environments: one has tetrahedral and the other octahedral, magnetic interaction between atoms on these sites: AB interaction via oxygen ions (super exchange) occurs and it decreases as the distance between the metals increases and as the angle of M-O-M decreases from 180 to 90°.

In spinel both A and B sites are equally capable of accommodating magnetic ions. Thus, magnetic ions are distributed throughout the crystal lattice which tend to interact through oxygen (super exchange) magnetically and hence exhibit magnetism. Interaction is maximum when M-O-M angle is 180° and distance between the metals is small. A look at the spinel structure (Fig 1.1) indicates an angle M_A-O-M_B, ~ 125° where M_A and

8
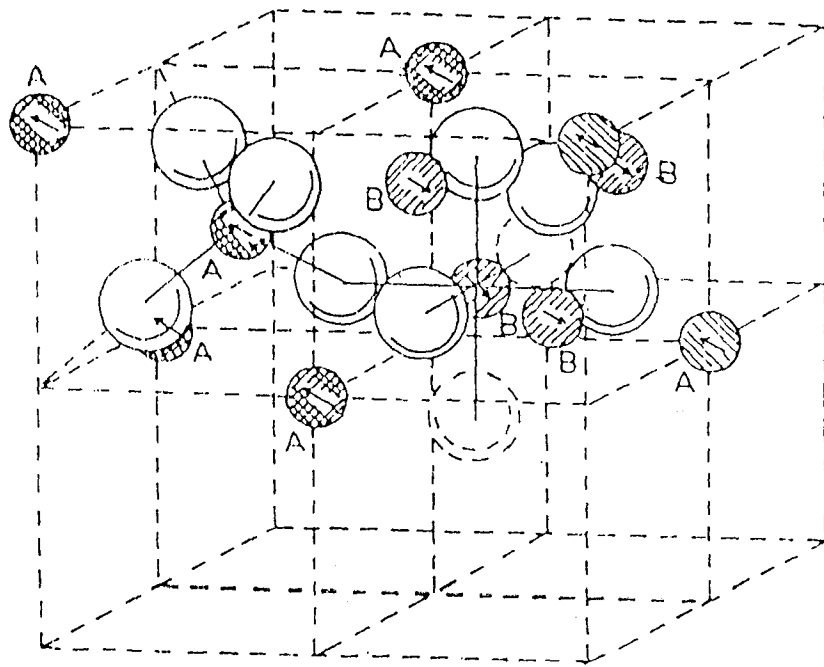
THE SPINEL STRUCTURE
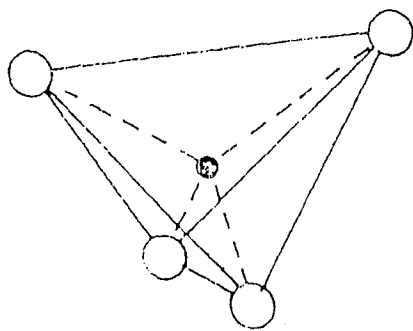
(a) Tetrahedral A site
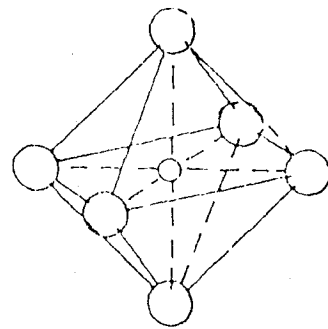
(b) Octahedral B site

FIG. 1.1   Crystal structure of spinel ferrites showing tetrahedral a id octahedral co-ordination

M_B are metals on A and B sites, respectively. On the other hand, M_B-O-M_B is $9)^O$ and interaction is minimum or negligible. The strength of interaction depends on the degree of orbital overlap of oxygen p orbits and the metal (mostly transition) d orbitals.

Based on these interaction knowledge [8-13] and the nature of metal ions possibly present on two sites, magnetic moments can be calculated and experimentally observed. Thus, Fe_3O_4, $Fe^{3+}[Fe^{2+}Fe^{3+}]O_4$ having $3d^5$ (Fe^{2+}) and $3d^5$ (Fe^{3+}) electrons contributing to magnetism gives experimentally magnetic moment, $\eta_B = 4.1$ which is close to the theoretical value of 4.0. Since B-B interaction is negligible and zero, the only significant interaction is A-B. If Fe^{3+} on A site (of $\mu_B = 5$) is considered to interact with Fe^{3+} of B site, then magnetic moment cancel as they are antiparallel to each other. And, hence, the magnetic moment is only due to $Fe^{2+}(\mu_B = 4)$. This confirms the cation distribution. Then, if $MgFe_2O_4$ is considered to be normal spinel, $Mg^{2+}[Fe^{3+}Fe^{3+}]O_4$, Mg on A site with no d-electrons, will not have interaction with B site Fe^{3+} ions. And, since B-B interaction is zero, the spinel should show no magnetic moment. However, it does show magnetic moment, $\eta_B = 1.1$. From the experimental value a cation distribution for $MgFe_2O_4$ is written and confirmed as $Fe_{0.9}Mg_{0.1}[Mg_{0.9}Fe_{1.1}]O_4$ and the calculated $\eta_3 = 1.0$ is thus very close to the experimental findings.

Experimental and calculated values of magnetic moments in ferrite may not necessarily guide one to the distribution of cations on A and B sites. For example, cobalt ferrite is known inverse spinel, $CoFe_2O_4$, $Fe^{3+}[Co^{2+}Fe^{3+}]O_4$. The $3d^7$ electrons ($\mu_3 = 3$) on octahedral sites make this spinel to possess magnetic moment of 3 Bohr magnetone but experiment indicates it to have 3.7 at 0 K. The higher value is due to orbital contribution of Co to the magnetic moment.

Thus, one can with some efforts make sure about the cation distributions in ferrites and confirm by other supporting experiments such as Mössbauer effect studies.

And, if cation distributions are thus confirmed, then there is no much difficulty in preparing such ferrites by chemical knowledge. Although preparation of ferrites is laborious, one is certain of the preparation. The synthesized material may be expected to give the desired properties like magnetization, Ms and Curie temperatures which are the intrinsic properties of ferrites. But they may not assure of the other properties considered to be extrinsic one.

Properties dependence on microstructure

Ferrites find applications in wide range of electronic appliances. MnZn ferrites are used [14-20] in devices, such as inductor, transformer, loading coil, flyback transformer, deflection yokes, recorder heads, power transformers. The desired properties for such device functions are permeability, μ, high stability of μ with temperature and time. But for transformer purpose a high μ and low hysteresis loss is needed. In loading coil applications high μ, high saturation Bs, high stability of μ with temperature are the requirements.

Ferrites for application at frequencies below 1 MHz the core materials should have high permeability but for high frequency signals to achieve, a high value of saturation magnetization is desired.

Ferrites designed for frequencies above 1MHz should possess high resistivities to avoid eddy current losses. Dielectric losses are minimised by choosing ferrites with resistivities $> 10^6$ Ω cm. Ferrites useful for storing information, cores should show square loop hysteresis having two equally stable magnetic states by +Br and –Br, the two remanent flux density states. Magnesium manganese ferrites, $Mg_{1-x}Mn_xFe_2O_4$ find use in such applications. Manganese ferrite, $MnFe_2O_4$ with saturation induction Bs = 5000 Gauss at room temperature and $MgFe_2O_4$ of Bs = 1800 Gauss are used to prepare a solid solution of these two to get induction values of desired level by careful choice of x.

11

Switch cores need ferrites of high flux density and is achieved by using a composition with high percentage of $MnFe_2O_4$.

Microwave devices for ultra high frequency applications demand ferrites exhibiting small saturation magnetization between 300-1900 G. Yttrium iron garnet (YIG), $Y_3Fe_5O_{12}$ ($4\pi Js = 1790$ G) and yttrium substituted YIG are most suitable for such applications [21] as depending on the required magnetization value the substitution may be effected without bringing any change in Curie temperature. Magnesium ferrite and substituted magnesium ferrites are also studied widely as they do find widespread applications in microwave devices.

Thus, it can be inferred that important properties of ferrites that make them useful for device applications are permeability, saturation magnetization, remanent flux, Curie temperature, resistivity, dielectric properties etc. But losses like eddy current, hysteresis loss, dielectric loss etc. required to be checked if ferrites are considered for device applications. For example, ferrites useful in radio frequency ranges the eddy current losses can be minimised by increasing resistivity, ρ. But the increase in frequency f, too enhances the loss, however, one can check this loss by decreasing the thickness of the ferrite core [22] as

$$\text{Eddy current loss} \quad \alpha \quad \frac{D^2 f}{\rho} \quad \text{------------------ (3)}$$

where D is the thickness of the core, f is the frequency of the a.c. field.

Permeability is an important property to be considered in ferrite applications. Permeability is governed by two mechanisms, namely, spin rotation in the magnetic domain and wall displacement. Although two mechanisms are well understood theoretically, when it comes interpreting the property from the experimental results, many difficulties arise. And, it has been described [7] that the intrinsic rotational permeability,

μ^R, and 180° wall permeability, μ^W depend, no doubt, on saturation magnetizati n but also on anisotropy, wall energy and diameter of the grains of the ferrite compacts,

$$\mu^R = 1 + 2\pi Ms^2/K \qquad\qquad \mu^W = 1 + {}^3/_4\pi Ms^2 D/\Upsilon \text{ ------------ (4)}$$

where Ms = saturation magnetization

D = grain size

K = total anisotropy = $K_1 + \lambda s\sigma$

K_1 = first order magnetocrystalline anisotropy

λs = magnetostriction or deformation with the field

σ = internal stress

Υ = wall energy = $K\delta u$

δu = wall thickness

The wall permeability, μ^W, may be written as

$$\mu^W = 1 + (3\pi/4\delta u)(Ms^2/K)D$$

Thus, wall permeability is dependent on intrinsic properties, Ms, K_1, λs and grain dependent properties (extrinsic). The rotational permeability, μ^R, on the other h nd, is dependent only on the intrinsic properties such as Ms, K_1, λs. Hence, the technolo ically important permeability property of magnetic materials if required to be adjusted, (ne has to have the knowledge of several above parameters.

The intrinsic properties such as Ms, K_1, λs are controlled by chemistry The permeability properties then depend, apart from these intrinsic properties, or grain dependent parameters such as grain size and intergranular defects such as p(rosity, second phase inclusions and dislocations that affecting the wall energy. Thus, microstructural aspects of ferrites compacts are required to be understood thor)ughly while establishing the required permeability values.

To obtain high permeability the ferrite core should possess small porosi y and pores must occur only between the grains and not inside the grain. A high purity s arting materials that yield quite homogeneous single phase ferrite may attain high permea bility. A linear increase in permeability with the gr. size has been realised technologica ly and a maximum permeability of ~ 40,000 is also reported [23] in MnZn ferrites by mod ifying sintering conditions.

The pores, impurities, inhomogeneity, inclusions, grain boundry all together act as an obstacle to rotation of the magnetization and hence permeability (μ^R) is hir dered. Pores inside the grain, on the other hand, effectively trap the walls of the domain ar d thus permeability due to wall movement is also hampered.

Hysteresis loss make ferrites unsuitable for many applications, especially in power ferrites. The factors that govern the hysteresis loss are

1. Magneto crystalline anisotropy (K_1)

2. Magnetostriction (λ)

3. Internal and external stress (σ)

4. Volume fraction of inclusions (include pores, dislocations, cavities and impuritie s)

5. Saturation magnetization (M_s)

To reduce hysteresis loss K_1, λ, σ and volume fraction of inclusions shc uld be small and M_s should be large. K_1, λ and M_s are primarily dependent upon ch emical composition (intrinsic properties). Internal stress and volume fraction of inclusic ns are determined by microstructure. It is, therefore, the microstructure of the fe rite is important in controlling the hysteresis loss as the intrinsic properties are easy to r lanage by chemistry.

Resistivity (ρ) determines eddy currents loss (equation 3). Because microstr icture controls resistivity, it can be expected that microstructure also controls the eddy cur rent

loss.

There are always efforts in ferrites industry to find best method to minimise the
above obstacles by adopting processes to obtain well compact ferrites. Hence, not only
chemistry but also microstructural aspects are required to be thoroughly studied while
looking for newer methods of synthesis of ferrites. Both intrinsic and extrinsic properties
need to be carefully considered in any ferrite studies.

Ferrite raw materials

Ferrites of general formula $MO.Fe_2O_3$, where M = divalent metals, Mg, Mn, Ni,
Fe, Cu, Co are derived from the ferrite when $M = Fe^{2+}$ and hence, in ferrites preparation it
is iron oxide which is the major raw material. The iron oxide sources (Table 1.2) for the
preparation of ferrites are mainly [24]: upgraded magnetite, upgraded hematite, oil free
mill scale, fluidized bed regenerated granules, spray roasted ferric oxide with high,
medium and little impurities, sulphate processed medium and little impurities and
carbonyl. In table 1.1 the world ferrite production projected [24] for year 1990, 1995 and
2000 indicates enormous requirement of iron oxides that are obtained from above
sources.

Table 1.1 Future utilisation of iron oxide raw materials for world ferrite production [24]

Year	1990	1995	2000
Estimated total world ferrite production in MTPY	516,000	665,500	974,000
Total ferric oxide consumption in MTPY Hard ferrites (x 0.87) Soft ferrites (x 0.70)	318,000 105,000	420,000 130,000	550,000 155,000
Sub total ferric oxide	423,000	550,000	705,000

Table 1.2 Iron oxide sources for ferrite preparation [24]

Iron oxide source	Year 1990	Year 1995	Year 2000
1. *Upgraded Magnetite	*5%	*5%	*5%
2. *Upgraded Hematite	*30%	*50%	*65%
3. *Oil free Mill Scale	*15%	*10%	*10%
4. * Fluidized bed regenerated granules	*50%	*35%	*20%
* Subtotal 1- 4 (MTPY)	127,000	192,500	2 ;2,000
5. Spray roasted ferric oxide, high content of impurities	20%	15%	10%
6. Spray roasted ferric oxide, medium content of impurities	70%	65%	60%
7. Spray roasted ferric oxide, little impurities (~200 ppm SiO_2)	10%	20%	30%
Subtotal 5-7 (MTPY)	275,000	330,000	3 37,000
8. * Sulfate processed medium impurity	*16%	*16%	*16%
9. * Sulfate processed little impurities	*80%	*80%	*80%
10. *Carbonyl	*4%	*4%	*4%
* Subtotal 8- 10 (MTPY)	21,000	27,500	;6,000

From Table 1.2 one can infer that in the coming years ferrite industry has to depend mainly on upgraded hematite ore and spray roasted ferric oxide for meeting the ever expanding ferrite industries requirement of the raw material. Ferrite industry itself is expected to increase its production to 974,000 metric tonnes per year (MTPY), by the turn of this century. And, the iron oxide required for such production is ~ 705,000 MTPY.

Indian ferrite production

Indian contribution in the world ferrite production (Table 1.3) [24] is insignificant. Comparing the world leaders in ferrite manufacturers from Table 1.3, India lags behind many developed and developing countries, as shown below.

Although, India is one amongst very few countries to have one of the best iron oxide sources in the world, yet there are no much improvement in the ferrite production capacity in India.

USA	1,40,000 (1979)	85,000 (1989) MTPY
G. Britain	17,000	12,000
France	21,500	2,21,500
Germany	21,500	20,500
Italy	21,500	18,200
USSR	45,000	45,000
China	35,000	37,000
Japan	1,35,000	1,80,000
India	9,000	9,000

India is dependent on the import of iron oxides of ferrite grade. Infact, Indian annual demand for the iron oxide to manufacture ferrites (both soft and hard)in 1977 was ~25 metric tonnes (MT) and was met through import [25]. Year 1988 was nc better than year 1977 and the ferrite grade iron oxide import remained the same (Busines India 11-24 July 1988).

Recently, India has begun in a small way to produce ferrite grade iron oxide and a pilot plant of capacity ~ 50,000 tonnes per year is already setup (The Economics Times, Bombay, India, 27 August 1990). A plant to manufacture very high grade iron oxide required for quality ferrites manufacturer is also installed, of capacity 10,000 tonnes year ferrite grade iron oxides.

Iron oxides required for ferrites (soft and hard) are mostly spray roasted iron chloride from acid (HCl) pickling solution in steel industries (Table 1.2). This is the synthetic ferric oxide, called as spray roasted iron oxide. Natural iron oxides of magnetic origin are also used in ferrites synthesis, after upgradation and this beneficiated ore along with the upgraded hematite are also used as raw material in ferrite industry.

Table 1.3 Estimated world ferrite production for 1990 in metric tonnes per year [24]

| Country | Metric tonnes per year estimated world ferrite production 1990 | | | |
| | Hard Ferrite | | Soft Ferrite | |
	Estimate 1979-ICF3	Estimate 1989-ICF5	Estimate 1979-ICF3	Estimate 1989-ICF5
Canada	4,000	4,000	3,000	300
USA	95,000	75,000	45,000	10,000
Mexico	3,500	2,500	2,800	400
Venezuela	2,500	1,000	1,500	200
Brasil	15,000	10,000	5,000	3,000
Argentina	3,000	1,500	2,000	500
Chile	600	600	400	200
Scandinavia	1,500	100	2,000	300
G. Britain	10,000	6,000	7,500	6,000
Spain	3,000	2,500	2,000	1,000
France	13,500	13,500	8,000	8,000
Germany	12,500	12,500	9,000	8,000
Italy	20,000	18,000	1,500	200
Holland	2,500	200	3,500	500
Yugoslavia	1,600	1,600	1,000	1,000
Bulgaria	1,200	1,500	600	800
Rumania	1,500	1,500	800	800
Hungary	1,500	1,500	1,500	1,000
CSSR	3,000	2,500	2,000	2,000
Poland	4,000	2,000	3,000	1,000
GDR	16,000	12,000	8,000	7,000
USSR	30,000	30,000	15,000	15,000
Egypt	1,500	1,000	1,000	200
Algeria	1,000	1,000	1,000	200
S. Africa	1,000	1,000	500	200
China	20,000	25,000	15,000	12,000
Japan	85,000	1,40,000	50,000	40,000
India	6,000	6,000	3,000	3,000
Indonesia	2,500	2,500	1,200	1,200
Singapore	-	6,000	-	500
Thailand	-	3,000	-	-
Malaysia	-	-	-	1,000
Philippines	1,500	1,500	1,000	500
Australia	1,200	1,000	600	500
Turkey	1,000	1,000	500	100
Israel	600	800	300	200
Iran	1,500	1,000	1,000	500
S. Korea	6,000	20,000	4,000	18,000
N. Korea	2,000	500	1,500	200
Taiwan	6,000	20,000	4,000	14,000
World ferrite production	3,82,200	4,31,100	2,09,700	1,59,500

18

Both the natural iron oxides and synthetic spray roasted iron oxides have inherent impurities which hinder them to use in high tech ferrites manufacture, however, routine ferrites are made by these.

Purity of any raw material is an important criterion in the synthesis of raw material of technological importance. There is no such thing as high purity or low purity when it comes to synthesizing any ferrite of optimum intrinsic or extrinsic properties. Without any reservation one can safely say that impurity free raw materials lead to high quality end products. Then it is difficult to always adhere to such specifications. One has to make some attempt, as far as possible, to free the impurities, as it is difficult to obtain nil impurity material.

Spray-roasted iron oxide

In ferrite synthesis, natural raw material (upgraded) as well as synthetic spray roasted iron oxides are bound to have impurities. The spray roasting of acid (HCl) pickle solution of steel industry into iron oxide normally retains all additive metals that are used in the steel making in the form of their respective oxides, along with the main constituent iron oxide. The technique of spray roasting is well developed by Ruthner [26-29] and put into large scale production by different countries in the name 'Ruthner Process'. In the spray roasting the pickle solution consist of the chlorides of metals.

Spray roasting process which was earlier recognized as pyrohydrolysis process [30] had been originally used to completely regenerate hydrochloric acid from the waste pickle acids produced by the steel industry. The process then underwent considerable development and not only the acid is being regenerated effectively but also a lot emphasis is put on the oxides that are the end product of the roasting. Many ceramic oxides such as Al_2O_3, MgO, Mn_2O_3, NiO, Fe_2O_3 have been synthesized in single step using pickle solution of steel industry and acid solution of mixed metals have further given scope to

prepare mixed metal oxides and by such spray roasting technique many indu strially important ferrites, $NiFe_2O_4$, $MnFe_2O_4$, MnZn ferrite etc. have been manufactured.

In spray roasting the metal chlorides are sprayed through ceramic spray no zzle at a pressure of 3 to 5 bars ($3x10^5$ to $5x10^5$ Pa) in the upper portion of the reactor (oil or gas fired cylindrical tower furnace). The droplets produced by the nozzle finally fall at the bottom in the form of oxide particles of an average particle size between 0.10 to 0.25 μ.

Impurities in spray roasted iron oxides originate from high temperatur : steel manufacturing process. Among the most significant impurities in these oxides a e Mn, Al, Cr, Ni and Si.

Control of impurities in ferrite grade iron oxide

Both upgraded iron ores, hematite and magnetite, do retain minor imp urities, depending upon ore sources and the use of beneficiation processes. The spray i oasted iron oxide also contains impurities, as mentioned earlier. The upgradation of iron ores is a physical beneficiation process and hence depending on the mineralogy of t ie ore deposits, the techniques [31-35] of oil agglomeration, froath flotation, se ective flocculation have been adopted to considerably increase the mineral content in the c re. In one such a study [31] the flotation beneficiation of low grade hematite ore ((f M/s Sallitho iron ores limited, Goa from the Pale mines) enabled to increase the iron c ontent from 43 (%) to 68-70 (%). The Si content was decreased from 9 (%) to 1.4 (%), while aluminium could be brought down to 1.1 (%) from 13.5 (%) present in the ore. I ut the ferrite industry needs still better improvement in the major impurities: Al and Si.

The pickle solution before spray roasting can also be purified by precipital ion or coprecipitation of the impurities, by solvent extraction, by ion exchange r by crystallization. The solvent extraction or ion exchange processes allow one to obt in th

desired metal chloride (iron chloride) in the concentrated form enabling the roasting process to yield pure oxide.

A new production method using solvent extraction technique to prepare iron oxide of high purity from waste acids from pickling plants has been described [36]. The extraction of iron (III) is effected by methyl isobutyl ketone (MIBK) and the iron precipitated subsequently from ammonia on heating yielded iron oxide of impurities (in ppm): Mn – 10, SiO_2 – 16, CaO – 10, Al_2O_3 – 10 and Cr – 10.

Use of γ-Fe_2O_3 in ferrite synthesis

In ferrites synthesis the iron oxide obtained, whether it is from spray roasted (Table 1.2) technique or sulphate processed method, is of alpha form, α-Fe_2O , with corundum structure having hexagonal close packing (hcp) of oxide ions. And Fe^{3+} ions occupy the octahedral sites of the hcp arrangement. The upgraded magnetite, on the other hand, is the magnetic oxide of iron, Fe_3O_4, the ferrouso-ferric oxide, $FeO.Fe_2O_3$, which has spinel structure. In the cubic close packed (ccp) arrangement of oxide ions of Fe_3O_4, the Fe^{2+} occupy the octahedral sites and the Fe^{3+} ions get accommodated on both tetrahedral and octahedral sites.

Sluggish reaction between α-Fe_2O_3 + MO

The method used in the most of the ferrite industries is a conventional ceramic technique which requires very high temperature to complete usually the sluggish solid-solid reactions. The raw materials iron oxide and oxides of divalent metals (or carbonates, nitrates, hydroxides of M^{2+}) are ground and heated to high temperatures.

The reaction between Fe_2O_3 and MO is sluggish. Causes for the sluggishness are many and one important factor for such delayed formation of a product can be considered based on the structure of the reactants and the product. The divalent oxides, MO, say

NiO, MnO, c. are cubic with rock salt structure while Fe_2O_3 (α-Fe_2O_3) is rhombohedral of hexagonal close packing. The product is MFe_2O_4, a spinel of ccp. Therefore, the main raw material α-Fe_2O_3 of corundum structure has to rearrange itself to react with cubic MO to form cubic spinel.

It is considered [37] that first α-Fe_2O_3 transforms at high temperatures into cubic spinel Fe_3O_4 as shown in equations 1 and 2. According to Richards and White [38] pure Fe_2O_3 dissociates into Fe_3O_4 evolving oxygen at $1385^{\circ}C$. But, in the presence of the other metal oxides like MgO, the dissociation occurs at lower temperature. The spinel Fe_3O_4 formation from α-Fe_2O_3 through a cation vacancy intermediate is dependent on

$$4 \, Fe_2O_{3 \, (rh)} \longrightarrow 3 \, Fe^{3+}{}_{8/3} \, \square_{1/3} \, O_4 \, {}_{(sp)} \longrightarrow 8/3 \, Fe^{2+}Fe_2{}^{3+}O_4 + O_2 \uparrow$$
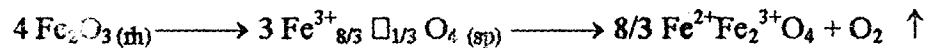
temperature and oxygen partial pressure as the cation vacancies decrease with the increase in temperature and the decrease in atmospheric oxygen.

At this high temperature the cubic spinel Fe_3O_4 formed easily reacts with the cubic MO present in the vicinity, thereby, completing the ferrite formation.

Upgraded magnetite if used, therefore, is expected to give easily ferrites, may be at lower temperature than the upgraded hematite when used, in ferrites synthesis. Natural magnetite Fe_3O_4 has been used [39] to make the high quality ferrite magnets and the large reserves of this mineral in Vietnam is being successfully exploited in ferrite synthesis. In the synthesis of barium ferrite from natural Fe_3O_4 and barium carbonate, the magnetite undergoes its usual phase transition from Fe_3O_4 to Fe_2O_3 in the heating process and the reactive Fe_2O_3 that formed now reacts with the reactive BaO that also formed *in situ* by the thermal decomposition of the carbonate. Thus, reactive Fe_2O_3 and BaO immediately form ferrite. Hence, it is considered that the ferritization is occurred well and even finished sooner when Fe_3O_4 is used [40] as a raw material than using the chemical oxide Fe_2O_3.

A systematic study is being done [41] to evaluate the processes of the formation of nickel ferrite $NiFe_2O_4$ from hematite, magnetite and magnetite like spinel iron sand found on the west coast of the North Island of New Zealand. From Differential thermal analysis (DTA) and evolved gas analysis (EGA) carried out on the reactants (and NiO) and their mixtures in different atmospheres, it was found that magnetite like iron sand, prior to their reaction with NiO, undergoes oxidation reaction $\sim220^{\circ}C$, while no such oxidation process is observed with hematite + NiO mixture. And, high reactivity found in magnetite + NiO and iron sand + NiO was attributed to the formation of reactive hematite *in situ* in the oxidation of the magnetite $\sim220^{\circ}$, which immediately reacts with the NiO, yielding $NiFe_2O_4$.

Mechanism of the solid state reactions

It is generally considered that the sluggish solid state reaction can be made reactive by rendering the reactants active. This can be done by increasing the surface area of the reactants by grinding them to the finer size or the best way is to use the starting material not in oxide form, but in the easily decomposable compound form, say carbonates, hydroxides. During the heat treatment these decompose to give oxides with particles showing high surface area and surface energy. On the basis of a considerable amount of experimental work Gregg [42] has postulated some general rules which can be applied in most of the cases where an active solid is prepared by the thermal decomposition of the precursors of any oxide. Therefore, the Fe_2O_3 formed from its precursors, Fe_3O_4, is reactive and such particles of Fe_2O_3 then interact with NiO to yield easily $NiFe_2O_4$. If NiO is also made to form *in situ*, by choosing a conventional precursor of it, say $NiCO_3$, then the formed NiO is active and reacts more easily with the active Fe_2O_3 formed from Fe_3O_4. Finally the spinelization takes place effectively, may be at lower temperature.

23

The formation of any product in solid state reaction involves two stages which are usually identified as,

i. Nucleation of the product

ii. Subsequent growth of the product.

Nucleation is facilitated if there is a structural similarity between the product and one or both of the reactants because this reduces the amount of energy required for structural reorganization that is necessary for the nucleation to occur. In the reaction of cubic MgO and hexagonal close packed Al_2O_3 to form $MgAl_2O_4$, for instance, the spinel product has a similar oxide ion arrangement to that in MgO. Spinel nuclei may therefore form at or on the surface of the MgO crystals such that the oxide arrangement is essentially continuous across the MgO-spinel interface,

$MgAl_2O_4$
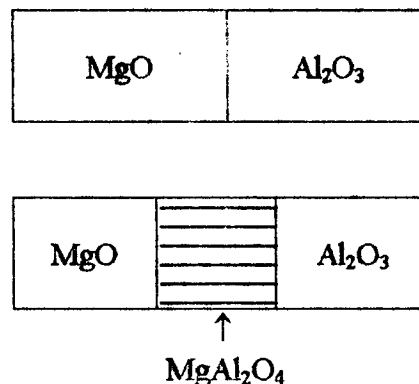
The nucleation product, spinel phase, makes use of a matching or partially matching of its own structure to that of existing phase, MgO, in the reaction mixture and the nucleation step is easier as a consequence.

High temperature makes possible this nucleation process easy because the heat helps the structural recognisation involving breaking up and reformation of bond by allowing the atoms to migrate (perhaps over considerable distance on an atomic scale).

The nucleation of the product phase thus leads to the growth of the product layer. Counter diffusion of Mg^{2+} and Al^{3+} through the product layer enables these ions to reach reaction interfaces.

In essence, the solid state reaction is an involved process wherein the crystal structure of the reactants and products, surface area or reactivity of the reactants, heat energy, breaking and forming of bonds, diffusion (or counter diffusion) of ions are all need to be understood.

However, high temperatures are usually adopted in ensuring the completion of the solid state reaction to form solid product, but, the solid product formed may not have an adequate stoichiometric composition as desired to obtain a uniform single phase spinel. Single phase products are difficult to achieve as there is every possibility of variation in the constitution elements concentration, say Mg rich phase of $MgAl_2O_4$ on MgO side and Mg deficient phase on the Al_2O_3 side are usually attained. This is due to the fact that the product of MgO + Al_2O_3 varies from $MgAl_2O_4$ to $Mg_{0.75}Al_{2.8}O_4$. And, therefore to achieve a single phase product further complications are encountered.

Rate of Reaction

Thus, in the solid state technique many factors are to be considered to achieve the desired product. The important factors that influence the rate of reaction between solids are i) the area of contact between the reacting solids and hence their surface areas ii) the rate of diffusion of ions through the various phases iii) the rate of nucleation of the product phases. The area of contact between the reactants can be increased by increasing the surface area. Grinding of the reactants into fine powder makes surface area high. But, very important factor is the structural aspects; at least one of the reactants should have similarity in the structure with the product to be formed. If both the reactants are chosen having similar structure with that of the product, then the rate of reaction can be further enhanced.

In Ni and barium ferrites synthesis Hunh [44] used iron oxide consisting of a large percentage of gamma ferric oxide, γ-Fe_2O_3, instead of the usual raw material alpha

ferric oxide, α-Fe_2O_3. And, it was observed that the rate of reaction is enhanced and ferrites occurred at lower temperatures than that indicated by using α-Fe_2O_3 as a starting material in the ferrite synthesis. In nickel-zinc ferrite preparation it has been noticed [45] that the magnetic performance parameter and resistivity values increased when cubic spinel γ-Fe_2O_3 is used as a starting material instead of α-Fe_2O_3. Although no explanations are given for such enhanced reaction rate between the reactants in zinc and barium ferrites formation, reason for the improved behaviour of γ-Fe_2O_3 as a starting material becomes quite obvious by considering different factors that influence the solid state reaction, as described in previous paragraphs, especially, the structural aspects may be considered as a main factor in influencing the solid state reactions, because high temperatures take care of all other factors if reactive reactants are used.

As it was mentioned, the nucleation of the reaction product is facilitated if there is a structural similarity between the product and one or both of the reactants, because this reduces the amount of energy that required for structural reorganisation that is necessary for the nucleation to occur. α-Fe_2O_3 is rhombohedral with hexagonal close packed oxide ions arrangement is not similar in structure with cubic close packed spinel product, although MO (the divalent metal oxide used in ferrites synthesis) may or may not be cubic, say NiO and MnO are cubic. Instead of α-Fe_2O_3 if cubic γ-Fe_2O_3 (vacancy ordered spinel) is used in the ferrite synthesis, say $NiFe_2O_4$, then both the reactants are now in cubic form (γ-Fe_2O_3 and NiO) which are similar in structure to that of the product spinel. And, hence, the rate of reaction is expected to be enhanced in the ferrite preparation when γ-Fe_2O_3 is used instead of α-Fe_2O_3, as a starting material.

It may be argued similarly as above the enhancement of reaction rate and improvement of ferrite character when magnetite is used as a starting material [39 41] in ferrite synthesis. Here Fe_3O_4 and NiO both are cubic so also their product $NiFe_2O$ [41].

The structural similarities, thus, influence the rate of reaction. However, although the starting material is Fe_3O_4, there is a phase transition to Fe_2O_3 is observed which is hexagonal close packed one. But, then, the formed oxide is reactive and thereby increases its activity with the NiO.

The phase transformation of Fe_3O_4 to Fe_2O_3 (α-Fe_2O_3) may also be considered to be through γ-Fe_2O_3 as,

$$(Fe^{3+})[Fe^{2+}Fe^{3+}]O_4 \longrightarrow (Fe^{3+})[Fe^{3+}_{5/3}\square_{1/3}]O_4 \longrightarrow Fe_2O_3 \quad \text{------------ (5)}$$

$$Fe_3O_4 \qquad\qquad \gamma\text{-}Fe_2O_3 \qquad\qquad \alpha\text{-}Fe_2O_3$$
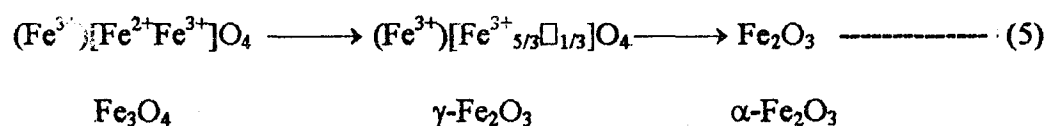
Hence, when magnetite is used as a starting material in ferrite synthesis, say $NiFe_2O_4$, the reaction of cubic Fe_3O_4 with cubic NiO, no doubt, is increased but further enhancement in the rate occurs as Fe_3O_4 transforms not only into yet another cubic form, γ-Fe_2O_3 but also a much more reactive oxide, γ-Fe_2O_3, as it is formed *in situ*. Thus, Fe_3O_4 and γ-Fe_2O_3 are found to be better starting materials in ferrite synthesis.

Since the preparation of ferrites by solid state technique is normally carried out in air with α-Fe_2O_3 as the starting material, little is known of the reaction or the properties of the products obtained using magnetite or γ-Fe_2O_3 when used as a raw material. In literature few studies are being made [39-41, 46] about such synthesis using γ-Fe_2O_3 and Fe_3O_4, however, nothing beyond that is explained excepting a statement that the phase transformation of Fe_3O_4 to hematite, α-Fe_2O_3, during heat process may be reactive and hence the reaction is speeded up giving ferrites well and even at lower temperatures

Other than structural aspects that are being considered in the easy formation of spinel product, when one or both the reactants have similar structures to that of the nucleating product, there appears to be no very apt explanations for such enhanced rate of reaction that take place when γ-Fe_2O_3 and Fe_3O_4 are used as a starting material instead of α-Fe_2O_3.

Aim of the present studies

Solid state reactions between hematite, α-Fe_2O_3, the usual starting material in ferrite synthesis and metal oxides leading to normal, inverse and random spinels of academic and industrial interest have been widely studied. However, a literature survey indicates that ferrites of better characteristics can be obtained by using magnetic iron oxides, magnetite (Fe_3O_4) and maghemite (γ-Fe_2O_3) instead of α-Fe_2O_3 as a starting material.

Since, literature is quite exhaustive about the preparation, characterization and correlation of electromagnetic properties of ferrites with their structural and microstructural aspects which depends on their preparative conditions and nature of starting materials, the studies of ferrites using α-Fe_2O_3 as a starting material do not require any further exploration. But, the investigation on ferrites prepared from γ-Fe_2O_3 / Fe_3O_4 need some attention of researchers to get to know whether ferrites can be produced with still better electromagnetic characteristics than those observed from ferrites obtained from routine raw materials, α-Fe_2O_3. And, we are aiming at this aspect of knowing how far the magnetic spinel iron oxide, γ-Fe_2O_3, is superior in their behaviour to α-Fe_2O_3 in yielding ferrites of better characteristics and that too at lower temperatures. A systematic study is, therefore, planned and the results of such investigations are presented in this thesis. These studies are not only aimed at knowing the superiority if at all of γ-Fe_2O_3 (or Fe_3O_4) in ferrites synthesis but also to see whether the knowledge thus acquired can be made applicable.

Scope

A preliminary studies done in our labe [46-47] with γ-Fe_2O_3 and $MgCO_3$ as starting materials indicates a single ph $MgFe_2O_4$ formation ~1000°C, while

α-Fe$_2$O$_3$ (hematite) + MgCO$_3$ at that temperature showed a mixture of MgFe$_2$O$_4$ (mainly) and α-Fe$_2$O$_3$ suggests that an incomplete reaction has taken place between hematite and the carbonate. The MgFe$_2$O$_4$ obtained from α-Fe$_2$O$_3$ showed many properties different from that of the ferrite synthesized from γ-Fe$_2$O$_3$. A variation in some properties are attributed not only to the non completion of the ferrite phase but also to non uniform particle size distribution in the ferrite prepared from α-Fe$_2$O$_3$. Although, the variation in properties could not be considered due to the only difference in the nature of reactants involved, but also to inadequate temperature adopted for the synthesis. Hence, many other different aspects are required to be ascertained. Only important outcome of these preliminary studies is that the γ-Fe$_2$O$_3$ and mixture of γ-Fe$_2$O$_3$ + α-Fe$_2$O$_3$ obtained from different sources gave ferrites of almost identical results which were distinctly different from the ferrite prepared from commercial α-Fe$_2$O$_3$. Though results in these studies could not give any inference, the ferrite synthesized from γ-Fe$_2$O$_3$ seemed to be formed ~1000°C, whereas, higher than this temperature is needed to achieve single phase ferrite from α-Fe$_2$O$_3$. But, most important results of these studies is that γ-Fe$_2$O$_3$ useful in ferrite synthesis could be prepared easily from iron ore rejects from chemical beneficiation route using hydrazine method to prepare easily decomposable precursors from acid extract of the ores.

Iron ore rejects are the main iron oxide sources for the synthesis of ferrites in our current research activities. From Table 1.3 it is seen that Indian contribution in the world ferrite production is insignificant. Considering the significant projected world ferrites production, by the turn of this century (Table 1.1), India can play an important role in world ferrites market as upgraded hematite (Table 1.2) expected to meet the huge iron oxide requirement needed for the manufacture of the ferrites (both soft and hard). This is due to the fact that India has rich iron ore reserves [43] of about 15265 million tonnes

29

(mt) which will last for another 250 years with the present rate of mining of ~ 60 mt per year. And Goa, a tiny state of India, was blessed with such rich iron source. But, because of rampant high grade iron ore exports, since 1950, amounting to about 300 mt, Goa now has an estimated researves of ~ 400 mt which is expected to last another 20 – 25 years with the present rate of production of 15 – 17 mt per year.

Iron ore mining industry in Goa is mostly export oriented. Considering the high grade iron of > 58 (%) Fe export (A and B in Table 2.1) for the last 50 years, a low grade (< 50 (%) Fe) iron ores are piling up as rejects – a national waste. In Goa, there is an estimate of > 900 mt of low grade iron ore rejects and tailing that are being dumped around mining areas which create environmental problems. And tapping of such low grade iron ore rejects to make useful in preparing iron oxide through chemical method is our objective. If we economically exploit the iron ore rejects and synthesize iron oxide useful in ferrites synthesis, we may look forward to be a leader in ferrites market, in future. And, this may be the reason why in his keynote address, Dr. B. B. Ghate (Bell Lab, USA) during the 5th International Conference on Ferrites (ICF – 5, Bombay, India, 1989) made it clear [48] that "there was ample opportunity for entrepreneurs, scientists and technologists trained in ferrites and related disciplines to contribute to the economic growth in India and to the world ferrite market". Prof. P. S. Deodhar (chairman, ICF – 5) in his inaugural address also made similar emphasis.

Any possible use of waste enhances the economic development. Our endeavour is therefore, lies in making use of iron ore reject in preparing active iron oxide for synthesizing ferrites.

Having done elaborate work in our laboratories to easily synthesize γ-Fe_2O from iron rejects, it was felt that some more systematic investigations are needed to chemically beneficiate iron ores to finally obtain γ-Fe_2O_3 economically useful in ferrite synthesis.

Objectives / Methodology

Aft.. aiming at the synthesis of ferrites from γ-Fe_2O_3 and considering the sc ope of the present work, it is natural to have objectives in our mind before actually planni ıg our research and adopting a methodology to successfully fulfill our aim.

The object' ;s are as under,

- Sampling of the ore rejects and choosing of a representative sample.

- Determination of the main impurity constituents of iron ore rejects and the chemi :ally beneficiated ore sample.

- Synthesizing α-Fe_2O_3 and γ-Fe_2O_3 from the ore.

- Using α-Fe_2O_3 and γ-Fe_2O_3 in the synthesis of ferrites, Mg ferrite and MnZn ferri te and comparing their characteristics with the ferrites that obtained from commercial α Fe_2O_3 (hematite) and a standard γ-Fe_2O_3 (maghemite).

- Studying the ferrite synthesis thoroughly, especially, MnZn ferrite whose prepara ion procedur .equires knowledge of exact atmospheric and thermal control.

- Investigating structural aspects of γ-Fe_2O_3 and look for their role in ferrite format on.

Organisation of the thesis

Chapter 1 General Introduction

An exhaustive literature survey made is used to introduce the subject matter of the thesis. Here it has been highlightened that India is insignificant in the world ferrite market, although it has one of the best iron sources in the world. Since the technoі ogical demand for ferrites (both soft and hard) is going to be increased considerably, India can play an important role in tapping its natural iron resources. Among various iron oxide sources like spray roasted iron oxide from acid pickle solution of steel industry, it is going

to be upgraded hematite ore which would meet major iron oxide requirement for ever increasing ferrite industry. And, hence India can look forward for such sources.

Importance of magnetic oxides, Fe_3O_4 (magnetite) and $\gamma\text{-}Fe_2O_3$ (maghemite) in ferrite synthesis in preference to usual starting material, hematite, $\alpha\text{-}Fe_2O_3$ has been sketched in this chapter. Therefore, upgradation of hematite ore, no doubt eases the iron oxide demand for ferrites industry but if $\gamma\text{-}Fe_2O_3$ could be prepared directly from ore, after chemical beneficiation, then one can effectively use this oxide for high tech ferrite preparation of better quality. To realise this importance of $\gamma\text{-}Fe_2O_3$ in the synthesis of ferrites, two known ferrites systems, magnesium ferrite $MgFe_2O_4$ and manganese zinc ferrite, $Mn_{1/2}Zn_{1/2}Fe_2O_4$ have been introduced.

Chapter 2 Chemical beneficiation of iron ore rejects

Although physically upgraded hematite ore is useful in ferrite synthesis, the ferrites may have impurities that are inherent in the ore. A chemical beneficiation resorts to acid treatment and hence pure iron oxide can be obtained by adopting suitable precipitation and heat treatment techniques. This is a energy consuming process. Hence, ferrite industry goes for spray roasted iron oxide from easily available acid pickle solution of steel industry. The iron oxide, $\alpha\text{-}Fe_2O_3$, may contain impurities depending on steel variety. Since $\gamma\text{-}Fe_2O_3$ is found to be superior to $\alpha\text{-}Fe_2O_3$ in ferrite synthesis, one can find out an easy method to directly prepare $\gamma\text{-}Fe_2O_3$ from acid pickle solution or acid leached ore. And when iron ore (of any grade now) can thus be used for the preparation of $\gamma\text{-}Fe_2O_3$ the energy burden in leaching can be profitably lessened if $\gamma\text{-}Fe_2O_3$ gives better ferrites than $\alpha\text{-}Fe_2O_3$ and that too at lower temperature.

Chapter 3 Preparation and characterization of iron oxides from iron hydroxides, iron formates and their hydrazinated complexes

32

The iron hydroxides and formates obtained from iron ore rejects as described in chapter 2 are utilised to synthesize iron oxides. Both iron hydroxides and iron formates are then hydrazinated. These precursors and their thermal end products are characterized.

Chapter 4 Studies on the magnesium ferrite and manganese zinc ferrites

The iron oxides, α-Fe_2O_3 and γ-Fe_2O_3 synthesized from iron ore rejects are made use as starting materials to synthesize magnesium ferrite and manganese zinc ferrites. The important properties of the ferrites are then compared with the characteristics of the ferrites that prepared from commercial hematite, α-Fe_2O_3 and standard gamma ferric oxide, γ-Fe_2O_3. The chapter is divided into three parts:

Part I: Microstructure and property correlation of $MgFe_2O_4$ (ore rejects [46])

Part II: Synthesis and characterization of $MgFe_2O_4$ (study sample I)

Part III: Synthesis and characterization of $Mn_{\frac{1}{2}}Zn_{\frac{1}{2}}Fe_2O_4$ (study sample II)

Chapter 5 Structural aspects of γ-Fe_2O_3: Hydrogen iron oxide or hydrogen ferrite

Ferrites prepared from γ-Fe_2O_3 seem to show superior characteristics to those synthesized from α-Fe_2O_3. Hence, it may be attributed to the structural aspect as α-Fe_2O_3 is different from that of γ-Fe_2O_3. The hexagonal close packed arrangement of oxide ions accommodate Fe^{3+} in their octahedral sites in the corundum structure of α-Fe_2O_3 which then reacts with MgO/MnO + ZnO which are cubic in nature giving cubic spinel. On the other hand, cubic spinel γ-Fe_2O_3 (vacancy ordered) reacts with MgO/MnO + ZnO giving cubic ferrite spinel. The cubic spinel γ-Fe_2O_3 and the other reactants which are also cubic find no difficulty in nucleating cubic ferrite phase, whereas corundum structured α-Fe_2O_3 may require an extra energy to break and form bonds.

The cubic spinel γ-Fe_2O_3 is not only similar in structure to that of nucleating

ferrites but it has vacancies in its unit cell, mainly on octahedral sites and these vacancies may help easy diffusion of cations which is indeed needed in solid state reaction to occur. Hence, a detailed structural aspects of γ-Fe$_2$O$_3$ is being studied and their results are compiled in the chapter.

Chapter 6   Conclusion

Chemical beneficiation of Iron ore rejects

2.1 Introduction

Demand for ferrites in ever expanding electronic industries is expected [24] to reach 974,000 metric tones per year (MPTY), by the turn of this century, and to meet this requirement the need of high quality ferrite grade iron oxide will also increase. About 705,000 MTPY of the iron oxide is required for the production of such a huge amount of ferrites, both soft and hard. Iron oxide is the major raw material in ferrite industry.

At present this need of iron oxide is normally met (Table 1.2) by using I) spray roasted ferric oxide from acid pickle solution of steel industry, ii) sulphate processed iron oxide, iii) fluidized bed regenerated processed iron oxide, iv) upgraded hematite ore and to some extent v) upgraded magnetite ore. It is the upgraded hematite ore which is, however, expected to play an important role in ferrite industry as a major raw material. All these sources supply iron in α-Fe_2O_3 form, excepting upgraded magnetite.

Although the spray roasted ferric oxide is widely used world over, the quality (or the impurity contents) of the iron oxide depends on the metal constituents of steel from which the pickle solution is obtained. However, depending upon the application of ferrites, low, medium and high impurity content iron oxides are prepared by further purifying the pickle solution before spray roasting. The purification of the pickle solution is carried out by chemical methods like precipitation or coprecipitation, solvent extraction, ion exchange or crystallization. A solvent extraction method [36] using methyl isobutyl ketone (MIBK) yields iron oxide of high purity consisting of impurities in ppm level. Direct use of spray roasted iron oxide from any pickle solution is therefore, restricted, if high quality ferrites are to be manufactured.

The upgraded hematites too are not useful for quality soft ferrites manufacture, although ceramic magnets can be synthesized from them. Again chemical methods are required to be adopted to obtain high quality iron oxide.

Ferrite industries in china use iron oxide synthesized from ferrous sulphate [49] but spray roasted iron oxides are also now available.

Chemical routes are being adopted to prepare iron oxides of better quality and such methods are now used to tap different iron sources which were until then considered as useless, especially the industrial effluents from iron / steel industries. A sol gel technique has been described [50].

Mine drainages, the other sources of iron which had been neglected so far, are now being effectively treated with $CaCO_3$ in Japan [51] to prepare ferrites directly. Infact, water base magnetic fluids have been prepared using this method. Magnetic fluids consisting of ultrafine Fe_3O_4 obtained by precipitation technique [52] find wide applications.

A modified ferrite process was developed [53] for the purpose of treating acid mine and mine drainages consisting of steps involving coprecipitation coupled with setting,

36

decantation and oxidative ageing followed by magnetic separation.

An improved recrystallization technology is proposed for pickle solution [54] to prepare pure iron oxide free from Ni and P to use in MnZn ferrites synthesis. New ferrite process has been adopted [55] in Korea to remove heavy metal ions from waste water.

Abandoned mines, after mining activities are terminated, create environmental problems, especially due to the accumulation of water in it which are acidic in nature. They are called as acid lakes. Lime treatment is usually adopted for portable or agricultural use. Lime treatment creates problem as the sludge obtained in the process is packed with many heavy toxic elements. Therefore, a novel method has been tried [56] by Canadian scientists to not only neutralise the water but also extract the heavy metals as ferrites. Sodium hydroxide is being used by these authors but the alkali being expensive they argue that such method would still be economically viable, considering very useful ferrites that are being processed easily, as well as, the water is made usable.

Chemical methods, thus, seem extensively used to obtain iron oxides of high quality and such methods have now opened up new iron sources, hitherto considered useless, like mine drainage etc. Chemical routes can also be made use in tapping yet another iron oxide sources which are going not only as a national waste but also creating environmental problems. They are iron ore rejects. And we are making an attempt to make use of such rejects in our present studies to prepare iron oxides through a chemical route.

2.2 Physico-chemical analysis of the ore rejects and preparation of study sample

2.2.1 Collection of ore samples

The iron ores of Goa are feebly magnetic attributing to the presence of FeO in addition to its basic major constituent Fe_2O_3. The Goan lumpy ore is soft and porous. A

typical chemical composition of lumpy ore of commercial importance is indicated in Table

2.1 shown below.

Table 2.1 Typical chemical composition of commercial iron ore

Analyte (%) Identification	Total Fe	Fe_2O_3	SiO_2	Al_2O_3
A	58.2	82.72	1.86	8.18
B	58.9	83.72	3.10	7.72
C	48.7	69.14	5.72	13.94

The silica and alumina contents vary from place to place and the present acceptable

combination is between 5 and 6 (%) maximum. Iron ores that are exported from Goa are

graded depending upon the Fe content as,

Fe (%)	Grade
54 - 57	Low
58 - 60	Medium
> 60	High

The typical ore reject sample 'C' in Table 2.1 above is of our interest which consist of >10

(%) Al_2O_3 and > 5 (%) SiO_2.

2.2.2 Iron ore rejects

Iron ore rejects from different places in Goan mining areas have been collected.

They were mixed thoroughly separately depending upon the area of collection, reduced by

cone and quartering method and the representative composite samples were prepared. In

all seven samples were taken for our studies and they are named as RPD-1 to RPD-7.

The samples thus prepared were jaw and roller crushed. These were then pulverised to obtain a fine powder to the extent of −100 # size. The seven samples were then confirmed to be homogeneous by rubber sheet mixing which were then analysed separately for the presence of various major and minor or trace (rare) element constituents.

a) Chemical analysis of ore samples

Iron ore samples were analysed for estimating the chemical constituents, both major and minor or trace elements, using standard methods [57-61].

i. Estimation of major elements:

Total iron

The estimation of total iron was carried out by a standard potassium dichromate method. The 0.5 g of the sample was dissolved in 50 (%) HCl and then reduced to ferrous state with minimum quantity stannous chloride solution. The excess $SnCl_2$ was removed by adding mercuric chloride solution. To this 10 ml of acid mixture (HNO_3+H_2SO) was added followed by 3-4 drops of 1 (%) solution of barium diphenylamine indicator and titrated against standard potassium dichromate solution. The colour of the solution changes from green to blue green and finally to intense purple or blue violet indicating the end point. The titre reading directly gives the total Fe (%) present in the sample.

Silica

The percentage of silica in the sample was estimated by gravimetric method. 2.5 g of the sample was decomposed with 50 (%) hydrochloric acid. The solution was then heated to dryness and extracted with dil.HCl containing about 2.5 ml of conc. HNO_2 The solution was filtered through Whatman no.1 filter paper and the residue was washed with

hot water, several times. The dry residue was charred in a platinum crucible and then weighed. After weighing, the ash was moistened by adding few drops of water followed by a drop or two of conc. H_2SO_4 and about 7 - 10 ml of 30 (%) hydrofluoric acid and kept on a sand bath. After evaporating silica as silicon fluoride the crucible was heated first on a low bunsen flame and then on a high flame to expel out the final traces of silicon fluoride. The crucible was then weighed and from the difference between the two weights, the silica percentage was calculated.

Alumina

Alumina estimation was carried out using complexometric method. 0.2 g of the sample was dissolved in 20 ml of 50 (%) HCl on a hot plate. To the cooled solution 25 (%) NaOH was added to precipitate iron as iron hydroxide.

The filtrate was acidified with dilute hydrochloric acid and the pH was maintained at about 2.8 to 3.2 by adding ammonium acetate solution. 20 ml of 1 (%) sulphos licylic acid was then added to identify any traces of Fe, which is indicated by the appearance of reddish colour to the solution. This final traces of Fe were removed by titrating the cold solution with the standard EDTA solution till colourless.

This solution was then boiled and 4 - 5 drops of copper pan indicator was added and titrated the hot solution against the standard EDTA till the colour changes from pink to permanent yellow. The completion of the end point was confirmed by further heating and adding one or two drops of the indicator followed by adding little ammonium acetate solution.

Manganous oxide

Manganous oxide is estimated by sodium arsenate method. 0.1 g of the sample was

dissolved in 10 ml of 50 (%) HCl and evaporated to dryness. Few drops of H_2SO_4 were then added into the dried mass and continued heating till all the chloride fumes were driven out.

After cooling, little water was added to the white mass. To this solution the 15 ml of dilute HNO_3, 10 ml of $AgNO_3$ and 15 ml of $K_2S_2O_8$ solution were added. The solution was warmed slightly till a pink colouration due to permanganic acid was formed. After cooling 1 - 2 ml of 2 (%) NaCl solution was added and then titrated against the standard sodium arsenate till the pink colour disappears leaving behind whitish straw colour.

ii) Determination of minor elements and trace (rare) elements

Estimation of minor or trace rare chemical constituents in the iron ores have been done complexometrically, colorimetrically, flame photometrically, alkalimetrically, volumetrically and gravimetrically using standard methods [57 – 61].

iii) Loss on Ignition

Dry sample of ore was weighed in a platinum / silica crucible and subjected to heat treatment on a burner flame at about $1050^{\circ}C$ for about 45 minutes to determine the loss on ignition from weight difference.

b) Preparation of study samples

The detailed major chemical constituents that present in RPD 1–7 are tabulated in Table 2.2a. The RPD-7 and RPD-4 were selected as study sample I and II, respectively. These study samples were then subjected for further analysis for determining minor elements and trace rare elements. The results are tabulated in Table 2.2a and 2.2b.

Table 2.2 a   Chemical analysis of various iron ore rejects (major elements)

Analyte Sample No.	Fe	FeO	Fe_2O_3	SiO_2	Al_2O_3	MnO	LOI	Other trace elements	Remarks (if any)
RPD/1	53.2	0.26	75.79	7.54	4.74	2.32	8.87	0.48	
RPD/2	55.2	1.28	77.51	7.76	5.70	0.90	6.44	0.41	
RPD/3	51.7	3.84	69.64	20.86	1.46	0.23	3.85	0.32	
RPD/4	53.4	Trs	76.36	5.24	6.41	3.04	7.62	1.33	Study sample II
RPD/5	25.4	0.13	36.18	30.79	15.61	7.36	9.25	0.68	
RPD/6	19.0	Trs	27.17	48.75	12.31	0.60	10.81	0.36	
RPD/7	41.0	1.02	57.49	23.33	9.15	0.83	7.83	0.35	Study sample I

The study sample I and II were so chosen that the sample I contains the ow Fe content and higher percentage of alumina and silica, while the sample II has higher percentage of Fe and lower percentage of alumina and silica.

No traces of rare elements were observed in both the study samples and the minor elements are also found to be nil or in traces. Titanium oxide is, however, found to be 0.535 ± 0.115 (%). The presence of phosphorus and sulphur too indicated but ir minor quantities.

2.3 Chemical beneficiation of study samples I & II: Preparation of metal (iron) hydroxides / formates

2.3.1 Acid Extraction

About 10 g of finely pulverised study sample was taken for the acid extraction (Flow sheet 1) of iron in each batch. A dilute HCl (1:1) was added to the ore sample in a

Table 2.2 b Trace (minor/rare) elemental analysis of the study samples and the hydroxides / formates precursors

Elements (%)	Study Sample I					Study Sample II		
				Using MIBK				
	RPD/ 7	FH/NaOH	FF/NaOH	FH/MIBK	FF/MIBK	RPD/ 4	FH-II/NaOH	FF-II/NaOH
Titanium dioxide	0.42	0.05	Traces	Traces	Nil	0.65	0.09	Traces
Calcium oxide	Traces	Nil	Nil	Nil	Nil	Traces	Nil	Nil
Magnesium oxide	Traces	Nil	Nil	Nil	Nil	Traces	Nil	Nil
Lead	Traces	Nil	Nil	Nil	Nil	Traces	Nil	Nil
Copper	Traces	Nil	Nil	Nil	Nil	Traces	Nil	Nil
Zinc	Traces	Nil	Nil	Nil	Nil	Traces	Nil	Nil
Arsenic	Nil	Nil	Nil	Nil	Nil	Nil	Nil	Nil
Chromium	Nil	Nil	Nil	Nil	Nil	Nil	Nil	Nil
Antimony	Nil	Nil	Nil	Nil	Nil	Nil	Nil	Nil
Tin	Nil	Nil	Nil	Nil	Nil	Nil	Nil	Nil
Nickel	Nil	Nil	Nil	Nil	Nil	Nil	Nil	Nil
Phosphorus	0.078	Traces	Nil	Traces	Nil	0.044	Traces	Nil
Sulphur	0.006	Nil	Nil	Traces	Nil	0.006	Traces	Traces
Sodium oxide	0.024	0.020	Traces	0.08	Traces	0.012	0.010	traces
Potassium oxide	0.045	0.019	Traces	0.02	Traces	0.047	0.021	Traces

FH – Ferric hydroxide, FF – Ferric formate, MIBK – Methyl isobutyl ketone

FLOW SHEET 1

-100 # Study sample of an ore rejects
(M-oxide Fe_2O_3 / Al_2O_3 / MnO / SiO_2)

|HCl (50:50)

↓Digest on hot plate

Acid extract

↓

Residue (discard)	Filtrate I

Filtrate I

boil ↓ con. HNO_3

Filtrate II (Chlorides of metals M = Fe/Mn/Al)	Residue (discard)

↓
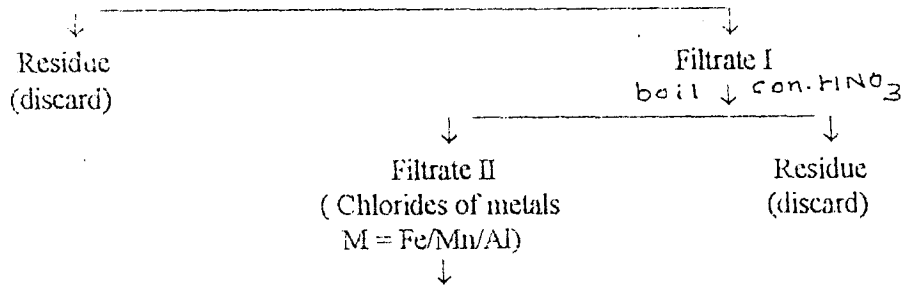
NaOH	NH₃	NaOH:NH₃ 50:50	Na₂CO₃	
↓	↓	↓	↓	Solvent
M-hydroxides	M-Hydroxides	M-hydroxides	M-Hydroxides	Extraction
｜Formic	｜Formic	｜Formic	｜Formic	MIBK
↓ Acid	↓ Acid	↓ Acid	↓ Acid	
M-formates	M-formates	M-formates	M-formates	
↓	↓	↓	↓	
Thermal products of hydroxide/ formates M-oxide	Thermal products of hydroxide/ formates M-oxide	Thermal products of hydroxide/ formates M-oxide	Thermal products of hydroxide/ formates M-oxide	

↓

Chlorides in MIBK	Aqueous layer

|Extract

↓with H_2O

Aqueous layer metal chloride	Organic layer

↓NH₃

M-hydroxide

↓

Thermal product
M-oxide

44
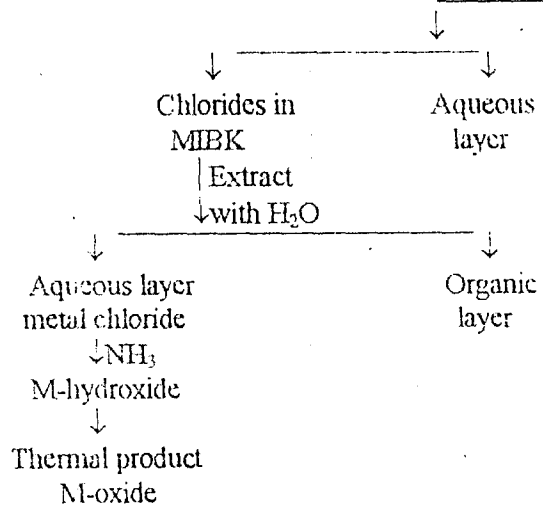
250 ml beaker and digested over a hot plate (sand bath) till the ore got completely opened up.

The cooled solution was then filtered through whatman no.1. The filtrate I (acid extract) was boiled after adding few ml of conc. HNO_3 to ensure the complete oxidation of metals. The cooled solution was filtered through whatman no.1. The filtrate I thus obtained was then used for the precipitation of metal hydroxides by,

i) Directly using precipitants like NaOH, NH_3, NaOH + NH_3, Na_2CO_3 and ii) After solvent extraction with methyl isobutyl ketone (MIBK) and then precipitating as hydroxide using NH_3.

The formates were then prepared from these metal hydroxides using formic acid.

2.3.2 Use of acid extract for metal (iron) hydroxide preparation:

a) Direct precipitation

The filtrate II obtained from acid extraction of iron ore reject as shown in Flow sheet 1, consists chlorides of metals mainly of iron and in minor quantities of manganese, aluminium and other trace metals, if any. The filtrate after adequate dilution is directly used to prepare metal hydroxides (FH) using precipitants like NaOH, NH_3, NaOH + NH_3, and Na_2CO_3.

i) NaOH Precipitant

A 25 (%) NaOH solution was added to the dilute metal chlorides solution slowly with constant stirring till the hydroxide precipitation was complete. Excess addition of the precipitant is avoided. The precipitate was digested over a hot plate, cooled and filtered through Whatman no.1. Sufficient washings with hot water were given till the filtrate is free from chloride ions. The chloride free precipitate was then dried ~ 105°C, crushed, sieved to -100 # and stored in a desiccator.

45

ii) NH₃ Precipitant

To the dilute metal chlorides (filtrate II) solution an ammonium chloride solution (2N) was added and then ammonia solution (eneral purpose reagent, GPR) was run down into it to get hydroxides precipitate. The precipitate was filtered through Whatman no.1, washed with hot water and then dried in oven ~ 105°C. The dried precipitate was crushed, sieved through -100 # sieve and stored in a desiccator.

iii) NaOH + NH₃ (50:50) Precipitant

A mixture of NaOH (25%) and ammonia solution (GPR) in 50 : 50 proportion was slowly added to the dilute metal chlorides solution till the precipitation is complete. The precipitate was filtered, washed with hot water, dried and stored in a desiccator.

iv) Na₂CO₃ Precipitant

A 15 (%) Na₂CO₃ solution was used to precipitate metal hydroxides from the metal chlorides (filtrate II) filtered, washed, dried and stored in a desiccator.

b) Preparation of metal hydroxide: After MIBK solvent extraction

The metal chlorides (filtrate II) were also used to prepare iron hydroxide of high purity adopting solvent extraction method. Methyl isobutyl ketone (MIBK) is found to be [36] very efficient solvent to selectively recover iron from the acid solution in the form of HFeCl₄. Hence, this method was utilised in our studies to see how far this procedure is superior to the direct precipitation methods in recovering iron, as discussed in 2.3.2 a. Here, the iron recovered from the filtrate II by MIBK extraction was precipitated as hydroxide using NH₃ as the precipitant to get metal hydroxides.

A diluted metal chlorides solution (Filtrate II) was taken in a separating funnel and to this an equal volume of MIBK was added and shaken well for 5 - 10 minutes. Then it

was allowed to stand for 10 minutes and the organic layer was made to remain in the funnel after draining away the lower aqueous layer. To this organic layer an equal volume of the deionised water was added and shaken well. The metal chlorides that were now in the aqueous layer was run down in a beaker and after adding NH_4Cl, an ammonia solution (GPR) was added to precipitate out the metal hydroxides. The precipitate was filtered, washed with hot water till free from chloride and dried ~ $105^{\circ}C$. The dry substance was crushed to -100 # and stored in a desiccator.

2.3.3 Preparation of Iron Formates from metal (Iron) hydroxides

The metal hydroxides prepared as in 2.3.2 (a) were then used to prepare metal formates (FF).

A calculated amount of formic acid plus 5 ml in excess was added to the required quantity of the metal hydroxide in a beaker. The beaker covered with a watch glass, placed on a water bath and the contents were intermittently agitated with a glass rod. A portion of 5 ml formic acid was added during 1½ hours heat treatment.

The syrupy contents in the beaker were then placed on sand bath carefully till a dry substance was obtained. The dried mass was then crushed in an agate mortar, sieved to -100 #, dried at $105^{\circ}C$ and preserved in a desiccator.

2.3.4 Characterization

a) Chemical Analysis: Metal estimations

The metal hydroxides and formates obtained from the ore rejects (section 2.3.2 and 2.3.3) were chemically analysed for estimating the presence of majority metals like Fe, Mn, Al, Si and trace elements as described in section 2.2.2a. The thermal products of these hydroxides and formates were also analysed for Fe contents in order to calculate the Fe_2O_3 percentage in them.

b) Thermal Analysis: Isothermal weight loss

The metal hydroxides and formates were isothermally heated at different predetermined temperatures to calculate the total weight loss leading to metal oxides.

c) X - ray diffraction studies

X-ray diffraction patterns of the thermal products of hydroxide / formate precursors were obtained by using Philips X-ray diffractometer (xrd) model PW 1710 using Cu $K\alpha$ radiations and Ni as a filter. The d_{hkl} values were matched with JCPDS fies for characterizing the oxide products.

2.3.5 Results and Discussion

a) Iron hydroxides (FH) and formates (FF): Study sample I

The chemical analysis for estimating total iron, silicon, aluminium, manganese in the hydroxides and formates done by standard methods are being given in the Table 2.3a (study sample I) and 2.3b (study sample II). The tables also include the chemical constituents present in the respective study samples from which the hydroxides and formates have been prepared.

1. Direct precipitation from acid extract (Filtrate II)

i) Using NaOH : Iron hydroxides (FH / NaOH)

The hydroxide is found to consist of 58 (%) Fe, 0.55 (%) Si, 0.228 (%) Al and 0.93 (%) Mn (Table 2.3a).

The isothermal mass loss studies indicate a total weight loss of 10.63 (%). The thermal product of the hydroxide $\sim 1050^{\circ}C$ is mainly Fe_2O_3. The x-ray characterization reveals α-Fe_2O_3 presence in the thermal product as d_{hkl} values in xrd match well with the JCPDS file [62] for α-Fe_2O_3. The chemical analysis of the thermal products suggests that

Table 2.3.a. Chemical analysis of Iron ore reject (study sample I) and precursors, Ferric hydroxides (FH) & Ferric formates (FF),

obtained using Iron chloride solution from the reject

Nature of Sample →	Study sample I	FH NaOH	FH NH$_3$	FH NaOH+NH$_3$	FH Na$_2$CO$_3$	FH/NH$_3$ MIBK	FF NaOH	FF NH$_3$	FF NaOH+NH$_3$	FF Na$_2$CO$_3$
Fe	41.00	58.00	56.00	56.50	57.00	64.20	45.76	44.33	43.62	34.10
Si (SiO$_2$)	---- (23.33)	0.55 ----	0.15 ----	0.17 ----	0.10 ----	0.08 ----	0.46 ----	0.07 ----	0.10 ----	0.04 ----
Al (Al$_2$O$_3$)	---- (9.15)	0.228 ----	2.90 ----	2.95 ----	2.64 ----	0.21 ----	0.10 ----	1.72 ----	1.63 ----	1.89 ----
Mn (MnO)	---- (0.83)	0.93 ----	0.62 ----	0.62 ----	1.05 ----	NIL ----	0.46 ----	0.38 ----	0.41 ----	0.60 ----
Total Weight Loss	----	10.63	16.32	8.52	11.80	7.46	41.06	52.00	53.00	53.12
Fe$_2$O$_3$	57.49	98.38	93.67	92.24	91.82	99.73	98.67	96.52	97.24	96.95

49

Table 2.3.b. Chemical analysis of Iron ore reject (study sample II) and precursors,

Ferric hydroxides (FH) & Ferric formates (FF), obtained using

Iron chloride solution from the reject

Nature of Sample ⟶	Study sample II	FH II NaOH	FF II NaOH
Fe	53.40	61.20	48.50
Si (SiO₂)	---- (5.24)	0.41 ----	0.30 ----
Al (Al₂O₃)	---- (6.41)	0.16 ----	0.11 ----
Mn (MnO)	---- (2.36)	2.10 ----	1.24 ----
Total Weight Loss	7.62	8.45	43.65
Fe₂O₃	76.36	96.80	97.10

it has 94.38 (%) Fe_2O_3. The remaining 1.62 (%) of metal oxides are due to the minor

constituent metals like Al, Mn, Si and other trace elements.

The oxide product, thus obtained from the ore reject, study sample I, shows an

improvement in Fe_2O_3 content from 57.49 (%) to 98.38 (%).

The total mass loss of the hydroxide amounts to 10.63(%). Since the main

constituent in the hydroxides is Fe-58 (%), a formula FeOOH is suggested to these

hydroxides consisting of the other metals of ~ 1.708 (%). The iron hydroxide on heating

yields Fe_2O by losing 10.63 (%) weight. Hence, a formula FeOOH is considered for this

hydroxide,

$$FeOOH \xrightarrow{\Delta} Fe_2O_3$$
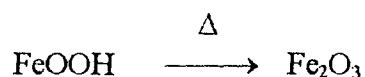
The calculated weight loss for FeOOH giving Fe_2O_3 is 10.13 (%). Since the observed

weight loss is 10.63 (%), the extra mass loss may be due to the hydroxides of the other

elements, Mn, Al, and Si converting into the respective oxides as admixture in Fe_2O_3.

ii) Using NH_3 (GPR) : (FH / NH_3)

The hydroxide obtained indicates 56.00 (%) Fe, 0.15 (%) Si, 2.9 (%) Al and 0.62 (%) Mn. A total of 16.32 (%) mass loss observed for the hydroxide is more than that of the hydroxide prepared from NaOH. Chemical analysis of the thermal product and x-ray characterization reveal it to be mainly α-Fe_2O_3. A 93.67 (%) Fe_2O_3 is found in the product.

iii) Using NaOH : NH_3 :: 50:50 (FH / NaOH + NH_3)

The elemental composition in the hydroxide is more or less similar to the one precipitation by using NH_3. The hydroxide consists of 56.5 (%) Fe, 0.17 (%) Si, 2.95 (%) Al and 0.60 (%) Mn (Table 2.3a).

The isothermal mass loss, however, indicates 8.52 (%) which is lower than in the hydroxides prepared by NaOH but much lower than that of FH / NH_3. The thermal product is characterized as α-Fe_2O_3 by x-ray diffraction (xrd). Percentage of α-Fe_2O_3 is 92.24 (%) in the thermal product suggesting the higher percentage of Al_2O_3 presence in it which gives this low percentage of Fe_2O_3.

iv) Using Na_2CO_3 : (FH / Na_2CO_3)

A 57.00 (%) Fe in the hydroxide is almost similar to that found in FH / NaOH, FH / NH_3 and FH / NaOH + NH_3 (Table 2.3a). The Si at 0.1 % is much less as compared in FH / NaOH which shows 0.55 (%), but in comparison to FH / NH_3 and FH / NaOH + NH_3 the Al content is marginally low.

The total loss observed on heating is 11.8 (%) which is near to the one found in FH / NaOH. The thermal product is mainly α-Fe_2O_3. The iron estimation of this product indicates that it consists of 91.82 (%) Fe_2O_3.

2. Hydroxides after solvent extraction (FH / MIBK)

The metal chlorides (Filtrate II; Flow sheet I) on extracting with methyl isobutyl ketone (MIBK) was precipitated as hydroxide by using ammonia (GPR). The elemental composition of this hydroxide (Table 2.3a) indicates 64.2 (%) Fe which is much higher than in the hydroxides obtained by direct precipitation methods as described in 2.3.5; (i).

The silicon content observed is just 0.08 (%) as compared to ~ 0.15 (%) in FH / NH_3, FH / NaOH + NH_3, FH / Na_2CO_3 and 0.55 (%) in FH / NaOH. Also, he Al percentage of 0.21 is very less as compared in the hydroxide prepared directly. There is no indication of Mn in the hydroxide.

Isothermal total weight loss of the hydroxide amounts to 7.46 (%) and the product is characterised by xrd as α-Fe_2O_3. The thermal product found to consist of 99.73 (%) Fe_2O_3 which suggests that the product is practically very pure excepting ~ 0.27 % oxide impurities due to Al, Si and other trace elements.

3. Formates from hydroxides prepared from study sample I

The formates of iron (FF) prepared from iron hydroxides (FH) obtained from filtrate II (acid extract of ore reject) of study sample I are analysed for metal constituents present in them. These results are presented in Table 2.3a along with the analysis of metal constituents in different FH samples for comparison. The elemental composition of the thermal products of the formates along with the products of iron hydroxides as Fe_2O_3 are also tabulated in the Table 2.3a.

i) Using FH / NaOH : Iron formate (FF / NaOH)

The iron formate (FF / NaOH) prepared from iron hydroxides (FH / NaOH) using formic acid shows 45.76 (%) Fe, 0.46 (%) Si, 0.1 (%) Al and 0.46 (%) Mn. The thermal product of this gives mainly α-Fe_2O_3 -98.67 (%) which shows an improvement in Fe_2O_3 as compared to the ore rejects containing 57.49 (%) Fe_2O_3. There are some improvements in Si – 0.46 (%) and Al – 0.1 (%) contents as compared to FH / NaOH which shows Si – 0.55 (%) and Al – 0.228 (%).

ii) Using FH / NH_3 : FF / NH_3

The formate obtained from FH / NH_3 indicates 44.33 (%) Fe, 0.07 (%) Si, 1.72 (%) Al and 0.38 (%) Mn. There is a marked decrease in Si – 0.07 (%) in FF / NH_3 as compared to in FH / NH_3: Si – 0.15 (%). Al content too decreases from 2.90 (%) in FH / NH_3 to 1.72 (%) in FF / NH_3. The Mn content is also decreased from 0.62 (%) in FH / NH_3 to 0.38 (%) in FF / NH_3. The thermal product contains 96.52 (%) α-Fe_2O_3.

iii) Using FH / NaOH + NH_3 : FF / NaOH + NH_3

The formate obtained from FH / NaOH + NH_3 gives 43.62 (%) Fe and 0.0 (%) Si, 1.63 (%) Al and 0.41 (%) Mn. There is some decrease in Si, Al and Mn contents here as compared to that found in FH / NaOH + NH_3. The thermal product contains 97.4 (%) α-Fe_2O_3.

iv) Using FH / Na_2CO_3 : FF / Na_2CO_3

The formate obtained using FH / Na_2CO_3 exhibits 34.1 (%) Fe, 0.04 (%) Si 1.89 (%) Al, 0.60 (%) Mn. A marked decrease in Si – 0.04 (%) content is observed as compared to that in FH / Na_2CO_3 which contains 0.10 (%) Si in it. There is some decrease

53

in Al, Mn contents too in comparison with FH / Na_2CO_3. Its thermal product marks 96.95 (%) α-Fe_2O_3.

b) Analysis of iron hydroxides and formates : Study sample - II

1. Hydroxide preparation directly from acid extract

i. Using NaOH : FH II / NaOH.

The hydroxide consists 61.2 (%) Fe, 0.41 (%) Si, 0.16 (%) Al and 2.10 (%)Mn. The thermal product yields 96.8 (%) Fe_2O_3 and the isothermal weight loss amounts to 8.45 (%). This hydroxide retains appreciable quantity 2.1 (%) Mn, as study sample II had already contained Mn to the same tune 2.36 (%) (Table 2.3b).

2. Formate from Hydroxide prepared:

i) Using FH II / NaOH : FF II / NaOH

The iron formate FF II / NaOH prepared from FH II / NaOH gives 48.5 (%) Fe, 0.30 (%) Si, 0.11 (%) Al and 1.24 (%) Mn. The overall upgradation of Fe_2O_3 reaches to 97.1 (%) (Table 2.3b).

c) Minor and trace (rare) elements

The minor elements like Ti, P, S, Na, K present in the study samples (Table 2.2b) are reduced to nil or traces on chemical beneficiation into the iron hydroxides / formates. The elements like Mg, Pb, Cu, Zn present in traces in the ore got reduced to nil on the chemical beneficiation.

2.4 Conclusions

1. Study sample I (RPD/7) is selected as the average quality of Goan ore reject consisting of 41 (%) Fe & high SiO_2 + Al_2O_3.

2. Study sample II (RPD/4) is chosen as it has a moderate level of SiO_2 + Al_2O_3 (%); and the presence of Mn is in appreciable quantity which is one of the major elements in Goan iron ores.

3. The presence of minor and trace (rare) elements are in negligible percentage in the study samples as well as in the hydroxides and formates prepared from the acid extracts.

4. The hydroxides and formates obtained from acid extracts of the ore rejects effectively help in increasing the iron recovery.

5. The iron recovery from the from the acid extracts is, however, maximum by solvent extraction method using methyl isobutyl ketone (MIBK).

6. The Fe_2O_3 obtained by the thermal decomposition of the iron hydroxides / formates that prepared from acid extract show purity in the range 92 – 98.38 (%). But 99.73 (%) pure iron oxide is obtained from the iron hydroxides prepared from acid extracts after solvent extraction.

Preparation and Characterization of Iron oxides from Iron hydroxides, Iron formates and their hydrazinated complexes.

3.1 Introduction

The synthesis and characterization of iron oxides from iron hydroxides and formates that obtained from iron ore rejects, as described in chapter 2, are being studied and presented in this chapter.

As our objective is to utilise beneficiated iron ore rejects in ferrite synthesis and since gamma ferric oxide, γ-Fe_2O_3 is reported [44-45] to be superior to α-Fe_2O_3 in such synthesis, we are looking for an easy method to prepare γ-Fe_2O_3 from iron ore rejects. The iron hydroxides that obtained from iron ore rejects on heating give usual iron oxide, α-Fe_2O_3. To obtain γ-Fe_2O_3 from these iron hydroxides, a systematic study is needed to be undertaken.

A knowledge acquired from preliminary studies done in our laboratories [46-47] to easily prepare gamma ferric oxide useful in ferrite synthesis from iron oxyhydroxides and

carboxylate by hydrazine method has been made use in the present work.

Hydrazine method is a versatile one used in the synthesis of metal and mixed metal oxides of technological importance [63-72]. Not only transition metal oxides and ferrites but also perovskite oxides have been synthesized by hydrazine method.

Lanthanum cobaltate, $LaCoO_3$ and doped $LaCoO_3$ are important conducting materials which are refractive in nature with high melting point ($>2400^{\circ}C$) having resistance to oxidation or corrosion. These materials are normally synthesized by solid state reactions at high temperatures above $1200^{\circ}C$ in air. But this needs repeated heating and grinding to complete the reaction due to slow diffusion process in solids. A new hydrazine method enabled [73] to synthesize these lanthanum cobaltates $< 800^{\circ}C$ which further allowed to properly go for sintering process to get dense ceramics.

By new hydrazine method [74-77] technologically important ZrO_2-Al_2O_3 solid solutions have been successfully synthesized, that too, of better quality than those obtained by usual ceramic technique.

In our laboratories hydrazine method has been utilized in the synthesis of γ-Fe_2O_3 from ferrous oxalate dihydrate [78], iron (II) carboxylates (Ferrous –fumarate,–succinate, –malonate, –tartrate, –maleate and –malate) [46], iron oxyhydroxides (α-FeOOH, γ-FeOOH and amorphous FeOOH) [46].

In hydrazine method gamma ferric oxide forms in one step from the hydrazinated precursors. Ferrous oxalate dihydrate, $FeC_2O_4.2H_2O$, for example, on hydrazination [78] forms $FeC_2O_4.1N_2H_4$ and $FeC_2O_4.2N_2H_4$ which decompose in an ordinary atmosphere into γ-Fe_2O_3. But the thermal decomposition of $FeC_2O_4.2H_2O$, in air, results into α-Fe_2O_3 and to obtain γ-Fe_2O_3, the α-Fe_2O_3 has to be reduced to Fe_3O_4 and then reoxidise to γ-Fe_2O_3.

A multistep reaction processes are adopted in the commercial manufacture of γ-Fe_2O_3 from α-FeOOH.

$$\alpha\text{-FeOOH} \xrightarrow{\text{dehydration}} \alpha\text{-}Fe_2O_3 \xrightarrow{\text{reduction}} Fe_3O_4 \xrightarrow{[O]} \gamma\text{-}Fe_2O_3$$
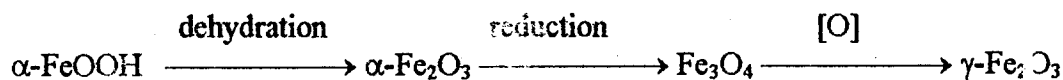
Thus, hydrazinate precursor, $FeC_2O_4.2N_2H_4$, easily transforms into γ-Fe_2O_3, whereas a controlled water vapour atmosphere is needed during the thermal decomposition of $FeC_2O_4.2H_2O$ to convert it into γ-Fe_2O_3 [79].

The other iron (II) carboxylates: ferrous fumarate, ferrous succinate, ferrous malonate, ferrous tartrate, ferrous maleate and ferrous malate too decompose in air mainly to α-Fe_2O_3, while a control water vapour atmosphere decomposition [80-85] then leads to γ-Fe_2O_3. But, then, their hydrazinate complexes studied in our laboratories [46] easily decompose to γ-Fe_2O_3.

The work done by Rane et al [79] on $FeC_2O_4.2H_2O$ in establishing the formation condition of γ-Fe_2O_3 from the precursor under a controlled atmosphere of water was continued in our laboratories by his group. The hydrazination of the oxalate then found to give directly γ-Fe_2O_3 [78] and the hydrazine method extended by Rane et al [46] on the other iron (II) carboxylates and iron oxyhydroxides further gave confidence in utilising this novel method in synthesizing γ-Fe_2O_3 easily.

Here, we are adopting a hydrazine method to synthesize γ-Fe_2O_3 from iron hydroxides and formates prepared from iron ore rejects as described in chapter 2. The results of such studies are presented here.

3.2 Preparation of Hydrazinated Iron Hydroxides and Formates

a) Preparation of Hydrazinated Iron Hydroxides (FHH)

Hydrazinated iron hydroxides were prepared by hydrazine equilibration method. The

finely crushed iron hydroxides (FH) that obtained by four different precipitants (section 2.3.2) were dried at 105°C, cooled in a desiccator, spread on Borosil glass petri dishes separately and were kept in a desiccators containing 100 % hydrazine hydrate for about 10 – 15 days. During this period the pale brown colour of iron hydroxides got changed into dark brown. They are coded as FHH/NaOH, FHH/NH₃, FHH/NaOH+NH₃ and FHH/Na₂CO₃.

Caution: Use of hand glows, eye glass and exhaust are to be made use while handling hydrazine hydrate as it is carcinogenic.

b) Preparation of Hydrazinated Iron Formates (FFH)

The hydrazinated iron formates were prepared using the four different iron formates (FF) described in section 2.3.3 by hydrazine equilibration method in a very similar fashion as in iron hydroxides. They are represented as FFH/NaOH, FFH/NH₃, FFH/NaOH+NH₃ and FFH/Na₂CO₃.

3.3 Thermal decomposition

3.3.1 Thermal analysis (DTA / DSC) of iron hydroxides / formates

Thermal decomposition of iron hydroxides and formates was carried out at 1000 – 1050°C and 300°C for ½ an hour respectively. Few representative samples of iron hydroxides: FH/NaOH, FH/NaOH+NH₃ and FH/Na₂CO₃ and iron formates: FF/NaOH, FF/NaOH+NH₃ and FF/Na₂CO₃ were also studied by Differential Thermal Analysis (DTA) and Differential Scanning Calorimetry (DSC).

3.3.2 Autocatalytic decomposition of hydrazinated complexes

Both iron hydroxide hydrazinates and formates on exposure to atmosphere from the desiccator immediately caught fire indicating an autocatalytic decomposition.

3.4 Characterization

3.4.1 Chemical Analysis

The total iron content estimation of the thermal products of iron hydroxides, formates and autocatalytically decomposed hydrazinated complexes of the hydroxides / formates was done by standard method that mentioned in section 2.2.2.a.

3.4.2 X-ray diffraction (xrd)

The thermal and autocatalytically decomposed products were characterized by x-ray diffraction technique on powder samples. Philips x-ray diffractometer model PW 1710 with Cu Kα radiations using nickel as a filter was utilised for such studies.

3.4.3 Magnetic characterization: Saturation magnetization

The saturation magnetization studies of the thermal products was carried out using a high field hysteresis loop tracer described by Likhite et al [86] and supplied by M/s Arun Electronics, Mumbai, India. The three major parts of this instruments are electromagnet, pick-up coil and balancing the integrating circuits.

The loop tracer consists of an electromagnet working on 50 Hz mains frequency. The alternating magnetic field of about 3600 Oersted is produced in an air gap of about 1 cm, in the instrument and a special balancing coil is used to measure the saturation magnetization of the sample in the air gap. Depending upon the magnetic induction in the specimen, pick-up coil produces a field proportional to the magnetic induction of the specimen. A supporting coil produces a signal which is equivalent to the strength of the magnetic field. When the respective signals are supplied to the vertical and horizontal plates of an oscilloscope, it displays a hysteresis loop on the screen.

A digital AC voltmeter which was connected to the output, was made to display peak or RMS value of the signal proportional to the saturation magnetization in milli volts.
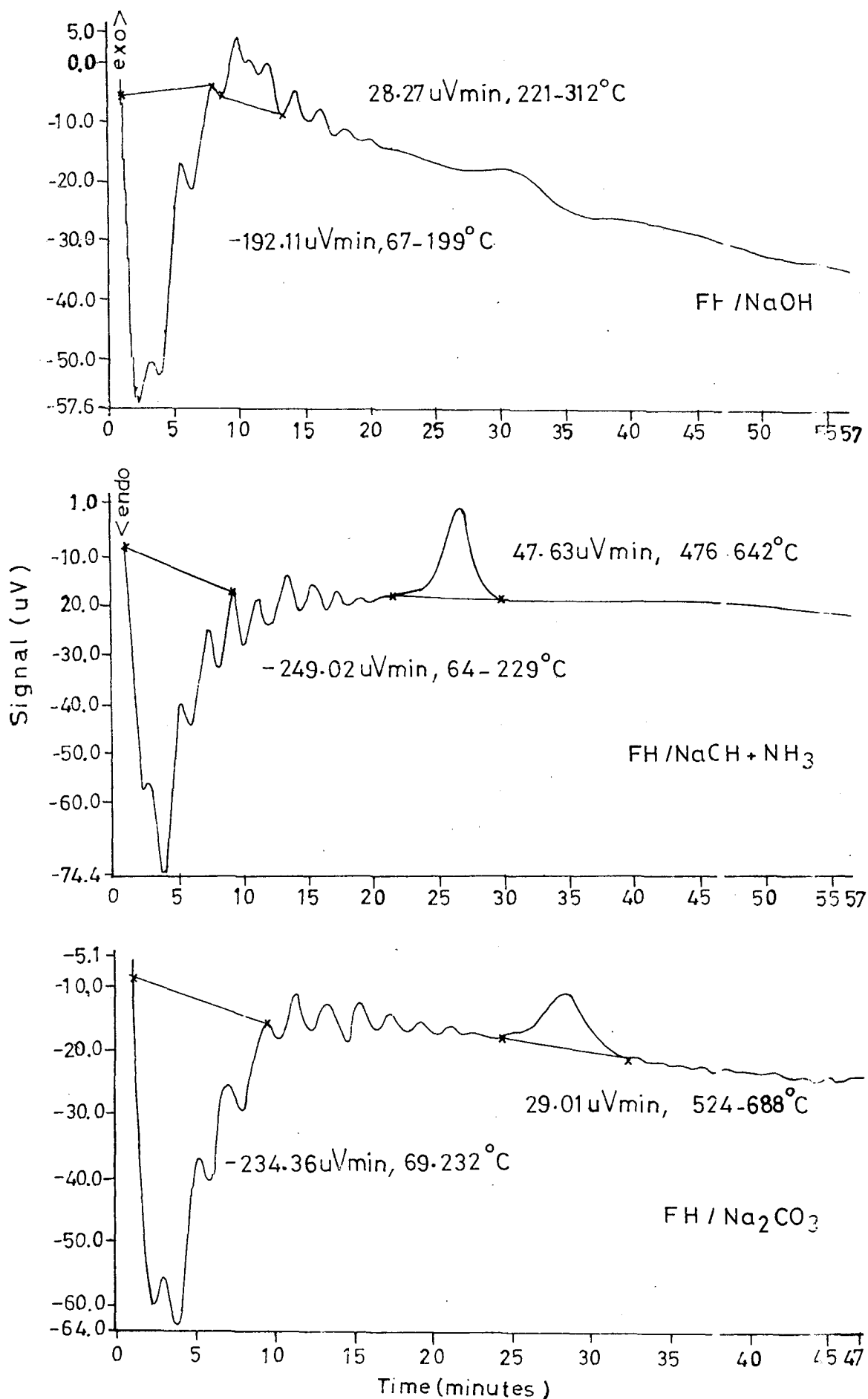
FIG. 3.1a :- Differential Thermal Analysis (DTA) of Iron hydroxide.

61

The calibration of the vertical scale corresponding to the magnetization value was done using pure nickel as a standard substance having saturation magnetization of 53.34 emu/g.

A known amount of synthesized iron oxide powder packed in a polythene bag was introduced in the instrument and signals were recorded with respects to the standard nickel, the σs values were thus obtained.

3.4.4 Infra red analysis

The infrared analysis of iron oxides were done on Shimadzu FTIR instrument, model 8101 A. The pellet used for recording spectra were prepared by mixing 1-2 mg of the sample with KBr. The IR spectra in the frequency range of 400 – 4600 cm^{-1} were recorded at room temperature.

3.5 Results

3.5.1 Thermal analysis: DTA/DSC

a) Iron hydroxides

The iron hydroxides: FH/NaOH, FH/NaOH+NH$_3$ and FH/Na$_2$CO$_3$ were analysed by DTA. In Fig. 3.1a the results of DTA from room temperature (RT) to 1000 C are given for these samples. FH/NaOH shows a broad endotherm between 67 – 199 C and an exothermic peak between 221 – 312°C. FH/NaOH+NH$_3$ indicates a broad endo therm between 64 – 229°C and an exothermic peak between 476 – 642°C. On the other hand, FH/Na$_2$CO$_3$, reveals an endothermic effect in the temperature range 69 – 232°C, while the exothermic peak is observed between 524 – 688°C. All these samples after an endothermic peak give exothermic peak and the end product after this peak is α Fe$_2$O$_3$ which is confined by xrd.

Only FH/NaOH decomposes at much lower temperature < 312°C giving α- Fe$_2$O$_3$, while the remaining two FH/NaOH+NH$_3$ and FH/Na$_2$CO$_3$ yield the oxide at much higher

temperatures. The chemical analysis indicates (Table 2.3a) that FH/NaOH has in t 0.55 (%) Si, 0.228 (%) Al and 0.93 (%) Mn as admixture whereas both FH/NaOH+NH$_3$ and FH/Na$_2$CO$_3$ contain < 0.2 (%) Si, but > 2.5 (%) Al. Hence, the higher temperature decomposition in these two samples may be attributed to the presence of high content of Al.

b) Iron formates

Iron formates FF/NaOH, FF/NaOH+NH$_3$ have been analysed by DTA, while FF/Na$_2$CO$_3$ is characterized by DSC (Fig. 3.1b). FF/NaOH shows an intense exotherm between 25° – 285°C, on the other hand, FF/NaOH+NH$_3$ indicates a small endothermic peak between 191 – 234°C followed by a sharp exotherm in the temperature range 235 – 306°C. The DSC trace of FF/Na$_2$CO$_3$ indicates change in heat contents in two ranges of temperatures with peak temperatures at 213.2°C and 310.9°C. From these observations it may considered that iron formate decomposes to Fe$_2$O$_3$ ~ 300°C. Only FF/NaOH decomposes to Fe$_2$O$_3$ at much lower temperatures ~ 270°C and this decomposition of the formate involves only one exothermic peak, while the remaining two show an endothermic peak followed by an exothermic reaction. The higher temperature decomposition in FF/NaOH+NH$_3$ and FF/Na$_2$CO$_3$ may be due to the presence of larger percentage of aluminium admixture (Table 2.3a) in them, 1.63 (%) and 1.8⁵ (%), respectively. Whereas, the FF/NaOH has aluminium content of ~ 0.10 (%) in it The silicon content is, however, more in FF/NaOH as compared to the other two formates.

3.5.2 Phase Identification of the thermal products:

a) Iron Hydroxides

The thermal products obtained ~ 1100°C from iron hydroxides FH/NaOH, FH/NH$_3$, FH/NaOH+NH$_3$, FH/Na$_2$CO$_3$ from study sample I and FH-II/NaOH from study sample II
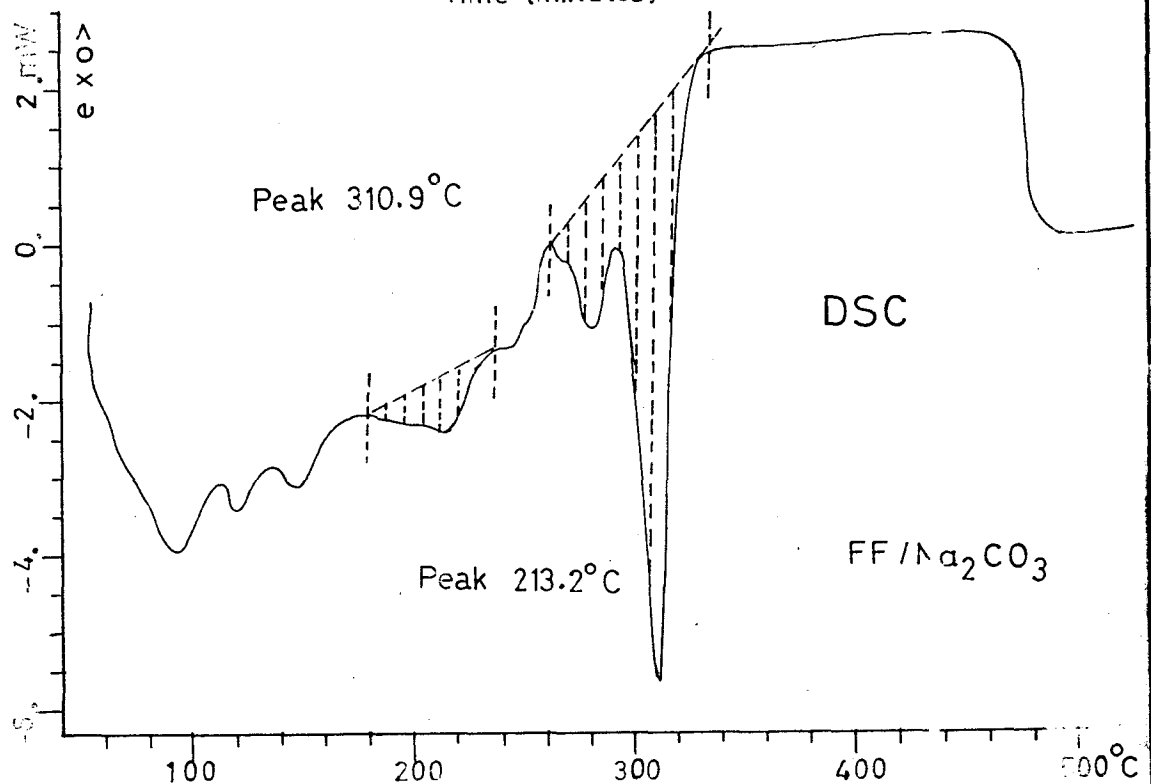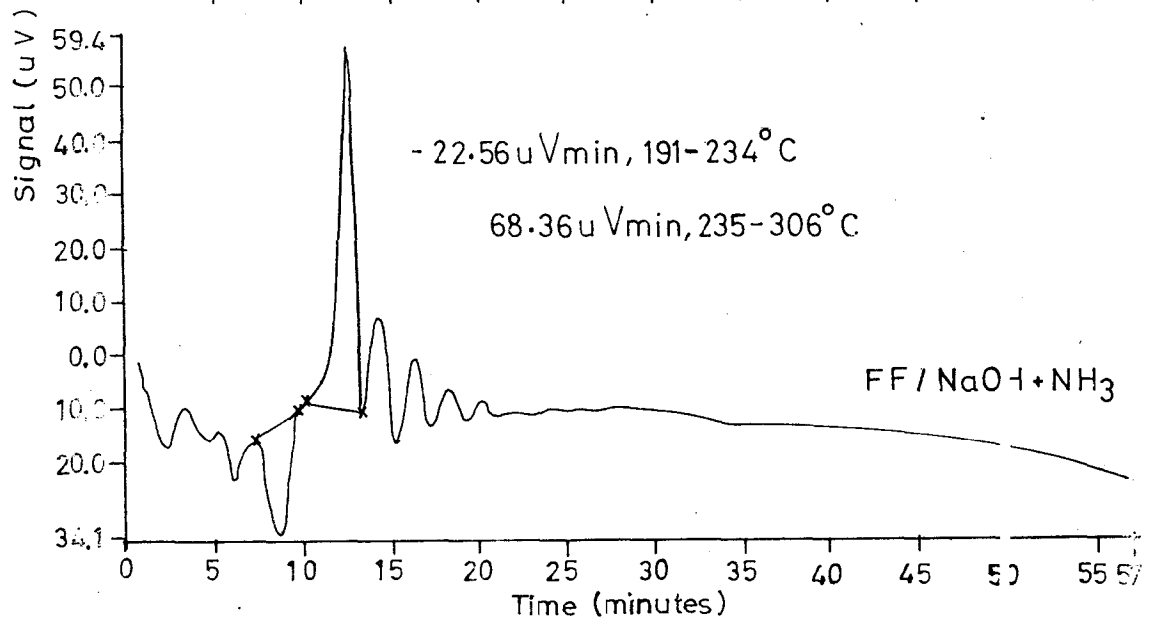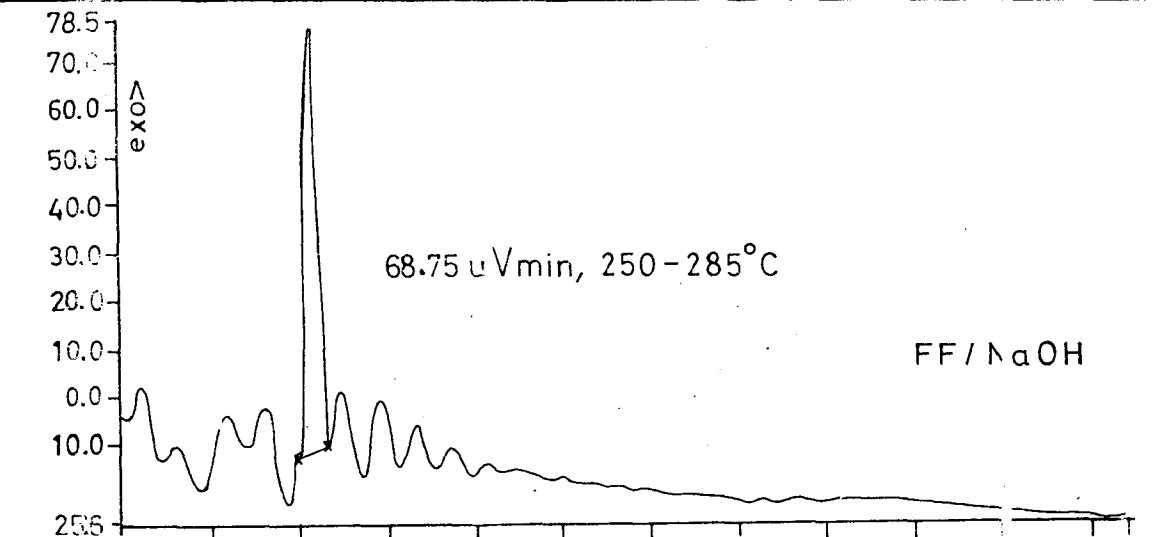
FIG. 3.1 b:– DTA Differential scanning colorimetry (DSC) of Iron formates.

Graph annotations:
- 68.75 uVmin, 250-285°C — FF / NaOH
- -22.56 uVmin, 191-234°C
- 68.36 uVmin, 235-306°C — FF / NaOH+NH₃
- Peak 310.9°C
- Peak 213.2°C
- DSC
- FF / Na₂CO₃

show x-ray diffraction (xrd) pattern similar to α-Fe$_2$O$_3$ and the d $_{hkl}$ values match well

with the values reported in JCPDS files [62]. The d $_{hkl}$ values of representatives samples

of these along with the different iron oxides reported are compiled in the Table 3.1.

Table 3.1. XRD data of Iron oxides obtained from the thermal decomposition of Iron

Hydroxides, Formates and autocatalytically decomposed hydrazinated

complexes

Oxides	d $_{hkl}$ (I/Io)											a (nm)
γ-Fe$_2$O$_3$ Tetragonal	--	2.95 (30)	--	--	2.51 (100)	2.086 (15)	--	1.7 (9)	1.60 (20)	1.47 (40)	1.2 (8)	0.8340
γ-Fe$_2$O$_3$ Cubic		2.95 (34)	--	--	2.52 (100)	2.08 (24)	--	1.7 (12)	1.61 (33)	1.48 (53)	1.2 (11)	0.8350
Fe$_3$O$_4$		2.96 (30)	--	--	2.53 (100)	2.09 (20)	--	1.7 (10)	1.61 (30)	1.48 (40)	1.2 (10)	0.8396
α-Fe$_2$O$_3$ Rhomboh-edral	3.66 (25)	--	--	2.69 (100)	2.51 (50)	--	1.838 (40)	1.690 (60)	--	1.452 (35)	--	
Red oxide commercial	3.67 (21)	--	--	2.70 (82)	2.52 (100)	2.07 (1)	1.838 (22)	1.70 (40)	1.60 (7)	1.45 (28)	1.2 (5)	
FH/NaOH	3.68 (31)	--	--	2.70 (100)	2.51 (70)	2.07 (2)	1.84 (36)	1.70 (32)	1.60 (9)	1.49 (28)	1.2 (7)	
FHH/ NaOH	--	2.95 (27)	--	--	2.52 (100)	2.09 (17)	--	1.70 (6)	1.61 (24)	1.48 (42)	--	0.8349
FF/NaOH		2.96 (10)	--	--	2.52 (100)	2.098 (5)	--	1.707 (9)	1.61 (8)	1.48 (13)	--	0.8383
FFH/NaOH	--	2.96 (36)	--	--	2.53 (100)	2.09 (17)	--	1.71 (10)	1.61 (19)	1.48 (26)	1.2 (5)	0.8375
FF/NH$_3$	--	2.95 (20)	--	--	2.52 (100)	2.08 (10)	1.84 (10)	1.70 (15)	1.60 (19)	--	1.2 (3)	0.844
FFH/NaOH + NH$_3$	3.68 (27)	--	2.89 (7)	2.69 (100)	2.51 (73)	--	--	1.69 (36)	1.60 (6)	1.48 (13)	1.2 (0.4)	0.8342
FHH / Na$_2$CO$_3$		2.95 (30)	--	2.69 (2)	2.51 (100)	2.09 (18)		1.71 (7)	1.61 (18)	1.48 (26)	1.2 (6)	0.8351

b) Iron Formates

Iron formates FF/NaOH, FF/NaOH+NH$_3$, FF/NH$_3$ and FF/Na$_2$CO$_3$ decompose

~ 300°C and give magnetic oxides. The xrd patterns of these thermal products show

mainly peak corresponding to γ-Fe$_2$O$_3$ (Table 3.1) and match well with the JCPDS files

[87]. Few peaks due to α-Fe$_2$O$_3$ are also observed. Only few representative samples are being entered in the table.

c) Hydrazinated Iron Hydroxides / Formates

The hydroxides and formates that equilibrated over hydrazine hydrate in a desiccator and on removing and exposing to air found to immediately fume. The chemical analysis to find the hydrazine content in the hydrazinated complexes could not be carried out. The samples FHH/NaOH, FHH/NaOH+NH$_3$, FHH/NH$_3$, FHH/Na$_2$CO$_3$, FFH/NaOH, FFH/NaOH+NH$_3$, FFH/NH$_3$, FFH/Na$_2$CO$_3$ that fumed, on cooling found to be magnetic and the x-ray characterization revealed them to be mainly γ-Fe$_2$O$_3$. Only few representative samples are being compiled in the Table 3.1.

3.5.3 Infra red analysis

The iron oxide that obtained from iron hydroxides, iron formates and their hydrazinates are characterized as γ-Fe$_2$O$_3$ and / or α-Fe$_2$O$_3$ (Table 3.1). The FH/NaOH, FH/NH$_3$, FH/NaOH+NH$_3$, FH/Na$_2$CO$_3$ and FH-II/NaOH on decomposition give α-Fe$_2$O$_3$. IR analysis of these on comparison with the reported band positions of α-Fe$_2$O$_3$ roughly suggest that the formed oxides are α-Fe$_2$O$_3$. In Fig. 3.2 ir spectra of few samples are placed along with the Std. γ-Fe$_2$O$_3$ and commercial red oxide (RO) for comparison. However, these iron oxides incorporate some admixture of Mn, Al, Si (Table 2.3 & b) that present in their precursors. The sample FH/MIBK is the only hydroxide (Table 2.3a) which has very low impurities and the oxide α-Fe$_2$O$_3$, that obtained from it is 99.3 (%) pure. Hence the ir spectra of it is considered to be of pure iron oxide, α-Fe$_2$O$_3$.

The band positions of α-Fe$_2$O$_3$ (FH/MIBK) and red oxide (RO) are more or less matching each other and also with the reported values [46, 92, 93, 95].

α-Fe$_2$O$_3$
FH / MIBK

RO
Fe$_2$O$_3$

γ-Fe$_2$O$_3$
FHH / Na$_2$CO$_3$

γ-Fe$_2$O$_3$
FHH / MIBK

Std γ-Fe$_2$O$_3$

γ-Fe$_2$O$_3$
FF / NaOH

FFH / NaOH

γ-Fe$_2$O$_3$

% T

4000.0   3000.0   2000.0   1500.0   1000.0   400.0

Wave number (cm-1)
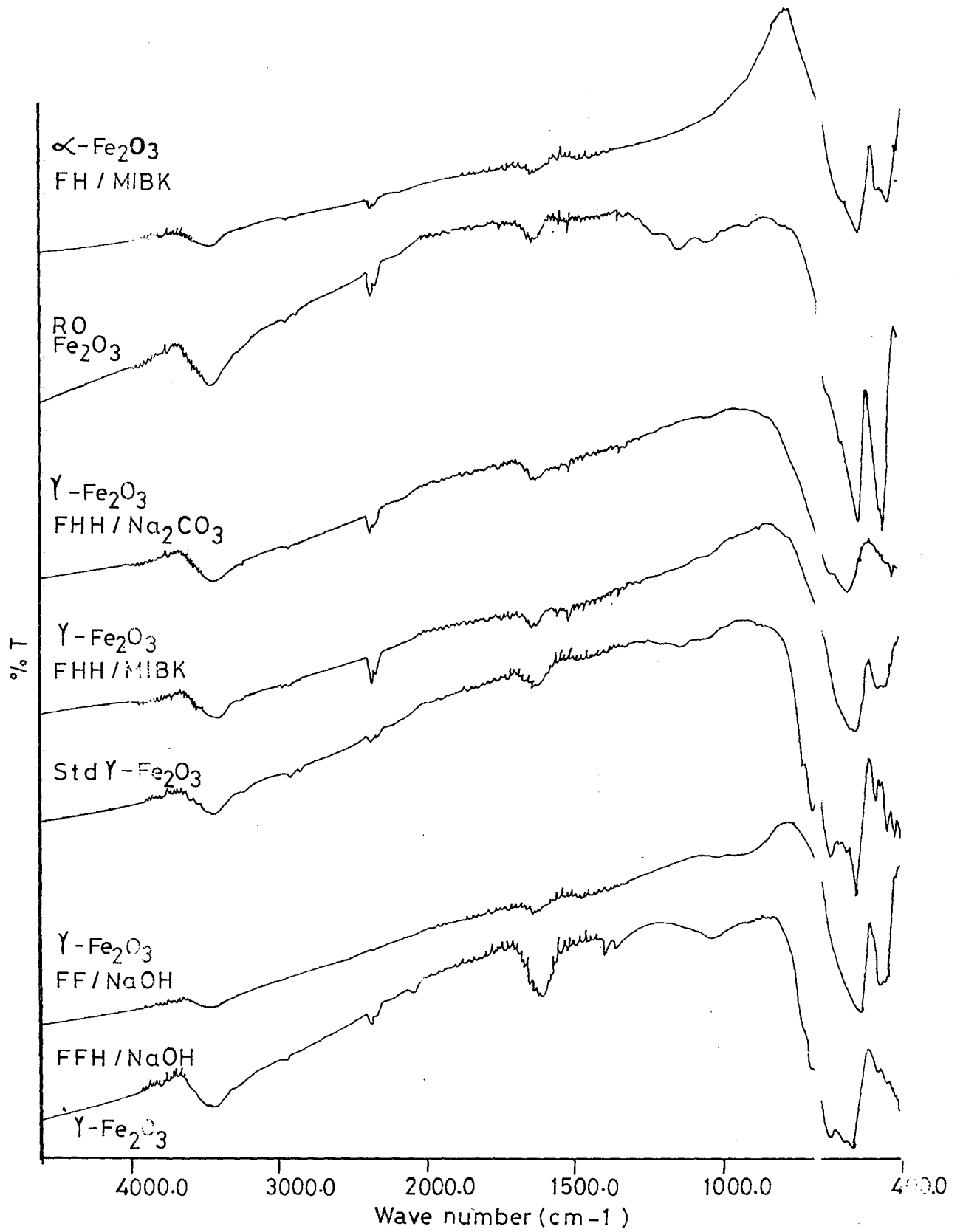
FIG.3.2:-IR spectra of Iron oxides of Chemically beneficiated Ore rejects

67

The iron hydroxides on hydrazination decompose autocatalytically and yield mainly γ-Fe_2O_3 which is confirmed by xrd (Table 3.1). The ir analysis of these oxides has been done and spectra of two representative samples, FHH/Na$_2$CO$_3$ and FHH/MIBK are given in Fig. 3.2. For comparison the spectra of Std. γ-Fe_2O_3 is also shown in the figure.

The ir band positions of Std. γ-Fe_2O_3 at 1646, 729, 694, 639, 609, 588, 55 \;, 483, 442 and 423 cm^{-1} are matching well with the reported values [46, 90-92, 94]. The FHH/Na$_2$CO$_3$ and FHH/MIBK also show more or less similar spectra to that of Std. γ-Fe_2O_3, but the close observation of these two samples that synthesized by us suggest that they have diffused spectra, indicating incomplete formation of the structure or the presence of impurities.

Iron formates and hydrazinated iron formates decompose mainly to γ-Fe_2O_3 The representative spectra of FF/NaOH and FFH/NaOH are given in Fig. 3.2. The oxide obtained from FFH/NaOH gives band positions at 1602, 1011, 687, 639, 560, 54ς, 479, 442 cm^{-1}. The spectra looks similar to Std. γ-Fe_2O_3 and also match with the reported values for γ-Fe_2O_3 [46, 90-92, 94]. However, the spectra of FF/NaOH is near to FFH/NaOH, but it seems the spectra is little diffused indicating incomplete formation of γ-Fe_2O_3.

3.5.4 Magnetic Characterization

Iron oxides prepared from iron hydroxides at ~1050°C temperature are non-magnetic.

The thermal products of hydrazinated iron hydroxides, iron formates and hydrazinated iron formates are all mainly magnetic. The saturation magnetization values, σs, are found to be in between 10 and 67 emu/g for samples (Table 3.2).

The maximum value of σs, 66.67 emu/g is observed for the thermal product of iron formate FF-II/NaOH.

Table 3.2 Saturation Magnetization of Iron oxides obtained from Iron hydroxide and Iron formate precursors

	γ-Fe$_2$O$_3$ from precursors	Using precipitants			
		NaOH	NH$_3$	NaOH+NH$_3$	Na$_2$CO
Study Sample I	FHH	10.37	25.02	27.06	33.77
	FF / Δ	24.35	----	----	27.65
	FFH	52.70	10.32	23.38	34.38
Study Sample II	FHH - II	62.97	--	--	--
	FF-II /Δ	66.67	--	--	--
	FFH - II	48.40	--	--	--

3.6 Discussion

3.6.1 Phase identification

The iron hydroxides, iron formates and the hydrazinated hydroxides and fo mates all decompose to iron oxide, Fe$_2$O$_3$. The iron hydroxides decompose to α-Fe$_2$O$_3$ The phase was identified by xrd. IR analysis too enabled us to confirm the formation (Fig.3.2) on comparing with red oxide, α-Fe$_2$O$_3$ (RO).

The iron hydroxides (FH) on equilibrating with hydrazine (FHH) and then exposing to air all decompose instantaneously to oxide. The xrd pattern of these ii dicate that the oxide obtained is mainly γ-Fe$_2$O$_3$ (Table 3.1) with some admixture of α-Fe$_2$O$_3$. This is expected as, in an explosive decomposition of the hydrazinated complexes there occurs an intense glow whose temperature is sufficient to transform few γ-Fe$_2$O$_3$ particles

to α-Fe$_2$O$_3$. The ir spectra (Fig. 3.2) of these oxides on comparing with the Std. γ-Fe$_2$O$_3$ reveal that the band position are more or less matching.

The Std. γ-Fe$_2$O$_3$ shows all band positions relevant to the oxide as reported. The FHH/Na$_2$CO$_3$, infact, resembles the Std. γ-Fe$_2$O$_3$ but with lower resolution of peak positions. FHH/MIBK too gives like FHH/Na$_2$CO$_3$ a diffuse spectra. The xrd data for FHH/Na$_2$CO$_3$ indicates d$_{hkl}$ values of γ-Fe$_2$O$_3$ (Table 3.1). It shows a weak peak ~ 2.69 Å which is 100 (%) peak of α-Fe$_2$O$_3$. The saturation magnetization value of 33.77 emu/g (Table 3.2) observed for the γ-Fe$_2$O$_3$ obtained from FHH/Na$_2$CO$_3$ is low as compared to the reported value of 71 – 74 emu/g [88]. However, the values in the range of 35 – 60 emu/g are also observed [89] depending upon the method of preparation. An admixture of α-Fe$_2$O$_3$ and also incomplete formation of structure and particle of optimum sizes may also contribute to low values in the magnetic saturation of γ-Fe$_2$O$_3$. And, this is expected in our samples when prepared from explosive hydrazine method. Thus, from xrd, ir and magnetic saturation values one may infer that all our samples, in general, are not anywhere near the reported values. Only iron formate FF/NaOH decomposition gives highest σs of 66.67 emu/g (Table 3.2). And, this FF/NaOH shows no α-Fe$_2$O$_3$ peak ~ 2.70 (Table 3.1).

Although our results indicate that hardly any one method enabled us to prepare pure γ-Fe$_2$O$_3$, we wish to emphasize here that we are interested only in an easy synthesis of γ-Fe$_2$O$_3$ from iron ore rejects. Since this oxide, even if it contains some admixture of α-Fe$_2$O$_3$, is good enough to enhance the reaction rate of ferrites preparation [44], we are not making any further efforts to improve the method of preparation of γ-Fe$_2$O$_3$ to achieve commercial grade properties. Here, therefore, we are looking into purity level of the oxides (γ-Fe$_2$O$_3$ or α-Fe$_2$O$_3$) thus obtained from two ore reject samples: study sample I

and II. The various precursors obtained from the ore rejects yield the oxides and we are reporting only the purity of the formed oxides. This is in accordance with our main objective to make use of iron ore rejects to obtain high purity iron oxide for ferrites preparation.

3.6.2 Thermal decomposition

a) Iron hydroxides

The study sample I of iron ore rejects consists of 57.49 (%) Fe_2O_3 (Table 2.3a). The hydroxide FH/NaOH obtained from the filtrate II (Flow sheet 1) on heating gives α-Fe_2O_3 of purity 98.38 (%). The other hydroxides, FH/NH$_3$, FH/NaOH+NH$_3$ and FH/Na$_2$CO$_3$ decompose to α-Fe_2O_3 and the percentage purity of these are, respectively, 93.67, 92.24 and 91.82 (%). The lower percentage of α-Fe_2O_3 in these is due to the presence of $>$ 2.64 (%) Al, $>$ 0.60 (%) Mn and $\sim$ 0.14 $\pm$ 0.03 (%) Si in the precursor hydroxides.

The iron hydroxide precipitated by NH$_3$ from filtrate II after solvent extraction, FH/MIBK, on decomposition gave 99.73 (%) pure α-Fe_2O_3. The hydroxide precursor shows 0.08 (%) Si, 0.21 (%) Al and nil (%) Mn.

From these results it may be seen that iron extraction by solvent method using methyl isobutyl ketone (MIBK), is superior to all the other methods adopted here.

The study sample II of iron ore rejects (Table 2.3b) containing 76.36 (%) Fe$_2$O$_3$ on extracting with HCl and precipitating iron as hydroxide, FH-II/NaOH, decomposes to α-Fe_2O_3 of purity of 96.8 %. The hydroxide precursor in this case retains about 2 1 (%) Mn that present in the ore of 2.36 (%). This may be the reason why purity of the iron oxide obtained is low as compared to FH/NaOH of study sample I.

71

b) Iron formate

The iron hydroxides that obtained from the study sample I and II have lowered the major impurity contents that present in the ore rejects. The iron formates obtained from these hydroxides showed further decrease in Al, Si, Mn contents (Table 2.3a & b). The iron formates, FF/NaOH, FF/NH$_3$, FF/NaOH+NH$_3$, FF/Na$_2$CO$_3$ and FF-II/NaOH on decomposition gave Fe$_2$O$_3$ (mainly γ-Fe$_2$O$_3$) and the purity of this is found, respectively, 98.67, 96.52, 97.24, 96.95 and 97.1 (%). Thus, iron oxides obtained from iron formates show low impurity iron oxides as compared to that prepared from iron hydroxides.

From these results it is seen that the iron ore rejects get chemically beneficiated to good purity iron oxides, mainly γ-Fe$_2$O$_3$ and α-Fe$_2$O$_3$. The hydrazinated iron formates give iron oxides, mainly γ-Fe$_2$O$_3$ easily.

These iron oxides, γ-Fe$_2$O$_3$ and α-Fe$_2$O$_3$ are then used in the synthesis of MgFe$_2$O$_4$ and Mn$_x$Zr$_y$Fe$_2$O$_4$ which is described in chapter IV.

3.7 Conclusions

1. Iron hydroxides decompose to non magnetic α-Fe$_2$O$_3$.

2. Iron hydroxides on equilibration with hydrazine and then exposing to air decompose instantaneously to magnetic iron oxide, mainly γ-Fe$_2$O$_3$ with some admixture of α-Fe$_2$O$_3$.

3. Iron formates decompose to γ-Fe$_2$O$_3$ and few admixture of α-Fe$_2$O$_3$.

4. Iron formate on equilibrating with hydrazine and then on exposing to air, decompose autocatalytically to γ-Fe$_2$O$_3$.

5. Hydrazinated iron hydroxides and formates are sensitive to air, hence, the detailed formula fixation of complex hydrazinates of these are not carried out.

Studies on the Magnesium Ferrite and Manganese Zinc

Ferrites

Part I

Microstructure and property correlation of $MgFe_2O_4$

(ore rejects [46])

Part II

Synthesis and Characterization of $MgFe_2O_4$

(Study Sample I)

Part III

Synthesis and Characterization of $(Mn_{1/2}Zn_{1/2})Fe_2O_4$

(Study Sample II)

General Introduction

Synthesis of ferrites of general formula MFe_2O_4 is carried out by bringing a solid state reaction between α-Fe_2O_3 and divalent metal oxides, MO, or their easily decomposable simple compounds such as MCO_3, $M(NO_3)_2$, $M(OH)_2$, etc. Since the solid state reactions are sluggish, a ceramic technique is usually adopted to get product of the desired stoichiometry having optimum intrinsic and extrinsic properties. In the ceramic technique the raw materials are first granulated, compacted, presintered, regranulated and recompacted. The recompacted materials are then heated to high temperatures. Many a times, one more grinding of the heated sample is needed. The ground materials are then compacted into the magnetic cores of the desired shapes and finally sintered at very high temperature generally $> 1200^{\circ}C$.

73

The ceramic technique is thus a laborious one and by adopting these different processes like granulation, compact formation, presintering, regrinding, reheating etc., it is fairly ascertained that an adequate rate of reaction can be achieved as homogeneity in reactant particle sizes is attained. These processes, hence, suggest that heterogene ties in the particle sizes should be avoided [96] in order to get a uniform and controlled microstructure. Chemical reactivity can be enhanced by increasing the surface area of the reactant particles and hence, finer the grain size (and also uniform) better is the reactivity and, in turn a speedy reaction rate leading to the desired product is assured.

Although other factors like temperature, atmospheres and the nature of the other metal constituents are essential in obtaining ferrites of the desired electromagnetic properties required for the applications in devices, many intrinsic properties depend solely on extrinsic properties and hence, microstructure of the products is also important criterion to be investigated in ferrites studies. Therefore, in ferrites research, an emphasis is put on the microstructure of the reactants, as well as, products, for that matter these aspects of microstructures are essential in any ceramic research.

Though solid state reactions are sluggish, the rate of reaction can, this, be enhanced by considering the aspects discussed above. In ferrites synthesis α-Fe_2O_3 and MO are effectively made to react by taking into consideration the microstructure, temperature, atmosphere control to get the desired products. But, there are few references [44,45] which report that the rate of reaction can be enhanced and also the temperature of formation can be lowered in ferrites synthesis by using γ-Fe_2O_3 as a starting material. This additional reactivity is due to the type of starting iron source for ferrite preparation. And, here the structural criterion may be considered to be playing an important role in enhancing the rate of reaction. Cubic γ-Fe_2O_3 reacts with the cubic MO giving the cubic

spinel product, while corundum α-Fe_2O_3 requires a lot of rearrangement to take place before reacting with cubic MO to form the spinel.

Other than structural aspects, the reason for the increased rate of reaction between γ-Fe_2O_3 and MO can be attributed to in situ transformation of γ-Fe_2O_3 to α-Fe_2O_3 during the heating process and the α-Fe_2O_3 thus formed has now more reactivity, because of energy change in the transformation and increase in surface area (energy) of the freshly formed α-Fe_2O_3 particles. Ferrites preparation from Fe_3O_4 and MO [39,41] found to occur at lower temperatures and also the spinels formed well with better characteristics or ferritization took place early. Here the phase transformation of Fe_3O_4 to Fe_2O_3 that occurs during the heating process supplies energetic Fe_2O_3 particles of better reactivity to react with the MO. And if MO is also formed in situ during the heating process from the starting compound like MCO_3, $M(NO_3)_3$ etc. then further enhancement in rate of the formation of ferrite is achieved.

In our laboratories [46,47] $MgFe_2O_4$ synthesized from freshly prepared γ-Fe_2O_3 gave better characteristics than that obtained from commercial α-Fe_2O_3. Already, a beginning has, thus, been made in our laboratory to explore the possibility of using γ-Fe_2O_3 in ferrite synthesis and the γ-Fe_2O_3 samples were obtained from the upgraded iron ore rejects. We are continuing such investigations on the usefulness of γ-Fe_2O_3 prepared from iron ore rejects in ferrite synthesis.

In the present work we are using γ-Fe_2O_3 samples synthesized from iron ore rejects, as described in chapter 2 and 3 to prepare once again $MgFe_2O$ and $(Mn_{1/2}Zn_{1/2})Fe_2O_4$. However, $(Mn_{1/2}Zn_{1/2})Fe_2O_4$ system is the new system in our on going research, but the $MgFe_2O_4$ is taken up here, not only to study and establish the preparation criterion using γ-Fe_2O_3 as a starting material, but also to investigate the micro-structural aspects in the synthesis. How the microstructure of the iron oxides

synthesized from iron ore rejects influence the products formation, as well as their properties are being investigated.

The present chapter, hence subdivided into 3 parts:

Part I: Microstructure and property correlation of MgFe$_2$O$_4$ (ore rejects [46])

Part II: Synthesis and Characterization of MgFe$_2$O$_4$ (study sample I)

Part III: Synthesis and Characterization of (Mn$_{1/2}$Zn$_{1/2}$)Fe$_2$O$_4$ (study sample II)

Both MgFe$_2$O$_4$ and (Mn$_{1/2}$Zn$_{1/2}$)Fe$_2$O$_4$ are being synthesized from iron oxides prepared from beneficiated iron ore rejects as described in chapter 2 and chapter 3 Part II and Part III of this chapter deals with the synthesis and characterization of these ferrites. However, the MgFe$_2$O$_4$ samples that had already been systematically studied in our laboratories [46,47] are being further studied and their results, especially, the microstructural aspects, are presented in the part I of this chapter. These Mg Fe$_2$O$_4$ samples too were prepared from iron oxides (mainly γ-Fe$_2$O$_3$) that had been obtained from beneficiated iron ore. Here we are making an attempt to correlate the microstructures with the electromagnetic characteristics of these ferrites. For the comparison of the results, the MgFe$_2$O$_4$ samples were also prepared from commercial α-Fe$_2$O$_3$ and standard γ-Fe$_2$O$_3$ and characterized. And these results are also presented here.

The microstructural studies were taken up to see whether the different precursors that had been used in producing iron oxides [46] from iron ore rejects have any influence in forming particles of uniform reactivity in ferrite synthesis. This is due to the fact that the MgFe$_2$O$_4$ sample prepared from γ-Fe$_2$O$_3$ obtained from different precursors: carboxylato-hydrazinate, iron oxyhydroxides and hydrazinated iron oxyhydroxides gave almost similar electromagnetic characteristics, while the ferrite synthesized from

76

commercial α-Fe$_2$O$_3$ indicated different properties [46,47]. And, hence, the microstructural studies are of significance and discussed here in Part I.

In part II the MgFe$_2$O$_4$ system is once again studied. Here iron oxides that used for the ferrite formation are prepared from beneficiated iron ore of Goan origin of different areas. Iron hydroxides were prepared from the acid extract of iron ore rejects (chapter 2) by treating with NaOH, NH$_4$OH, NaOH + NH$_4$OH and Na$_2$CO$_3$. These hydroxides were then used for the preparation of iron formates. And, their chemical analysis (Table 2.3a and b) indicate different percentage of main impurities, Mn, Al, Si. Both the iron hydroxides and formates were then hydrazinated. These hydroxides and formates of iron and their hydrazinated complexes all gave (chapter 3) iron oxides, mainly α-Fe$_2$O$_3$ or γ-Fe$_2$O$_3$ or the mixture of these (Table 3.1 and 3.2). Thus, here we are studying MgFe$_2$O$_4$ system synthesized from only these iron oxides, while in par I the ferrites were synthesized [46] from iron oxides prepared from different precursors : Iron (II) carboxylato-hydrazinates (Ferrous fumarato-hydrazinate, ferrous succinato-hydrazinate, ferrous malonato-hydrazinate, ferrous tartrato-hydrazinate, ferrous maleato-hydrazinate and ferrous malato-hydrazinate), iron oxyhydroxides (γ-FeOOH, α-FeOOH and amorphous FeOOH) and their hydrazinates. Therefore, the present studies use iron oxides prepared from simple precursors: hydroxides and formates and their hydrazinates.

(Mn$_{1/2}$Zn$_{1/2}$)Fe$_2$O$_4$ system, however, is studied with a view to standardize the method of synthesis of this most complex ferrite, as Mn is susceptible to variation in its oxidation state. We used different preparation techniques. Not only the ceramic technique using iron oxide (from iron ore rejects) + MO but also a coprecipitation techniques are being adopted and presented in the part III. In coprecipitation technique the iron hydroxide obtained from iron ore rejects were dissolved in acid and after adding the required stoichiometric amount of Mn and Zn, the solution was treated with ammonia

77

to get hydroxides. From these hydroxides, formates were then prepared. The hydrazinated complexes of these were also then synthesized. We are reporting only the preparation of the precursors and their thermal decomposition leading to ferrite The studies are restricted only to phase identification by x-ray diffraction and magnetic characterization by determining saturation magnetization values with respect to the different heat treatments.

Microstructure and property correlation of MgFe$_2$O$_4$

(ore rejects [46])

4.1 Introduction

Magnesium ferrite, $MgFe_2O_4$, prepared in our laboratory [46] from chemically beneficiated iron ore reject of one particular region of Goa was thoroughly studied by xrd to establish the phase formation, magnetic characterization: saturation magnetization, A. C. susceptibility and initial permeability as a function of temperature, and electrical characterization to evaluate the temperature dependence of resistivity. The properies of the ferrite samples synthesized from iron oxides prepared from iron ore rejects by using different precursors were then compared with the ferrites prepared from commercial iron oxide, $\alpha-Fe_2O_3$. As the ferrite prepared from iron oxides (mainly $\gamma-Fe_2O_3$) that obained from iron ore rejects gave superior properties compared to the one prepared from commercial iron oxide, hematite, it was considered that the inferior properties in $MgFe_2O_4$ from hematite may be due to the presence of impure $\alpha-Fe_2O_3$ phases n the

ferrite. Whereas, the iron oxides from ore rejects indicated the formation of single phase $MgFe_2O_4$. Although, this reason for the inferior properties is fairly correct, we thought of inspecting the microstructures of the precursor iron oxides and the ferrites. And we in the present Part-I are presenting the results of the scanning electron microscopic (SEM) studies done on these samples [47].

4.1.1 Preparation and characterization of iron oxides and $MgFe_2O_4$

   a) Chemical beneficiation of iron ore rejects

   A representative iron ore reject dump sample of Goan origin containing 35 5 (%) Fe, 3.3 (%) Al_2O_3, 40.28 (%) SiO_2 and traces of manganese, calcium and magnesiu n was chemically beneficiated [46] by acid extraction with dil.HCl + dil.HNO$_3$. The acid extract was treated with 20 (%) NaOH to get metal hydroxides, mainly iron hydroxides. The hydroxide of iron was then used to prepare iron (II) carboxylato-hydrazinates and iron oxyhydroxides: α-FeOOH, γ-FeOOH and amorphous FeOOH and their hydrazinates. The thermal products of these precursors are coded as [46,47],

1. Ferrous fumarato-hydrazinates (FFHA)

2. Ferrous succinato-hydrazinate (FSHA)

3. Ferrous malonato-hydrazinate (FMHA)

4. Ferrous tartrato-hydrazinate (FTHA)

5. Hydrazinated γ-FeOOH (γ-FA)

6. Hydrazinated amorphous FeOOH (Amp FA)

7. Hydrazinated α-FeOOH (α-FA)

The thermal products are mainly γ-Fe$_2$O$_3$ (Table 4.1.1). Few products also contained α-Fe$_2$O$_3$ in minor quantities. These iron oxide samples were then used to prepare $MgFe_2O_4$.

TABLE 4.1.1 XRD data of iron oxides [46]

Sample	d										
γ-Fe$_2$O$_3$*	-	2.95	-	-	2.51	2.09	-	1.70	1.60	1.47	1.20
γ-Fe$_2$O$_3$*	-	2.95	2.78	-	2.52	2.08	-	1.70	1.61	1.48	1.27
Fe$_3$O$_4$*	-	2.97	-	-	2.53	2.09	-	1.71	1.61	1.48	1.28
α-Fe$_2$O$_3$*	3.66	-	-	2.70	2.51	2.20	1.83	1.69	-	1.45	-
FFHA	3.68	-	2.78	2.70	2.52	2.08	1.84	1.70	1.60	-	-
FSHA	-	2.95	2.78	-	2.51	2.09	-	1.71	1.61	-	-
FMHA	-	2.97	2.78	2.70	2.52	2.09	1.83	1.70	1.61	-	-
FTHA	-	2.95	2.78	2.70	2.52	2.09	1.84	1.70	1.61	-	-
γFA	-	2.96	-	-	2.52	2.09	-	1.70	1.61	1.48	1.27
AmpFA	-	2.95	-	-	2.51	2.08	-	-	1.60	1.47	1.27
αFA	-	-	-	2.70	2.52	-	1.83	1.69	1.60	1.48	1.27

(The header spans: d$_{hkl}$ (Å))

* - Reported [62, 87, 94, 176]

b) Preparation of MgFe$_2$O$_4$

The iron oxides mainly γ-Fe$_2$O$_3$ synthesized as in 4.1.1a were mixed in the required proportion with MgCO$_3$, pelletised and preheated $\sim$ 800°C for 12 h in ai. The cooled samples were ground, pelletised and then heated to 1000°C for 24h in an o dinary atmosphere. The samples thus prepared are named as below.

Iron oxide source   Code name of magnesium ferrite

(1) FFHA $\longrightarrow$ MgFFHA

(2) FSHA $\longrightarrow$ MgFSHA

(3) FMHA $\longrightarrow$ MgFMHA

(4) FTHA $\longrightarrow$ MgFTHA

F = ferrite

$\alpha = \alpha\text{-Fe}_2\text{O}_3$

Mg HEM

Mg FMHA
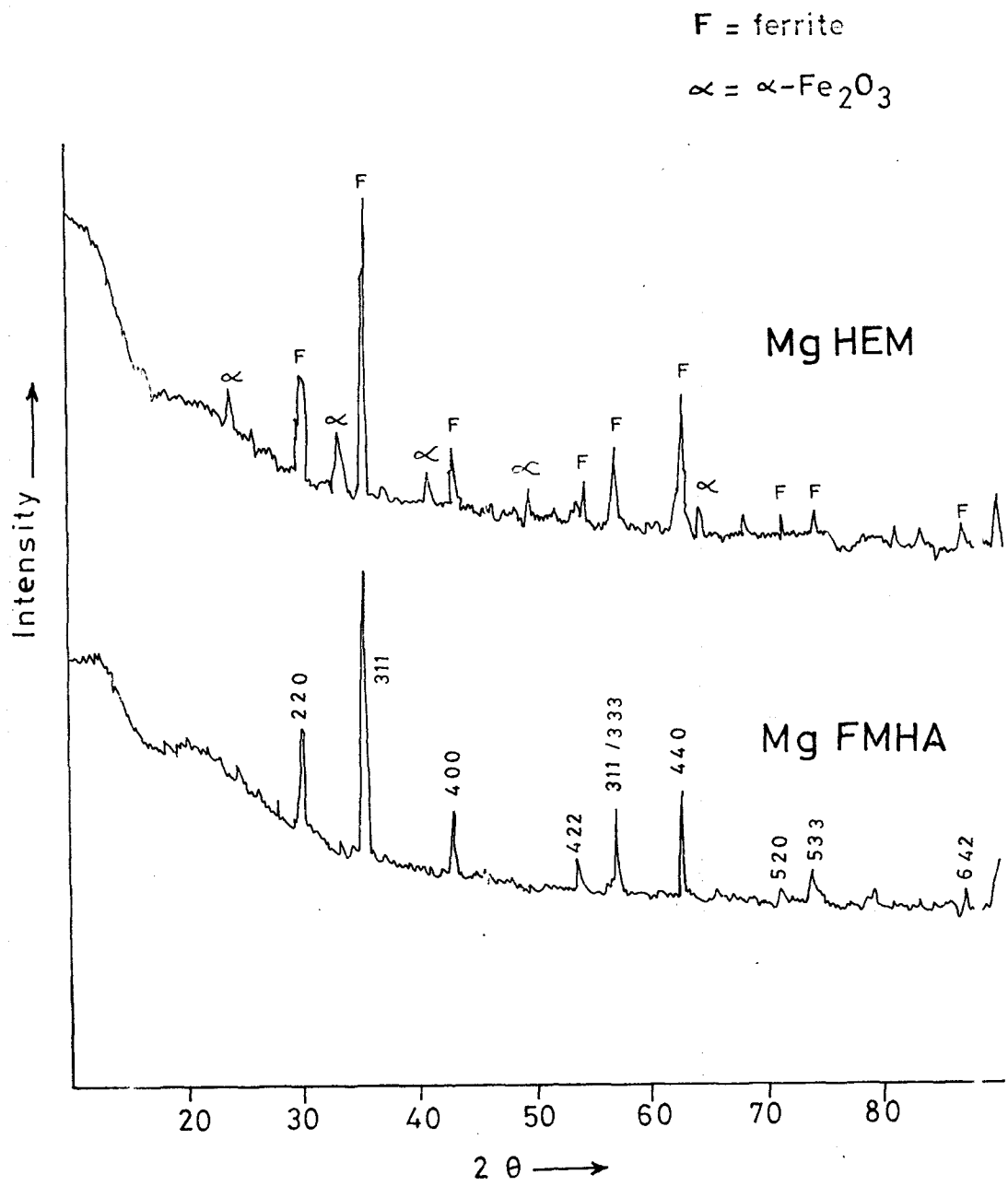
FIG. 4·1·1:– X–ray pattern of MgFe$_2$O$_4$

(5) γFA ⟶ MgγFA

(6) AmpFA ⟶ MgAmpFA

(7) αFA ⟶ MgαFA

A commercial iron oxide, hematite, α-Fe₂O₃, was also mixed with $MgCO_3$ a ᴉu ᴛᴉɪᴄ sample of $MgFe_2O_4$ was prepared as above and coded it as MgHem.

All these were characterised with xrd technique and the observed d $_{hkl}$ value s were matched wi꞉꞉ JCPDS files [97] for $MgFe_2O_4$. All samples excepting MgHem (pr ꞉pared from hematite) give single phase $MgFe_2O_4$. The xrd pattern of one representative s imple, MgFMHA is given in Fig 4.1.1 along with the MgHem. The MgHem clearly shows unreacted α-Fe₂O₃ in the $MgFe_2O_4$.

c) Lattice parameter, porosity of $MgFe_2O_4$

The lattice parameter of all $MgFe_2O_4$samples are given in Table 4.1.2. They are all found to be 0.839 to 0.841 nm which are within the range of the reported values [9ʃ -101]. X-ray densities, dx, of all the samples are in the range 4.45 to 4.49 g cm^{-3} which are close to the reported value of 4.52 and from the actual density, da, porosity, P, is calc alated using formula

$$P\ (\%) = \frac{dx - da}{dx} \times 100$$

All ferrites samples prepared from γ-Fe₂O₃ show porosity ~25 (%) (Table 4.1.2), w ʉereas the spinel ꞉ ꞉gHem prepared from hematite indicates a high porosity of 42 (%). A porosity of 31 (%) and 27 (%) [102 - 103] are reported for $MgFe_2O_4$ in the literature

d) Magnet꞉ and electrical characterization of $MgFe_2O_4$

Saturation magnetization, σs, in emu/g values of all $MgFe_2O_4$ samples me sured at RT fall i꞉ ᴛhe range of 22 – 28 [Table 4.1.2] excepting MgHem which show 17.2

emu/g. The saturation magnetization, $4\pi Ms$, in Gauss are found to be in the range of 922 – 1168 excepting the ferrite prepared from hematite, MgHem which shows the lowest value of 609.5 Gauss. The magnetone number, n_B, calculated (Table 4.1.2) for MgHem is the lowest, 0.62, while all other samples indicate values in the range of 0.79 – 1.01 which are close to the reported values of 0.93 – 1.2 [105].

TABLE 4.1.2 Lattice parameter, porosity, Magnetization data and Curie temperatures of magnesium ferrite samples [46]

Sample	Lattice Parameter 'a' (nm)	Porosity P (%)	Magnetization Data			Curie Temperatures (^{o}C)		
			$4\pi Ms$ (Gauss)	n_B	σs (emu/g)	Magnetic suscepti-bility	Initial Permeability	Resi-stivity
MgFFHA	0.8393	26.04	1082	0.93	25.96	385	416	399
MgFSHA	0.8391	29.58	967.2	0.87	24.36	397	-	399
MgFMHA	0.8388	26.24	922.3	0.79	22.15	369	394	385
MgFTHA	0.8400	21.31	1097	0.89	24.79	387	409	412
MgαFA	0.8410	23.63	1110.2	0.93	25.96	427	452	439
MgγFA	0.8415	26.41	1042.6	0.91	25.34	407	439	426
MgAmpFA	0.8414	25.92	1168.4	1.01	28.20	407	444	425
MgHem	0.8417	42.19	609.5	0.62	17.20	457	469	466

From alternating current susceptibility (section 4.2.3d) and initial permeability measurements (section 4.2.3d), Curie temperatures have been obtained and those are tabulated in Table 4.1.2. By a.c. susceptibility, the Curie temperature, Tc, for all $MgFe_2O_4$ samples are found to be within a range of 369 – 427°C while the spinel obtained from α-Fe_2O_3, MgHem, shows the higher value of 457°C. Similarly the Curie

temperature measured from initial permeability for all $MgFe_2O_4$ samples ranges from 394 – 452°C, whereas the MgHem shows highest value of 469. The reported values show rather a wide range of Tc from 320° to 440°C [106,107].

Direct current electrical conductivity measurements (section 4.2.3d) also used to locate Curie temperature by studying the temperature dependence of resistivity of all ferrite samples. A transition temperature from ferrimagnetic to paramagnetic is observed by the change in slope of the log ρ Vs 1/T plots. And the Tc values in the range 385 – 439°C for $MgFe_2O_4$ obtained from γ-Fe_2O_3 are tabulated in Table 4.1.2. A high value of Tc of 466°C is observed for MgHem.

4.1.2 Microstructural studies by SEM

The $MgFe_2O_4$ prepared from γ-Fe_2O_3 samples obtained from chemical beneficiated iron ore rejects, thus, show fairly uniform magnetic and electric characteristics, as described in 4.1.1, while the ferrite prepared from commercial hematite, α-Fe_2O_3 (MgHem) indicated higher porosity, low saturation magnetization value and high Curie temperature. The xrd studies revealed an admixture of α-Fe_2O_3 in $MgFe_2O_4$ prepared from α-Fe_2O_3 (commercial), on the other hand, all other $MgFe_2O_4$ samples obtained from γ-Fe_2O_3 showed single phase in the xrd pattern. Although, this admixture of α-Fe_2O_3 in $MgFe_2O_4$ may be considered due to incomplete reaction in the present investigation which may be causing different characteristics that observed, it is important to look into microstructure of these ferrites. This is due to the fact that all $MgFe_2O_4$ samples show porosity ~ 25 % excepting MgHem (from α-Fe_2O_3) which shows ~ 40 % porosity.

Grain size and porosity are the important factors which influence magnetic and electric properties in ceramics. And, therefore, the samples on which all above results

were obtained in our laboratories [46] were used to get microstructural information through scanning electron microscopy (SEM) and the results of such studies [47] are presented here.

Microstructure of all γ-Fe_2O_3 samples and commercial hematite, α-Fe_2O_3 used for the $MgFe_2O_4$ preparation and all the ferrite samples synthesized were studied by using SEM, Model: Cambridge Stereoscam S 250 MK LH having accelerating voltage range from 500 V to 40 kV and magnification range from 20x to 3,00,000x at 10 mm WD with resolution 40Å.

The samples in the pellet form and in powder form were used in obtaining SEM results in the form of a micrographs on 35 mm B/W film.

From SEM micrographs the grain size is calculated as follows,

i) Drawing a diagonal on the photograph

ii) Measuring the maximum unidirectional particle size in the vertical direction against diagonal

iii) Averaging the maximum unidirectional particle size

The distributions of grain sizes are then plotted as percentage (%) variation versus size of particles in μm and presented in the form of bar chart (Fig.4.1.2) for $MgFe_2O_4$ samples. Few representative micrographs of iron oxides and the ferrites prepared from these oxides are also given here.

a) Particle size distribution

Scanning electron micrographs of all $MgFe_2O_4$ samples prepared from γ-Fe_2O_3 show a particle size distribution (Fig 4.1.2) upto 3 μm, excepting the ferrite that prepared from α-Fe_2O_3 (MgHem) in which a wide range in sizes upto 6 μm is observed.
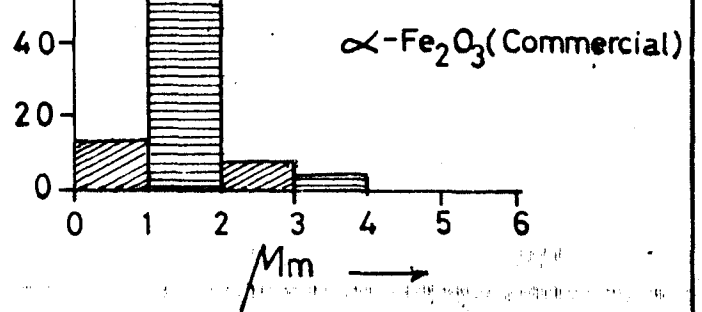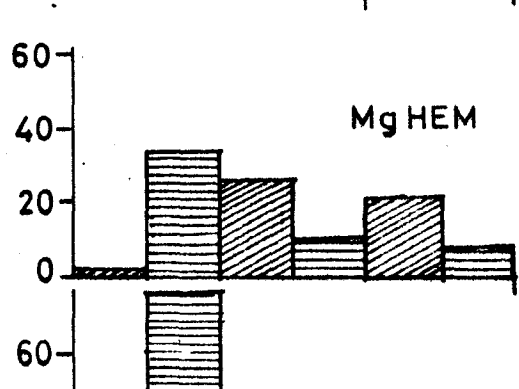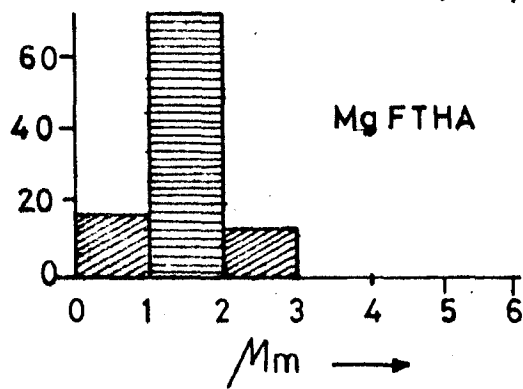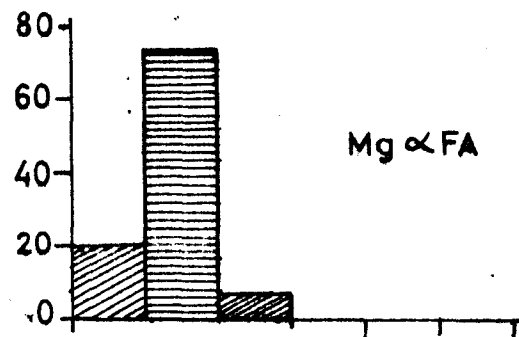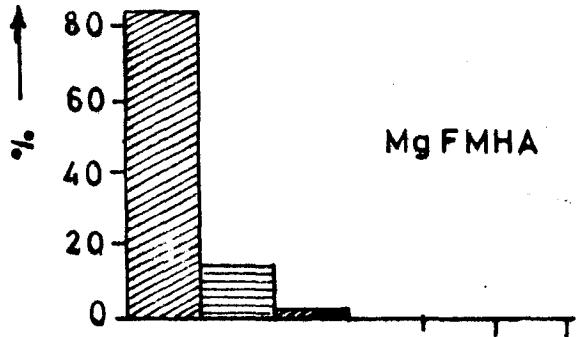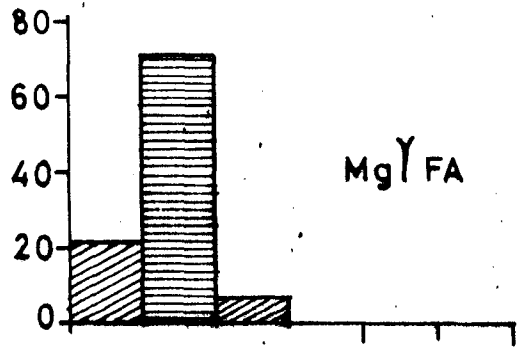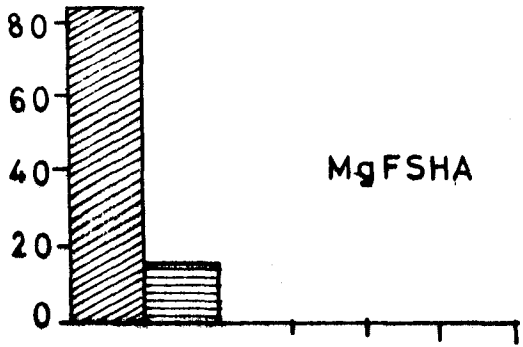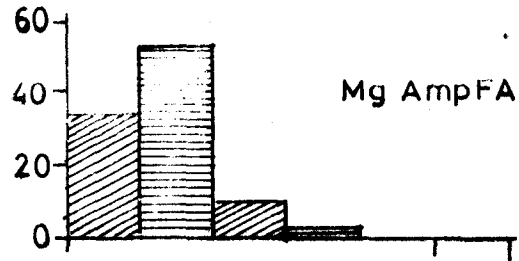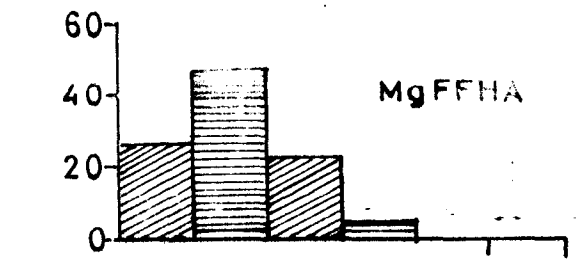
FIG. 4.1.2:-Particle size distribution of Mg Fe$_2$O$_4$ (ore reject [46])
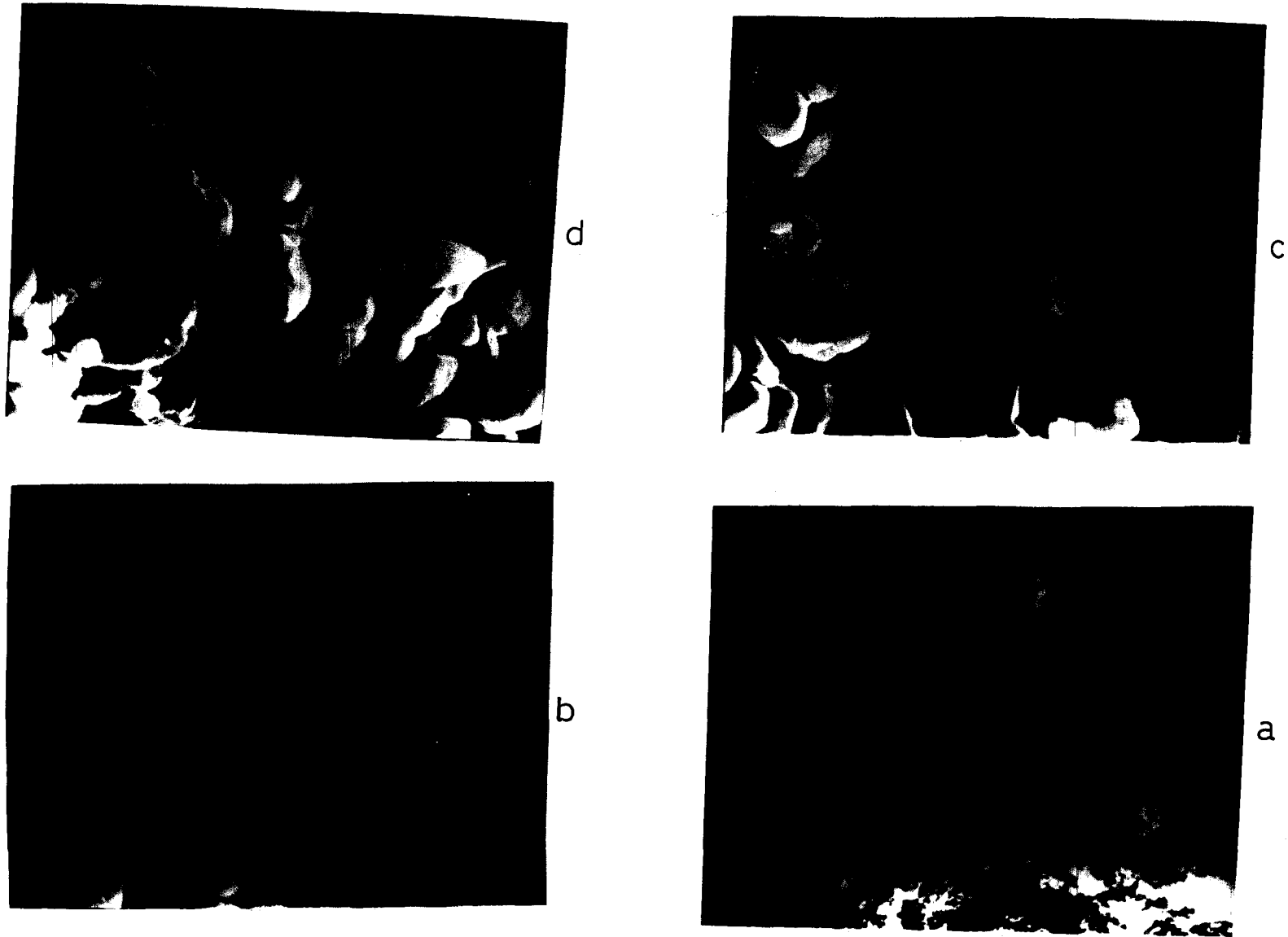
FIG. 4.1.3:- Scanning Electron Micrographs of a) Y-Fe_2O_3 : YFA & b) $Mg Fe_2O_4$ from YFA : $MgYFA$
c) & d) $Mg Fe_2O_4$: $Mg\alpha FA$ & $Mg Amp FA$
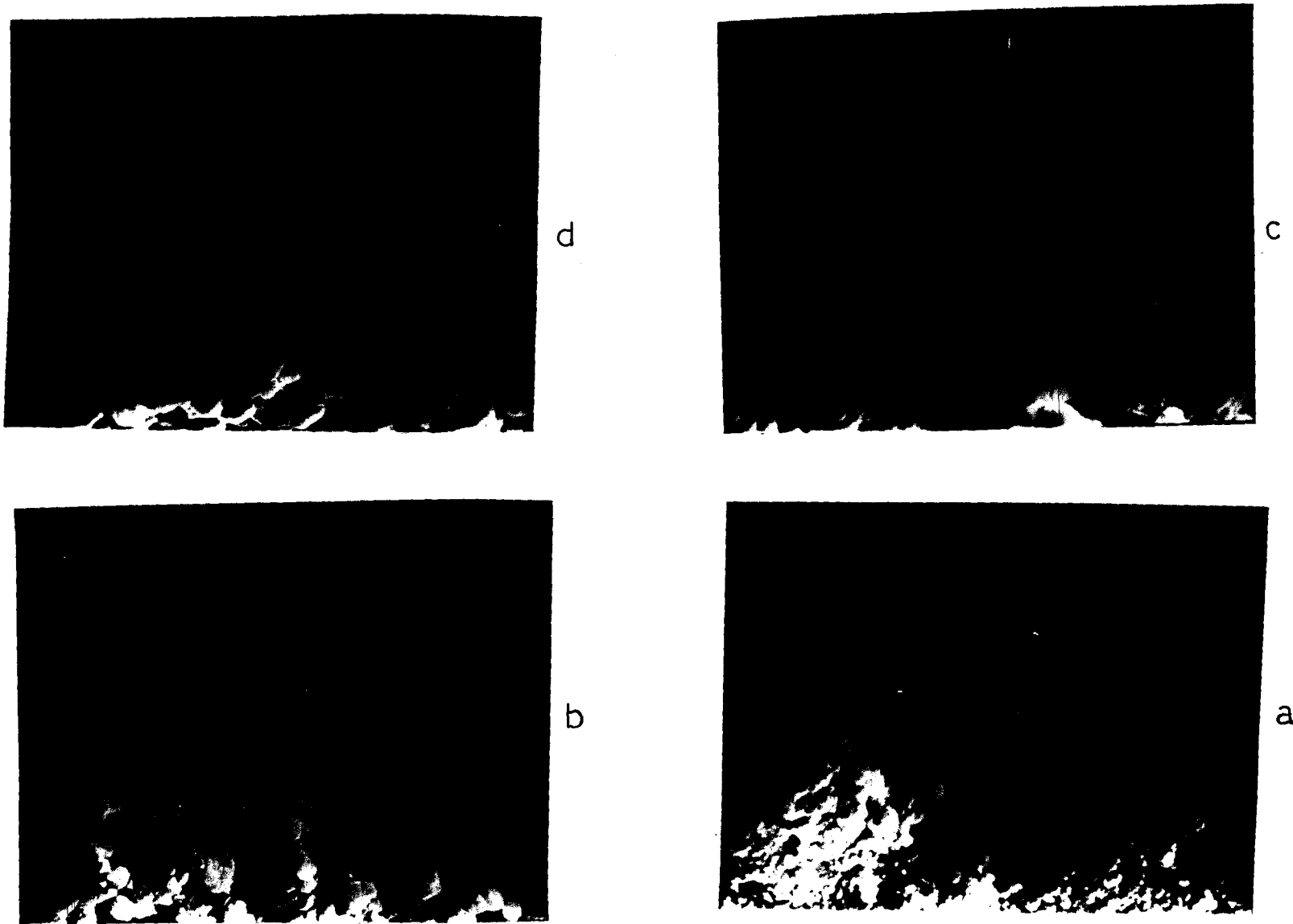
FIG 4·1·4:— Scanning Electron Micrographs of a) γ-Fe_2O_3: FSHA & b) $MgFe_2O_4$ from FSHA: Mg FSHA;
c) & d) $Mg Fe_2O_4$: Mg FFHA & Mg FTHA

a

b

FIG 4.1.5 — Scanning Electron Micrographs of a) $MgFe_2O_4$; MgHEM (from commercial α- Fe_2O_3) .
b) Commercial α-Fe_2O_3 .

MgγFA, MgαFA and MgAmpFA

The MgFe$_2$O$_4$, MgγFA, prepared from γ-Fe$_2$O$_3$ (γ-FeOOH autocatalytic), shows ~ 72 (%) particle between 1 - 2 μm, 22 (%) grains < 1μm and 6 % in the range of 2 - 3 μm. The sample MgαFA (γ-Fe$_2$O$_3$ source from α-FeOOH) and MgAmpFA (γ Fe$_2$O$_3$ from amorphous FeOOH) also show more or less the similar grain size distribution as MgγFA. The micrographs of these are shown in Fig. 4.1.3. There is a uniform grain size distribution in these samples. The measured porosity from x-ray density and actual density of these are almost similar: 23.63 - 26.41 (%) (Table 4.1.2).

MgFFHA, MgFSHA, MgFMHA and M3FTHA

The MgFe$_2$O$_4$ synthesized from γ-Fe$_2$O$_3$ obtained from iron (II) carbo: ylato-hydrazinates (FFHA, FSHA,FMHA and FTHA) show a grain distribution (Fig.4. .2) of upto 3 μm. The MgFMHA and MgFSHA have ~ 85 (%) grains < 1 μm and ~ 14 4 (%) particles of 1 - 2 μm. A few particles of 2 - 3 μm are also observed in MgFMHA. On the other hand, MgFFHA and MgFTHA show a majority of grains in 1 - 2 μm. The SEM micrographs are shown in Fig. 4.1.4 and the porosity of these ranges from 21 - 29 (%).

MgHem

The MgFe$_2$O$_4$ prepared from commercial α-Fe$_2$O$_3$ (MgHem) shows a wide range of grain size distribution (upto 6 μm). In Fig. 4.1.2 it can be seen clearly that 34 (%) of particles are of 1- 2 μm, 26 (%) are in 2 - 3 μm, 10 (%) in 3 - 4 μm, 20 (%) are in 4 - 5 μm and 8 (%) in 5 - 6 μm range. Such a distribution of grains effectively makes these sample more porous and the porosity observed from x-ray density & actual density is 42 (%). The SEM micrographs of commercial α-Fe$_2$O$_3$ and MgHem are shown n Fig 4.1.5.

Thus, all samples excepting the ferrites prepared from α-Fe$_2$O$_3$ (MgHem) sh w

uniform microstructure. And this leads to different magnetic characteristics that has been observed in our studies.

b) Reactivity of iron oxides leading to $MgFe_2O_4$

The $MgFe_2O_4$ synthesized from iron oxide (mainly γ-Fe_2O_3) obtained from different sources show almost similar micro-structural characteristics with majority of grains of size < 2 μm. The $MgFe_2O_4$ obtained from commercial α-Fe_2O_3 (MgHem), however, shows particles upto 6 μm with different grain sizes. The iron oxide (mainly γ-Fe_2O_3) sources used for the synthesis of $MgFe_2O_4$ are from autocatalytically decomposed iron (II) carboxylato-hydrazinates and hydrazinated iron oxyhydroxides. The autocatalytic decomposition leads to oxides of uniform particle size with very high surface area.

The BET surface area of iron oxides (mainly γ-Fe_2O_3) measured on few samples show to have 30-70 m^2/g and SEM micrographs also indicated a uniform distribution of particles of 10-30 nm size. A representative micrographs of γFA (Fig. 4.1.3a) and γSHA (Fig. 4.1.4a) are shown along with the ferrite prepared from them. These iron oxides then react with $MgCO_3$ and the ferrite samples that sintered at 1000°C show < 3 μm size grains in the ferrite, as described above.

On the other hand, the wide distribution of particle size in $MgFe_2O_4$ (MgHem) obtained from commercial α-Fe_2O_3 may be due to the large grain size of 1 - 2 μm observed in this oxide. In Figures 4.1.2 and 4.1.5b it can be clearly seen that α Fe_2O_3 (commercial) has 76 (%) of grains 1 - 2 μm, 13 (%) grains < 1 μm, 7 (%) particles are 2 - 3 μm, 4 (%) are in 3 - 4 μm. Such a large grain sized α-Fe_2O_3 material in contrast to small nanometre sized γ-Fe_2O_3 is responsible for the wide range of particles in the ferrites with large porosity as observed in MgHem (Fig. 4.1.5a). The small grain γ Fe_2O_3 samples, however, give uniform and smaller particles of ferrites with uniform porosity

but less than MgHem. These observations indicate nanometre size particles give uniform 1 - 3 μm size ferrites at 1000°C allowing further scope to increase the particle size by increasing sintering temperature, giving better characteristics. Whereas, non uniform particles in MgHem may further enhance non-uniform grains.

4.1.3 Conclusions

1. Iron (II) carboxylato-hydrazinates and iron oxyhydroxides obtained from iron ore rejects decompose autocatalytically giving mainly γ-Fe_2O_3. Few traces of α-Fe_2O_3 are found in few samples.

2. The iron oxides (mainly γ-Fe_2O_3) yield single phase $MgFe_2O_4$ when mixed with $MgCO_3$ and heated ~ 1000°C.

3. Commercial α-Fe_2O_3 (hematite) plus $MgCO_3$ ~ 1000°C give mainly $MgFe_2O$, with few traces of α-Fe_2O_3, suggesting single phase spinel is not formed.

4. $MgFe_2O_4$ prepared from commercial α-Fe_2O_3 shows high porosity of ~ 42 %, while γ-Fe_2O_3 sources result in the ferrites of porosity ~ 25 %.

5. A low saturation magnetization value of 609 Gauss is observed for $MgFe_2O_4$ prepared from α-Fe_2O_3 where as the ferrite obtained from all γ-Fe_2O_3 sources show the value between 922 – 1168 Gauss.

6. Curie temperature, Tc, of 457, 469 and 466°C is observed for $MgFe_2O_4$ obtained from α-Fe_2O_3 from temperature variation of magnetic susceptibility, initial permeability and resistivity. All other samples showed Tc lower than this, which are close to the reported values.

7. Uniform grain size in the range of 0 - 3 μm is observed for $MgFe_2O_4$ from nanometre size γ-Fe_2O_3 prepared from hydrazine precursors. A large distribution in particle size

0 - 6 μm is indicated by $MgFe_2O_4$ synthesized from commercial grade α-Fe_2O_3 of mainly 1 - 2 μm size grains.

Synthesis and Characterization of MgFe$_2$O$_4$

(Study Sample I)

4.2 Introduction

In Part I, we have described a detailed microstructural aspects of $MgFe_2O_4$ prepared from iron oxides containing γ-Fe_2O_3 that obtained from chemically benef ciated iron ore rejects. Iron (II) carboxylato-hydrazinates and hydrazinated iron oxyhydroxides were the precursors for these iron oxides. The $MgFe_2O_4$ samples thus obtained were characterized for their important electronic and magnetic properties. These properties were then compared with the properties of $MgFe_2O_4$ prepared from commercial hematite, α-Fe_2O_3. Since, $MgFe_2O_4$ prepared from α-Fe_2O_3 (MgHem) showed low saturation magnetization value compared to the ferrite prepared from γ-Fe_2O_3 obtained from ore rejects, we had suspected that MgHem differed in its characteristics due to an incomplete formation of $MgFe_2O_4$ as it had some admixture of α-Fe_2O_3 in it. Also, MgHem showed higher porosity ~ 42 (%) as compared to all the other samples, we considered this may be

the reason for the inferior characteristics in MgHem. The microstructural studies too indicated large particle size distribution in MgHem, while all the other samples showed almost uniform particles. Thus, from these studies we conclude that the starting iron oxide consisting of γ-Fe_2O_3 is required for $MgFe_2O_4$ formation of better quality. Hence, the γ-Fe_2O_3 seems to be a better precursor as mentioned in the literature [44 – 45] for ferrite preparation. We have, therefore, investigated this aspect further and the results of such studies are presented in this Part II.

In the present studies too iron ore rejects are being used to obtain γ-Fe_2O_3 The detailed procedure to obtain the iron oxides from study sample I has been described in chapters 2 and 3. These iron oxides are then used for $MgFe_2O_4$ preparation and characterized. For comparison the ferrite samples were also prepared from commercial red oxide (a fresh sample other than that used in 4.1) and a standard γ-Fe_2O_3.

4.2.1 Preparation of $MgFe_2O_4$

a) From iron oxides (study sample I)

The iron oxides mainly in the form of γ-Fe_2O_3, α-Fe_2O_3 and γ-Fe_2O_3 with some admixture of α-Fe_2O_3 that obtained from iron ore reject study sample I (chapter 3)are mixed with $MgCO_3$ in the required proportion and performed heat treatment as in 4 1.1.b. The sintering temperature was $1000^{\circ}/24h$. The samples thus obtained were coded as below, depending on the iron oxide source from which they are prepared.

Iron oxide source	Code for $MgFe_2O_4$

Mainly α-Fe_2O_3 (from hydroxides)

FH / NaOH	$\longrightarrow$	MgFH / NaOH
FH / NH_3	$\longrightarrow$	MgFH / NH_3
FH / NaOH + NH_3	$\longrightarrow$	MgFH / NaOH + NH_3

$$\text{FH / Na}_2\text{CO}_3 \longrightarrow \text{MgFH / Na}_2\text{CO}_3$$
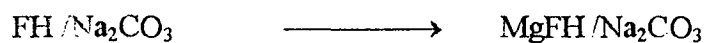
Mainly γ-Fe_2O_3 (from hydroxide hydrazinates)

$$\text{FHH / NaOH} \longrightarrow \text{MgFHH / NaOH}$$

$$\text{FHH / NH}_3 \longrightarrow \text{MgFHH / NH}_3$$

$$\text{FHH / NaOH + NH}_3 \longrightarrow \text{MgFHH / NaOH + NH}_3$$

$$\text{FHH / Na}_2\text{CO}_3 \longrightarrow \text{MgFHH / Na}_2\text{CO}_3$$
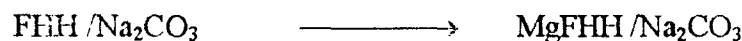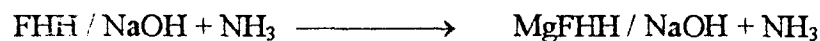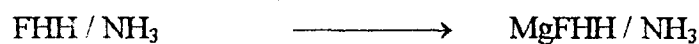
Mainly γ-Fe_2O_3 (from formate / formate hydrazinate)

$$\text{FF / NaOH} \longrightarrow \text{MgFF / NaOH}$$

$$\text{FF / NH}_3 \longrightarrow \text{MgFF / NH}_3$$

$$\text{FF / NaOH + NH}_3 \longrightarrow \text{MgFF / NaOH + NH}_3$$

$$\text{FF / Na}_2\text{CO}_3 \longrightarrow \text{MgFF / Na}_2\text{CO}_3$$

$$\text{FFH / NaOH} \longrightarrow \text{MgFFH / NaOH}$$

$$\text{FFH / NH}_3 \longrightarrow \text{MgFFH / NH}_3$$

$$\text{FFH / NaOH + NH}_3 \longrightarrow \text{MgFFH / NaOH + NH}_3$$

$$\text{FFH / Na}_2\text{CO}_3 \longrightarrow \text{MgFFH / Na}_2\text{CO}_3$$
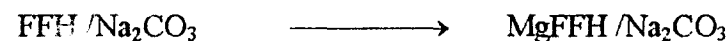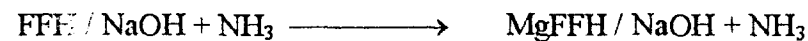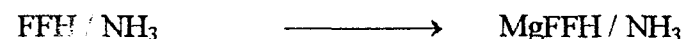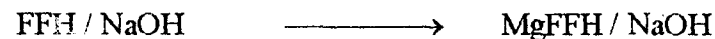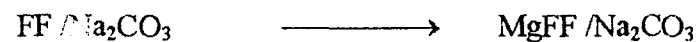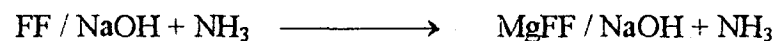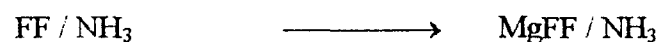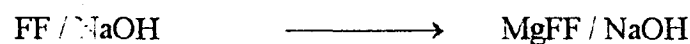
b) From commercial red oxide, RO

A commercial grade iron oxide, red oxide (RO), α-Fe_2O_3, was mixed w th the required amount of MgCO_3 and the heat treatment was followed as in 4.2.1. The product was coded as MgRO.

c) From standard γ-Fe_2O_3

A commercial γ-Fe_2O_3 that procured was used to prepare magnesium ferr te. A mixture of MgCO_3 + γ-Fe_2O_3 was heat treated in air as well as in an inert atmosph re and sintered ~ $1000^\circ/24$. The samples are coded as Mgγ-air and Mgγ-N_2.

4.2.2 Shaping of $MgFe_2O_4$

Although the ferrite samples were synthesized and sintered in pellet form, in general, as in 4.2.1, they were then crushed to fine size and used for x-ray characterization to establish the single phase ferrite formation and magnetic characterization. However, samples for initial permeability measurements were required to be in the torroid form and for dielectric and resistivity measurements in the pellet form. They are prepared as follows.

a) Pellets and torroids

The ferrite sample prepared were crushed in an agate mortar to fine size and used to prepare pellets and torroids.

Pellets

A finely ground ferrite sample was compressed into a pellet using a die. A pellet of 1–1.5 cm diameter and 0.2 – 0.3 cm thickness was obtained by applying pressure of 5 – 10 ton/cm^2 for a duration of 2 minutes.

Torroids

Torroids of size of internal diameter 1 cm and outer diameter of 2 cm were prepared from ground $MgFe_2O_4$ samples.

b) Sintering

Pellets and torroids were heat treated in a muffle furnace. All were heated initially to 700°C for 24 hours and then increased the temperature to 1000°C and maintained at that temperature for 24 hours. Samples were then furnace cooled.

4.2.3 Characterization

a) X-ray diffraction (XRD): Phase identification

The magnesium ferrite samples were x-ray analysed on Philips x-ray diffractometer model PW 1710 with Cu Kα radiation and nickel as a filter. The x-ray diffraction in the present study is used to (1) observe the impurity phase (2) confirm the completion of solid state reaction and (3) determine the lattice constants, inter planar distances, octahedral and tetrahedral site radii, bond length, x-ray density etc. As the crystallites are randomly oriented, a reflection at the particular position is due to the set of atomic planes satisfying Bragg's condition. The Bragg's law is given as,

$$n\lambda = 2d_{hkl} \sin \theta$$

where d_{hkl} is the interplanar spacing of crystal planes of miller indices (hkl), θ is the glancing angle, λ is the wavelength of x-ray radiation and 'n' is the order of diffraction.

For a cubic lattice, lattice parameter 'a', miller indices (hkl) and interplaner distance d_{hkl} are related by relation,

$$d_{hkl} = \frac{a}{\sqrt{h^2 + k^2 + l^2}}$$

The planes that diffract x-rays in inverse cubic spinel systems are (220), (311), (400), (422), (440), (533) etc. The interplaner distance (d) for each diffraction angle was calculated by the above given relation and then the lattice parameter 'a' was calculated. Finally the values of 'a' for all $MgFe_2O_4$ samples were computed by the least square method.

Measurement of bond length

The values of bond lengths (R_A and R_B) and site radii (r_A and r_B) were calculated by using the relations given below.

$$R_A = a \sqrt{3} \ (\delta + \tfrac{1}{8})$$

$$R_B = a \sqrt{1/16 - \delta/2 + 3d^2}$$

$$r_A = (u - 1/4) a \sqrt{3} - R_0$$

$$r_B = (5/8 - u) a - R_0$$

where R_A = The shortest distance between A-site (tetrahedral) cation and oxygen ion

R_B = The shortest distance between B-site (octahedral) cation and oxygen ion

r_A = Tetrahedral site radius

r_B = Octahedral site radius

R_0 = Radius of oxygen ion (1.35 Å)

δ = Deviation from oxygen ion parameter (u)

$\delta = u - u_{ideal}$ [$u_{ideal} = 0.375$ Å]

b) X-ray density, Physical density & Porosity

The x-ray density (dx), physical density (dp) and porosity (P) of the ferrite samples were calculated from the relations

$$dx = 8M/N a^3$$

$$dp = m/v$$

and

$$P(\%) = ((dx - dp)/dx) * 100$$

Where M= Molecular weight of the sample

N = Avagadro's number

a = lattice parameter.

m = Mass of the pellet in air

v = Volume of the pellet measured using mercury balance by the relation

$$v = \frac{W_1 + W_2}{d}$$

where W_1 = Weight of pellet in air

W_2 = Weight of pellet in mercury

d = Density of mercury

c) Infra - Red Analysis

The infra red analysis of all the magnesium ferrite samples were done on Shimadzu FTIR, model 8101 A. The pellets used for recording spectra were prepared by mixing small amount of ferrite powder in KBr. The IR spectra in the frequency range of 400 - 4600 cm^{-1} were recorded at room temperature.

d) Magnetic and Electric Characterization

i. Saturation magnetization

The saturation magnetization in Gauss (G) is determined by formula $4\pi Ms$. Ms is calculated as

$$Ms = (1-P)\, dx \cdot \sigma s$$

Where P is the Porosity

dx is the X-ray density

σs is saturation magnetization in emu/g

The magnetone number, that is the magnetic moment per formula unit (1_B) in Bohr magnetons is given by

$$n_B = M \cdot \sigma s / 5585$$

Where M is the molecular weight of the sample.

ii. A.C.Susceptibility

The curie temperature and domain structure of the ferrite samples were determined by a.c. susceptibility method developed by Likhite et al [132]. The powdered ferrite was taken in a quartz sample tube and placed at the centre of the pick up coil and Pt-Rh thermocouple was used to read the temperature of the sample. The sample was heated by passing d.c. current through platinum heating coils and the signal from the thermocouple was converted to temperatures. The magnetic moment and temperature were recorded till this moment becomes zero. The relative susceptibility ie. magnetic moment at higher temperature to the moment at room temperature was plotted against temperature. The curves are called χ- T curves.

iii. Initial Permeability

The initial permeability as a function of temperature was measured at 1000 Hz over the temperature range from 27 to 527°C using Hawlett Packard 4234 A, 20 Hz –1 MHz precision LCR meter. The furnace temperature was regulated within $\pm$ 3°C. The initial permeability was calculated from the low field inductance measurements with a torroidal core of 85 turns using the formula,

$$L = 0.0046 \ \mu i \ N^2 \ h \ \log d_1/d_2$$

where L is the inductance in Hz

d_1 is the outside diameter of a torroid

d_2 is the inside diameter of a torroid

μi is the initial permeability of the core

h is the height of the core in inches.

iv Resistivity

The electrical resistivity measurements of the magnesium ferrite samples were

carried out using the two terminal d.c. method, in a range of temperature from 27 to 527°C. The pellets of dimensions 10 mm diameter and 2-3 mm thickness were pressed between two platinum electrodes and then measurements were taken. The resistivity was determined by the relation,

$$\rho = \pi r^2 / t * R.$$

Where r is the radius of pellet

t is the thickness of pellet

R is the resistance

The Curie temperature of ferrites were determined from the plot log ρ against 1/T.

v Dieletric Constant and Dielectric loss Tangent

The dielectric measurements were made using the two - probe method. The pellets of 10 mm diameter and 2-3 mm thickness were used for the dieectric measurements which were carried out against frequency on Hawlett Packard 4234 A, 20 Hz – 1 MHz precision LCR meter with 16048 C test leads. The capacitance, c, was measured and used in the calculation of dielectric constant, ϵ', using the relation

$$\epsilon' = cd / \epsilon_0 \ A$$

where d is the thickness of the pellet

A is the cross-sectional area of the flat surface of the pellet and ϵ_0 is the free - space permittivity.

The variation of tan δ with the frequency is also measured along with the dielectric constant.

e) Microstructural (SEM) studies

SEM of magnesium ferrite samples were taken on a Cambridge Stereoscan S 250

Table 4.2.1 XRD data of $MgFe_2O_4$ obtained using Iron oxides prepared from Iron hydroxides / formates and their hydrazinates

MgFe₂O₄	d hkl (I/Io)								'a' (nm)	Form
MgFe₂O₄ JCPDS 17-464 low	4.84 (4)	----	2.96 (40)	----	2.53 (100)	----	----	----	1.48 (35)	0.8375	Low
MgFe₂O₄ JCPDS 17-465 high	4.85 (8)	----	2.97 (35)	----	2.53 (100)	----	----	----	1.49 (40)	0.8397	High
α-Fe₂O₃ JCPDS 13-534	----	3.66 (25)	----	2.69 (100)	----	2.51 (50)	2.20 (30)	1.84 (40)	----	----	
Mg γ- air	4.85 (3)	----	2.97 (42)	----	2.53 (100)	2.52 (44)	----	----	1.48 (41)	0.8388	
Mg γ- N₂	4.86 (4)	----	2.97 (41)	----	2.53 (100)	----	----	----	1.48 (22)	0.8391	
Mg.RO air	4.84 (4)	----	2.97 (43)	----	2.53 (100)	----	----	----	1.48 (40)	0.8386	
Mg.FH / NaOH air	4.85 (3)	----	2.97 (37)	----	2.53 (100)	----	----	----	1.48 (40)	0.8398	
Mg.FHH / NaOH air	4.85 (3)	----	2.97 (35)	----	2.53 (100)	----	----	----	1.48 (36)	0.8393	
Mg.FHH / NaOH N₂	4.81 (2)	----	2.96 (36)	----	2.53 (100)	----	----	----	1.48 (25)	0.8380	
Mg.FF / NaOH air	4.84 (3)	----	2.97 (42)	----	2.53 (100)	----	----	----	1.48 (44)	0.8388	
Mg.FF / NaOH N₂	4.85 (3)	----	2.97 (40)	----	2.53 (100)	----	----	----	1.48 (44)	0.8407	
Mg.FFH / NaOH air	4.85 (4)	----	2.97 (40)	----	2.53 (100)	----	----	----	1.48 (40)	0.8394	
Mg.FFH / NaOH N₂	4.88 (2)	----	2.97 (34)	----	2.54 (100)	----	----	----	1.48 (46)	0.8407	
Mg.FH / NH₃ air	4.81 (3)	----	2.95 (34)	2.69 (1)	2.52 (100)	----	----	1.84 (2)	1.48 (39)	0.8349	
Mg.FHH / NH₃ air	4.83 (5)	3.69 (1)	2.95 (33)	2.70 (5)	2.51 (100)	----	2.21 (1)	1.84 (3)	1.48 (42)	0.8353	
Mg.FF / NH₃ air	4.83 (3)	3.69 (4)	2.96 (40)	2.70 (12)	2.52 (100)	----	2.21 (3)	1.84 (4)	1.48 (42)	0.8360	
Mg.FFH / NH₃ air	4.83 (3)	3.69 (4)	2.96 (33)	2.70 (11)	2.52 (100)	2.51 (56)	2.21 (3)	1.84 (4)	1.48 (38)	0.8363	
Mg.FH / NaOH + NH₃ air	4.80 (2)	----	2.95 (35)	2.69 (2)	2.51 (100)	2.51 (57)	----	----	1.48 (43)	0.8343	
Mg.FHH / NaOH + NH₃ air	4.81 (3)	3.69 (2)	2.95 (39)	2.71 (6)	2.52 (100)	----	2.21 (1)	1.84 (2)	1.48 (40)	0.8356	
Mg.FF / NaOH + NH₃ air	4.81 (4)	----	2.95 (36)	2.70 (1)	2.52 (100)	2.51 (51)	2.21 (0.3)	----	1.48 (37)	0.8355	
Mg.FFH / NaOH + NH₃ air	4.84 (2)	----	2.96 (38)	----	2.52 (100)	----	----	----	1.48 (47)	0.8356	
Mg.FH / Na₂CO₃ air	4.84 (3)	----	2.96 (38)	2.69 (2)	2.52 (100)	----	----	1.84 (1)	1.48 (45)	0.8365	
MgFHH/Na₂CO₃ air	4.81 (4)	3.69 (0.4)	2.95 (35)	2.69 (2)	2.52 (100)	2.51 (52)	2.21 (0.4)	1.84 (0.6)	1.48 (39)	0.8357	
Mg.FF / Na₂CO₃ air	4.83 (4)	3.68 (0.5)	2.95 (36)	2.71 (2)	2.52 (100)	----	2.21 (0.7)	1.84 (1)	1.48 (38)	0.8359	
Mg.FFH/Na₂CO₃ air	4.83 (4)	----	2.96 (36)	----	2.52 (100)	----	----	----	1.48 (35)	0.8370	

Table: 4.2.2 X-ray density, physical density and porosity of magnesium ferrites usi ig

iron oxides prepared from iron hydroxides, iron formates and their

hydrazinates

Sr. Nos.	Mg- Ferrite Sample	X-ray density g/cm^3	Physical density g/cm^3	Poros ty (%)
1	Mg.RO	4.50	3.22	28.5 }
2	Mgγ	4.50	3.34	25.7
3	Mgγ (N₂)	4.50	----	----
4	Mg.FH / NaOH	4.49	----	----
5	Mg.FHH / NaOH	4.49	3.35	25.3)
6	Mg.FHH / NaOH (N₂)	4.51	3.35	25.7)
7	Mg.FF / NaOH	4.50	3.17	29.6)
8	Mg.FF / NaOH (N₂)	4.47	---	---
9	Mg.FFH / NaOH	4.49	---	---
10	Mg.FFH / NaOH (N₂)	4.47	---	---
11	Mg.FH / NH₃	4.57	3.37	26.1)
12	Mg.FHH / NH₃	4.56	3.87	15.0)
13	Mg.FF / NH₃	4.55	3.71	18.4 '
14	Mg.FFH / NH₃	4.54	3.15	30.7 .
15	Mg.FH / NaOH+NH₃	4.57	3.27	28.5 }
16	Mg.FHH / NaOH+NH₃	4.55	3.15	30.8)
17	Mg.FF / NaOH+NH₃	4.56	3.26	28.3)
18	Mg.FFH / NaOH+NH₃	4.55	---	---
19	Mg.FH / Na₂CO₃	4.54	3.12	31.1)
20	Mg.FHH / Na₂CO₃	4.55	3.47	23.8)
21	Mg.FF / Na₂CO₃	4.55	---	---
22	Mg.FFH / Na₂CO₃	4.53	2.87	36.8)

The values of bond lengths (R_A and R_B) and site radii (r_A and r_B) are presented in Table 4.2.3 The bond length R_B is greater than R_A as expected is observed.

Table 4.2.3 Lattice parameter, bond length (R_A & R_B) and site radii (r_A and r_B) for magnesium ferrites .

Sr. Nos	Precursors	Mean Lattice parameter 'a'(nm)	Bond Length (nm)		Site radii (nm)	
			R_A-O	R_B-O	r_A	r_B
1	Mg.RO	0.8386	0.1903	0.2047	0.0553	0.0696
2	Mg-γ	0.8388	0.1903	0.2048	0.0553	0.0697
3	Mg-γ (N_2)	0.8391	0.1904	0.2049	0.0554	0.0697
4	Mg.FH / NaOH	0.8398	0.1905	0.2050	0.0555	0.0699
5	Mg.FHH / NaOH	0.8393	0.1904	0.2049	0.0554	0.0698
6	Mg.FHH / NaOH (N_2)	0.8380	0.1901	0.2046	0.0551	0.0695
7	Mg.FF / NaOH	0.8388	0.1903	0.2048	0.0553	0.0697
8	Mg.FF / NaOH (N_2)	0.8407	0.1908	0.2053	0.0558	0.0701
9	Mg.FFH / NaOH	0.8394	0.1905	0.2049	0.0555	0.0698
10	Mg.FFH / NaOH (N_2)	0.8407	0.1908	0.2053	0.0558	0.0701
11	Mg.FH / NH_3	0.8349	0.1894	0.2038	0.0544	0.0687
12	Mg.FHH / NH_3	0.8353	0.1895	0.2039	0.0545	0.0688
13	Mg.FF / NH_3	0.8360	0.1897	0.2041	0.0547	0.0690
14	Mg.FFH / NH_3	0.8363	0.1898	0.2042	0.0548	0.0691
15	Mg.FH / NaOH+NH_3	0.8343	0.1893	0.2037	0.0543	0.0686
16	Mg.FHH / NaOH+NH_3	0.8356	0.1896	0.2040	0.0546	0.0689
17	Mg.FF / NaOH+NH_3	0.8355	0.1896	0.2040	0.0546	0.0689
18	Mg.FFH / NaOH+NH_3	0.8356	0.1896	0.2040	0.0546	0.0689
19	Mg.FH / Na_2CO_3	0.8365	0.1898	0.2042	0.0548	0.0691
20	Mg.FHH / Na_2CO_3	0.8357	0.1896	0.2040	0.0546	0.0689
21	Mg.FF / Na_2CO_3	0.8359	0.1897	0.2041	0.0547	0.0690
22	Mg.FFH / Na_2CO_3	0.8370	0.1899	0.2044	0.0549	0.0692

MK III. A well polished surface of the pellet was used for taking micrographs. The average grain size of these samples were computed from these SEM micrographs.

4.2.4 Results

a) X-ray analysis

The observed d_{hkl} values and their respective intensities of all samples of ferrite are matched with the JCPDS files for $MgFe_2O_4$ [97]. Some of the important d_{hkl} values and respective I/Io percentages are tabulated in Table 4.2.1 along with the JCPDS file values for $MgFe_2O_4$, both the low and high temperature forms and α-Fe_2O_3 [62]. The d_{hkl} values of α-Fe_2O_3 are presented in the table to identify the presence of any unreacted iron oxide in the ferrite formed to confirm the completion of the reaction. The table also includes lattice 'a' parameter (in nanometre, nm) of all ferrite samples.

Lattice parameter for $MgFe_2O_4$ samples ranges from 0.8343 to 0.8407 nm and the values indicate that they cover the lattice parameter of the ferrite from low temperature form, 0.8375 nm to the high temperature form, 0.8397 nm.

$MgFe_2O_4$ prepared from standard γ-Fe_2O_3 (Mgγ) in air and N_2 show lattice parameter of 0.8388 and 0.8391 nm, respectively, while the ferrite from commercial red oxide, Mgα, indicates a = 0.8386 nm.

The ferrites synthesized in N_2 from γ-Fe_2O_3 / mixture of γ-Fe_2O_3 + α-Fe_2O_3 that obtained from iron formate / formate hydrazinate, MgFF/NaOH and MgFFH/NaOH show a = 0.8407 nm, whereas that sintered in air indicates lattice parameter, respectively 0.8388 and 0.8394 nm.

X-ray densities, dx of all samples and physical densities, dp of few are presented in Table 4.2.2. Porosity measured from these densities are also included in the table. A porosity range from 15 to 36 (%) is observed.

b) Infra red analysis

The IR spectra of all the magnesium ferrite samples are shown in Fig 4.2. . The IR spectroscopy is an important technique to describe the local symmetries in cry talline [109] and non-crystalline solids [110] and, various ordering phenomena in spinels [111 – 112].

In the present IR studies, the high frequency band v_1 between 565 – 580 cr 1^{-1} and low frequency band v_2 at ~ 410 cm^{-1} and between 425 – 440 cm^{-1} match well w th the reported $MgFe_2O_4$ [113]. This confirms the formation of $MgFe_2O_4$. Since mag esium ferrite is sensitive to humidity, the absorption bands are also observed at ~ 340(cm^{-1}. Then bands are due to stretching and bending vibrations of water molecule [114].

The lattice vibrations of oxide ions with cations give rise to absorption b; nds in spinel ferrites, producing various frequencies for the unit cell. Generally the spinel ferrites show four IR bands, v_1, v_2, v_3 and v_4 in the range of 100 – 1000 cm^{-1} The occurrences of these four bands have been computed on the basis of group thec retical calculations, using space groups and symmetries.

The first three fundamental bands are due to [115] tetrahedral and oct hedral complexes and the fourth one due to some type of lattice vibrations. It has been pointed out [116] that vibrational frequencies depend on the mass of the cation, bonding for ;e and unit cell dimensions.

For inverse and partially inverse spinels these four active models are triply degenerate and may split [117] into three vibrations. If the splitting is not too lar ;e and there is certain statistical distribution of various cations over tetrahedral and oct hedral sites, one c not observe the splitting but only broadening of the spectral lines in he IR spectra. This may be the reason why such behaviour is observed in our samples.

Mg FH / NaOH / air

Mg FHH / NaOH / air

Mg FFH / NaOH / air

Mg FHH / NH$_3$ / air

Mg FFH / Na$_2$CO$_3$ / air

Mg RO / air

Mg FHH / NaOH / N$_2$

Mg FF / NaOH / N$_2$

Mg Y / N$_2$

%T

Wave number (cm-1)
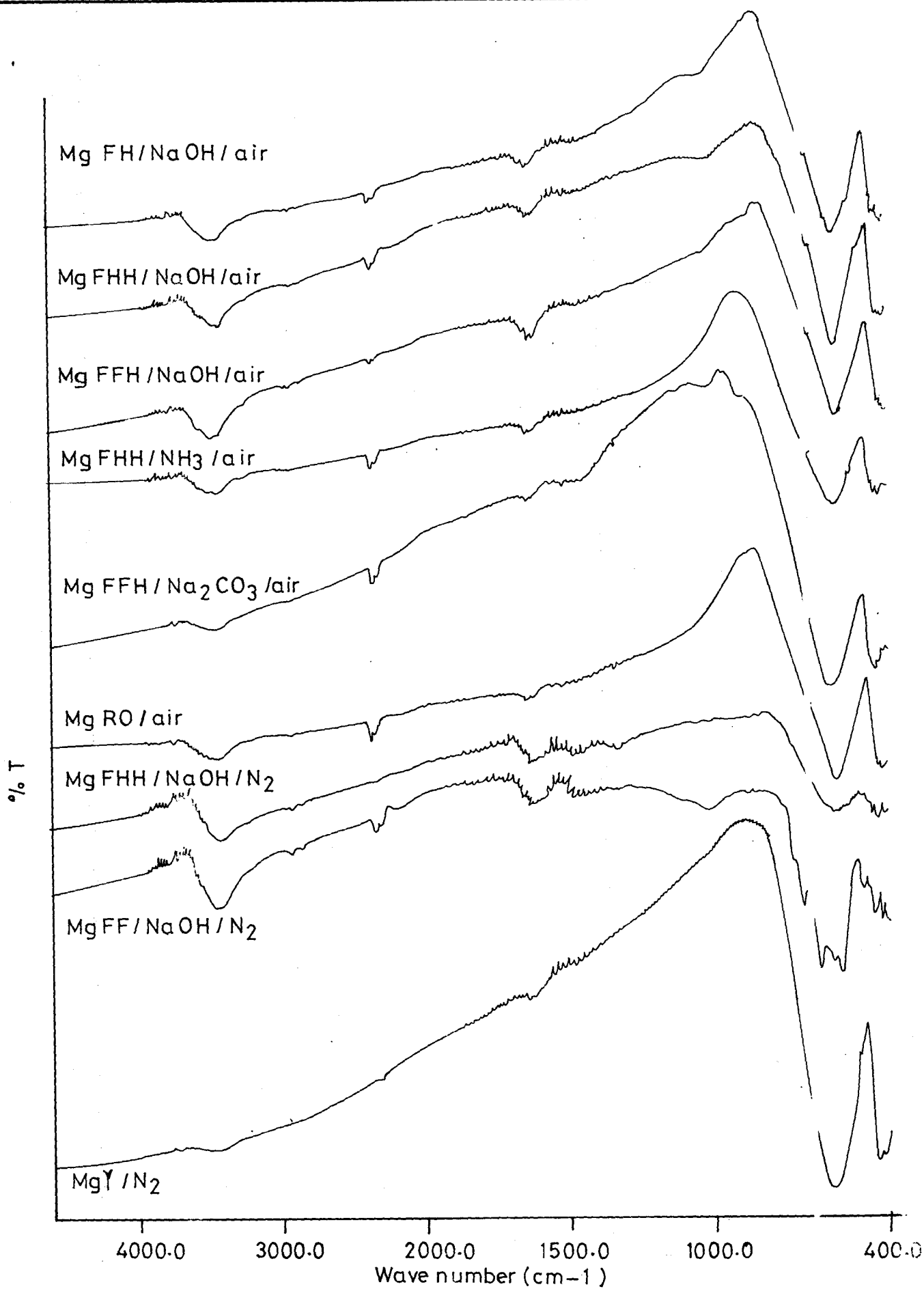
FIG. 4.2.1:—IR Spectra of MgFe$_2$O$_4$.

Table 4.2.4   Saturation magnetization (σ_S), $4\pi MS$, and magneton number (n_B) of

magnesium ferrites

Sr. Nos.	Mg- Ferrite Samples	Saturation magnetization		Magneton number (n_B)
		σ_S (emu/g)	$4\pi MS$ (Gauss)	
1	Mg.RO	23.05	----	0.82
2	Mg-γ	22.56	949	0.80
3	Mg-γ (N_2)	18.86	----	0.67
4	Mg.FH / NaOH	27.28	----	0.98
5	Mg.FHH / NaOH	27.45	1158	0.98
6	Mg.FF / NaOH	29.75	1185	1.06
7	Mg.FFH / NaOH	20.45	----	0.73
8	Mg.FH / NH_3	23.05	----	0.83
9	Mg.FHH / NH_3	21.46	1044	0.77
10	Mg.FF / NH_3	19.57	912	0.70
11	Mg.FFH / NH_3	20.45	----	0.73
12	Mg.FH / NaOH+NH_3	24.34	----	0.87
13	Mg.FHH / NaOH+NH_3	----	852	----
14	Mg.FF / NaOH+NH_3	21.25	872	0.76
15	Mg.FFH / NaOH+NH_3	27.14	----	0.97
16	Mg.FH / Na_2CO_3	20.81	----	0.75
17	Mg.FHH / Na_2CO_3	22.78	----	0.82
18	Mg.FF / Na_2CO_3	26.33	----	0.94
19	Mg.FFH / Na_2CO_3	27.77	----	0.99

ii. A. C. Susceptibility

Variation of normalized susceptibility, χ_{ac} /χ_{RT} with temperature for $MgFe_2O_4$

samples are given in Figures 4.2.2 a, b & c. It is seen that the χ_{ac} is, in general,

dependent on the increase in temperature upto Curie temperature. The nature of such

dependence gives an idea about whether the domains are single domain (SD),

Legend (top right):
Mg FH / Na(H + NH$_3$
Mg FHH / N$_{10}$H + NH$_3$
Mg FF / Na(H + NH$_3$
Mg FFH / N$_{10}$H + NH$_3$

Y-axis: $\dfrac{X_T}{X_{RT}}$ →

X-axis: Temperature (K) →

FIG. 4.2.2a:- Temperature dependence of low field a.c. Susceptibility of Mg Fe$_2$O$_4$.
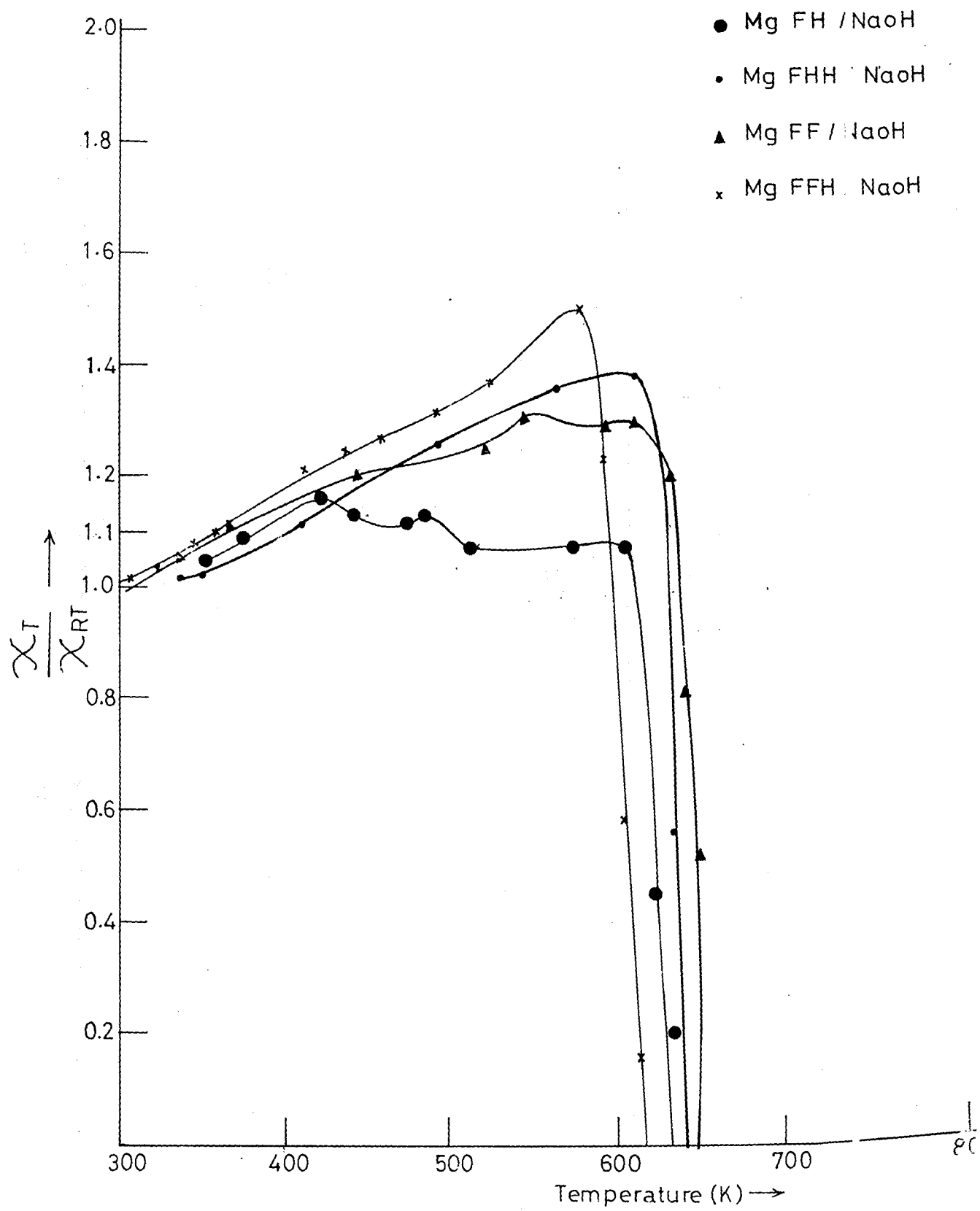
FIG. 4.2.2 b:- Temperature dependence of low field a. c. Susceptibility of $Mg\,Fe_2O$
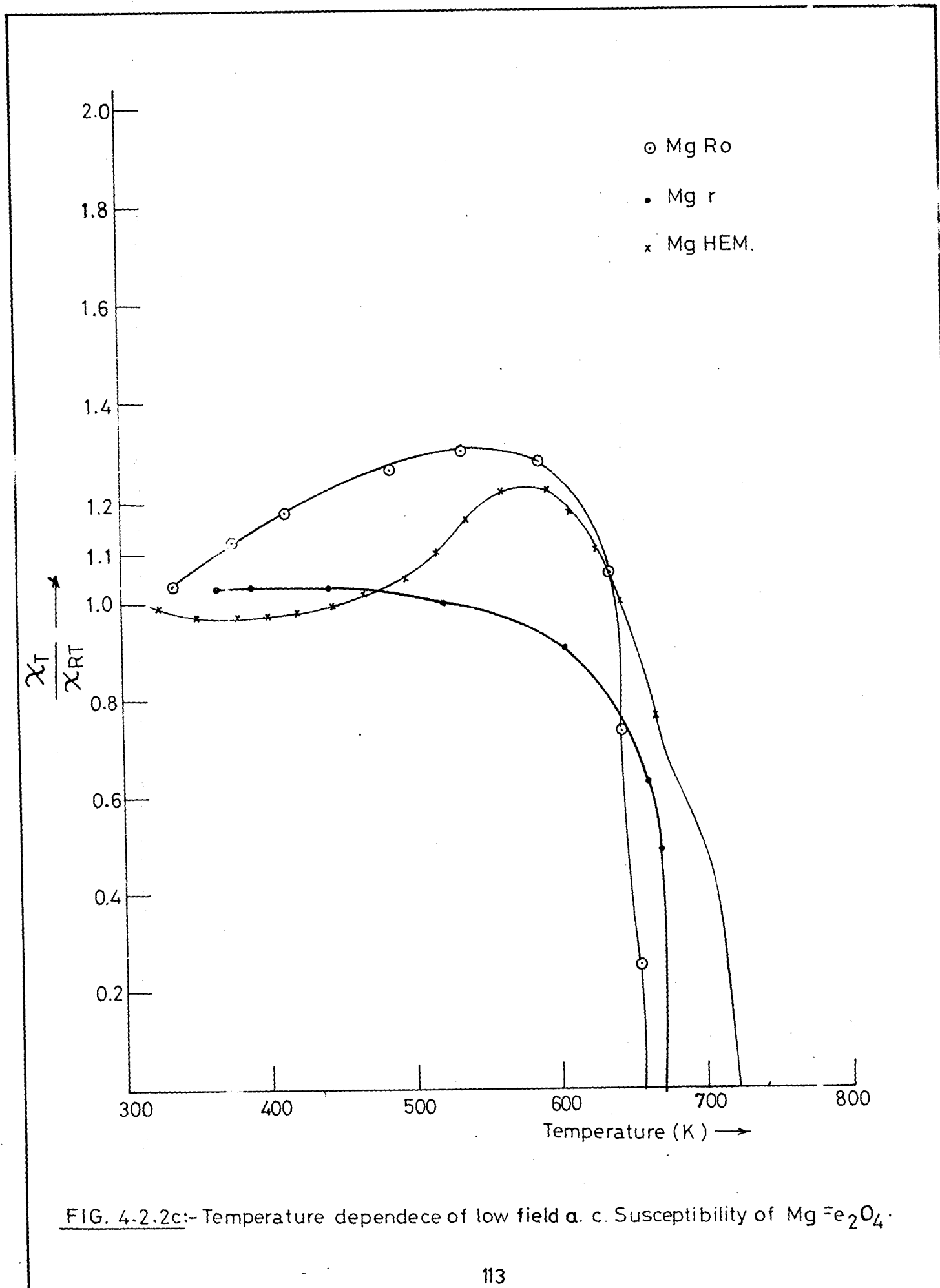
FIG. 4.2.2c:- Temperature dependece of low field a. c. Susceptibility of $Mg\ Fe_2O_4$.

113

The v_1 band is assigned to intrinsic vibrations of the tetrahedral group and v_2 to

the octahedral group [113, 118]. The absorption band v_1 is caused by stretching of

tetrahedral metal – oxygen and v_2 by the oxygen vibrations in the direction perpendicular

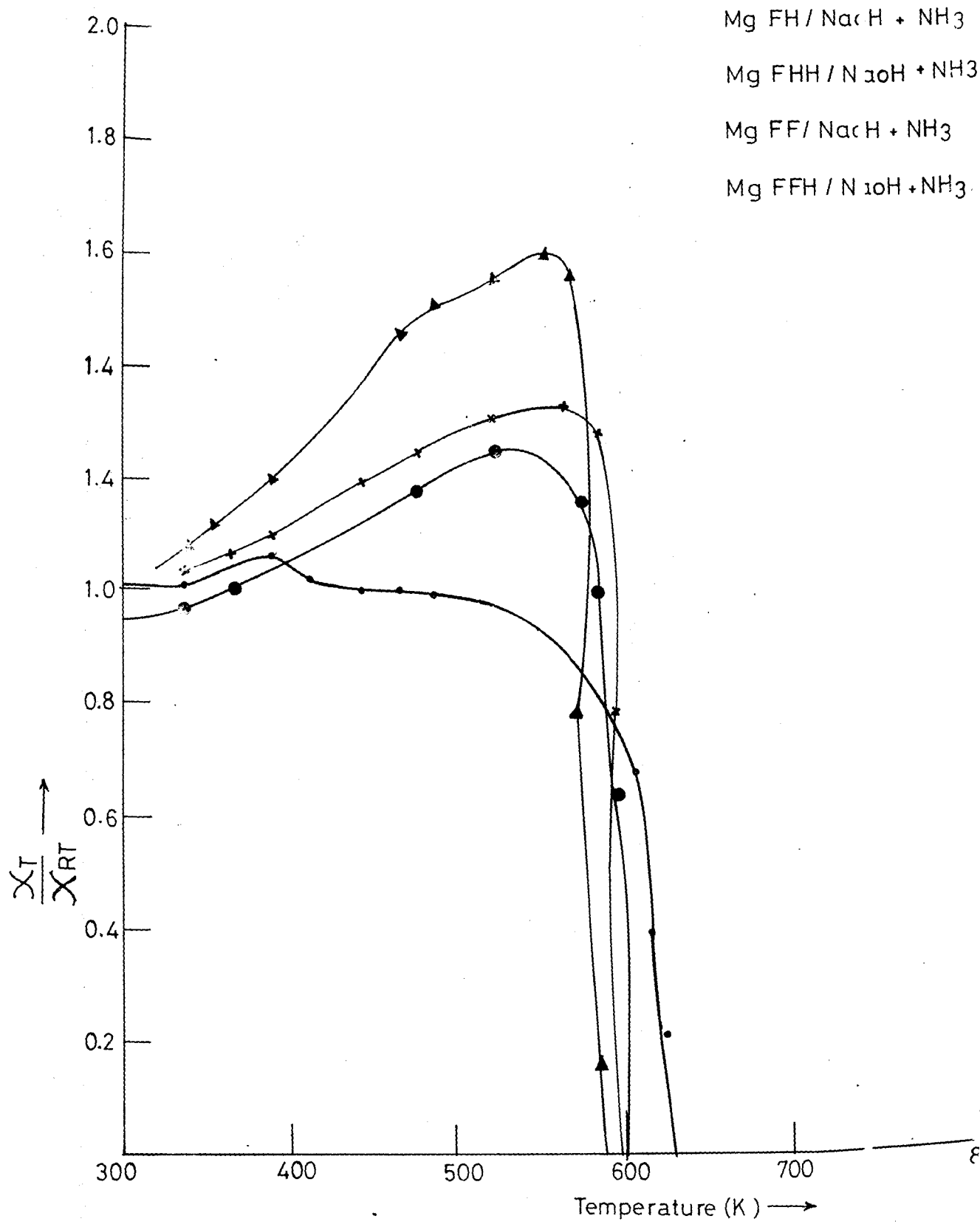to the tetrahedral oxygen ion axis. These two have been associated with the vibrations of

the metal ions in the isotropic force fields to their octahedral and tetrahedral

environments. The bands v_3 and v_4 are not observed in spinel ferrites [119].

Cubic lattice distortion or Jahn - Teller effect have marked influence on the IR

spectra [120 – 122] of spinels and the presence of ferrous ions, Fe^{2+}, in spinel car cause

[123] splitting of absorption bands. The absence of such split or double band ~ 600 cm^{-1}

(v_1 band) indicate no impurity Fe^{2+} ions in our samples. However, few samples do show

such presence (Fig. 4.2.1) of the band or just slight dent in the region or a shoulder in the

spectra ~ 600 cm^{-1}.

c) Magnetic and Electric Characterization

i. Saturation magnetization

A saturation magnetization value, σs in emu/g, for all ferrite samples are given in

Table 4.2.4. The values at RT are found to be in the range of 18 – 30 emu/g. These are in

the comparable range of 22 – 28 emu/g reported for $MgFe_2O_4$ [104, 124 – 126, 132].

Magnetization, $4\pi Ms$, values calculated from relation mentioned above are also presented

in the table and they are in the range 852 – 1185 Gauss. These values are low as

compared to the reported values of 1140 – 1530 G [99, 127 – 128]. The magnetone

number, n_B between 0.67 and 1.06 is observed for all samples of which few are

comparable to the reported values [104 – 105, 108] of 0.93 – 1.2 Bohr magnetone.
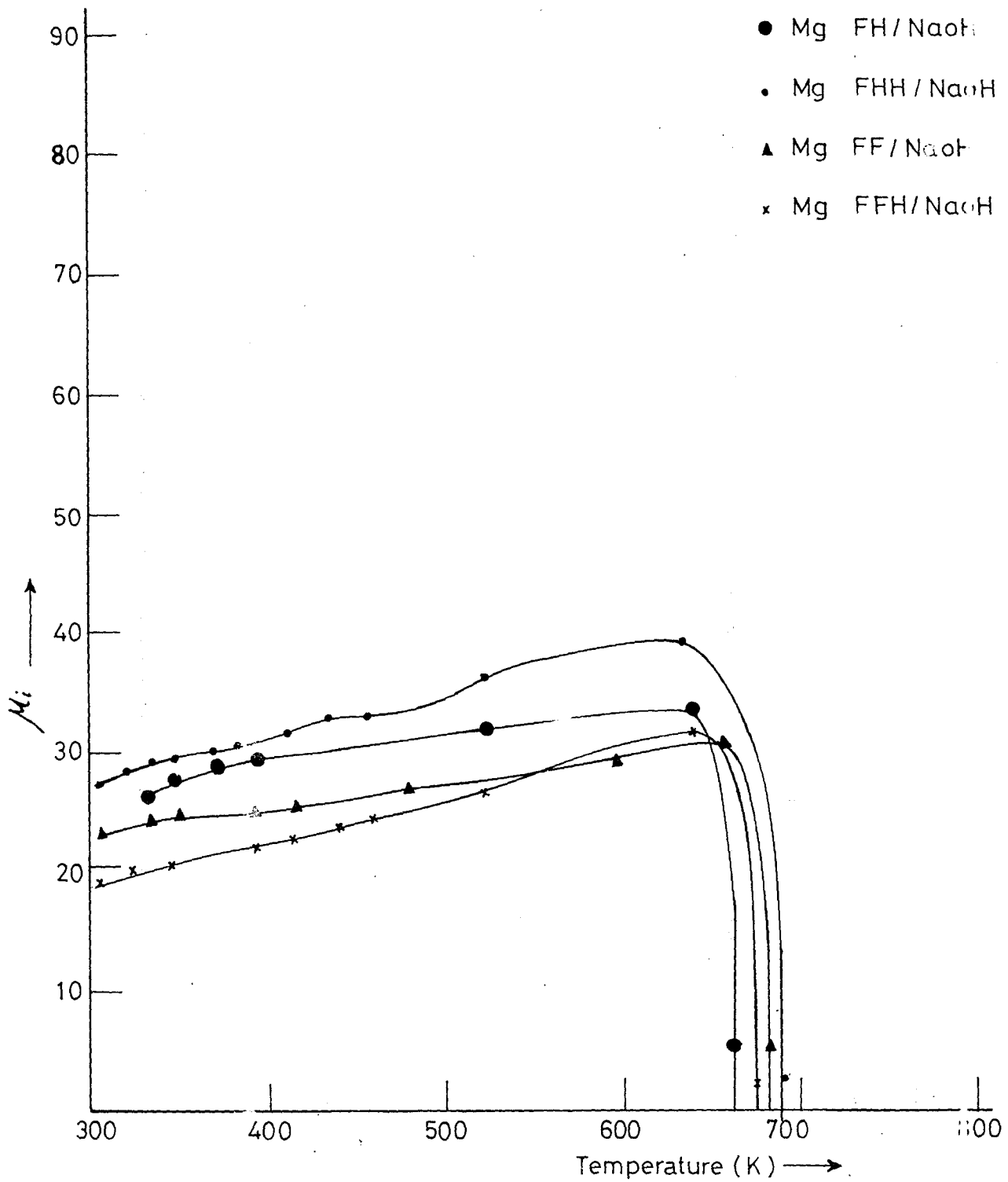
FIG. 4.2.3a:– Thermal Variation of Permeability of $MgFe_2O_4$.

Legend:
- ● Mg FH/NaoH
- • Mg FHH/NaoH
- ▲ Mg FF/NaoH
- × Mg FFH/NaoH
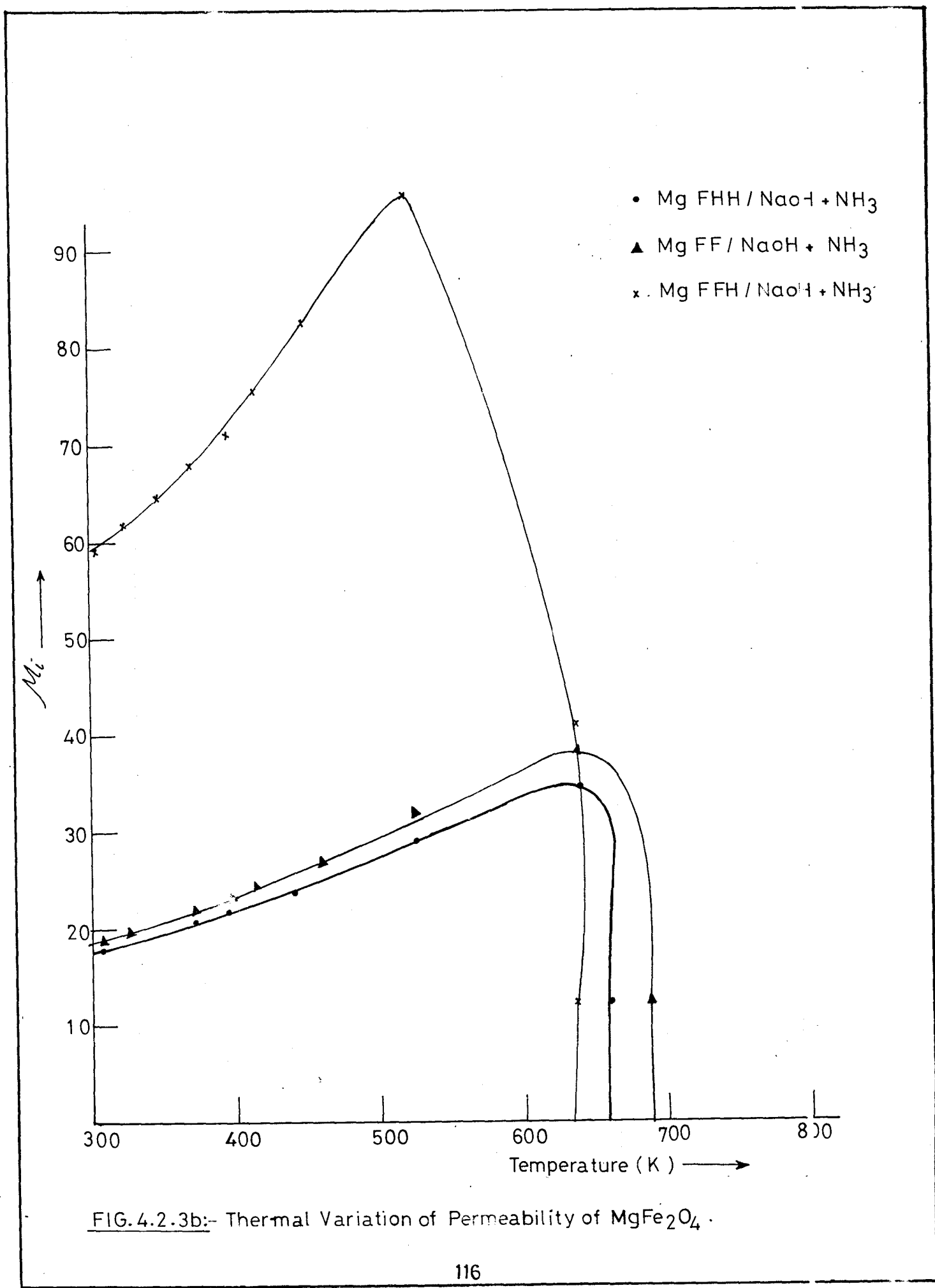
FIG.4.2.3b:- Thermal Variation of Permeability of MgFe$_2$O$_4$.
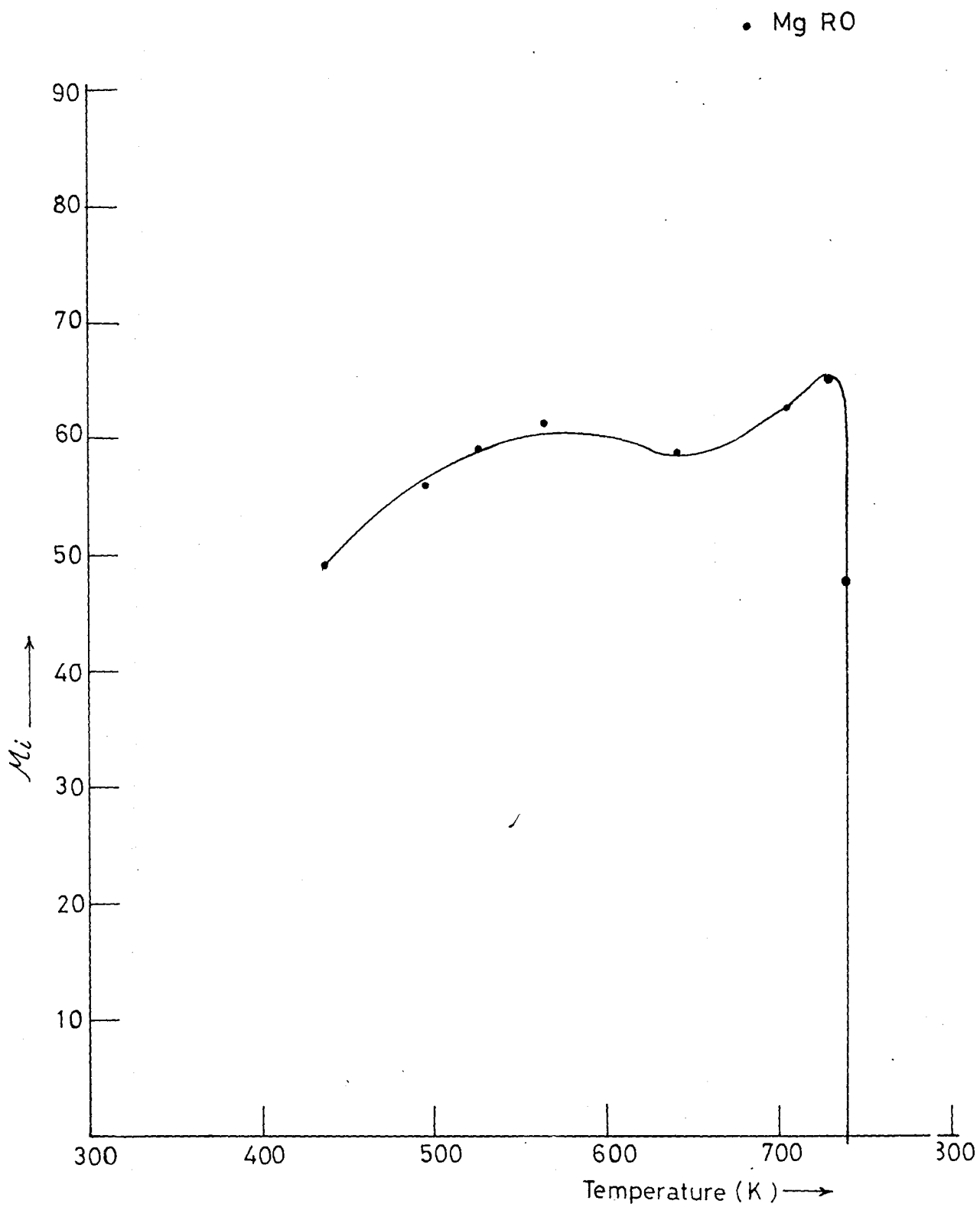
FIG. 4.2.3c:-Thermal Variation of Permeability of $MgFe_2O_4$.
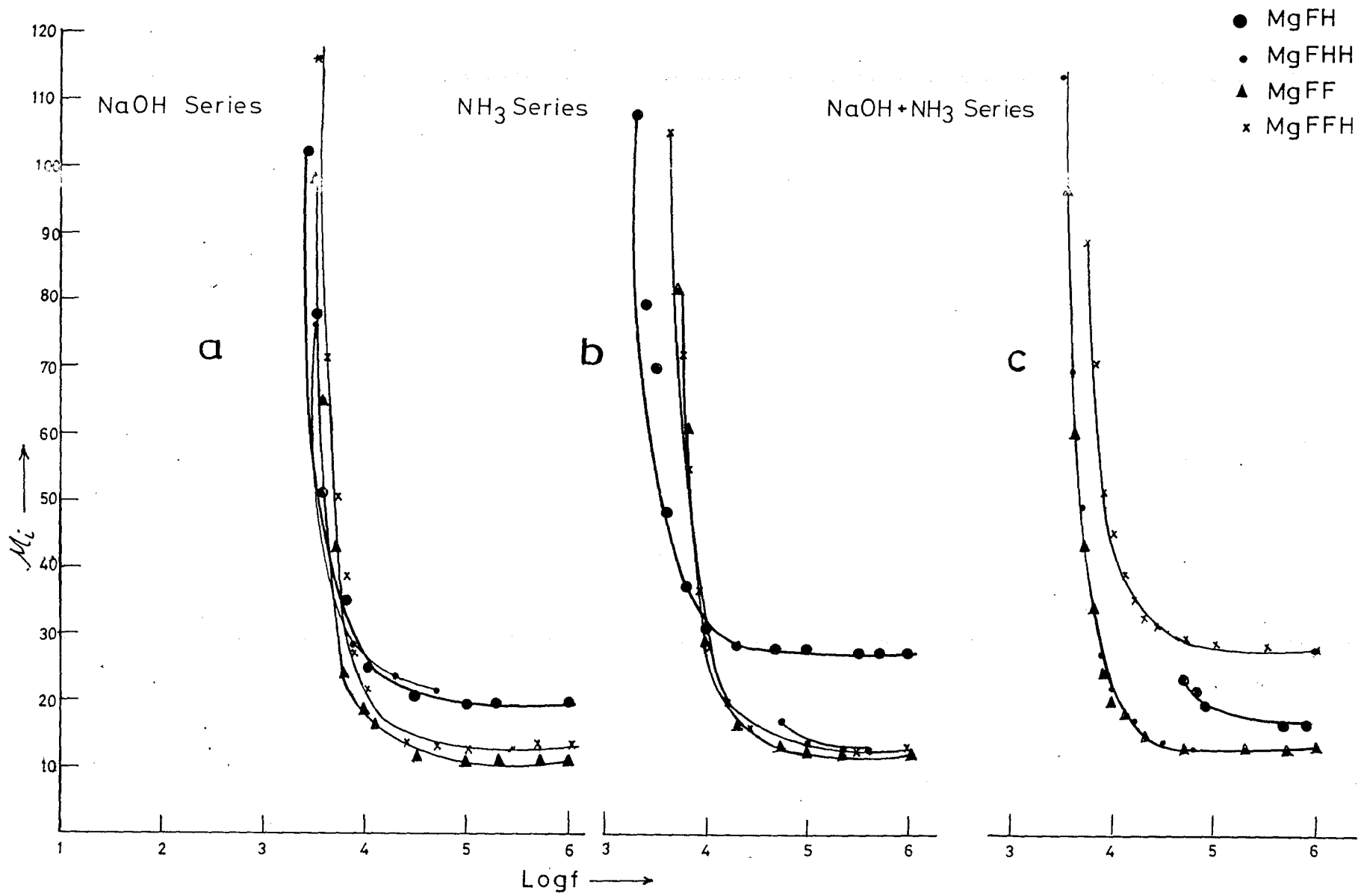
FIG. 4.2.4 :— Frequency dependence of Permeability of $MgFe_2O_4$.
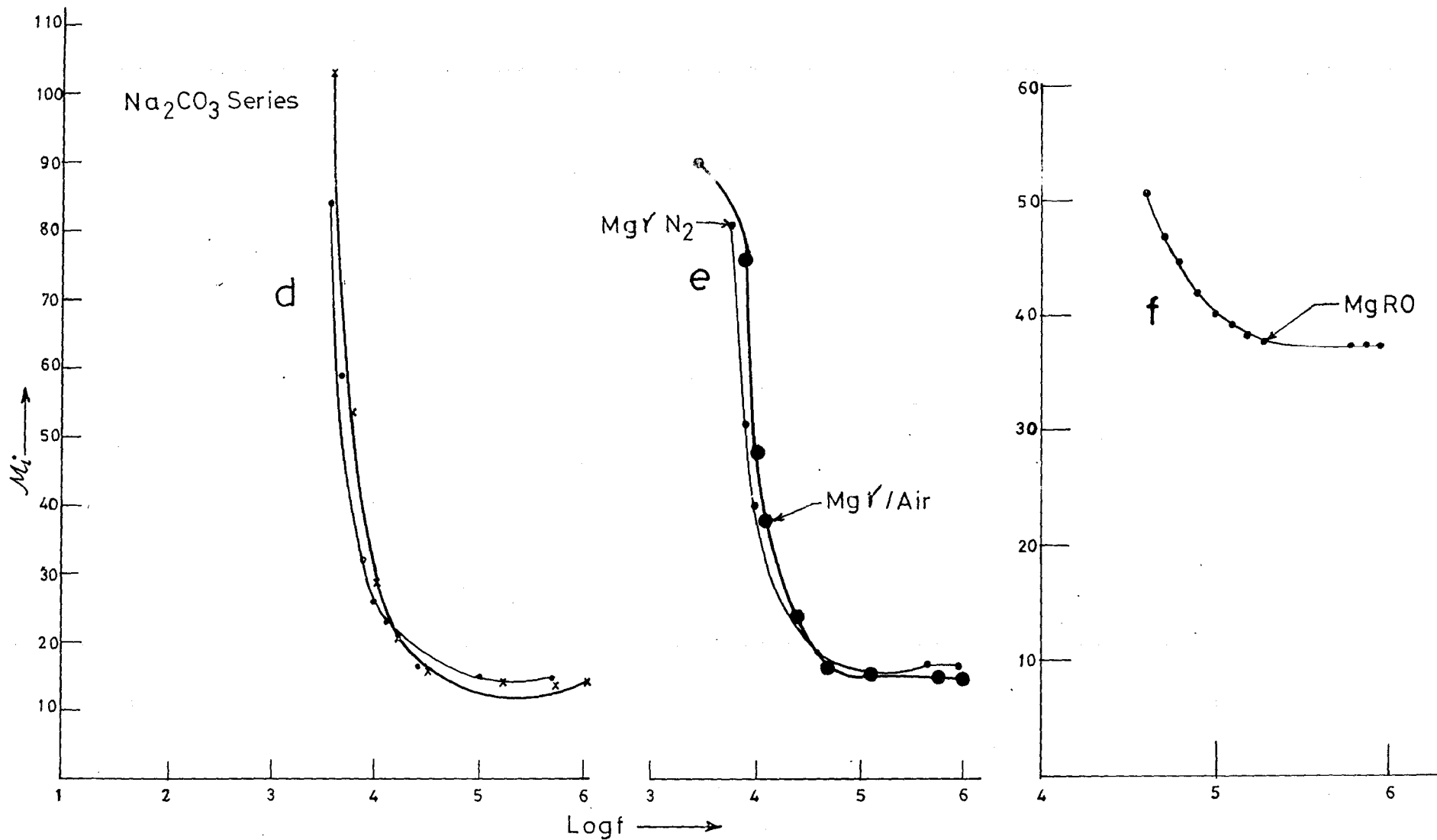
FIG. 4.2.4 :- Frequency dependence of Permeability of $Mg\,Fe_2O_4$.
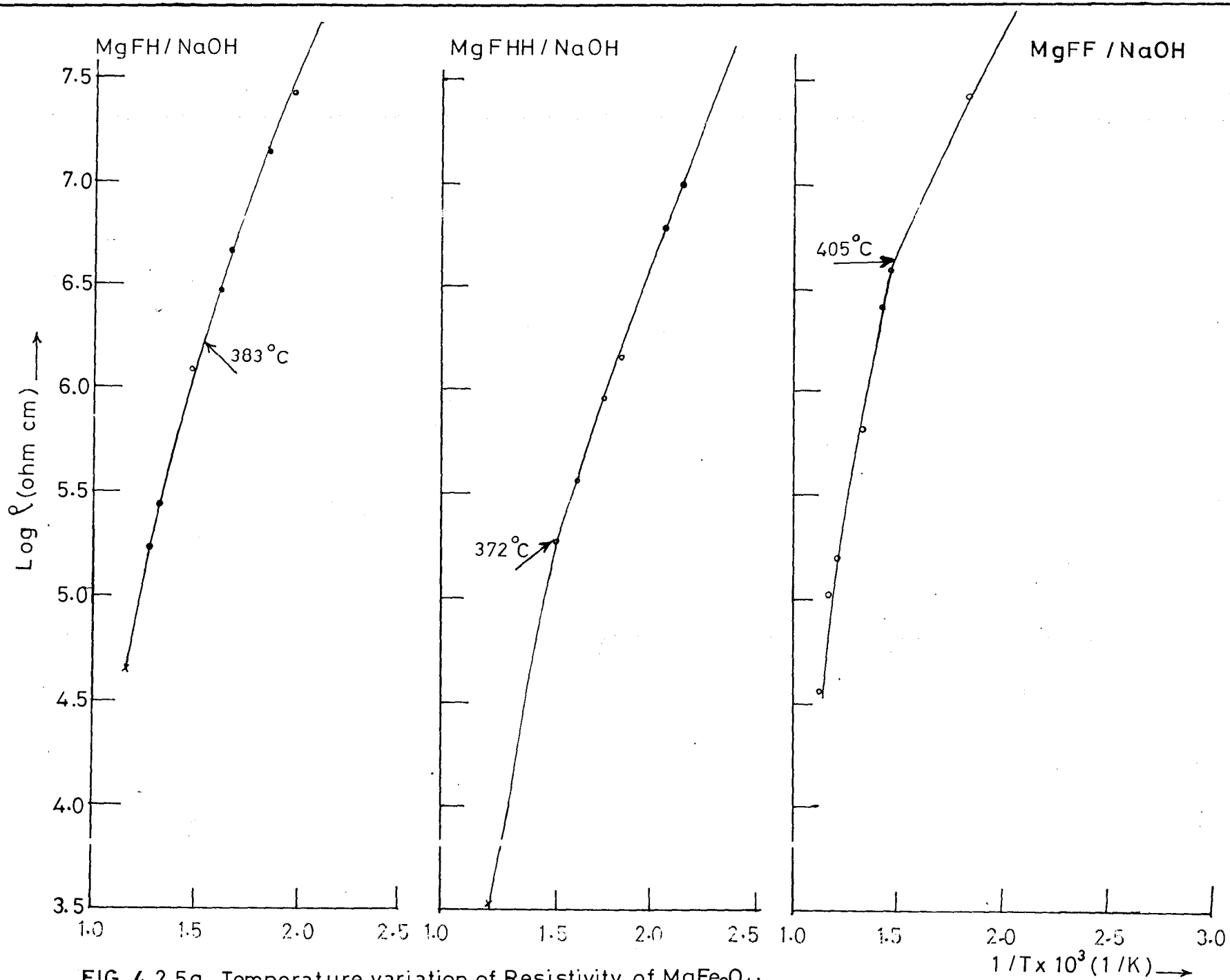
FIG. 4.2.5a Temperature variation of Resistivity of MgFe$_2$O$_4$.
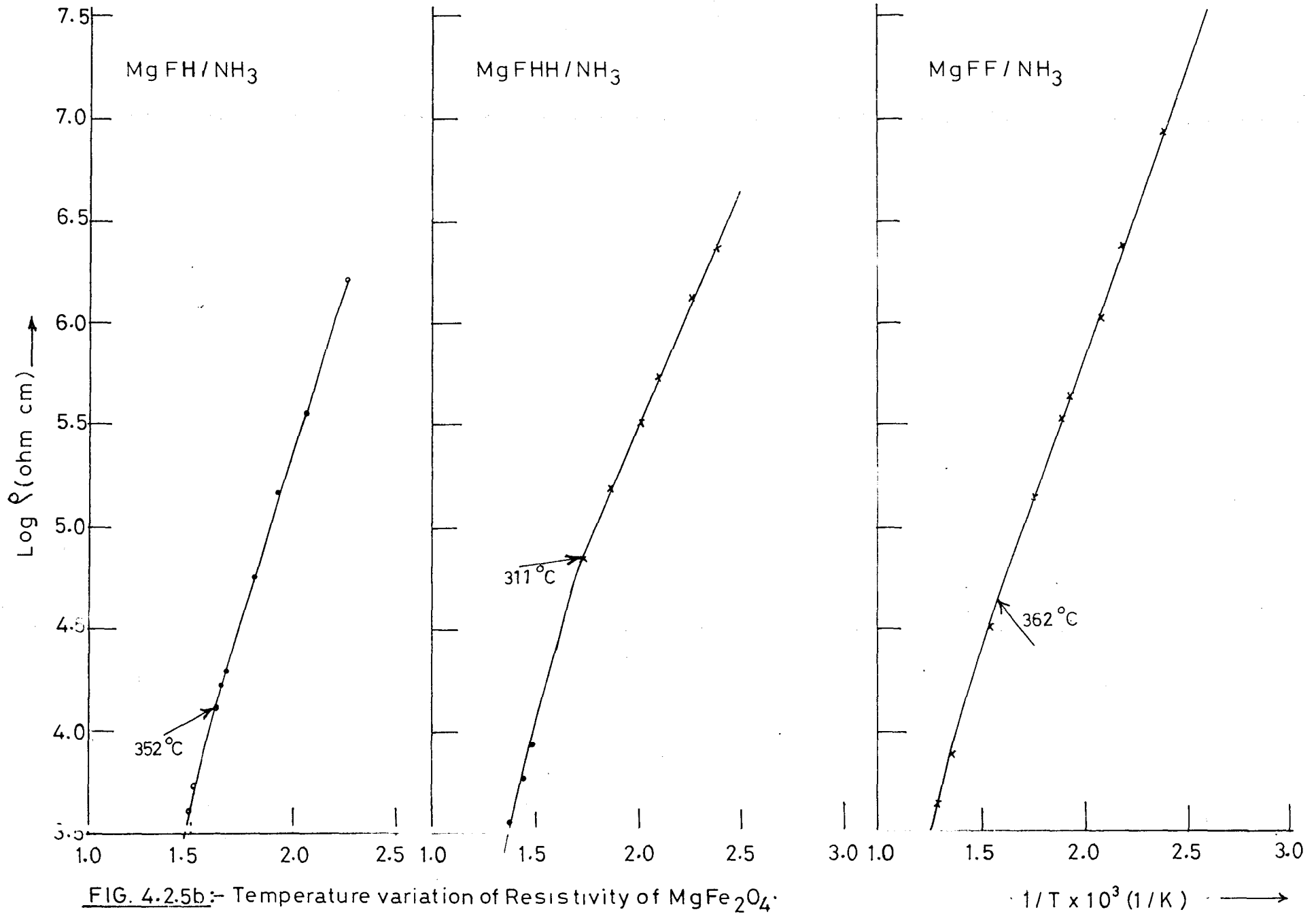
FIG. 4.2.5b :- Temperature variation of Resistivity of $MgFe_2O_4$.

FIG. 4.2.5c:- Temperature variation of Resistivity of $MgFe_2O_4$.

FIG. 4.2.5d :— Temperature variation of Resistivity of MgFe$_2$O$_4$.
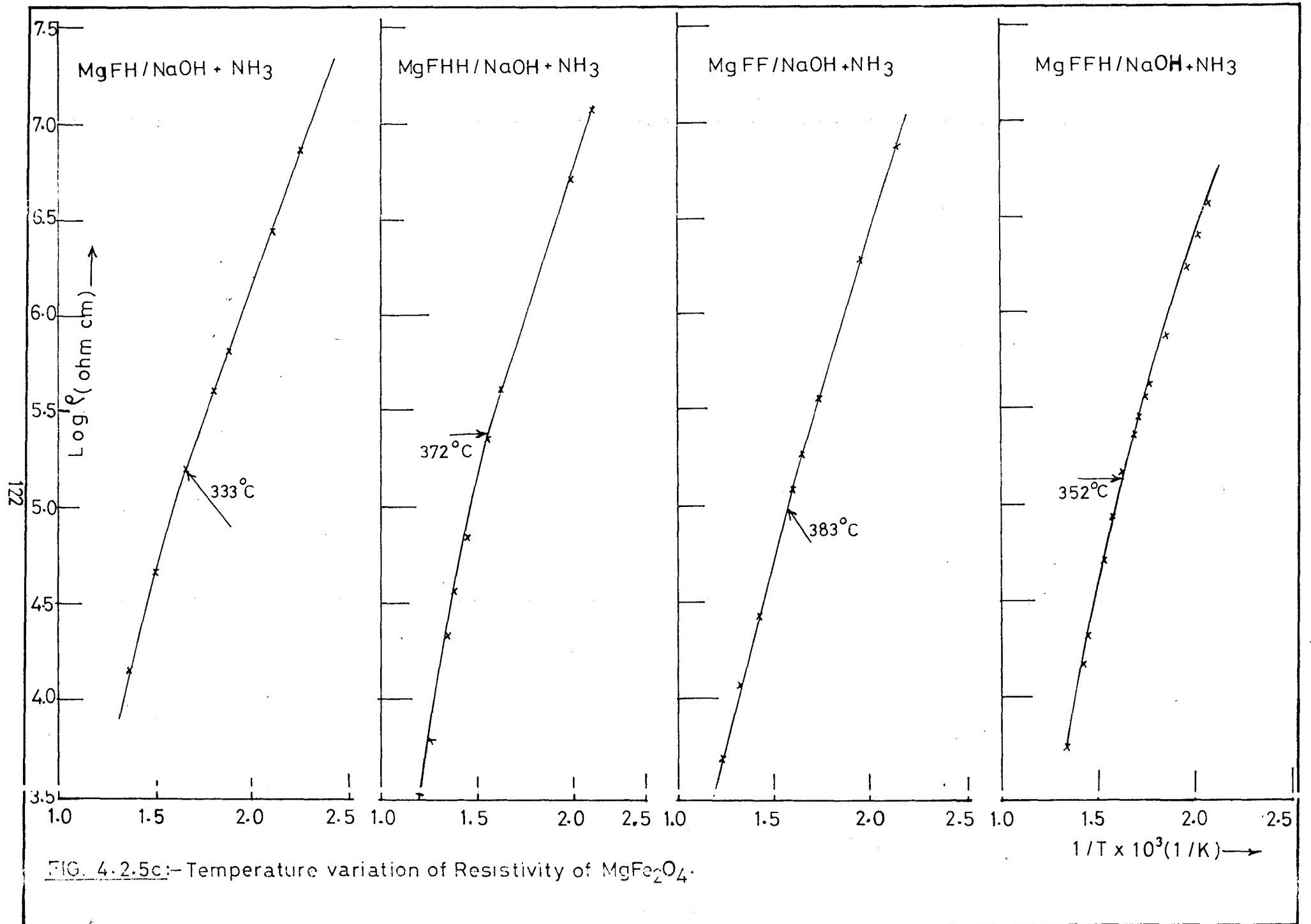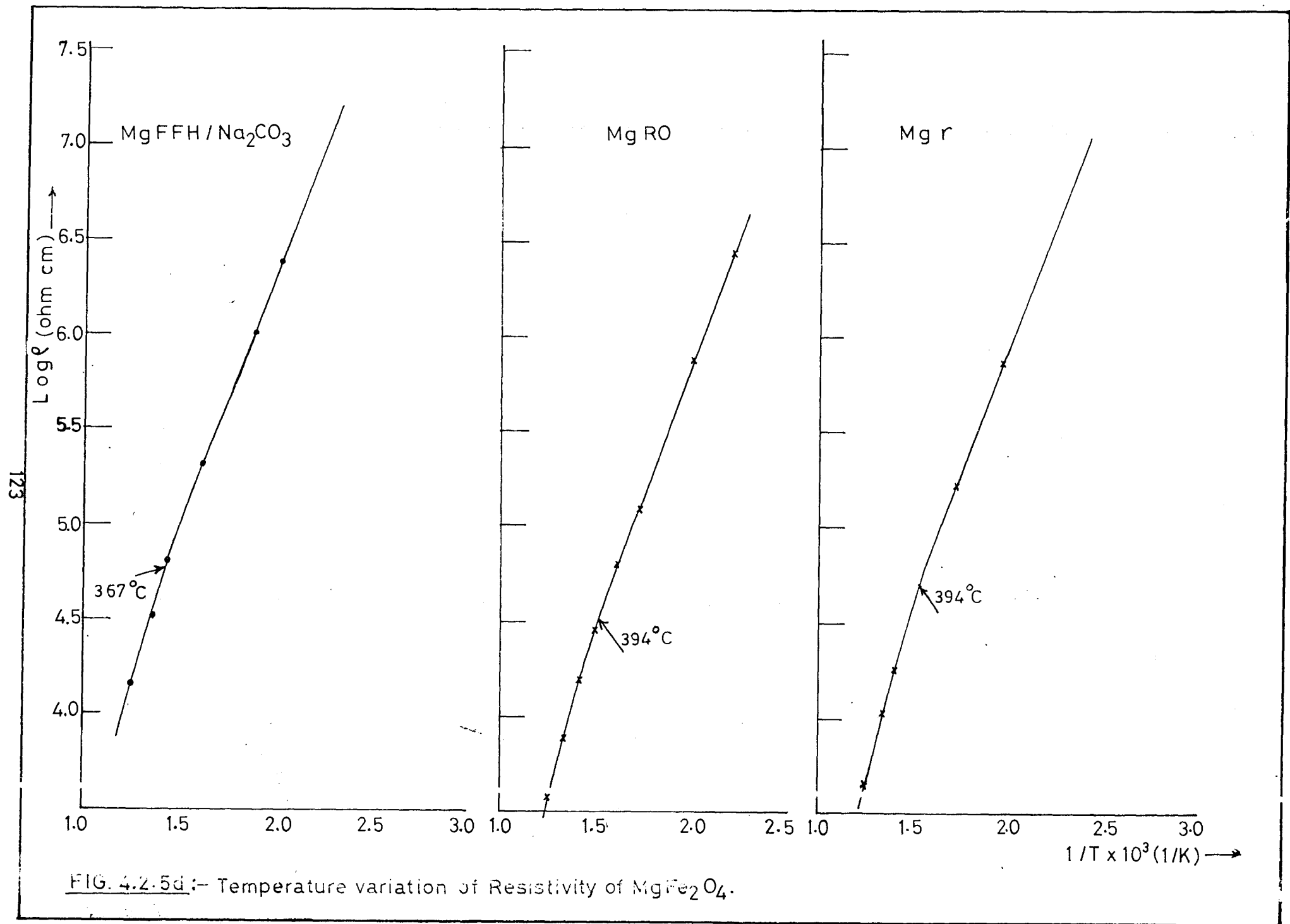
the ferrite preparation from red oxide, MgRO, shows cusps like behaviour which may be due to the presence of single domains: For comparison the ferrite prepared from commercial hematite, MgHem (section 4.1.1b), which clearly shows a Hopkinson effect is also included in the figure.

χ_{ac} Vs temperature plots are not showing a smooth increase in χ_{ac} in case of MgFH/NaOH, MgFF/NaOH (Fig 4.2.2b).

iii. Initial Permeability, μ_i

The thermal variation of initial permeability, for all $MgFe_2O_4$ samples have been measured and few representative sample plots are presented in Figure 4.2.3a-c. In general μ_i is found to increase and near Tc a sharp decrease in the value observed. From these plots the Curie temperature of the samples are spotted and put in the Table 4.2.5.

The frequency variation of initial permeability, μ_i – f, of all $MgFe_2O_4$ samples upto 1 MHz are plotted and shown in Figure 4.2.4 a-f.

There is μ_i decrease in all samples upto 50 – 100 kHz and then the permeability is observed to be frequency independent.

iv. Direct Current Resistivity

D.C. resistivity measurements done on all $MgFe_2O_4$ samples as a function of temperature are shown as log ρ Vs 1/T x 10^3 plots in Figure 4.2.5 a-d. A linear plots of the resistivity show break in plot showing two different inclinations of different slopes. At the break in the plot a temperature indicates [63, 130] a change in ferrimagnetic state to paramagnetic state. This temperature is taken as a Curie temperature, Tc. These values of Tc are placed in Table 4.2.5.

multidoma.. (MD) or super paramagnetic (SP). Temperature at which a decrease in χ_{ac}

is observed is followed to obtain Curie temperature, Tc. The Curie temperatures of few

samples are placed in Table 4.2.5.

Table 4.2.5 Comparative values of Curie temperatures for magnesium ferrites by

different methods

Sr. Nos.	Mg-Ferrite Sample	Curie Temperatures (^{O}C) From		
		Magnetic susceptibility	Initial permeability	Resistivity
1	Mg.RO	384	467	39
2	Mg-γ (N₂)	396	----	39
3	Mg.FH / NaOH	370	390	38
4	Mg.FHH / NaOH	367	417	37
5	Mg.FF / NaOH	374	410	40
6	Mg.FFH / NaOH	380	404	37
7	Mg.FH / NH₃	----	----	35
8	Mg.FHH / NH₃	----	----	31
9	Mg.FF / NH₃	----	----	36
10	Mg.FH / NaOH+NH₃	327	----	33
11	Mg.FHH / NaOH+NH₃	357	384	37
12	Mg.FF / NaOH+NH₃	317	417	38
13	Mg.FFH / NaOH+NH₃	327	364	35
14	Mg.FFH / Na₂CO₃	----	----	39

χ_{ac}/χ_{RT} Vs temperature plots in general show increase in χ_{ac} just before decrease

to almost zero, indicating Curie temperature. This nature of plot is indicative of single

domain type particles in the ferrite. An increase in χ_{ac} just before Curie temperature

indicates Hopkinson effect. The temperature independent χ_{ac} upto just before Curie

temperature is found in the ferrite preparation from Std. γ-Fe₂O₃, Mgγ (Fig. 4.2.2c) while

v. Dielectric Constant and Dielectric Loss Tangent

Frequency variation of dielectric constant, ε' and the dielectric loss tangent tan δ, at room temperature was carried out from 100 Hz to 1 MHz on all $MgFe_2O_4$ samples from study sample I of ore rejects and presented in Fig. 4.2.6. It can be seen that the value of dielectric constant decreases continuously with the increasing frequency upto 50 – 100 kHz, beyond that there is almost frequency independent behaviour is observed upto 1 MHz, in all samples. The plots of dielectric loss tangent (tan δ) against frequency, in general, indicate a decrease in the value with the increase in frequency. However, in some samples a decrease in tan δ ~1 kHz is followed by slight increase and plots of such samples show a broad hump peaking ~ 10 – 20 kHz.

The $MgFe_2O_4$ sample that had been synthesized from a representative iron ore reject [46] on which we conducted microstructural studies as described in 4.1.2. The same samples were then used to investigate dielectric constant and tan δ behaviour as a function of frequency. The results are presented in Fig. 4.2.7. These samples were sintered in air ~ $1000^{\circ}C$ / 24h. However, our objective was to explore all the possible reasons to achieve a ferrite of good quality, therefore, these samples were further sintered at $1100^{\circ}C$ and their ε' and tan δ variations as a function of frequency are presented here in Fig.4.2.7. For better comparison of the influence of heat treatment / sintering, the results of ε' and tan δ on samples sintered at 1000 and $1100^{\circ}C$ are given in the figure.

d) Microstructure (SEM) studies

In part I the microstructural studies on $MgFe_2O_4$ samples, synthesized and characterized in our laboratory [46] from iron ore rejects of one representative iron ore reject, were discussed. In the present Part II the microstructures of the ferrite samples
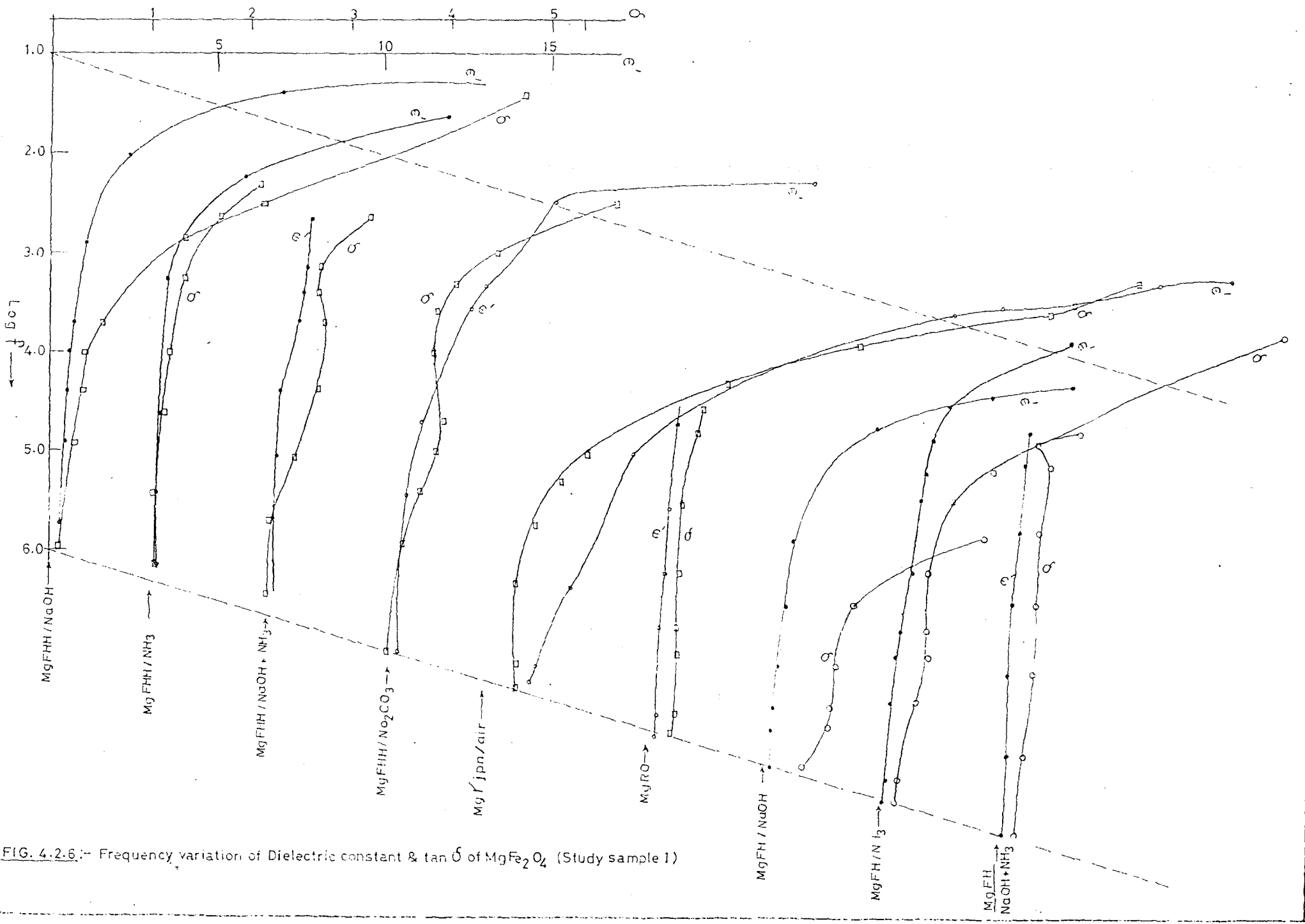
FIG. 4.2.6:— Frequency variation of Dielectric constant & tan δ of MgFe₂O₄ (Study sample I)
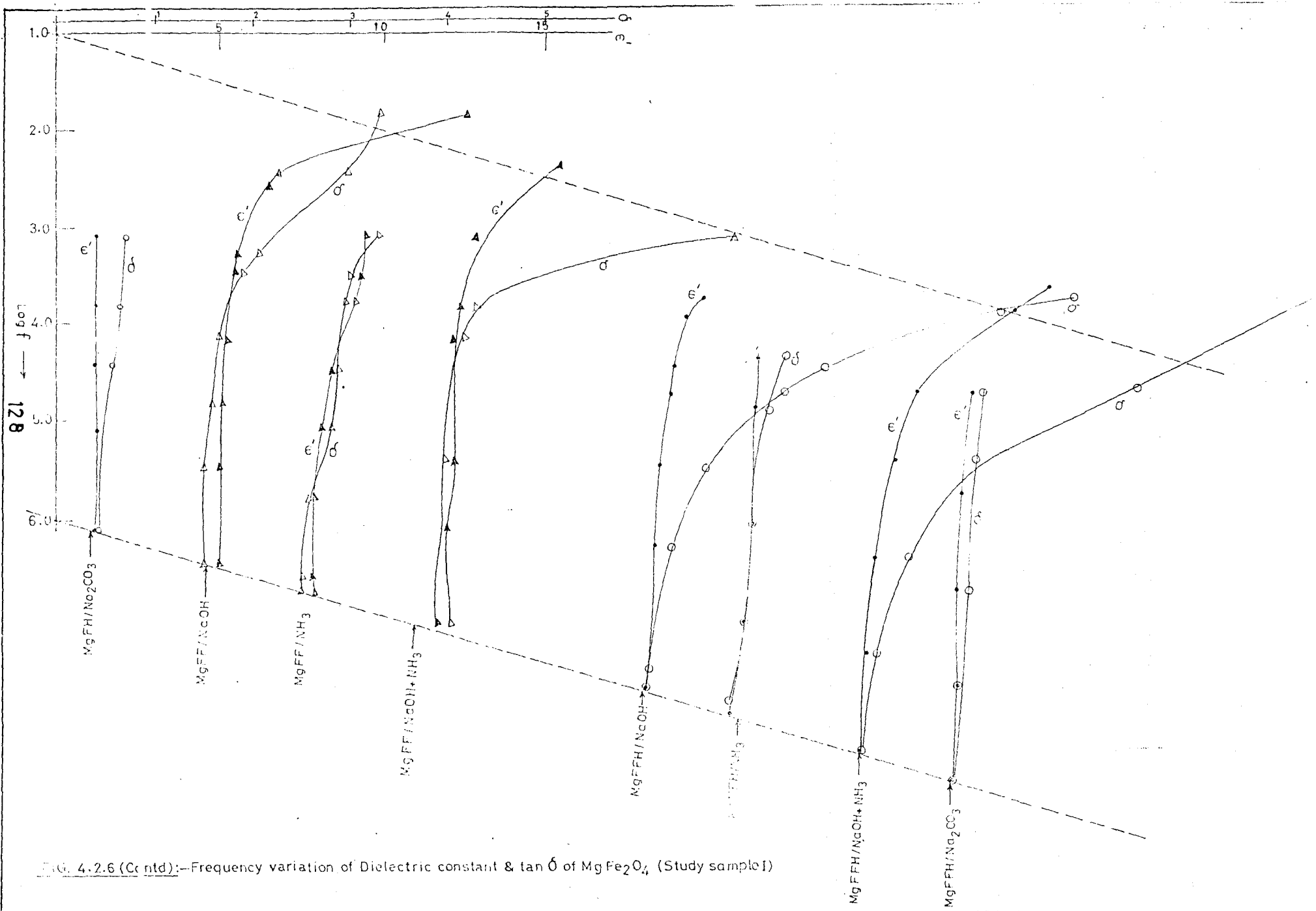
FIG. 4.2.6 (Contd):—Frequency variation of Dielectric constant & tan δ of MgFe₂O₄ (Study sample I)

128
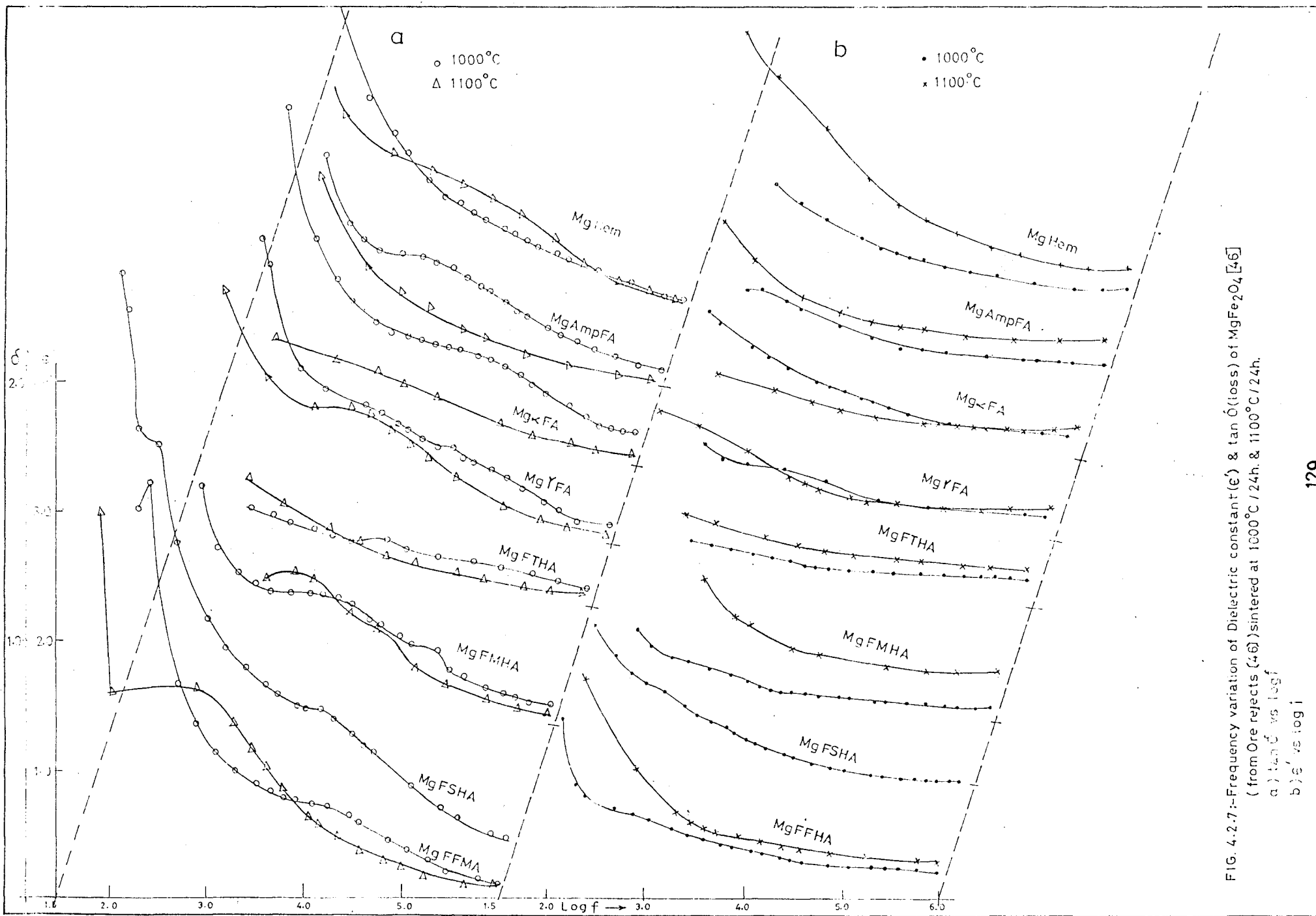
FIG. 4.2.7:-Frequency variation of Dielectric constant(ϵ') & tan δ(loss) of MgFe$_2$O$_4$ [46] (from Ore rejects [46])sintered at 1000°C/24h. & 1100°C/24h.

a) tan δ vs log f

b) ϵ' vs log f

129

std γ-Fe$_2$O$_3$

Comm RO

130

Mg γ
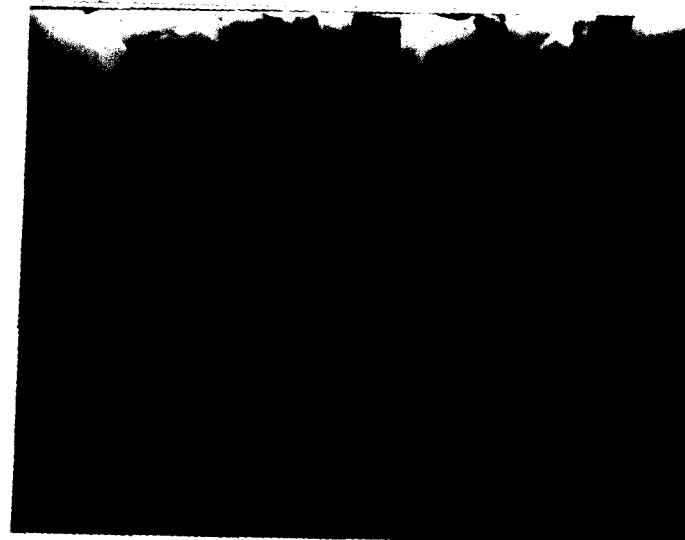
Mg RO

FIG. 4·2·8A Scanning Electron Micrographs of std γ-Fe$_2$O$_3$, Commercial RO, Mgγ & Mg RO
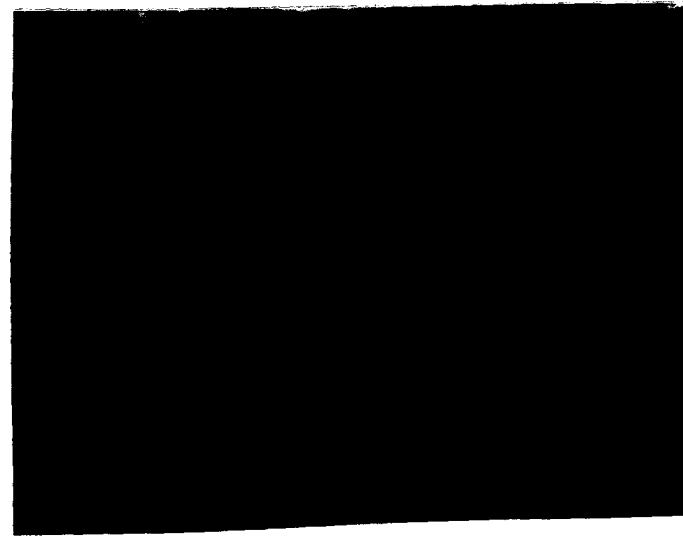
FH / NaOH

Mg FH / NaOH

FIG.4.2.8b :- Scanning Electron Micrographs of FH/NaoH, MgFH/NaoH

FHH/NaOH

MgFHH/NaOH
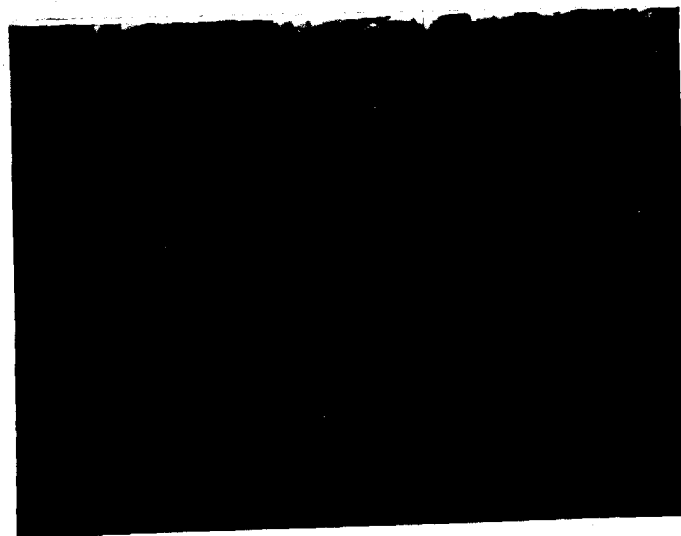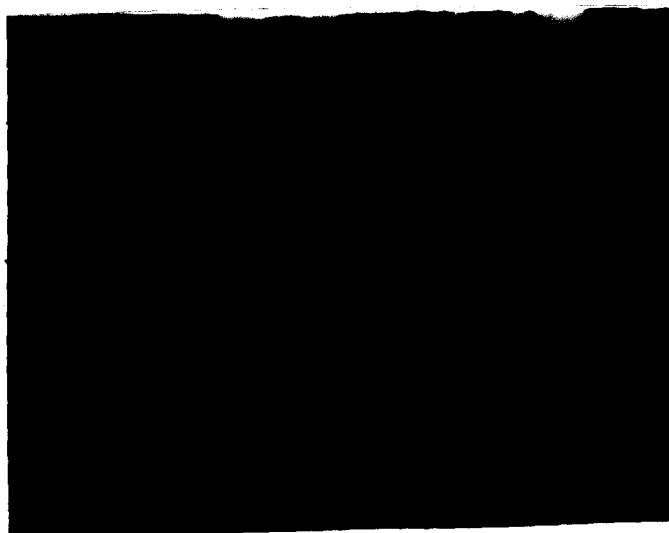
MgFHH/Na$_2$CO$_3$

FIG 4.2.8.C Scanning Electron Micrographs of FHH/NaoH, MgFHH/NaoH & MgFHH/Na$_2$CO$_3$
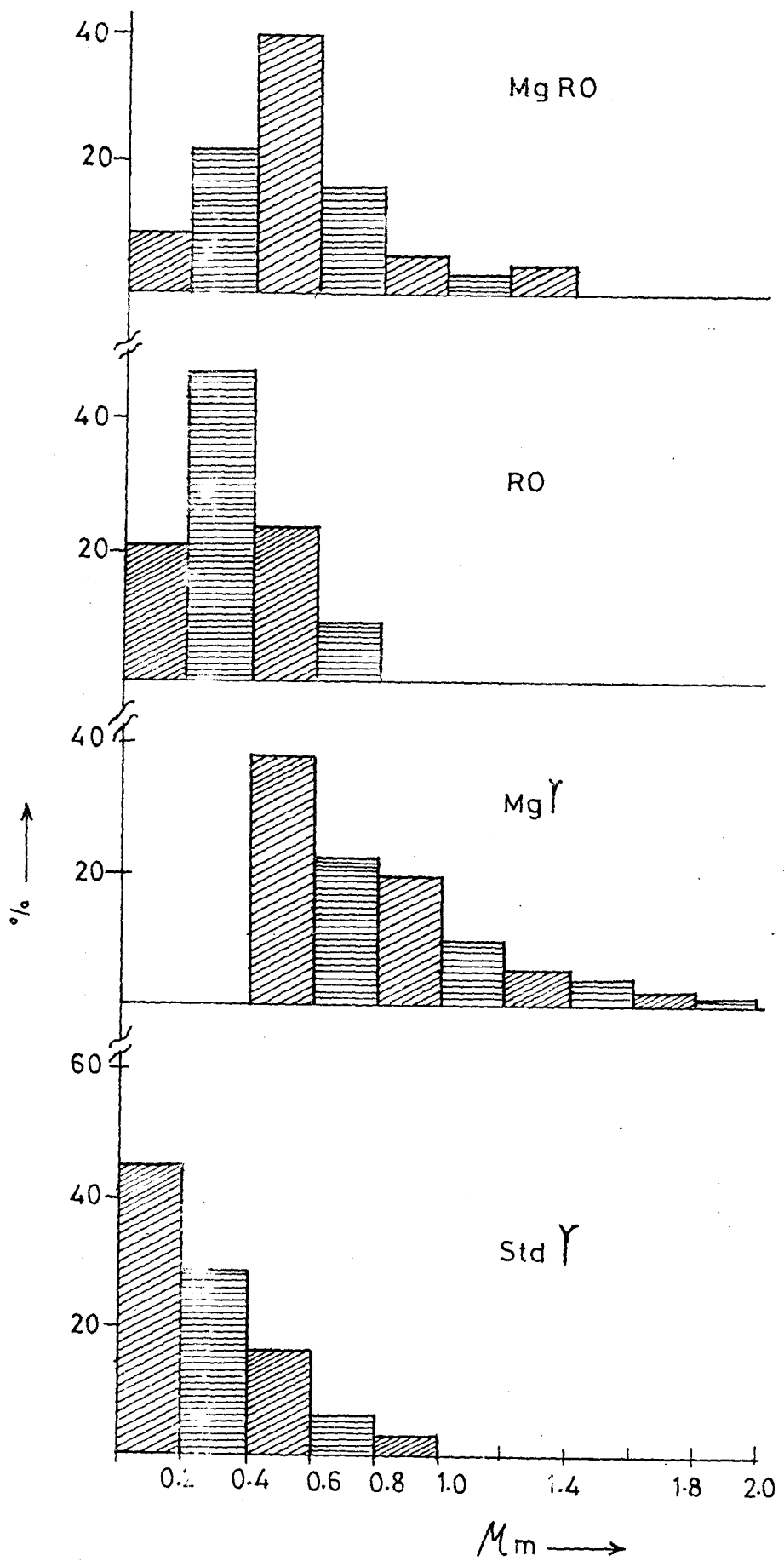
FIG 4·2·9a:-Particle size distribution of standard Iron oxides & $Mg\,Fe_2O_4$
obtained from the oxides.
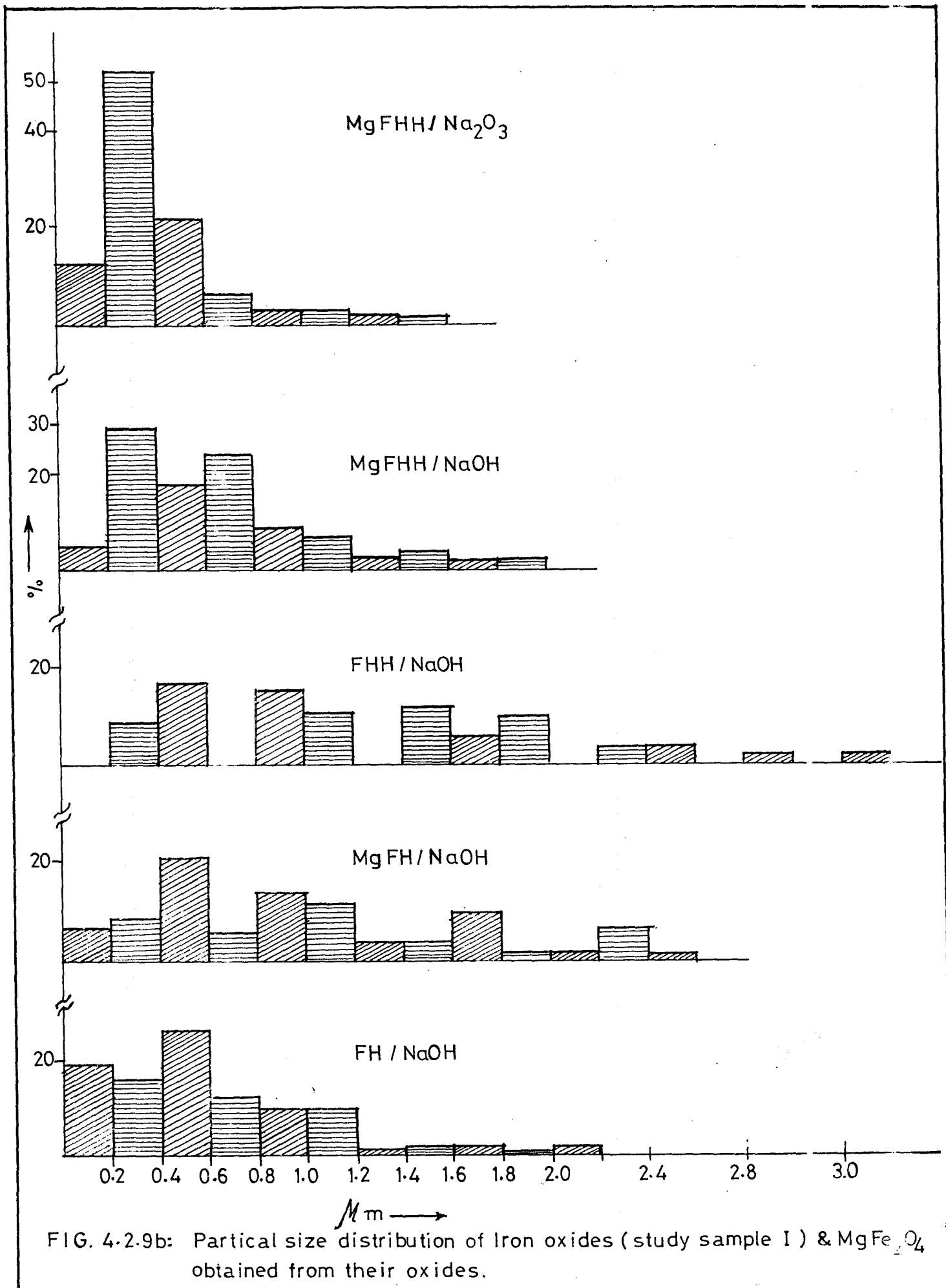
FIG. 4·2·9b: Partical size distribution of Iron oxides (study sample I) & MgFe$_2$O$_4$ obtained from their oxides.

134

from study sample I of iron ore rejects have been characterized and their result; have been presented in this section.

The SEM micrographs of few representative ferrite samples have been given in figure 4.2.8 a-c.

The micrographs of the iron oxides used for the preparation of these ferri es are also presented in the figures. The particle size distributions have been plot ed as percentage of the particles verses size of the particles in μm and the bar chart c f such measuremen;s are shown in Fig. 4.2.9 a-b.

The standard γ-Fe_2O_3 shows spindle shape particles of sizes, 0.0 – 0.2 μm (15 %), 0.2 – 0.4 μm (28 %), 0.4 – 0.6 μm (17 %) and the rest between 0.6 and 1 μm. Th is, the particles are, in general, of very small sizes. The $MgFe_2O_4$ prepared from this oxide, Mgγ-, give dumb-bell shape grains of sizes more than 0.4 μm. It is clearly seen t at the 0.00 – 0.4 μm spindle shape particles of Std. γ-Fe_2O_3 have grown into dumb-be 1 type particles of the ferrite of > 0.4 μm particles. The Mgγ- indicates a size distributio 1 upto 2 μm .

The commercial red oxide (α-Fe_2O_3), RO, has 48 (%) 0.2 – 0.4 μm p rticles which look rod like. There are about 20 (%) 0.00 – 0.20 and 24 (%) 0.4 to 0.6 μ n size particles and the rest > 0.6 μm. The ferrite prepared from this oxide, MgRO, ho vever, shows a wide variations in the particles upto 1.4 μm. The particles of 0.0 to 0.4 μm of RO have grown to the sizes upto 1.4 μm in MgRO.

The iron oxide (mainly α-Fe_2O_3) obtained from the ore reject, FH/NaO I, has distribution of particles upto 2.2 μm. But, mainly, the majority particles are < 1 2 μm. The ferrite, MgFH/NaOH, obtained from this oxide shows a wide variation in p rticles upto 2.6 μm.

On the other hand, the iron oxide (mainly γ-Fe$_2$O$_3$) that obtained from the ore rejects by hydrazine method, FHH/NaOH indicates very wide distributions in particle sizes, upto 4 μm. It looks quite uneven distribution of particles. However, the ferrite MgFHH/NaOH that obtained from this oxide show particles of good distribution below 1.2 μm. The ferrite MgFHH/Na$_2$CO$_3$ obtained from γ-Fe$_2$O$_3$ that obtained from FHH/Na$_2$CO$_3$ gives rather particles of even distribution below 0.8 μm; the majority particles are in the range of 0.2 – 0.4 μm (52 %). From these results it can be inferred that γ-Fe$_2$O$_3$ samples show better reactivity with MgO leading to uniform particles in the ferrite. Whereas, the α-Fe$_2$O$_3$ samples give the ferrite of uneven distribution. It is important to make note that the ferrite MgFHH/Na$_2$CO$_3$ has better particle distribution than MgFHH/NaOH. Although both the ferrite samples are prepared from γ Fe$_2$O$_3$ obtained from hydrazine method, the γ-Fe$_2$O$_3$, FHH/Na$_2$CO$_3$, has lower impurities as compared to the oxide FHH/NaOH.

4.2.5 Discussion

a) Phase Identification

The phase identification by xrd reveals that all samples synthesized in the present investigations are MgFe$_2$O$_4$. Only samples MgFHH/NH$_3$, MgFF/NH$_3$, MgFFH/NH$_3$, MgFHH/NaOH+NH$_3$, MgFHH/Na$_2$CO$_3$, MgFF/Na$_2$CO$_3$ (Table 4.2.1) indicate the presence of minor quantities of α-Fe$_2$O$_3$ in them.

The lattice parameter, a, ranging from 0.8343 to 0.8407 nm observed (Table 4.2.3) in these samples indicate that most of the samples show the parameter pertaining to low temperature phase of MgFe$_2$O$_4$ (a = 0.8375). the high temperature form of the ferrite is reported to be having a = 0.8397 and here it is observed that Mgγ- sintered in air and N$_2$ give, respectively, the parameter 0.8388 and 0.8391. Also, the high temperature form is

136

observed in MgFHH/NaOH sintered in air, while that sintered in N_2 gave a = (.8380.

Both MgFF i/NaOH (air) and MgFFH/NaOH (N_2) give the parameter pertaining to the high temperature form.

From these results it is difficult to give any reason for such behaviour in the lattice parameter, although all are being synthesized $\sim 1000^\circ C$ / 24h and furnace cooled. In the literature both these forms are observed in $MgFe_2O_4$ depending on the preparation conditions. Those prepared from MgO + α-Fe_2O_3 at $\sim 1320^\circ C$ and quenching [9?, 129] yield a high temperature form, while the annealed samples show a low temperature form of the ferrite. The thermal decomposition of mixed metal oxalato-hydra zinate, $MgFe_2(C_2O_4)_3.5N_2H_4$ $\sim 120^\circ C$ leads [130] to a high temperature form. The hydroxides obtained by coprecipitation of nitrates of Mg and Fe from NH_4Cl + NH_4OH at pH 9.5 - 10 decompose $\sim 950^\circ C$ giving $MgFe_2O_4$ of high temperature form [131] The variations in lattice parameter of the low temperature form is observed for $M_4Fe_2O_4$ prepared by methods [104] like chemical (0.8323 nm), ceramic (0.8367 nm) and annealing (0.8354 nm).

Lattice parameter, thus, seems to depend on the method of preparation. The lattice parameter of 0.8375 nm, the low temperature form of $MgFe_2O_4$ is found [99] to be increased to 0.840 nm when it was quenched from $1302^\circ C$. At high temperatures the migration of Mg^{2+} ions from the octahedral sites (B) to the tetrahedral sites (A) in the otherwise inverse spinel, $MgFe_2O_4$, $(Fe^{3+})_8 [Mg^{2+}_8Fe^{3+}_8]O_{32}$ causes an increase in the average radius of the A (tetrahedral) sites.

Bond lengths between A sites cation and oxygen ion (R_A–O) and B site cation and oxygen (R_B–O) and radii of A site cation (r_A) and B site cation (r_B) measured for all $MgFe_2O_4$ samples are given in Table 4.2.3.

137

In general, R_B–O, 0.20369 – 0.20525 nm and R_A–O, 0.1852 – 0.19054 nm are observed which are close to the reported values [100]. A careful observation of the table indicates that site radii of cation in the tetrahedral (A) site for the high temperature form is higher than that of the low temperature form. The MgFFH/Na_2CO_3, for example, shows lattice parameter 0.8370 nm (low temperature form) and r_A = 0.05451 nm, whereas, the high temperature form, MgFH/NaOH gives a = 0.8398 and r_A = 0.055 nm.

The migration of Mg^{2+} ion (radius 0.078 nm) from octahedral site to the tetrahedral (A site) by substituting Fe^{3+} ion (radius 0.067 nm) can cause an increase in the radii of the A site (r_A). Since the high temperature form has higher r_A than the low temperature form of $MgFe_2O_4$, the migration of the Mg^{2+}ions may be causing the increase in the lattice parameter. A cation distribution of $Mg_{0.12}Fe_{0.88}[Mg_{0.88}Fe_{1.12}]O_4$ for annealed sample (low temperature form) [99] and $Mg_{0.225}Fe_{0.745}[Mg_{0.745}Fe_{1.255}]O_4$ for quenched sample (high temperature form) have been suggested. From neutron diffraction studies [146] a degree of inversion 0.88 ± 0.01 and 'u' parameter of 0.381 ± 0.001 have been observed. These studies suggest that the migration of Mg^{2+} ions to A sites and the higher percentage of Mg^{2+} ion in the high temperature form of $MgFe_2O_4$ hence causes the higher lattice parameter.

Our all samples were prepared ~1000°C and furnace cooled and hence they should have shown low temperature form of the ferrite. Both the low temperature and high temperature forms of $MgFe_2O_4$ that observed in our samples, prepared from different iron oxide precursors and are sintered in air and N_2. Hence, any conclusion can not be arrived at. May be detailed cation distribution studies required to be done.

Further, the migration of Mg^{2+} may also be influenced by the other impurity cations that present in the iron oxide obtained from ore rejects. There are major impurities like (Table 2.3a) Si, Al and Mn in our precursor iron oxides which may

compete for the sites in the spinel $MgFe_2O_4$. A competition in site occupancy of S^{4+} (on tetrahedral sites), Al^{3+} (on B sites) and Mn^{2+}/Mn^{3+} (on tetrahedral sites) may, hence, contribute to the Mg^{2+} ion distribution over A and B sites.

b) Magnetic and Electric Characterization

All $MgFe_2O_4$ samples show (Table 4.2.4) σs, $4\pi Ms$ and n_B in the range 13 – 30 emu/g, 635 – 1185 G and 0.67 – 1.06 Bohr magnetone, respectively. Ferrites, MFe_2O_4, in which divalent ions M^{2+} like Mn^{2+}, Fe^{2+}, Co^{2+} and Ni^{2+} that present on the octahedral sites, $Fe^{3+}_A[M^{2+}Fe^{3+}]_BO_4$, are called inverted spinels and they all are ferrimagnetic with saturation magnetic moments appropriate to the divalent ions alone. According to the Neel theory [133] there exists a strong negative exchange coupling between the atoms on A sites and the atoms on the B sites. This results in a spin alignment in which the A site moments are all antiparallel to the B site moments. In the inverted ferrites the iron moments on A sites just cancel those on B sites, leaving the crystal with a net moment equal to that of the divalent ion.

The case of magnesium ferrite, $MgFe_2O_4$, is some what exceptional. Its structure was originally reported [134] to be inverted, $Fe^{3+}_A[Mg^{2+}Fe^{3+}]_BO_4$. On the basis of Neel theory it would then be expected to have zero magnetic moment. However, it is not what is observed experimentally. The saturation is found to vary within 1 – 2.4 Bohr magnetone depending on the condition of preparation. This discrepancy has been explained on the assumption that magnesium ferrite is incompletely inverted, the number of iron atoms on the B sites thus exceeding the number on A sites. But, this inversion is ~ 10 – 15 (%) and hence the ferrite shows low saturation magnetization values, in general. Hence, a wide variation in σs, $4\pi Ms$ and n_B observed (Table 4.2.4) indicates different percentage of inversion in our samples of $MgFe_2O_4$.

139

Not only this degree of inversion which causes large variations in the magnetic characteristics in our samples but also the impurities present in the precursor iron oxides may too be responsible.

The standard γ-Fe$_2$O$_3$ contains no measurable impurities in it and the ferrite prepared from this in air (Mg γ-air), however, shows, n_B = 0.81, while that synthesized in inert atmosphere (Mg γ-N$_2$) gives the value of 0.67 Bohr magnetone (Table 4.2.4). Both these samples indicate lattice parameters (a = 0.8388 ±0.0003) close to the high temperature form. The ferrite obtained from iron ore rejects, MgFF/NaOH, in air, shows the maximum n_B = 1.06. This too has the lattice parameter similar to Mgγ-/air (a = 0.8388), but then MgFF/NaOH has major impurities: Al, Si, Mn. Thus, it is difficult to give any conclusive reasons for such variations in the magnetic values in the present investigations.

Bulk magnetic behaviour can generally be understood starting from the domain structure. The temperature variation of the a. c. magnetic susceptibility and hysteresis provide useful data on the domain structure. The thermal variation of χ_{ac} for MgFe$_2$O$_4$ prepared from standard γ-Fe$_2$O$_3$, Mgγ- (Fig. 4.2.2c) shows a temperature independent behaviour and then it falls to zero ~ 396°C. This is the Curie temperature, Tc. The temperature dependence of χ_{ac} is observed, however, in the ferrite prepared from commercial red oxide, MgRO, the increase in χ_{ac} upto Tc is followed by sharp decrease at Tc = 384°C. A multidomain (MD) type behaviour is observed in Mgγ, while single domain (SD) behaviour observed in MgRO. For comparison the ferrite prepared from commercial hematite, MgHem (as described in 4.1)is also given in the same figure and this shows a temperature independent χ_{ac} followed by a sharp peak before falling to zero

at ~ 457°C. This is a typical single domain behaviour with a Hopkinson effect [135]. The behaviour of MgRO, is not typical for single domain.

Ferrites when prepared by a ceramic method, mixed domain states tend to be formed resulting in the bulk magnetic properties appropriate to a mixture of SD, MD and super paramagnetism (SP). In few ferrites MD or SD behaviour is determined primarily by the composition and the structure [135]. Such mixed domain type of behaviour in χ_{ac} - temperature curves are observed in most of our samples [Fig. 4.2.2 a&b). The sharp decrease in χ_{ac} at Tc is indicative of single phase ferrite. A tailing of χ_{ac} near Tc is also observed in few samples. The Tc between 317 – 396°C found in our samples are falling in the range normally observed in $MgFe_2O_4$ from 320 – 440°C [107].

The domain behaviour and also the saturation magnetization values are usually determined by the composition and structure of ferrites. Hence, they can be contro led by fixing the stoichiometry of the desired ferrite. But the technological importance of the ferrites primarily lies in their high resistivity. All ferrites prepared here show high resistivities at RT of ~ 10^7 Ω cm [Fig. 4.2.5] and ferrites in the range of 1 to 10^{12} Ω cm are being used depending on the applications. Resistivities of ferrites decrease with the temperatures and the log ρ Vs 1/T plots in our samples show a break in the linear plot indicating the switch over from ferrimagnetic to paramagnetic region. Curie temperatures measured from these breaks are given in Table 4.2.5. Tc between 311 and 405°C found in the ferrite samples match well with the reported values [107].

Although high resistivity ferrites are preferred in device application as the important eddy current losses can be minimised and hence joule losses, the knowledge of the losses due to other mechanism are also equally important to establish the efficiency of these materials having desired properties. Initial permeability is one such property which is being studied. The initial permeability, μ_i called simply [136] the permeability of a

material is defined as the derivative of the induction B with respect to the internal field H in the demagnetized state

$$\mu_i = \frac{dB}{dH} \qquad H \longrightarrow 0, \quad B \longrightarrow 0$$

In the case of polycrystalline materials containing a large number of randomly oriented crystallites the permeability will be a scalar, at least at low frequencies.

Permeability measured as a function of temperature and frequencies of few representative samples are shown in figures 4.2.3 and 4.2.4. μ_i, in general, shows low frequency dispersion upto 10-20 kHz and then there is frequency invariant behaviour of permeability in all ferrites studied. The ferrite Mgγ prepared from standard γ-Fe$_2$O$_3$, both in air and nitrogen shows almost similar behaviour. The ferrite from red oxide, MgRO, also indicates the low frequency dispersion but upto 100 kHz. The low frequency dispersion in ferrites have been attributed to [137] the domain wall displacements. Pores hinder domain wall motion and also give rise to a local demagnetization field. The hindrance to the domain wall motion results in low values of μ_i.

The porosities observed in most of our samples (Table 4.2.2) lie in the range 25-30 (%) with few exception showing 15 and 36 (%). μ_i value of $\sim$ 100 that observed at 100 Hz for all samples decrease upto 100 kHz, while the ferrite prepared from red oxide, MgRO, however, starts showing μ_i = 50 at 40 kHz which then decreases upto 100 kHz and then it remains frequency invariant.

The thermal variation of permeability of all samples of MgFe$_2$O$_4$ (Fig. 4.2.3) indicates an increase in μ_i with temperature upto Curie temperature and then it falls sharply at Tc. Curie temperatures measured from these show 364 - 417°C which are in the range of 320 - 440°C as reported [107]. The μ_i variation with temperature of the ferrite prepared from red oxide, MgRO shows one broad hump (Fig. 4.2.3c) in the value

before reaching a peak at Tc and then sharply decreases at Tc = 467°C. A very high Tc is observed.

The susceptibility behaviour of MgRO with temperature (χ_{ac} Vs temperature) shows (Fig. 4.2.2c) mixed domain type behaviour. Since all other samples show a single peak in the thermal variation of μ_i, and indicate sharp decrease in the value at Tc, a single phase ferrite may be present in these samples. The MgRO, therefore, may be multi phase one, but the xrd rules out this.

The initial permeability is reported [138, 139] to be dependent on the method of preparation, porosity within the material and grain size.

The frequency variation of dielectric constant, ε', and tan δ (loss) for all $M_f Fe_2O_4$ samples are given in Fig. 4.2.6.

The ε' and tan δ values fall upto 10 kHz in all samples and after that they remain frequency invariant. The dispersion of these is found to be maximum in MgFHH/NaOH, MgFHH/NH$_3$, Mgγ-air and MgFH/NaOH, MgFFH/NaOH + NH$_3$.

In case of MgFHH/Na$_2$CO$_3$ there is a maximum dispersion in ε', but the tan δ decrease is followed by a small increase which then finally decreases. A hump ~ 8 kHz thus indicates that there occurs some increased loss. Such increased loss is indicated by a hump ~ 7 kHz in MgFHH/NaOH and ~ 12 kHZ in MgFF/NH$_3$.

Almost invariance in ε' and tan δ is observed from 100 Hz to 1 MHz for MgFFH/Na$_2$CO$_3$ and in MgFH/Na$_2$CO$_3$ from 1 kHz to 1 MHz.

Polycrystalline ferrites are very good dielectric materials. This is because [140], in the process of preparation of ferrites when the powders are sintered under slightly reducing conditions, the divalent iron ions formed in the body leads to high conductivity grains. When such materials are cooled in an oxygen atmosphere, it is possible to form layers of very low conductivity over their constituents grains. Almost all the ferrites in

the polycrystalline form have such high conductivity grains separately by low conductivity layers so that they behave as inhomogeneous dielectric materials. A; such the dielectric properties of ferrites are dependent on several factors including the method of preparation, sintering temperature, sintering atmosphere, chemical composition, microstructure etc. As a consequence of the inhomogeneous dielectric behaviour, dielectric constants as high as 10^6 are found in the case of ferrites at low frequencies. Ferrites having very high dielectric constants are useful in designing good microwave devices such as isolators, circulators etc.

In our samples the dielectric constant values at low frequencies at room temperatures lie between $10 - 22$ and decrease to $1 - 2$ beyond 10 kHz.

Room temperature dielectric constant of $CdFe_2O_4$ at 5 kHz found to be 52.01 [140]. On adding lithium to the ferrite, $Li_{0.1}Cd_{0.8}Fe_{2.1}O_4$, the ε' value decreases to 29.49 and further decrease is found in $Li_{0.3}Cd_{0.4}Fe_{2.3}O_4$ which indicated the value of 39.9ς. The $CdFe_2O_4$ has RT conductivity (σ), 1.10×10^{-5} $\Omega^{-1}cm^{-1}$ and this is attributed to the presence of Fe^{2+} about 1.586 (%) on the octahedral sites which play a dominant role in the process of conduction due to hopping of electrons between $Fe^{2+} \Leftrightarrow Fe^{3+}$. The Fe^{2+} concentration decreases with the substitution of Cd^{2+} by Li^{1+} ions and a 0.684 (%) of Fe^{2+} is found in $Li_{0.3}Cd_{0.4}Fe_{2.3}O_4$ and hence low conductivity of 4.37×10^{-6} $\Omega^{-1}cm^{-1}$ The dielectric constant of $CdFe_2O_4$ decreases with the addition of lithium in it, hence, suggests that there is a strong correlation between the conduction mechanism and the dielectric behaviour of ferrites. Higher ferrous ions which exchange with Fe^{3+} ions thus give rise to maximum dielectric polarization. A correlation between conduction and dielectric processes has been done on several ferrites [141 – 146].

The $MgFe_2O_4$ samples in the present investigations have all high resistivity (low conductivity) of $\sim 10^7$ Ωcm (Fig. 4.2.5) and hence they all may have negligible or very

low concentration of Fe^{2+} (chemically not measurable). The low dielectric constant observed here may be due to this. The frequency dependence of ε' in all these are similar to the ferrites mentioned above; there is continuous fall in ε' with frequency.

The frequency dependence of loss tangent (tan δ) in all $MgFe_2O_4$ show, in general, decrease. But in few samples there occurs a slight increase in the loss ~ 8 - 12 kHz. Lithium substituted $CdFe_2O_4$ samples too [140] show such a maximum ~ 10 - 20 kHz, specially a maximum loss in $CdFe_2O_4$ and least in $Li_{0.3}Cd_{0.4}Fe_{2.3}O_4$ and this can be correlated with their electrical conductivity behaviours. The least loss observed in the sample which has low concentration of Fe^{2+} ions. The tan δ maximum around a particular frequency is considered to be due to the equalisation of the externally applied field with the hopping frequencies in the samples. And, this may be the reason why few samples in the $MgFe_2O_4$ show, in our case, a maximum ~ 8 - 12 kHz. Although, we are unable to detect Fe^{2+} presence in these samples, the infra red data analysis on our samples reveal some presence of Fe^{2+} in few of them as shown in Fig. 4.2.1, especially a slight split in the band ~ 600 cm^{-1}.

c) Frequency dependence of ε', and tan δ of $MgFe_2O_4$ (ore reject [46])

The samples of $MgFe_2O_4$ that prepared from a representative iron ore rejects as described [46], in our laboratories on which we have presented microstructural aspects in 4.1 are being studied by us and their results are presented here. As it was observed that the $MgFe_2O_4$ synthesized from the ore rejects show almost similar behaviour in their magnetic characteristics with the exception of the ferrite prepared from commercial $\alpha-Fe_2O_3$, McHem, we undertook dielectric constant and tan δ measurements on these samples as a function of temperature to get further insight in their property differences. The samples that obtained ~ 1000° / 24h from our laboratory [46] were used as such and

the measurements were carried out. Also, few samples were then further sint ired ~ 1100°C and the measurements were done. The results of such measuremer ts are presented here and discussed.

It can be seen from the Figure 4.2.7 that there is a normal dispersion in ε' with frequency. However there is no much difference in ε' values at low frequencies of 1000° and 1100°C sintered samples. MgHem, however, shows maximum dispersion in the sample sintered at 1100°C; the ε' values at low frequency also increased. MgFFI A too showed maximum dispersion in ε'. Increased ε' is found to be more for MgFM IA on sintering to 1100°C.

MgHem sintered at 1100°C which showed increased ε' value and ma imum dispersion with frequency also indicated a tan δ maximum (hmp) ~ 9 kHz (Fig. 4.2.7), while that sintered at 1000°C showed normal dispersion. But the MgFFHA which showed increased ε' on 1100°C sintering now shows normal dispersion in tan δ, whereas the 1000°C sintering gives an increased tan δ ~ 12 kHz. MgαFA sintered at 1)00°C gives frequency independent tan δ which is in general lower through out the frequency range as compared to that sintered at 1100°C.

Thus, higher temperature sintering has some beneficial effect on tan δ va ues in $MgFe_2O_4$ excepting MgHem. The maximum dielectric dispersion observed in N gHem sintered at 1100°C suggests that it may have some Fe^{2+} ions present in it whic 1 then reflected in its tan δ loss maximum.

d) Microstructure (SEM) analysis

The standard γ-Fe_2O_3 has spindle shape particles (Fig. 4.2.8) of sizes, 45 (%) upto 0.2 μm (Fig. 4.2.9a), 45 (%) of 0.2 – 0.6 μm and the ferrite Mgγ, prepared from this oxide show dumb-bell shape particles of sizes more than 0.4 μm. The commercial red oxide,

α-Fe$_2$O$_3$ (RO), indicate particles rod like of sizes 0.2 – 0.4 μm (48 %) and 44 (% upto 0.6 μm, but the ferrite obtained from this, MgRO, show particles upto 1.4 μm. The ferrite MgHem prepared from commercial α-Fe$_2$O$_3$ (section 4.1; Fig. 4.1.5) shows a wide variations in the particle distributions and has a porosity of 42 (%) (Table 4.1.2). These are the ferrites obtained ~ 1000°C using commercial iron oxides.

The MgHem shows the saturation magnetization, σs, values (Table 4.1.2) of 17.20 emu/g, while the Mgy and MgRO indicate (Table 4.2.4) the values of 22.56 and 23.05 emu/g, respectively. Both the MgRO and Mgy have single phase MgFe$_2$O$_4$, while MgHem has few admixture of α-Fe$_2$O$_3$ indicating incomplete formation of the ferrite and hence the lowest σs may be observed.

These three MgFe$_2$O$_4$ samples, however, show temperature variation of susceptibility (Fig. 4.2.2c) quite different from each other. A multidomain type behaviour is observed in Mgy and a single domain type nature in MgRO. But, the MgHem shows a Hopkinson effect.

Although, the particle size distribution and shapes may not directly influencing the nature of γ - T plots, the different domain types observed in these three ferrite samples can be roughly considered due to variations in particle distribution. Also, the particle shapes and sizes are not influencing the saturation magnetization values and hence the lowest σs values of 17.2 emu/g observed in MgHem may be due to incomplete MgFe$_2$O$_4$ formation. The dumb-bell shape Mgy and MgRO having usual particles, however, have σs values of 22.56 and 23.05 emu/g, respectively. But the permeability of ferrites is much influenced by factors such as imperfections, porosity and crystalline shape and distribution. Permeability values are dependent, hence, on the method of preparation.

The frequency dependence of permeability of Mgγ (Fig. 4.2.4e), both sintered in air and nitrogen, show almost 6 order dispersion. The MgRO, however, indicates the frequency dispersion but of 1½ order. The low frequency permeability values are also low in MgRO compared to Mgγ. The Mgγ has dumb-bell shape particles, while MgRO has normal size particles of wide distributions.

The frequency dependence of dielectric constant (ε') and tan δ loss of MgHem (Fig. 4.2.7) sintered at 1000°C show usual dispersions. The sample that sintered at 1100°C indicates maximum dispersion in ε' but then it also shows a low frequency tan δ maximum (a hump). As particle size distribution in MgHem that sintered at 1000°C led to high porosity, the sintering to 1100°C must have increased porosity due to uneven growth of the particles.

The MgRO, on the other hand, has usual particle size distribution (Fig. 4.2.5 a) and it has both frequency independent ε' and tan δ (Fig. 4.2.6) in the frequency range of our measurements. The dumb-bell shape Mgγ, however, shows (Fig.4.2.8) very large dispersions in both the ε' and tan δ values as a function of frequency.

Thus, there seems to be some influence of particle sizes, shapes on the electromagnetic properties in MgFe$_2$O$_4$ in our studies. However, further systematic investigations are required to correlate the electromagnetic properties with that of the nature of particles. In part I of this chapter we did make some attempt in this regard. However, one important aspect has not been taken into consideration here about the influence of impurities on the particle size distribution and electromagnetic properties, especially on the other ferrite samples that prepared from iron ore rejects. The three ferrite samples discussed so far are obtained from commercial grade iron oxide.

Synthesis and Characterization of (Mn½Zn½)Fe2O4

(Study Sample II)

4.3 Introduction

Mn-Zn ferrites are technologically important soft magnetic materials [14'] find use as cores in high frequency coils and transformers. High permeability and low losses along with good stability of permeability with temperature and time are the characteristics of such ferrites and as such fine control of Fe^{2+} (ferrous) ions is essential to achieve these. The large permeability is primarily associated with low crystal anisotropy in Mn-Zn ferrites and attains maximum value as the crystal anisotropy K approaches zero. And this is achieved by introducing a small calculated amount of Fe^{2+} ions which contribue to a positive anisotropy; Mn-Zn ferrite has a negative crystal anisotropy and hence the Fe^{2+} nullifies this resulting it into 0. Hence, in the synthesis of Mn-Zn ferrites a proper care has to be taken to have this compromise in the concentration of Fe^{2+} ions and crystal anisotropy. Temperature and atmosphere controls are needed in processing the ferrites.

Apart from there compositional restrictions in the ferrite preparation a strict control of microstructures of the final products is also to be carried out as these to a great extent also allow the ferrites to achieve final magnetic properties. Grains with large grain size and trapped porosity make the ferrite cores susceptible to eddy currents. Among ferries the preparation of MnZn ferrites is further complicated because of variable manganese oxidation states and the ferrites should have Mn^{2+} in its normal sites. Therefore, a systematic synthetic research is still in progress. And, we in the present investigations restricting ourselves to the synthesis, xrd phase characterization and magnetic characterization (saturation magnetization, σs in emu/g) of $Mn_{1/2}Zn_{1/2}Fe_2O_4$ from up graded iron ores, especially from a study sample II. The results of such studies are discussed here.

In ferrite processing the properties of the starting materials are of critical importance [148 - 149] because they greatly influence the process parameters and, especially in less flexible production processes, determine the quality of the final products. Iron oxide, α-Fe_2O_3, is the starting material, which represents about 70% of the raw materials in ferrite synthesis. The quality of the oxide is of paramount importance as iron oxide for ferrites preparation are drawn from various sources, especially from steel pickle solution (spray roasted) and upgraded hematite. Both cation impurities, as well as anion impurities in iron oxide [149 – 150] have been found to influence the ferrite properties.

The iron oxide if exhibits self sintering at lower temperatures before it reacts with the other metal ion constituents of ferrite raw material, the product formation gets delayed. The self sintering means the oxide shrinks (compresses) and becomes inactive. This is in accordance with the general observation that the lower the decomposition temperature of the basic salts from which the oxide (say from metal hydroxides/

nitrates/carbonates) the lower the temperature region where the decomposition product reaches its optimum reactivity. The free surface of Fe_2O_3 in the starting mixture will strongly decrease during heating, thus impeding the solid state reaction between the starting oxides. Such observations are made [151] during the Mn-Zn ferrite formation. And it is observed here that ~ $600^{o}C$ the raw mix containing Fe_2O_3 + ZnO + Mn_3O_4 shows mainly $ZnMn_2O_4$ leaving aside Fe_2O_3 unreacted. The ferrite formation is then delayed.

The reactivity of iron oxide and its solid state reaction with the other metal oxides in ferrite preparation is an important study one has to carry out to get well dense products. And, this is our main objective in the present research activities. Therefore, we have been working with different iron oxide samples that obtained from iron ore rejects. We are not only using iron oxide, α-Fe_2O_3, thus prepared but also γ-Fe_2O_3 or mixture of γ-Fe_2O_3 + α-Fe_2O_3 that obtained by special technique in preparing ferrites. In Part I and II of this chapter we have described our studies on $MgFe_2O_4$ and in this chapter we are presenting our data on Mn-Zn ferrite. The γ-Fe_2O_3 may have added advantage in ferites preparation as it during heating of raw mix of ferrites transforms into α-Fe_2O_3 which may be now more reactive and hence ferrite formation may occur readily or it may become inactive by self sintering and hence ferritization may be delayed.

4.3.1 Experimental

a) Preparation

The iron oxide obtained from study sample II of iron ore rejects, FH-II/NaOH, FHH-II/NaOH , FF-II/NaOH and FFH-II/NaOH are being used for the synthesis of $Mn_{1/2}Zn_{1/2}Fe_2O_4$.

i) Ceramic technique

Iron oxides as mentioned above were mixed in the desired percentage with manganese formate (MF') and zinc formate (ZF') and ground in an agate mortar and then pelletised. The pellets of 15 mm diameter and 5 – 6 mm thickness (compressed in a ... ... 5 – 10 tons/inch^2) were then heated slowly to 700°C in air or nitrogen for 24 hours. The cooled samples were crushed, ground and then repelletised. Binder PVA (Polyvinyl alcohol) was used in few cases. The pellets were then heat treated at 1150 – 1200°C for 3 – 6 hours in air or N$_2$. The samples were furnace cooled.

Few samples were heated to 1200°C and then quenched by dropping samples in water. They are coded as MF'/ZF'/FH, MF'/ZF'/FHHz, MF'/ZF'/FF' and MF'/ZF'/FF'Hz.

ii) Coprecipitation method

The iron oxides as mentioned above from study sample II were brought into solution by adding HCl and adequate amounts of MnCl$_2$ and ZnO were then put in the same solution. The solution was then coprecipitated with NaOH. The mixed metal hydroxides, MZFH (from FH-II/NaOH) were filtered, washed and dried. The dried mass was then used to prepare the mixed metal formates by same method as described earlier for iron formates.

The dry MZFH and MZFF' were then equilibrated in hydrazine hydrate atmosphere in a desiccator. The samples are named as MZFHH and MZFF'Hz.

The coprecipitated samples MZFH and MZFF' were pelletised and then decomposed in air or nitrogen ~ 700°C/24 hr. the cooled samples were crushed, ground and repelletised. Then they were heated slowly in air or nitrogen to 1150 – 1200°C/3-6 hours. Furnace cooled samples were stored in desiccator. They are coded as MZFH/air, MZFH/N$_2$, MZFF'/air and MZFF'Hz/N$_2$. The hydrazine equilibrated samples fumed soon after they were removed from the desiccator. They were then crushed, ground, pelletised

as above and samples sintered in air or nitrogen at 1150 – 1200°C are named as

MZFHHz/air and MZFHHz/N$_2$, MZFF Hz/air and MZFF Hz/N$_2$.

b) X-ray characterization

The samples were x-ray characterized as described in section 2.3.4.

c) Magnetic characterization

The saturation magnetization, σs in emu/g of the samples were calculated as in

section 3.4.3

4.3.2 Results and Discussion

The observed d $_{hkl}$ values of all samples studied here are given in Table 4.3.1. All

xrd peaks are matching well with each other. However, the Mn-Zn ferrite prepared in the

present studies is to get Mn$_{½}$Zn$_{½}$Fe$_2$O$_4$. The JCPDS file [152] mentions only about

Zn$_{0.6}$Mn$_{0.8}$Fe$_{1.6}$O$_4$ (Franklinite (ZnMnFe)(FeMn)$_2$O$_4$ with lattice parameter a = 0.8474

nm. The d $_{hkl}$ values of Franklinite are also given for comparison in the table and there is

a close resemblance of these with our values. Our samples have lattice parameter

between 0.8426 and 0.8543. The lattice parameter variation between 0.854 and 0.855 is

observed [153] with zinc content for Mn-Zn ferrite of composition between

Mn$_{0.6}$Zn$_{0.4}$Fe$_2$O$_4$ and Mn$_{0.5}$Zn$_{0.5}$Fe$_2$O$_4$. Since all our samples show more or less same d $_{hkl}$

values as observed [14] for Mn$_{0.5}$Zn$_{0.5}$Fe$_2$O$_4$, we consider that we have achieved the

ferrite of same composition.

The saturation magnetization values measured at room temperature of all samples

are presented in Table 4.3.2.

The ferrite synthesized by ceramic technique using iron oxides from iron ore

rejects (study sample II) indicate σs values between 34 and 86 emu/g. The iron oxide,

α-Fe$_2$O$_3$, obtained in air from iron hydroxides, FH-II/NaOH when mixed with manganese

153

Table 4.3.1 XRD data of $Mn_{1/2}Zn_{1/2}Fe_2O_4$

Ferrite Samples	d_{hkl} values (I/I$_0$)										a (nm)	d_X	porosity
(ZnMnFe)(FeMn)$_2$O$_4$ reported	4.88 (10)	2.99 (70)	2.55 (100)	2.44 (5)	2.12 (40)	1.730 (30)	1.632 (70)	1.499 (80)	1.340 (5)	1.293 (20)	0.8474	--	--
MZFH 6h/N$_2$/1150	4.91 (58)	3.00 (64)	2.56 (100)	-- --	2.12 (45)	1.73 (38)	1.63 (51)	1.50 (53)	1.38 (33)	1.29 (35)	0.8473	5.15	20.83
MZFHH$_z$ 6h/N$_2$/1200	4.95 (72)	3.02 (66)	2.57 (100)	2.46 (50)	2.13 (54)	1.74 (41)	1.64 (55)	1.50 (56)	-- --	1.30 (38)	0.8426	5.11	--
MZFF 6h/N$_2$/1000	4.95 (72)	3.03 (64)	2.58 (100)	2.47 (50)	2.13 (55)	1.74 (41)	1.64 (57)	1.51 (60)	1.33 (38)	1.30 (40)	0.8543	5.03	14.44
MZFF H$_z$ 6h/N$_2$/1150	4.93 (58)	3.01 (59)	2.57 (100)	2.46 (40)	2.13 (46)	1.73 (34)	1.64 (52)	1.50 (51)	1.34 (30)	1.29 (33)	0.8509	5.08	14.46
MF/ZF/FH 6h/N$_2$/1150	4.90 (8)	3.00 (38)	2.56 (100)	2.45 (5)	2.12 (21)	1.73 (10)	1.63 (43)	1.499 (39)	1.34 (3)	1.29 (10)	0.8482	5.15	--
MF/ZF/FHH$_z$ 6h/N$_2$/1150	4.91 (10)	3.00 (34)	2.56 (110)	2.45 (9)	2.12 (18)	1.73 (12)	1.63 (40)	1.51 (1)	--	--	0.8491	5.12	--
MF/ZF/FF 6h/N$_2$/1150	4.93 (60)	3.00 (64)	2.56 (100)	2.46 (46)	2.12 (49)	1.73 (42)	1.63 (52)	1.50 (56)	--	1.30 (38)	0.8498	5.11	

formate (MF') and zinc formate (ZF'), leads to the ferrite MF'/ZF'/FH and gives a σ_s of 55 emu/g, while that prepared in N_2, shows a lower value of 34 emu/g.

Table 4.3.2 Saturation Magnetization of $Mn_{1/2}Zn_{1/2}Fe_2O_4$

Sr. No.	$Mn_{1/2}Zn_{1/2}Fe_2O_4$ samples	Type & nature of Sample	Sintering	Saturation Magnetization σ_s (emu/g)	Quenched at $1200^\circ C$ σ_s (emu/g)
1	MZFH	Coppt^n Hydroxide	$1150/N_2/3h$	86	
2	MZFHH$_z$	Coppt^n Hydroxide Hydrazinate	$1200/N_2/6h$	79.92	
3	MZFF'	Coppt^n Formate	1200 / air	39	54.8
4	MZFF'	Coppt^n Formate	$1000/N_2/6h$	39	
5	MZFF'H$_z$	Coppt^n Formate Hydrazinate	$1150/N_2/3h$	53	
6	MF'/ZF'/FH	Solid State	1150/air/3h	55	
7	MF'/ZF'/FH	Solid State	$1150/N_2/3h$	34	61.5
8	MF'/ZF'/FHH$_z$	Solid State	1150/air/3h	56	
9	MF'/ZF'/FHH$_z$	Solid State	$1150/N_2/6h$	56	59.9
10	MF'/ZF'/FF'	Solid State	1150/air/6h	49	
11	MF'/ZF'/FF'	Solid State	$1150/N_2/6h$	54	
12	MF'/ZF'/FF'H$_z$	Solid State	$1150/N_2/6h$	44	

M = Mn, Z = Zn, F = Iron, H = Hydroxide, F' = Formate, Hz = Hydrazinate.

The ferrite (MF'/ZF'/FHHz) that prepared in air from the iron oxide, mainly $\gamma-Fe_2O_3$, that obtained from FHHz/NaOH, shows a value of σ_s = 56 emu/g, while that sintered in N_2 also gives the value of 56 emu/g.

The iron oxides, $\gamma-Fe_2O_3$ + $\alpha-Fe_2O_3$, that prepared from iron formate, FF'-II/NaOH, give the ferrite in air of σ_s = 49 emu/g (MF'/ZF'/FF'), while that synthesized in N_2 shows a value of 54 emu/g.

A saturation magnetization of 55.85 emu/g was obtained for $Mn_{0.5}Zn_{0.5}Fe_2O_4$ [154] from a solid state reaction between $MnFe_2O_4 + ZnFe_2O_4 \sim 1000^{\circ}C/24h$. Our values are found to be very close to this reported value.

The $Mn_{1/2}Zn_{1/2}Fe_2O_4$ prepared in N_2, however, from coprecipitation technique gave very high σs of the order of 79.92 to 86 emu/g. The MZFH is the ferrite obtained from precursor hydroxides of manganese zinc iron shows a value of 86 emu/g. The hydroxide precursor on equilibrating in hydrazine hydrate and on decomposition and sintering in N_2 give a ferrite MZFHHz of value 79.92 emu/g. On the other hand, the coprecipitation of manganese, zinc and iron as formates on decomposition and sintering in air and N_2, MZFF/N_2/air, gives σs value of 39 emu/g. The formate on equilibrating with hydrazine and then decomposing and sintering in N_2 gives a value of 53 emu/g.

A study carried out to see the reactivity of iron oxide in the synthesis of $Mn_{0.4}Zn_{0.6}Fe_2O_4$ and its influence in microstructure development from the mixture of α-$Fe_2O_3 + ZnO + Mn_3O_4$ precalcined at different temperatures before final sintering at high temperatures, the authors [151] observed low σs values for the ferrite of < 30 emu/g when sintered and cooled in air, while higher values with maximum 85 emu/g were obtained when sintered in air and then cooled in N_2. The variations in σs values observed in our samples may, hence, due to the processing conditions. Although 55.85 emu/g was observed [154] for $Mn_{0.5}Zn_{0.5}Fe_2O_4$, we do get values in this range. But, then higher values that obtained in our studies from coprecipitation technique of ~ 80 - 86 emu/g is surprisingly very high.

The Mn-Zn ferrites preparation is very sensitive to the methods of preparation and atmospheres of sintering. Sintering of Mn-Zn ferrite is an important and elaborate step [147]. Among many reasons for getting variation in magnetic, permeability etc values, zinc loss posses a problem when high sintered density is required. This sintering reports

to high temperatures and hence loss in zinc is possible. If atmospheres are not controlled the oxidation of Mn^{2+} may lead to high valence states (and consequent reduction of Fe^{3+} to lower valence state) may occur. As concentration of Fe^{2+} in the ferrite is also needed, controlled atmospheric sintering is essential. Inert gas atmosphere sintering or cooling of the ferrite (after heating in air / oxygen) is required to be undertaken. The cooling in N_2 also helps in avoiding reoxidation of Mn^{2+} and Fe^{2+}. A systematic heat schedules are normally adopted to avoid microcracks development in the dense samples. Thus, many precautionary measures are required in the synthesis of Mn-Zn ferrites. Many a times, to freeze the obtained composition at higher temperatures, one needs to quench the samples. This way, magnetic and electric characteristics of the ferrites can be optimised.

Few samples of the ferrites in the present investigations have been quenched The sample MZFF/air having σs = 39 emu/g on quenching from $1200^{\circ}C$ showed an increase in the value to 54.8 emu/g. Similarly, the MF'/ZF'/FH sample of 34 emu/g increased to 61.5 emu/g on quenching.

Structural aspects of γ-Fe_2O_3: Hydrogen iron oxide or hydrogen ferrite

Gamma ferric oxide, γ-Fe_2O_3, is an oxidation product of spinel magnetite, Fe_3O_4.

Magnetite is a ferrouso – ferric oxide, $FeO.$ Fe_2O_3, and it is an inverse cubic spinel,

$(Fe^{3+}_8)_{tet}$ $[Fe^{2+}_8 Fe^{3+}_8]_{oct}$ O_{32}. The ferrous ions are on the octahedral sites. The oxidation

of this Fe_3O_4 leads to cubic γ-Fe_2O_3. The cubic γ-Fe_2O_3 on further heating transforms into

a hexagonal corundum α-Fe_2O_3.

It was found that synthetic magnetite transformed more easily into γ-Fe_2O_3 than

the natural magnetite. While oxidising synthetic magnetite it was observed that there are

four forms of γ-Fe_2O_3. Three of them belongs to cubic system and the fourth belongs to

the tetrahedral system [155 – 156]. The synthetic and natural magnetites during oxidation

created a lot of interest among researchers because of their difference in behaviour The

synthetic Fe_3O_4 oxidised first to γ-Fe_2O_3 and then to α-Fe_2O_3, whereas the natural

magnetite oxidised mainly to α-Fe_2O_3. Even in the synthetic magnetite [157] the

specimen which on oxidation gave γ-Fe$_2$O$_3$ invariably contained an appreciable percentages of water, while the specimens prepared under dry conditions oxidized with great difficulty, never yielding γ-Fe$_2$O$_3$. From x-ray study [158] it was found that the natural single crystal of Fe$_3$O$_4$ when heated to 600°C gave mainly α-Fe$_2$O$_3$.

The early workers found on oxidation of Fe$_3$O$_4$ to γ-Fe$_2$O$_3$ some extra lines in the x-ray photographs. These extra lines could be accounted for if γ-Fe$_2$O$_3$ had a primitive cell (Fe$_3$O$_4$ is face centred cubic) of the approximate dimensions of Fe$_3$O$_4$. In recent years, however, various workers have expressed doubt about the structure of γ-Fe$_2$O$_3$ which was proposed in 1931 [159] and concluded [160] that the changes in the intensities of the diffraction lines and also in the density of γ-Fe$_2$O$_3$ from that of Fe$_3$O$_4$ were produced by the vacant sites in the iron atom lattice in the spinel that formed on oxidation. The oxygen during oxidation of Fe$_3$O$_4$ is certainly not added to the lattice. A suggestion thus came stating that structure of γ-Fe$_2$O$_3$ is defective one with cation vacancies in an oxygen ion frame work. Hence, when Fe$_3$O$_4$ is written as Fe^{2+}$_8$Fe^{3+}$_{16}$O^{2-}$_{32}$ the γ-Fe$_2$O$_3$ can be written as Fe^{3+}$_{21.33}$ $\square_{2.67}$ O^{2-}$_{32}$, where $\square_{2.67}$ denotes the cation vacancies.

Thus, on oxidation of Fe$_3$O$_4$, for every 3 Fe^{2+} ions there appears 2 Fe^{3+} ions and corresponding number of vacancies arise and hence a composition Fe$_{64/3}$ $\square_{8/3}$ O$_{32}$ is the result of such oxidation which represents γ-Fe$_2$O$_3$. And, the vacancies were considered [161 – 162] to be present preferentially on the octahedral sites of the spinel structure of Fe$_3$O$_4$ from which the γ-Fe$_2$O$_3$ is obtained. The spinel structure is thus considered as consisting of octahedral vacancies, (Fe^{3+}$_8$)$_{tet}$ [Fe^{3+}$_8$ Fe^{3+}$_{5\ 1/3}$ $\square_{8/3}$]$_{oct}$ O$_{32}$. However, some authors [163 – 165] also report that the vacancies may also enter both the octahedral and tetrahedral sites of the spinel.

The moisture containing magnetite [157] transformed into γ-Fe_2O_3 and the gamma ferric oxide thus obtained retained in its lattice small amount of water. Any attempt to remove this water ended the transformation into α-Fe_2O_3. This findings confirmed the earlier studies [166].
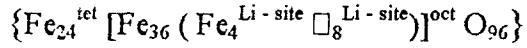
Although the oxidation of Fe_3O_4 yields γ-Fe_2O_3, it is considered that the oxidation process is crucial and water is found to essential [155,157, 167 – 175] in stabilizing the metastable phase of the iron oxide. In the absence of this water the oxidation proceeds to thermodynamically more stable oxide of iron, α-Fe_2O_3.

The importance of the water in γ-Fe_2O_3 preparation is also studied by Rane et al [79] and the others [78, 80 – 85]. The essential requirement of water in stabilizing γ-Fe_2O_3 and the structural similarity of this oxide with that of lithium ferrite, $LiFe_5O_8$, $(Fe^{3+})_8$ $[Li^{1+}_4 Fe^{3+}_{12}] O_{32}$, allowed the researchers [155, 157, 169] to assume that the vacancies are occupied by some 1+ charged species. Since water promotes the stabilization of γ-Fe_2O_3, protons H^{1+} were considered to be incorporated in the lattice. A fully protonated γ-Fe_2O_3, hence, may be written similar to $LiFe_5O_8$ as HFe_5O_8, $(Fe^{3+})_8$ $[H^{1+}_4 Fe^{3+}_{12}] O_{32}$.

The γ-Fe_2O_3 stabilized under controlled water vapour decomposition of ferrous oxalate dihydrate was considered [176] to have a composition in between (Fe^{3+}_8) Fe^{3+}_{12} $Fe^{3+}_{4/3} \square_{8/3}]O_{32}$ and $(Fe^{3+})_8$ $[H^{1+}_4 Fe^{3+}_{12}]O_{32}$, which may be given as $(Fe^{3+})_8$ $[Fe^{2+}_x H^{1+}_{4-2x} \square_x Fe^{3+}_{12}] O_{32}$. Some Fe^{2+} ions may thus be introduced due to the proton incorporation. An extreme case would be $(Fe^{3+})_8$ $[Fe^{2+}_2 \square_2 Fe^{3+}_{12}] O_{32}$.

This protonated phase of γ-Fe_2O_3 is called [169] as a hydrogen iron oxide, $H_{1-x}Fe_{5+x/3}O$ or hydrogen doped iron oxide with an upper limit [170] of the presence of H^{1+} is put at $H_{0.1}Fe_{5 1/3}O_8$. And it was also considered as hydrogen ferrite type of phase

by Nikumbh, Rane, Mukhedkar [176]. From the similarity with the lithium ferri e, the protons, H^{1+}, may now be thought to be occupying the so called 'Lithium sit es' of γ-Fe$_2$O$_3$ [177 – 178]. The γ-Fe$_2$O$_3$ is actually Fe$_{64}$O$_{96}$,

$$\{Fe_{24}^{tet} \; [Fe_{36} \; (\; Fe_4^{Li\text{-}site} \; \square_8^{Li\text{-}site})]^{oct} \; O_{96}\}$$
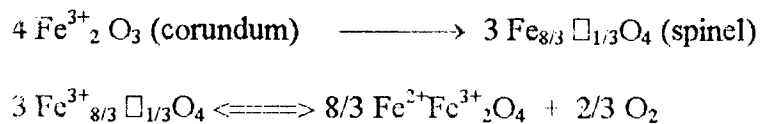
The presence of protons in γ-Fe$_2$O$_3$ is being investigated by Nikumbh, Rane, Mukhedkar [176] after carefully studying the thermal decomposition of ferrous (xalate dihydrate in a controlled atmosphere of water vapour as described by Rane et al [9], by adopting a direct current electrical conductivity measurements as a functi n of temperature in different atmospheres. This method gave a qualitative idea abc ut the presence of protons in γ-Fe$_2$O$_3$. The method was further extended to γ-Fe$_2$O$_3$ ob tained from variety of precursors [46] and such studies also qualitatively revealed the pr sence of protons in it. However, since protons occupy the lithium sites of γ-Fe$_2$O$_3$, it was felt to carry out the lithiation studies on the oxide and then study this by electrical condt ctivity measurements. The results of such studies [179] are presented in this chapter.

The detailed structural aspects of γ-Fe$_2$O$_3$ is important in our present re search activities as we are aiming at synthesizing ferrites using γ-Fe$_2$O$_3$, γ-Fe$_2$O$_3$ + α- Fe$_2$O$_3$, α-Fe$_2$O$_3$ as raw materials. This use of γ-Fe$_2$O$_3$ is thought to enhance the rate of re action of spinel formation if used in the ferrite synthesis, instead of usual α-Fe$_2$O$_3$.

One possible reason for such enhanced reactivity of γ-Fe$_2$O$_3$ may be because it has cubic structure similar to the end products in ferrites synthesis, ie Cubic spinel The reactivity is further enhanced if the other metal oxides (MgO / MgCO$_3$, MnO, ZnO) are also cubic. The structural compatibility between the reactants now may lead to better reaction as explained in the introduction.

Another possible reason for the increased reactivity of γ-Fe_2O_3 is due to the fact that it transforms during heat treatment in ferrite preparation to active α-Fe_2O_3 which may cause the better reactivity with the other oxides. Also, it is being thought that [7] in the ferrite preparation from usual raw material α-Fe_2O_3 and if the oxide is in excess then this may change to the γ- variety which may be in equilibrium with α-Fe_2O_3.

$$4 \, Fe^{3+}_2 O_3 \text{ (corundum)} \longrightarrow 3 \, Fe_{8/3} \square_{1/3} O_4 \text{ (spinel)}$$

$$3 \, Fe^{3+}_{8/3} \square_{1/3} O_4 \Longleftrightarrow 8/3 \, Fe^{2+}Fe^{3+}_2 O_4 + 2/3 \, O_2$$

The presence of oxygen in the atmosphere during preparation of ferrites may shift the second equilibrium backwards and cause cation vacancies which are favourable to grain growth. In the study of manganous-zinc ferrite synthesis the authors [181] invoked this aspect of the cation vacancies to get crack free grains of the ferrite.

γ-Fe_2O_3 has cation vacancies hence they may help at lower temperature to allow the other cation enter these vacancies when used as raw material in the ferrite synthesis. Also, if the H^+ ions leave in the lattice then there will be a driving force for the cations to enter these sites. And, the substitution of the protons by Ni, Gd has also been studied by Nikumbh, Rane and Mukhedkar [182]. All these factors, thus, may lead to better cation diffusion and hence lead to the early spinelization, if γ-Fe_2O_3 is taken as a starting material.

The protons of γ-Fe_2O_3 are found to leave the lattice ~ $180^{\circ}C$ [176]. The proton eliminated γ-Fe_2O_3 now is similar to the usual vacancy ordered γ-Fe_2O_3. And hence, the presence of such important protons in γ-Fe_2O_3 is being investigated here by lithiation.

5.1 Experimental

a) Standard γ-Fe_2O_3

The standard γ-Fe_2O_3 sample on which several studies being done in the present

investigations has been used for conducting thermal analysis like DTA, TG and measuring electrical conductivity as a function of temperature in different atmospheres.

b) Lithiation of γ-Fe$_2$O$_3$

γ-Fe$_2$O$_3$ is considered to consist of protons, H^{1+} in its lattice on the octahedral sites and it may contain the protons in the upper limit which is put at $H_{0.1}Fe_{5\,1/3}O_8$ The protons incorporated samples may contain ~ 0.75 (%) H^{1+} in the lattice. The fully protonated sample, $H_1Fe_5O_8$ has 7.14 (%) H^{1+} in the lattice. If lithium ions are capable of substituting these protons, then two samples of lithium added γ-Fe$_2$O$_3$ are needed for further studies to be carried out. Hence we prepared two samples of lithium incorporated γ-Fe$_2$O$_3$: one lithium exact consisting of 1 – 2 (%) Li and the other lithium excess having 7 – 8 (%) Li.

i) Lithium exact γ-Fe$_2$O$_3$

3.766 ml of n-butyl lithium in hexane (15 % solution) was stirred with 3g of γ-Fe$_2$O$_3$ in an inert atmosphere. The dried sample is stored in a desiccator.

ii) Lithium excess γ-Fe$_2$O$_3$

6.513 ml of 15 (%) solution of n-butyl lithium in hexane with 3g γ-Fe$_2$O$_3$ was stirred well in an inert atmosphere. The dried sample was then stored in a desiccator.

c) Preparation of pellet

Sample of γ-Fe$_2$O$_3$ and lithium doped γ-Fe$_2$O$_3$ were pressed in the form of pellets of dimensions 10 mm diameter x 3 – 4 mm thickness.

5.2 Characterization

a) Chemical analysis

The percentage of FeO in the lithiated samples was determined by standard potassium dichromate method.

b) Thermal analysis

DTA and TG analysis was done on STA 1500 instrument in air. DSC analysis was carried out on TA instrument 2000 Thermal analyser -- DSC modulated.

c) Phase identification

X-ray diffraction studies were carried out on Rigaku D Max II x-ray diffractometer using Cu and Fe targets. The observed d $_{hkl}$ values were compare 1 with JCPDS files [87] to identify the phases.

d) Infra red analysis

The infra red analysis of the samples was done on Shimadzu FTIR, model 8101A.

5.3 Direct current (dc) electrical conductivity

Direct current electrical conductivity, σ, as a function of temperature in air, N_2 and again in air after moisture equilibration was done on a home built conductivi y cell system.

Pellets of known dimension were pressed between two platinum electrodes. Temperature of the furnace is well controlled.

For passing nitrogen and moisture a special arrangement was adopted. For moisture equilibration a carrier gas was bubbled through a container containing water
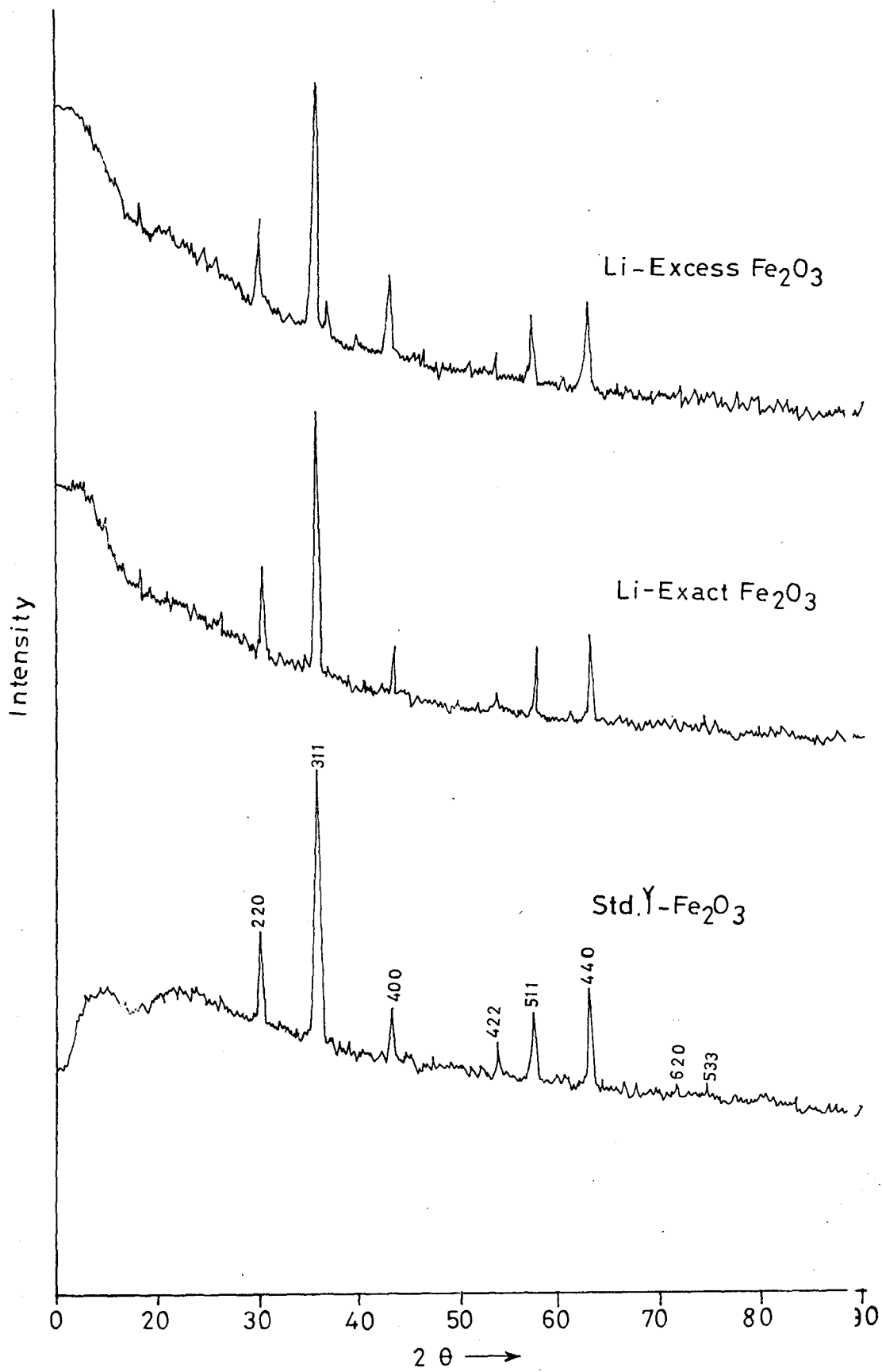
FIG. 5.1:- XRD pattern of std γ -Fe$_2$O$_3$ & lithiated γ-Fe$_2$O$_3$.

kept at ~ 60°C. The moisture that carried by the carrier gas was preheated ~ 150°C before passing over the conductivity cell. Nitrogen gas was used as a carrier gas.

5.4 Results and Discussion

5.4.1 Phase identification

The x-ray diffraction patterns of γ-Fe$_2$O$_3$ and the lithiated samples are presented in Fig. 5.1. the xrd pattern and the d $_{hkl}$ values of γ-Fe$_2$O$_3$ match well with the reported JCPDS files for γ-Fe$_2$O$_3$. Lithium exact γ-Fe$_2$O$_3$ and the lithium excess samples show an identical pattern to that of Std. γ-Fe$_2$O$_3$. The maximum 100 (%) peak due to d $_{hkl}$ = 311, however, showed a slight decrease in intensity in the lithiated samples. Otherwise, all the other peaks show almost similar intensity behaviour with that of the Std. γ-Fe$_2$O$_3$. These results indicate qualitatively that the lithiation has not converted γ-Fe$_2$O$_3$ into any other phase.

5.4.2 Chemical analysis

Sample of γ-Fe$_2$O$_3$ does not indicate any chemically measurable ferrous ions presence in the form of FeO. The lithium exact γ-Fe$_2$O$_3$, however, shows a presence of 6.12 (%) FeO, while the lithium excess γ-Fe$_2$O$_3$ found to consists of 25.77 (%) FeO. The lithium excess γ-Fe$_2$O$_3$ is slightly blackish in its appearance, whereas the brown γ-Fe$_2$O$_3$ does not indicate any change in colour on lithiating 1 – 2 (%) lithium. The xrd pattern of the lithium excess γ-Fe$_2$O$_3$ does not show any change in the peak position, but then if it has more FeO then it may have turned to ferrouso-ferric oxide, FeO.Fe$_2$O$_3$ (Fe$_3$O$_4$) The magnetite, Fe$_3$O$_4$, is also a cubic spinel and is a precursor of γ-Fe$_2$O$_3$. It is difficult to identify Fe$_3$O$_4$ in γ-Fe$_2$O$_3$ as d$_{hkl}$ values for both are almost identical. The lattice

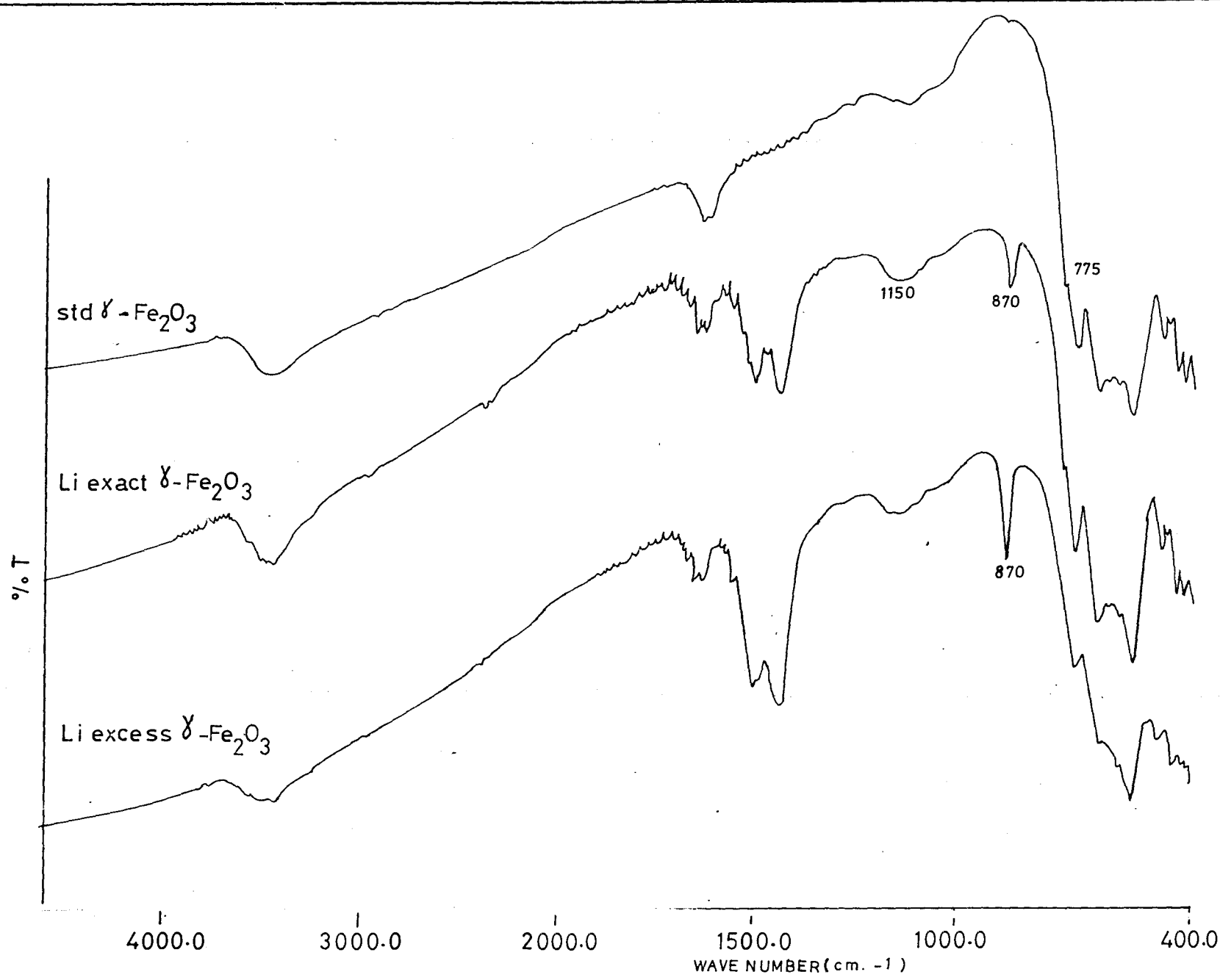FIG. 5.2:—IR Spectra of std γ-Fe$_2$O$_3$ & lithiated γ-Fe$_2$O$_3$.
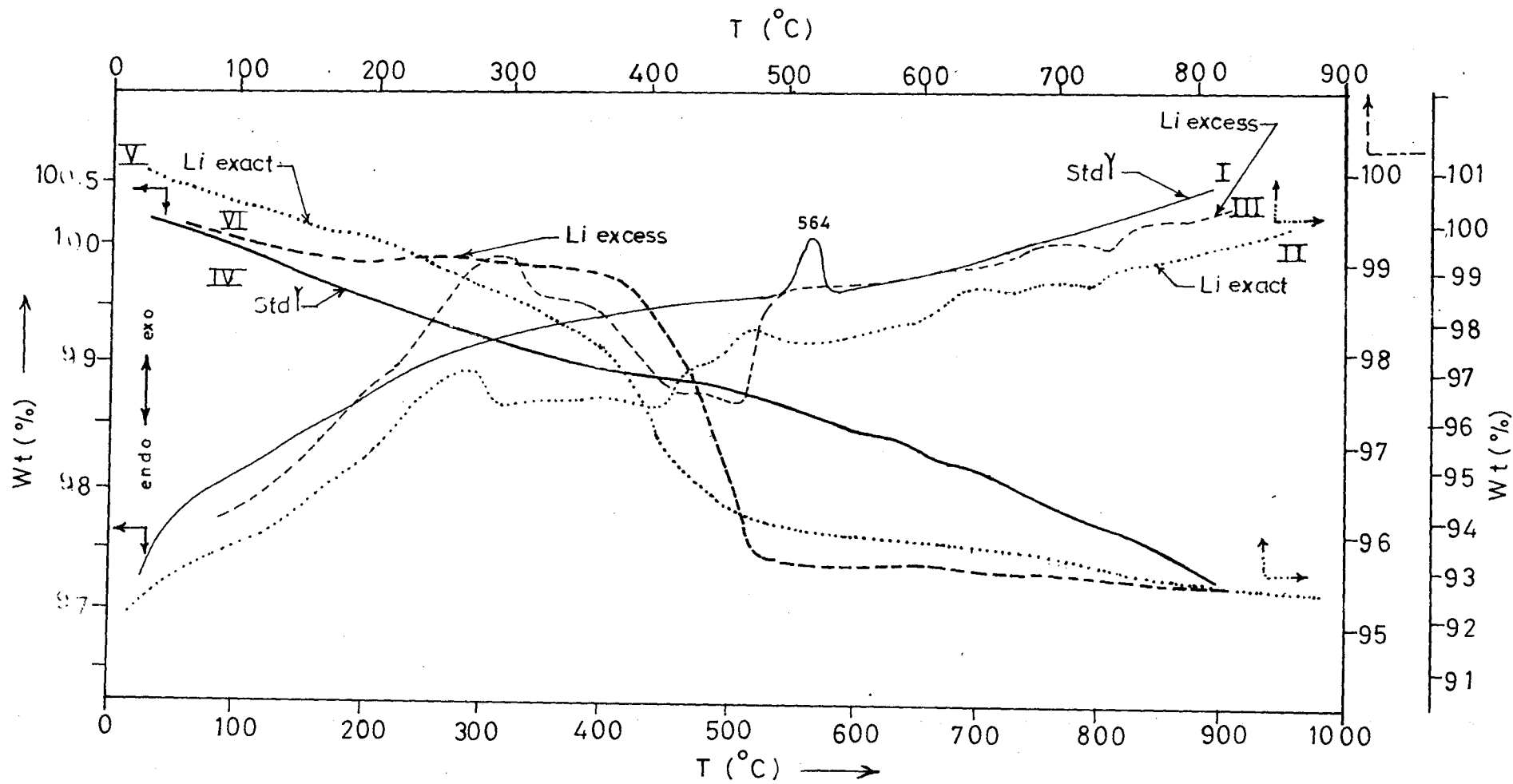
FIG. 5.3:—DTA / TG traces of stdγ-Fe$_2$O$_3$ & lithiated γ-Fe$_2$O$_3$.

parameter calculation also does not show any change in the 'a' parameter. However, quantitative studies on the x-ray analysis is being done separately in our laboratorie.

5.4.3 Infra red analysis

The IR band positions of γ-Fe_2O_3 and the two lithiated samples are given n Fig. 5.2. The IR band positions of Std. γ-Fe_2O_3 (curve I) at 550, 640, 700, 725 cr $^{-1}$ are retained in Li exact γ-Fe_2O_3 (curve II), while a new band appeared at ~ 870 cm^{-1}. n Li - excess γ-Fe_2O_3 (curve III) all the four bands are present as in Std. γ-Fe_2O_3 but th(band that appeared ~ 870 cm^{-1} in Li - exact showed an increased intensity. The 1125, 16.5 and 3420 cm^{-1} bands are present in all three samples. However, there appears bands ~ 1425 and 1500 cm^{-1} in Li - exact which are not present in Std. γ-Fe_2O_3; the bands show increased intensity in Li - excess sample. A weak band also appears ~ 2180 cm^{-1} in the lithiated samples.

The results of ir studies thus reveal some change on lithiation in the fine structure of γ-Fe_2O_3 which was not detected in γ-Fe_2O_3. Chemical analysis did show the presence of FeO in both the lithiated samples.

The band positions in standard γ-Fe_2O_3 are, however, agree well with the reported for gamma ferric oxide.

5.4.4 Thermal analysis

The DTA and TG traces of Std. γ-Fe_2O_3 and both the lithiated γ-Fe_2O_3 samples are given in Fig. 5.3. An exothermic effect ~ 564°C on DTA (curve I) for Std. γ-Fe_2O_3 is due to the transformation of γ-Fe_2O_3 to α-Fe_2O_3. The transformation is confirmed by xr l. A gradual loss of mass of 1.5 (%) between 42° and the onset of exothermic reaction at ~ 538°C on TG (curve iv) suggests that the water absorbed is lost from the as prepared γ-Fe_2O_3.
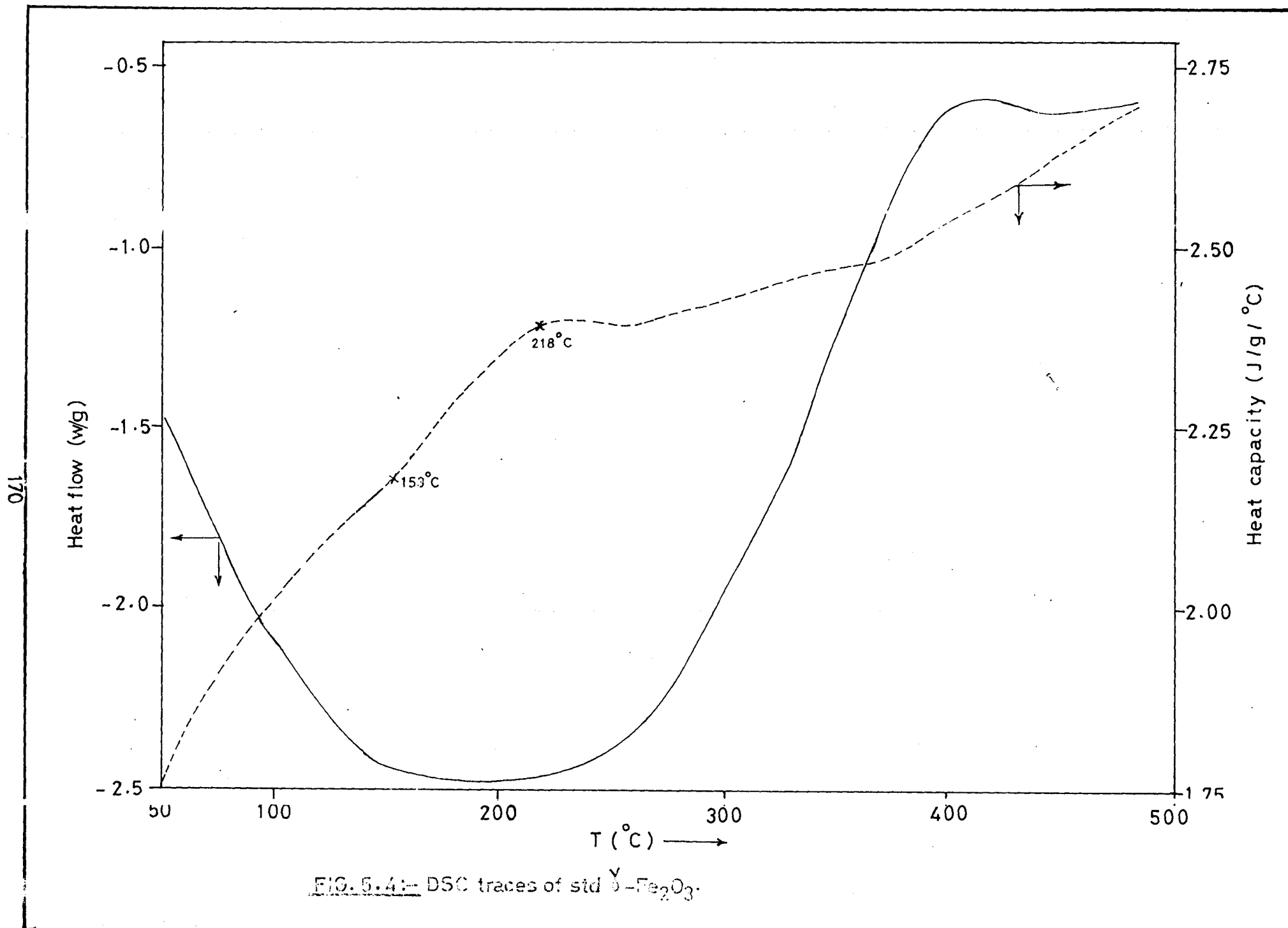
FIG. 5.4:– DSC traces of std γ–Fe_2O_3.

DTA / TG traces of both the lithiated samples, however, show several thermal effects in the temperature range where Std. γ-Fe_2O_3 gives one exothermic peak.

The lithium exact γ-Fe_2O_3 indicates (curve II) an exothermic peak ~ $265^{\circ}C$ while that of Li – excess γ-Fe_2O_3 (curve III) shows the effect ~ $289^{\circ}C$. The mass losses observed on TG traces (curve v and vi) for these samples upto these temperatures are ~ 1 (%). Beyond these temperatures there occurs further exothermic effects in both the samples. Since our interest in these samples is to look into any variation upto $350^{\circ}C$, we have not analysed the full pattern of DTA / TG studies. This work is taken up separately by our research group for further studies.

Chemical analysis carried out on the samples of lithiated γ-Fe_2O_3, after the exothermic effects (~265 and ~ $289^{\circ}C$), revealed the absence of FeO in them. This suggests that the exothermic effects are due to the oxidation of Fe^{2+} to Fe^{3+}. The phase transformation of γ-Fe_2O_3 to α-Fe_2O_3 is observed ~ $540^{\circ}C$ in standard γ-Fe_2O_3 and the lithiated samples may then be transformed to α-Fe_2O_3 in case of Li – exact sample around this temperature as indicated by a weak exotherm ~ $500^{\circ}C$. But the Li – excess γ-Fe_2O_3 which contained ~ 7 – 8 (%) lithium in it is found to show an exotherm ~ $560^{\circ}C$. This may be the transformation of lithiated γ-Fe_2O_3 to α-Fe_2O_3 or it may give lithium ferrite of $LiFe_5O_8$ type (as in it lithium is ~ 7 – 8 %). We have not done any phase analysis of these. High temperature x-ray studies may reveal some interesting results.

Differential scanning calorimetry (DSC) studies have been done only on standard γ-Fe_2O_3. The DSC traces are given in Fig. 5.4. Both the heat capacity and heat flow changes from RT to $400^{\circ}C$ are given in the figure. It may be seen from DSC traces that there is some change in heat capacity ~ 153° and $218^{\circ}C$. The heat flow trace shows correspondingly an increase in the temperature range 50 – $150^{\circ}C$ and between 30 – $225^{\circ}C$ it remains constant then there is an increase till $350^{\circ}C$. Although, the analysis of
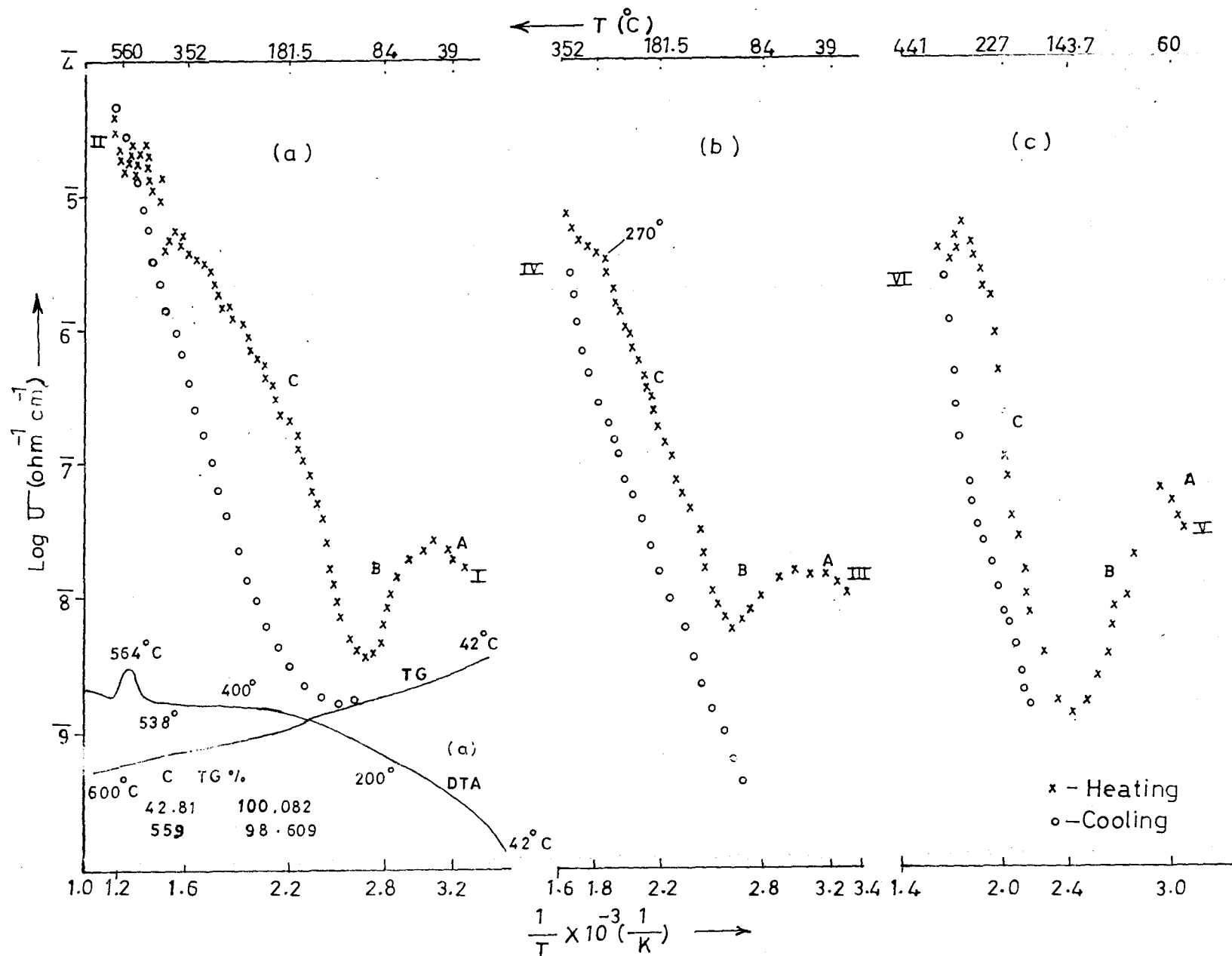
FIG.5.5:– Temperature variation of conductivity of :–
a) std γ-Fe$_2$O$_3$ → α-Fe$_2$O$_3$ b) std γ-Fe$_2$O$_3$ c) moisture equilibrated std γ-Fe$_2$O$_3$.

this sample as well as the lithiated samples are not complete, the elementary observations reveal that γ-Fe$_2$O$_3$ undergoes some changes in ~ 150^0 and 218°C. TG and DTA studies, however, do not show any traceable changes around these temperatures. DSC hence gives better insight in the fine structural changes that occur in γ-Fe$_2$O$_3$.

5.4.5 D. C. Electrical conductivity

Direct current (dc) electrical conductivity (ec) measurements by two probe method were conducted [46 - 47] on all γ-Fe$_2$O$_3$ samples that have been mentioned n Part I of chapter IV. The conductivity results were then compared with the data o1 Std. γ-Fe$_2$O$_3$. Although these results have enabled to qualitatively confirm the prese ice of protons in the lattice of γ-Fe$_2$O$_3$ that had been detected from the condu ctivity measurements by Rane et al [79, 90, 182], the studies on lithiated γ-Fe$_2$O$_3$ done by Rane et al [179] are being discussed here.

The Std. γ-Fe$_2$O$_3$ transforms to α-Fe$_2$O$_3$ ~ 560°C (Fig. 5.3) and the condu ctivity behaviour as a function of temperature has been done in the full range of temperat ire of this transformation. The log σ Vs 10^3/T plot of Std. γ-Fe$_2$O$_3$ from RT – 600°C is hown in Fig. 5.5a. The DTA / TG traces in this temperature range are also given in the same figure again for quick consultation. A conductivity increase measured in air during heating (curve I) from RT to 50°C (region A) is followed by a decrease in the valu upto 90°C (region B). From 90°C onwards there is a steep increase in σ till 360°C. Between 360° and 560°C there occurs several breaks in the plot. From 560°C onwards the e is a steep increase in σ till 600°C. The break ~ 560°C in the log σ Vs 1/T plot ar d the exothermic peak in DTA ~ 564°C suggests that the γ-Fe$_2$O$_3$ at this temperature range transforms into α-Fe$_2$O$_3$. Hence, the conductivity behaviour > 560°C is due to α-Fe$_2$O$_3$ that formed. The cooling curve is now due to α-Fe$_2$O$_3$ (curve II) and there is a conti iuous

decrease in the conductivity and this curve is not expected to overlap the heating curve I of γ-Fe$_2$O$_3$.

Hysteresis in conductivity

As we are interested only in the conductivity behaviour of γ-Fe$_2$O$_3$, the region C (of curve I) between 90° and 360°C is of our concern. In Fig. 5.5b the regions A B, C (curve III) of a fresh Std. γ-Fe$_2$O$_3$ sample during heating from RT to 360°C are shown. The sample then on cooling, the conductivity plot (curve IV) is found not retracing the heating curve III. There is thus a hysteresis behaviour in the conductivity plot of heating and cooling of γ-Fe$_2$O$_3$ (curves III and IV).

Once cooled, further heating of the sample shows a conductivity behaviour similar to the cooling curve IV and the σ values more or less overlap the values of the cooling curve. This suggests that the regions A, B and C that observed during the first heating of the fresh sample (curve III) are not observed during the second heating of the sample. The subsequent heating and cooling of the sample now found to show conductivity values overlapping the first cooling curve IV. The sample on further heating and cooling in nitrogen atmosphere too showed values overlapping curve IV. The sample, thus , consisting of no A, B and C regions then flushed with dry nitrogen ~ 200°C and then a known partial pressure of moisture in N$_2$ is passed over the sample for 2 hours and finally cooled in that atmosphere. Such moisture equilibrated sample on heating (Fig. 5.5c) showed regions A, B and C (curve V) as fresh γ-Fe$_2$O$_3$. The cooling curve V now followed other path, not overlapping the heating curve V. Thus, once again a hysteresis behaviour in the conductivity during heating and cooling is observed.

The sample is then further heated and cooled and the values, once again, as before, overlapped on the cooling curve VI. That means, the sample has no regions A, B

and C.

Arrhenius plot

Direct cureent electrical conductivity, σ, of Std. γ-Fe_2O_3 measured here show, in general, an increase in conductivity with the elevation in temperature in region C and obey Arrhenius equation $\sigma_T = \sigma_0\, e^{-\Delta E / kT}$, where σ_T is the conductivity value at a particular temperature T, σ_0 is a constant, ΔE is an activation energy of the conduction process and k is a Boltzman constant, hence, will give a straight line plot of log σ Vs 1/T of negative slope. The region of straight line plot, therefore, may be used to calcu ate an activation energy for conducting process. The break in the plot are due to diferent mechanism for conduction processes.

A careful observation of curve III (Fig. 5.5b) of log σ Vs 1/T Arrhenis plot during heating of a fresh sample of Std. γ-Fe_2O_3 in the temperature range 113° – $;50^\circ C$ indicates that there is a definite break ~ $270^\circ C$. the region C between 113 and $;70^\circ C$ shows three inclinations in the otherwise straight line in the temperature regions: 113 – $150^\circ C$, 150 $215^\circ C$ and 215 – $270^\circ C$. The cooling curve IV is not overlapping the region C and also regions A and B of heating curve. The sample ~ $113^\circ C$ in the heating curve is now free from all adsorbed moisture. The region C is therefore the electrical conductivity of moisture free γ-Fe_2O_3. This γ-Fe_2O_3 shows three inclinations n the region C suggesting that there may be three different mechanisms possible for conductivity.

TG does not show any traceable mass loss for Std. γ-Fe_2O_3 between $113^\circ C$ and $270^\circ C$ and DTA is not indicating any thermal effect in the temperature range. DSC traces (Fig. 5.4), however, show some change ~ 153 and ~ $218^\circ C$. The log σ Vs 1/T plot does show change in the slope in the regions: 113 – $150^\circ C$, 115 – $215^\circ C$ and $;15$ –

270°C. Hence, DSC and conductivity studies reveal some measurable changes in moisture free γ-Fe_2O_3 in region C. such sample on cooling and reheating does no show these changes. That means the γ-Fe_2O_3 during the first heating shows conductivity between 113 and 270°C due to some fine structural and phase changes which are reversible on moisture equilibration. Hence, the moisture may be playing some ole in γ-Fe_2O_3.

Importance of water

If in A and B regions sample losses adsorbed moisture then the region C may be considered to be due to hydroxylated or hydroxyl containing γ-Fe_2O_3. David and Welch [157] in their detailed oxidation studies on wet and dry magnetite prepared by different methods considered a composition in between $(Fe^{3+}_{20} \Box_4)(OH)_4O_{28}$ and $(Fe^{3+}_{21\ 1/3} \Box_{2/3})O_{32}$ for γ-Fe_2O_3 obtained from wet magnetite. And, the authors are of the view that small proportion of combined water is essential for the stability of γ-Fe_2O_3. Water incorporates OH in the lattice.

If such hydroxylated γ-Fe_2O_3 is considered in our case then region C may be due to such OH containing oxide which on heating ~ 270°C results into hydroxyl free γ-Fe_2O_3 and hence the cooling curve is due to hydroxyl free γ-Fe_2O_3 and hence the cooling curve IV is not overlapping the heating curve III. Equilibration of such sample with moisture, therefore, may be considered to incorporate the hydroxyls ions in the lattice.

On the other hand, if protons incorporated γ-Fe_2O_3 is considered, then the composition in between $(Fe^{3+})_8 [Fe^{3+}_{12} Fe^{3+}_{4/3} \Box_{8/3}]O_{32}$ and $(Fe^{3+})_8 [Fe^{3+}_{12} H^{1+}_4]O_{32}$ may also be proposed to γ-Fe_2O_3 in our case. But the choice between these two proposals,
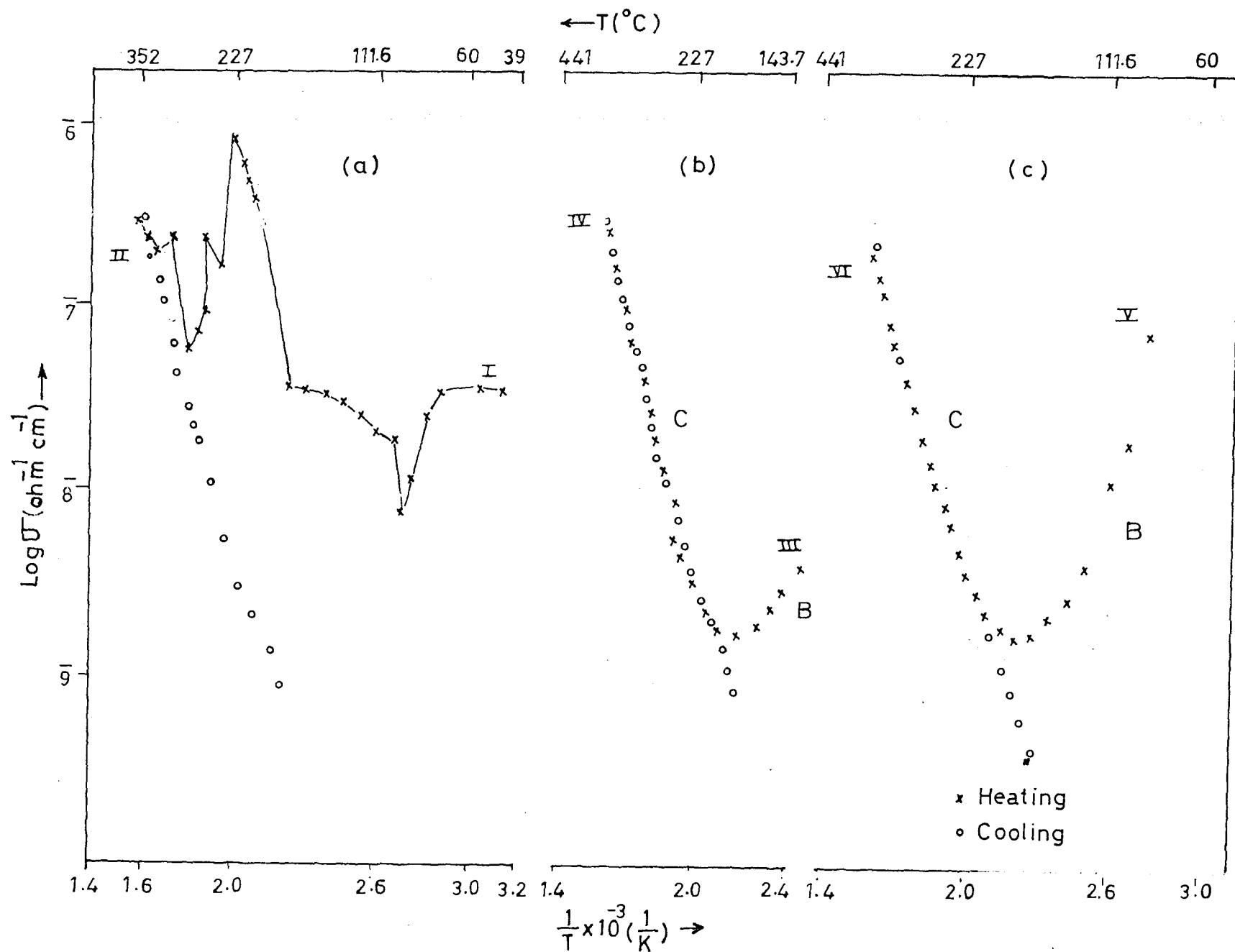
FIG. 5.6:— Temperature variation of conductivity of Li-exact η–Fe_2O_3

a) in air   b) in air/N_2 c) Moisture equilibrated

hydroxylated and protonated, requires further experimentation. And, therefore, lithium insertion studies were being carried.

Conductivity behaviour of lithiated γ-Fe$_2$O$_3$

Lithiation may incorporate Li^{1+} on vacancies or it may replace H$^+$ but not OH in the above two proposed structural composition of γ-Fe$_2$O$_3$. If Li^{1+} occupies vacancies, then hydroxyl groups will still be retained in the lattice of γ-Fe$_2$O$_3$ (hydroxylated). Then region C is expected to be due to the removal of the OH$^-$ on heating and hence they may be reintroduces on moisture equilibration. A hysteresis behaviour is therefore expected. If protons are substituted by Li, then lithium insertion in proton incorporated γ-Fe$_2$O$_3$ should not show any hysteresis behaviour even on moisture equilibration. And, this will decide about the protons presence in our γ-Fe$_2$O$_3$. Hence, conductivity behaviour of such samples may be of interest. Our results on such studies are discussed here.

Conductivity of Li – exact γ-Fe$_2$O$_3$

The d.c. electrical conductivity of Li – exact (approx. 2% Li) shows a decrease in conductivity (curve I, Fig. 5.6a) from RT to 98°C and then it increases slowly upto 181°C followed by a steep increase upto ~ 225°C. A decrease in conductivity is then observed till 280°C in two steps followed by an increase upto 340°C. A slight decrease in σ then is followed by an increase. On cooling the sample from 360°C the values show curve II in log σ Vs 1/T plot. Further heating and cooling the values overlap curve II.

The sample was then left in air in the conductivity cell for ten days and on continuing the measurements in air or N$_2$ the heating curve III (Fig. 5.6b) after an initial decrease in conductivity from RT showed an increase in the values upto 360°C. Cooling curve IV overlaped the heating curve. A 2 (%) lithium insertion does not show any change in xrd pattern (Fig. 5.1) of the Std. γ-Fe$_2$O$_3$. A chemical analysis, however,

indicates ~ .12 (%) FeO in it which means the lithiation reduced few Fe^{3+} ions in the spinel to Fe^{2+}. Lithiation of Fe_3O_4 [183 -184] and γ-Fe_2O_3 [185 – 186] have been studied by x-ray and neutron diffraction and shown that the $[B_2]O_4$ sublattice of the $A B_2]O_4$ spinel structure remains intact upon lithium insertion. Lithium enters the octahedral sites of the spinel and reduces few Fe^{3+} ions present on tetrahedral sites (8a) and pushes them into adjacent unoccupied octahedral sites (16c) thereby producing rock salt like structure in Fe_3O_4 and γ-Fe_2O_3 when large percentage of lithium is inserted ($Li_{0.85}Fe_2O_3$ and $Li_{1.2}Fe_2O_3$). However, the 2 (%) lithium insertion in the present studies that introduces ~ 4 (%) Fe^{2+} on octahedral sites is not expected to change the structure from spinel to rock salt like. This Fe^{2+} is oxidised ~ $265^{\circ}C$ to Fe^{3+} as shown by exothermic peak (Fig. 5.3) and chemical analysis. The electrical conductivity between 225 and $280^{\circ}C$ (curve I, Fig. 5.6a) may be, therefore, attributed to the oxidation process of Fe^{2+} ions. This lithium insertion sample on cooling from $360^{\circ}C$ shows curve II (Fig. 5.6a) which is different from curve I. And subsequent heating and cooling now naturally show conductivity behaviour of lithiated sample overlaping curve II or curve IV (Fig. 5.6b)

No A, B, C regions peculiar to γ-Fe_2O_3 are observed here, although, there is a region of decrease in conductivity (curve III, Fig. 5.6b) in the lithiated sample that left exposed to air for several days. This may be considered as region B. No hysteresis in region C is observed during heating and cooling.

The sample on moisture equilibration show a continuous decrease in conductivity which may be taken as region B (curve V, Fig. 5.6c). But, then, region C in heating cycle and cooling cycle overlap each other indicating clearly no hysteresis.

These results suggests us that lithiated sample has neither H^{1+} nor OH in it. If H^{1+} had been still retained even after Li insertion hysteresis behaviour would have been noticed. On the other hand, if OH had still remained in the lithiated sample then it would

FIG. 5.7:– Temperature variation of conductivity of Li-excess γ-Fe_2O_3 :– a) in air b) in air/N_2 & moisture equilibrated.

have shown the hysteresis behaviour. And also, moisture equilibration would have introduces them. Since no hysteresis in conductivity during heating and cooling of fresh and moisture treated sample observed, we may safely say that lithiated sample do not have H^{1+} or OH^-.

Conductivity behaviour of Li – excess γ-Fe₂O₃

Li-excess γ-Fe₂O₃ showed 25.7% FeO (~20% Fe^{2+}) in it and x-ray pattern (Fig. 5.1) did not show much of the change in main peaks of Std. γ-Fe₂O₃. But, urther detailed structural determination of the lithiated sample are being taken up separately. However, in the present investigation we are only looking for any hysteresis in conductivity of such samples.

A fresh Li-excess γ-Fe₂O₃ on heating shows a continuous conductivity increase upto ~ $300^{\circ}C$ then it decreases (curve I, Fig. 5.7). DTA shows (Fig. 5.3) ~ $290\,^{\circ}C$ an exotherm and chemical analysis of the product indicates no Fe^{2+}. Hence, the break in conductivity ~ $300^{\circ}C$ may be due to oxidation of Fe^{2+} to Fe^{3+}. Cooling from $360^{\circ}C$ (curve II, Fig. 5.7 a) shows a linear decrease in conductivity. On further heating and then cooling, the conductivity values found to overlap curve II.

The sample when left in the cell for several days, and then on measuring the conductivity during, heating and cooling (curves III, IV, Fig. 5.7b) showed no hysteresis behaviour. Moisture equilibrated sample also did not show hysteresis behaviour. These result clearly indicate absence of H^+ or OH^- in the lithiated sample.

CHAPTER VI

Conclusions

1. Low grade iron ore, Fe_2O_3 – 57.49 (%) and a high grade one with the oxide 76..6 (%) are extracted with acid and the metal (mainly iron) chlorides are precipitated as hydroxides.

2. The metal (iron) hydroxides on decomposition yielded α-Fe_2O_3 of purity 92 – 98.38 (%). The acid extract on solvent extraction with methyl isobutyl ketone (MIBK) and then precipitating it into hydroxide on decomposition gave 99.73 (%) pure iron oxide.

3. The metal (iron) formates prepared from the hydroxides on decomposition gave γ-Fe_2O_3 + α-Fe_2O_3 (minor quantity) of purity 96.52 – 98.67 (%).

4. Metal (iron) hydroxides and metal (iron) formates on hydrazinating by equilibration in a desiccator containing hydrazine hydrate when exposed to air decomposed easily to mainly γ-Fe_2O_3.

182

5. The iron oxides, α-Fe_2O_3 and γ-Fe_2O_3 on mixing with $MgCO_3$ and heat treating (ceramic technique) at $1000^\circ C$ / 24h yielded single phase $MgFe_2O_4$.

6. The commercial hematite, α-Fe_2O_3, however, when used as a precursor in the $MgFe_2O_4$ preparation indicated incomplete formation of the ferrite phase (MgHem) with some admixture of α-Fe_2O_3.

7. Standard γ-Fe_2O_3 also yielded a single phase $MgFe_2O_4$.

8. Particle size distribution (SEM studies) of the $MgFe_2O_4$ samples showed uniform particles and a porosity < 25 (%) is observed in all, while the ferrite (MgHem) prepared from commercial hematite, α-Fe_2O_3, indicated a high porosity ~ 42 (%).

9. The $MgFe_2O_4$ obtained from spindle like standard γ-Fe_2O_3, however, showed dumb – bell shape particles.

10. The saturation magnetization, σs, values between 20 – 28 emu/g are observed for all $MgFe_2O_4$ samples, excepting the ferrite that obtained from hematite (MgHem).

11. Curie temperatures of all $MgFe_2O_4$ are within the range reported, while MgHem showed the highest Tc.

12. Curie temperature Tc of all $MgFe_2O_4$ samples are also obtained from temperature variation of susceptibility, permeability and resistivity.

13. Frequency variation of permeability, dielectric constant, tanδ loss are being investigated. Although, any critical analysis could not be done, but results need careful attention to establish the importance of these properties.

14. The $Mn_{1/2}Zn_{1/2}Fe_2O_4$ samples prepared from the iron oxides, α-Fe_2O_3 and γ-Fe_2O_3, however, indicate single phase ferrite formation. The investigations are only restricted to the measurement of saturation magnetization. However, further studies are required to be carried out.

15. The present investigations are done keeping in mind the usefulness of γ-Fe$_2$O$_3$ in ferrites synthesis. The literature survey indicates that ferrites of better properties can be prepared easily at lower temperatures if γ-Fe$_2$O$_3$ is used as a precursors, instead of α-Fe$_2$O$_3$.

Although this difference in properties of ferrites prepared from α-Fe$_2$O$_3$ and γ-Fe$_2$O$_3$ is not clearly visible in the present investigations, the studies done here clearly indicate that better quality ferrites can be obtained from freshly prepared iron oxides from iron ore rejects. The commercial hematite, however, yielded poor quality MgFe$_2$O$_4$.

16. Further work is required to be carried out to establish any enhancement in reaction rate between synthetic γ-Fe$_2$O$_3$ (from ore rejects) and divalent metals compared to the reaction between α-Fe$_2$O$_3$ + MO. However, in the present investigation we have also explored some structural aspects of γ-Fe$_2$O$_3$.

17. γ-Fe$_2$O$_3$ is a vacancy ordered inverse spinel obtained by the oxidation of inverse spinel magnetite, Fe$_3$O$_4$, (Fe^{3+})$_8$ [Fe^{3+}$_8$Fe^{2+}$_8$]O$_{32}$. This oxidation yields γ-Fe$_2$O$_3$, (Fe^{3+})$_8$ [Fe^{3+}$_{40/3}$ $\square_{8/3}$]O$_{32}$, where, $\square$, and vacancies on the octahedral sites.

18. The Fe$_3$O$_4$ oxidation is crucial and water has been considered to be essential in stabilizing the oxidation product, γ-Fe$_2$O$_3$.

19. The essential requirement of water in stabilizing γ-Fe$_2$O$_3$ and its crystal structure similarity with lithium ferrites, LiFe$_5$O$_8$, (Fe^{3+})$_8$ [Li^{1+}$_4$Fe^{3+}$_{12}$]O$_{32}$ has made researchers to consider the γ-Fe$_2$O$_3$ to have protons, H^{1+}, in its structure. And the fully protonated γ-Fe$_2$O$_3$, hence, may have chemical formula similar to LiFe$_5$O$_8$ as HFe$_5$O$_8$, (Fe^{3+})$_8$ [H^{1+}$_4$Fe^{3+}$_{12}$]O$_{32}$.

20. The protons are present in the octahedral sites and $\gamma\text{-Fe}_2\text{O}_3$ may have structural formula in between vacancy ordered $\gamma\text{-Fe}_2\text{O}_3$

$$(Fe^{3+})_8 \, [Fe^{3+}{}_{12}Fe^{3+}{}_{4/3} \, \square_{8/3}]O_{32} \text{ -------------------- (1)}$$
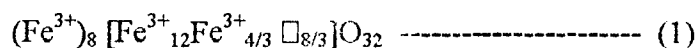
and fully protonated HFe_5O_8,

$$(Fe^{3+})_8 \, [Fe^{3+}{}_{12} \, H^{1+}{}_4]O_{32} \text{ ---------------------- (2)}$$

A protonated $\gamma\text{-Fe}_2\text{O}_3$ is thought to be a hydrogen iron oxide, $H_{1-x}Fe_{5+x/}O_8$ or hydrogen doped iron oxide with an upper limit of H^{1+}, $H_{0.1}Fe_5 \, _{1/3}O_8$. And this was considered as hydrogen ferrite type of phase by Nikumbh, Rane, Mukhedkar [50].

21. The presence of H^+ in the $\gamma\text{-Fe}_2\text{O}_3$ may be 1-2 (%). Since water is crucial in the synthesis of $\gamma\text{-Fe}_2\text{O}_3$, our studies reveals the presence of H^+ qualitatively in the oxide. In order to further investigate this presence of H^+ in $\gamma\text{-Fe}_2\text{O}_3$, studies have been carried out by measuring the direct current electrical conductivity measurement on $\gamma\text{-Fe}_2\text{O}_3$ in different atmosphere.

22. The $\gamma\text{-Fe}_2\text{O}_3$ loses H^+ ~ $170^\circ C$ and the same is reintroduced on moisture equilibration of the proton free $\gamma\text{-Fe}_2\text{O}_3$.

23. The protons are occupying the lithium sites of the lithium ferrite. Hence, lithiation studies are being carried out to see whether protons are being substituted by Li^{1-}.

24. The lithiation studies on $\gamma\text{-Fe}_2\text{O}_3$ reveal the presence of H^+ on the octahedral sites of the oxide.

25. X-ray, IR, chemical analysis of the lithiated $\gamma\text{-Fe}_2\text{O}_3$ are being done to investigate the presence of protons. The electrical conductivity measurement in different atmosphere too helped in confirming the findings.

The detailed neutron diffraction studies to investigate the presence of protons in $\gamma\text{-Fe}_2\text{O}_3$ are being taken up in our laboratories.

References

1. H. E. Du Bois, Phil. Mag. 29(1890)293.

2. J. L. Snoek, Philips Technical Review 8(1946)353.

3. S. Hilpert, Ber. Deut. Chem. Ges. 42(1909)2248.

4. F. J. Schnettler, Physics of Electronic Ceramics, Part 'B', edited by L. L. Hench and D. B. Dove, Marcel Dekker Inc. New York, 1972.

5. Alex Goldman, Future Trends in Soft Ferrite Processing, Proceedings of V International Conference on Ferrites (ICF – 5), 1989, India, pp. 13 – 20.

6. Handbook of Microwave Ferrite Materials, edited by Withelm H Von Aulock, Academic Press, New York, London, 1965 (Chapter 4).

7. P. I. Slick, 'Ferromagnetic Materials', edited by E. P. Wohlfarth, North Holland Publishing Company, Amsterdam, New York, Oxford, 1980 (Chapter 3).

8. J. Smit and H. P. J. Wijn, "Ferrites", John Wiley Sons, New York, 1959, pp.36?.

9. J. H. Van Vleck, Phys. Rev. 78(1950)266.

10. Y. Yafet C. Kittel, Phys. Rev. 87(1952)290.

11. P. W. Anderson, Phys. Rev. 79(1950)350.

12. C. G. Shull, W. A. Strauser, Phys. Rev. 81(1951)483.

13. J. M. Hastings and L. M. Corliss, Rev. Mod. Phys. 25(1953)114.

14. Tahir Abbas, Y. Khan, Mushtaq Ahmad and Shahid Anwar, Solid State Comm. 82(1992)701.

15. M. Bremer, St. Fischer, H. Langbein, W. Tipelmann and H. Scheler, Therm ochim Acta 209(1992)323.

16. Silke Christen, Hubert Langbein and Klaus Jaenicke - Rößler, Thermochim Acta 209(1992)253.

17. M. N. Sankarshana Murthy, C. E. Deshpande and J. J. Shrotri, Proc. Ind. Acal. Sci. 87(1978)49.

18. Yung – Tsen Chien, Yung – Chao Ko, J. Mater. Sci. 26(1991)5859.

19. L. Stanciulea, J. Nematu, M. Feeder, E. Segal, P. Cristea and L. Gal, J. Mater. Sci. Lett. 11(1992)961.

20. T. Y. Tseng, S. Y. Jou, J. Mater. Sci. Lett. 8(1989)777.

21. G. R. Harrison and L. Rees Hodges, 'Microwave Garnets Physics of Electronics Ceramics', Part B, edited by L. L. Hench and D. B. Dove, Marcel Dekker Inc., New York, 1972 (Chapter 26).

22. Jan Verweel, "Magnetic Properties of Materials", edited by Jan Smit, McGraw-Hill book company, Inter University Electronics Series, Vol. 13, 1971.

23. A. Beer and J. Schwarz, IEEE Trans. MAG-2, 470 (1966).

24. M. J. Ruthner, in 'Proceedings of the Vth International Conference on Ferrites', Bombay, India, 1989, pp. 23.

25. S. G. Patil, Electronics, Information and Planning 4(1977)979.

26. M. J. Ruthner, H. G. Richter and J. L. Steiner, in 'Proceedings of the Intern itional Conference on Ferrites', Japan, 1970.

27. M. J. Ruthner, J. physique Colloque, Cl. Supplement au no. 4, Tome 38, Avril 1977) pp. Cl – 311.

28. M. J. Ruthner, 'Ceramic Powders', edited by P. Vincenzini, Elsevier Scientific Publishing Co., Amsterdam, 1983, pp. 513.

29. M. J. Ruthner, 'Spray Roasted Iron Oxides: The Nature of Minor Impurities', 1989, pp. 103.

30. W. I. Kiading and W. Karner, Ceramic Bulletin 69(1990)814.

31. K. A. Natarajan, Transaction of the Indian Institute of Metals 31(1978)169.

32. K. A. Natarajan, International Symposium on Recent Advances in Particulate Science and technology, Madras, India, (1982).

33. K. A. Natarajan and R. Upadhyaya, Transactions of the Indian Institute of Metals 39(1980)627.

34. S. Subramanian and K. A. Natarajan, ibid, 40(1987)489.

35. G. G. O. O. Uwadiale, Minerals and Metallurgical Processing (1989)117.

36. A. Chiba and O. Kimura, in 'Proceedings of the Vth International Conference on Ferrites', Bombay, India, 1989, pp. 35.

37. E. P. Wohlfarth, 'Ferromagnetic Materials', North Holland Publishing Co. Vol. 1 & 2, (1980).

38. R. G. Richards and J. White, Trans. Brit. Ceramic Soc. 53(1954)422.

39. P. A. Tuan, D. Minh, N. Chau and B. T. Cong, in 'Proceedings of the VIth International Conference on Ferrites', Japan, 1992, pp. 370.

40. N. T. Mai, Doctoral Thesis, Honoi, 1987.

41. K. J. D. Mackenzie and C. M. Cardile. Thermochim. Acta 165(1990)207.

42. S. J. Gregg, J. Chem. Soc. A (1953)3940.

43. S. M. Rege, in 'Earth Resources for Goa's Development', Goa. 1985, pp. 89.

44. H. J. Hunh, Z. Chem. 27(1987)334.

45. J. J. Shrotri, A. G. Bagul, S. D. Kulkarni, C. E. Deshapande and S. K. Date, in 'Proceedings of the VIth International Conference on Ferrites', Japan, 1992, pp. 104.

46. V. M. S. Verenkar, Ph.D. Thesis, Goa University, 1997.

47. K. S. Rane, V. M. S. Verenkar and P. Y. Sawant, J. Mater. Sci.: Mater. in Electronics 9(1998).

48. B. B. Ghate, in 'Proceedings of the Vth International Conference on Ferrites', Bombay, India, 1989, pp. 23.

49. Sun Yi - dong, J. Ren - Pei, Z. Hongru, Z. Xi, in 'Proceedings of the Vth International Conference on Ferrites', Bombay, India, 1989, pp. 1107.

50. V. Jha and A. K. Bhanthia, in 'Proceedings of the Vth International Conference on Ferrites', Bombay, India, 1989, pp. 961.

51. T. Tsutaoka, S. Ema and H. Salo, in 'Proceedings of the Vth International Conference on Ferrites', Bombay, India, 1989, pp. 1113.

52. R. V. Mehta, V. Ravikumar, S. D. Bhagat and R. Srivastav, in 'Proceedings of he Vth International Conference on Ferrites', Bombay, India, 1989, pp. 1119.

53. R. K. Mehta and L. Zhans, in 'Proceedings of the VIth International Conference on Ferrites', Japan, 1992, pp. 348.

54. Y. Yamazaki and M. Matsue, in 'Proceedings of the VIth International Conference on Ferrites', Japan, 1992, pp. 1.

55. Jaehyur Oh, in 'Proceedings of the Vth International Conference on Ferrites', Japan, 1992, pp. 256.

56. N. Fell, New Scientist Vol.151, No. 2042, pp. 23.

57. Japanese Industrial Standards, JIS M 8212 – 8228 – 1971, Translated and Published by Japanese Standards Association (Reaffirmed: 1983).

58. Indian Standard Institution, IS: 1493, Methods of Chemical Analysis of Iron Ores.

59. IS: 1917 Determination of Alkalies by the Flame Photometric Method.

60. IS: 1473, Methods for Volumetric Determination of Ca and Mg using EDTA.

61. British Standards, BS: 4158 Part I – III, Method of Analysis of Iron Ores.

62. JCPDS File No. 13 – 534.

63. K. C. Patil, D. Gajapathy and V. R. Pai Vernekar, Mat. Res. Bull. 17(1982)29.

64. D. Gajapathy and K. C. Patil, Mater. Chem. Phy. 9(1983)423.

65. S. Sundar Manoharan and K. C. Patil, in 'Advances in Ferrites' edited by C. M. Srivastava and M. J. Patni, Oxford and IBM Pub. Co. Pvt. Ltd., New Delhi, 1(1989)43.

66. T. T. Srinivasan, P. Ravindranathan, L. E. Cross, R. Roy, R. E. Newnham, S. G. Sankar and K. C. Patil, J. Appl. Phys. 63(8)(1988)3789.

67. P. Ravindranathan and K. C. Patil, Am. Ceram. Soc. Bull. 66(4)(1987)688.

68. P. Ravindranathan, T. T. Srinivasan, R. Roy, R. E. Newnham, S. G. Sankar and K. C. Patil, in 11th International Symposium on 'Reactivity of Solids', Princeton U.S.A.,1988.

69. P. Ravindranathan, Ph.D., Thesis, Indian Institute of Science, Bangalore, 1986, pp. 70.

70. P. Ravindranathan and K. C. Patil, J. Mater. Sci. 22(1987)3261.

71. J. S. Budkule and K. C. Patil, Synth. React. Inorg. Met – Org. Chem. 19(9)(1989)909.

72. J. S. Budkule and K. C. Patil, Synth. React. Inorg. Met – Org. Chem. 21(4)(1991)709.

73. T. Kikkawa, M. Yoshinaka, K. Hirota and O. Yamaguchi, J. Mater. Sci Lett. 14(1995)1071.

74. K. Ishida, K. Hirota, O. Yamaguchi, H. Kume, S. Inamura and H. Miyamoto, J. Am. Ceram. Soc. 77(1994)1391.

75. S. Kimoto, K. Hirota, O. Yamaguchi, H. Kume, S. Inamura and H. Miyamoto, Ibid. 77(1994)1694.

76. K. Yamakata, K. Hirota, O. Yamaguchi, H. Kume, S. Inamura and H. Miyamoto, Ibid. 77(1994)2207.

77. K. Goto, K. Hirota, O. Yamaguchi, H. Kume, S. Inamura and H. Miyamoto, J. Mater. Sci. 31(1996)204.

78. V. Moye, K. S. Rane and V. N. Kamat Dalal, J. Mater. Sci.: Mater. in Electronics 4(1993)241.

79. K. S. Rane, A. K. Nikumbh and A. J. Mukhedkar, J. Mater. Sci. 16(1981)2387.

80. A. Venkataraman, V. A. Mukhedkar, M. M. Rahman, A. K. Nikumbh and A. J. Mukhedkar, Thermochim. Acta 115(1987)215.

81. A. Venkataraman, V. A. Mukhedkar, M. M. Rahman, A. K. Nikumbh and A. J. Mukhedkar, Thermochim. Acta 112(1987)231.

82. M. M. Rahman, V. A. Mukhedkar, A. Venkataraman, A. K. Nikumbh, S. B. Kulkarni and A. J. Mukhedkar, Thermochim. Acta 125(1988)173.

83. A. Venkataraman, V. A. Mukhedkar and A. J. Mukhedkar, J. Therm. Anal. 35(1989) 2115.

84. A. Venkataraman and A. J. Mukhedkar, J. Therm. Anal. 36(1990)1495.

85. A. K. Nikumbh, A. A. Latkar and M. M. Phadke, Thermochim. Acta 219(1993)269.

86. S. D. Likhite, C. Radhakrishnamurthy and P. W. Sahasrabudhe, Rev. Sci. Instr. 25(1965)302.

87. JCPDS File No. 24 – 81.

88. D. Khalafalla and A. H. Morrish, J. Appl. Phy. 43(1972)624.

89. J. M. D. Coey and D. Khalaffala, Phy. Stat. Sol.(a) 11(1972)229.

90. A. K. Nikhumbh, K. S. Rane and A. J. Mukhedkar, J. Mater. Sci. 17(1982)2503.

91. M. P. Morales, M. Ocana, T. Gonzalez – Carreno and C. J. Serna, in 'Fine Particles Science and Technology, Edtd. E. Pelizzetti, Kluwer Academic Publishers, Netherlands, 1996, pp. 197.

92. D. G. Klissurski, J. Subrt, V. N. Blaskov, J. Lipka, P. Hanousek and K. Bech ne, J. Mater. Sci. 19(1984)183.

93. J. E. Iglesias and C. J. Serna, Miner. Petrogr. Acta 29-A(1(1985)363.

94. JCPDS File No. 19 – 629.

95. E. Mendelovici, R. Villalba and A. Sagarzazu, Mater. Res. Bull. 17 (1982) 241.

96. Arjan Noordermeer and Marijike M. E. Severin-Vantilt, Adv. Mater. 3 (1991) 394.

97. JCPDS, Powder diffraction File no.17-464 and 17-465.

98. K. C. Patil, D. Gajapathy and V. R. Pai Vernekar, Mater. Res. Bull. 17 (1982) 29.

99. K. Seshan, A. L. Shashimohan, D. K. Chakrabarty and A. B. Biswas, Phys. Stat. Sol. (a) 68 (1981) 97.

100.G. K.Joshi, S. A. Deshpande, A. Y. Khot, S. R. Sawant, Ind. J. Phys. 61 A (1987) 251.

101.C. M. Srivastava, S. N. Shringi and M. Vijaybabu, Bull. Mater. Sci 6 (1984) 27.

102.E. Weiser, H. Schröder and K. Kleinctiick, Phys. Stat. Sol. (a) 1 (1970) 749.

103.S. H. Patil, S. J. Patil, S. M. Kadam, S. R. Patil and B. K. Chowgule, Bull. Mater. Sci. 14 (1991) 1225.

104.R. G. Kulkarni and H. H. Joshi, J. Solid State Chem. 64(1986)141.

105.C. S. Narasimhan and C. S. Swamy, Phys. Stat. Sol. (a) 59(1980)817.

106.J. S. Smart, Phys. Rev. 94(1954)847.

107.C. Guillnd and R. Bertrand, J. des rech. du centre Nat. dela Rech. Sci. 3 (1950) 73.

108.J. I. Powar, S. A. Patil and R. N. Karekar, Ind. J. Pure & Appl. Phy. 20 (1982) 267.

109.S. A. Chim, Ann Chim. (Fr) 9(1974)31.

110.W. L. Konijnendijk, Philips Research Reports 30(1975)

111.W. B. White and B. A. De Angelis, Spectrochim. Acta 23-A(1967)985.

112.J. Preudhomme, Spectrochim. Acta, 26-A(1970)985.

113.R. D. Waldron, Phys. Rev. 99(1955)1727.

114.K. Nakamoto, 'Infra red and Raman Spectra of Inorganic and Coordination Compounds', Wiley-Interscience, 1976, pp. 142.

115.P. Tarte and Preudhomme, J. Acta. Cryst. 16(1963)227.

116.V. R. K. Murthy, S. Chitrasankar, K. V. Reddy and J. Sobhanadri, Ind. J. Pure and Applied Phy. 36(1978)79.

117.V. A. M. Brabers, Phys. Stat. Sol. (a) 33(1969)563.

118.V. S. Hafner, Z. Fur. Krist. 115(1961)331.

119.K. Satomi, J. Phys. Soc. Japan 16(1961)286.

120.K. Siratori, J. Phys. Soc. Japan 23(1967)948.

121.N. W. Grimes and A. Collet, Phys. Stat. Sol. (b) 43(1971)591.

122.J. Kanturek and Z. Simsa, Phys. Stat. Sol. (a) 36(1969)47.

123.V. R. Potakova, N. D. Zervey and V. P. Romanov, Phys. Stat. Solidi (a) (Germ.) 12(1972)623.

124.H. H. Joshi and R. G. Kulkarni, J. Mater. Sci. 21(1986)2138.

125.K. B. Modi, H. H. Joshi and R. G. Kulkarni, J. Mater. Sci. 31(1996)1311.

126.S. H. Patil, S. I. Patil, S. M. Kadam, S. R. Patil, and B. K. Chougule, Bull. Mater. Sci. 15(1992)127.

127.S. A. Oliver, R. T. Welley, H. H. Hamdeh, G. Oliveri and G. Busca, Scripta Metallurgica et Materialia 33(1995)1695.

128.S. H. Patil, S. I. Patil, S. M. Kadam, S. R. Patil and B. K. Chougule, J. Mag. Mag. Mater. 110(1992)147.

129.K. Seshan, M. J. Patni and D. K. Chakrabarty, J. Solid State Chem. 42(1982)206.

130.Y. P. Irkhin, E. A. Turov, Sov. Phy. JETP 33(1957)673.

131.M. D. Sundararajan, A. Narayanasamy, T. Nagarajan, L. Haggström, C. S. Swamy and K. V. Ramanujachary, J. Phy. C. Solid State Phys. 17(1984)2953.

132.S. D. L'White and C. Radhakrishnamurty, Curr. Sci. 35(1966)534.

133.I. Neel, Ann. Phys. 3(1948)139.

134. T. F. W. Barth and E. Posnjak, Krist. 82(1932)325.

135. C. Radhakrishnamurthy, S. D. Likhite, E. R. Deutsch, G. S. Murthy, Physics of Earth and Planetary Interiors 30(1982)281.

136. 'Magnetic Properties of Materials', Edited by Jan Smit, McGraw-Hill Book Company, 1971.

137. G. T. Rado and A. Terris, Phys. Rev. 83(1951)177.

138. C. Guillaud, Compt. Rend. 232(1951)944.

139. K. J. Standley, 'Oxide Magnetic Materials', Clarendon Oxford, 1972, pp. 98.

140. K Radha and D. Ravinder, Ind. J. Pure & Appl. Physics 33(1995)74.

141. D. Ravinder, J. Mater. Sci. Lett. 11(1992)1498.

142. K. Latha, K. Satya Mohan and D. Ravinder, Phys. Status Solidi (a) 142(1994)K 103.

143. K. Iwanchi, Jpn. J. Appl. Phys. 10(1971)1520.

144. N. Rezlescu and E. Rezlescu, Phys. Stat. Solidi (a) 23(1974)575.

145. V. R. kulkarni and A. J. Vaingankar, J. Mater. Sci. 22(1987)4087.

146. L. M. Corliss, J. M. Hastings and F. G. Brockman, Phy. Rev. 90(1953)1013.

147. C. E. Deshpande and S. K. Date, Ind. J. Chem. 35A(1996)353.

148. Y. H. Hung, Y. T. Chien, Y. C. Ko, J. Mater. Sci. Lett. 13(1994)639.

149. U. Wagner, J. Mag. Magn. Mat. 23(1981)73.

150. U. Wagner, J. Mag. Magn. Mat. 4(1971)116.

151. S. Urek and M. Drofenik, J. Mater. Sci. 31(1996)4801.

152. JCPDS File No. 10 – 467.

153. K. Latha and D. Ravinder, Phys. Stat. Sol. (a) 139(1993) K 109.

154. K. Suresh and K. C. Patil, in 'Proceedings of Vth International Conference of Ferrites, Bombay, India, 1989, pp. 103.

155. G. M. Van Oosterhout and C. J. M. Rooijmans, Nature 181(1958)44.

156.J. D. Bernal, D. R. Dasgupta and A. L. Mackey, Clay Min. Bull. 4(1959)15.

157.I. David and A. J. E. Welch, Trans. Faraday Soc. 52(1956)1642.

158.D. R. Dasgupta, Ind. J. Phys. 35(1961)401.

159.J. Thewlis, Phil. Mag. 12(1931)1089.

160.G. Hass, Z. Krist. B 29(1953)95.

161.W. E. Henry and M. J. Boehm, Phys. Rev. 101(1956)1253.

162.G. A. Ferguson and M. Hass, Phys. Rev. 112(1958)1130.

163.J. R. Armstrong, A. H. Morrish and G. A. Sawatzky, Phys. Lett. 23(1966).

164.H. Annersten and S. S. Hafner, Z. Kristallog. 137(1973)321.

165.K. Haneda and A. M. Morrish, Solid State Commun. 22(1977)779.

166.E. J. W. Verwey, Z. Krist. 91(1935)65.

167.M. A. Anantharaman, K. Seshan, D. K. Chakrabarty and H. V. Keer, Bull. Mater. Sci. 3(3)(1981)278.

168.T. Elder, J. Appl. Phys. 36(1965)1012.

169.P. B. Braun, Nature 170(1952)1123.

170.C. Greaves, J. Solid State Chem. 49(1983)325.

171.A. Aharoni, E. H. Frei and M. Schieber, J. Phys. Chem. Solids 23(1962)545.

172.F. Gazzarini and G. Lanzavecchia, in 'Reactivity of Solids' edited by J. W. Mitchell et al, Wiley – Interscience, 1969, pp. 57.

173.G. D. Renshaw and C. Roscoe, Nature 224(1969)263.

174.V. Rao, A. L. Shashimohan and A. B. Biswas, J. Mater. Sci. 9(1974)430.

175.F. E. Deboek and P. W. Selwood, J. Amer. Chem. Soc. 76(1954)3365.

176.JCPDS File No. 25 – 1402.

177.R. Giovanoli and R. Brütsh, Thermochim. Acta 13(1975)15.

178.M. P. Morales, C. Pecharronman, T. Gonzalez Carreno and C. J. Serna,

Chem. 108(1994)158.

179.K. S. Rane, V. M. S. Verenkar, R. M. Pednekar and P. Y. Sawant, J. Mater. S.

Mater. in Electronics (Accepted).

180.M. A. Semary, M. A. Ahmed and Y. Abbas, J. Mater. Sci. 18(1983)2890.

181.C. E. Deshpande, P. P. Bakre and M. N. Sankarshana Murthy, Bull. Mater. Sci.

5(1983)1.

182.A. K. Nikumbh, K. S. Rane and A. J. Mukhedkar, J. Mater. Sci. 18(1983)341.

183.M. M. Thackeray, W. I. F. David and J. B. Goodenough, Mat. Res. Bull.

17(1982)785.

184.M. S. Islam and C. R. A. Catlow, J. Solid State Chem. 77(1988)180.

185.M. Pernet, J. Rodriguez, M. Gondrand, J. Fontcuberta, P. Strobel and J. C. Joubert, in

Proceedings of the Vth International Conference on Ferrites, Bombay, India, 1989,

pp. 61.

186.M. Pernet, P. Strobel, B. Bonnet and P. Bordet, Solid State Ionics 66(1993)259.